OPTIMISATION OF A SEMI-EMPIRICAL MODEL FOR ACCURATE DETERMINATION OF EXCITATION ENERGIES AND ABSORPTION SPECTRA OF QUANTUM DOTS

BY

OYENIYI, EZEKIEL

B.TECH. Physics (LAUTECH), M.Sc. Physics (Ibadan)

Matric Number: 153244

A thesis in the Department of Physics

Submitted to the Faculty of Science in partial fulfilment of

the requirement of the Degree of

DOCTOR OF PHILOSOPHY

of the

UNIVERSITY OF IBADAN

May, 2021

ABSTRACT

Quantum dots are nanomaterials that have several potential applications including the production of efficient solar cells. Accurate theoretical studies of excitation energies and absorption spectra of quantum dots are essential for harnessing such potentials. The existing high-level *ab-initio* methods for obtaining excitation energies and absorption spectra are computationally expensive for quantum dots. However, the semi-empirical methods, including the Intermediate Neglect of Differential Overlap for spectroscopy (INDO/s) model, are computationally cheap but are generally less accurate. Unlike some ground-state semi-empirical methods, INDO/s has not attracted significant attention to improving its level of accuracy because of some difficulties associated with optimising its parameters. Therefore, this research was aimed at developing an improved INDO/s model that will be computationally cheap and capable of producing accurate excitation energies and absorption spectra for quantum dots.

A semi-empirical Hamiltonian based on INDO/s was parameterised with benchmark excitation energies from Equation-Of-Motion Coupled-Cluster Singles Doubles (EOM-CCSD) for Si, S, Cd and Zn diatomics at different interatomic separations. The Mean Absolute Errors (MAE) were calculated for different sets of parameters and the optimised set of parameters were those with the least MAEs. The optimised model was called optimised for excitation Intermediate Neglect of Differential Overlap (oeINDO). The oeINDO was validated by computing the MAEs of the oeINDO and INDO/s excitation energies and absorption spectra maxima for Si_n, S_n, Zn_n ,Cd_n, $(ZnS)_n$ and $(CdS)_n$ (n is the number of atoms) clusters. The validation was carried out relative to EOM-CCSD for small clusters ($n<6$) and Time-Dependent Density Functional Theory (TDDFT) for large clusters ($n \geq 6$). All computation times were recorded. The oeINDO was then employed to predict the absorption spectra of Si, S, Zn, Cd, ZnS, and CdS quantum dots, and the optimal size of CdS and ZnS quantum dots for solar cell applications.

The optimised parameters obtained for Si, S, Zn and Cd diatomics had MAEs 0.21, 0.19, 0.23,and 0.29 eV, respectively. The oeINDO produced excitation energies with MAEs 0.18, 0.56, 0.25, 0.22 eV for small Si, S, Zn, and Cd clusters, respectively, and MAEs 0.22, 0.36, 0.15, 0.24, 0.36 and 0.23 eV, for large Si, S, Zn, Cd, ZnS, and CdS clus-

ters, respectively. The unoptimised INDO/s however, produced excitation energies with MAEs 1.23, 1.29, 0.70, and 1.23eV for small Si, S, Zn, Cd clusters, respectively, and MAEs 1.05, 2.51, 2.49, 0.63, 0.76 and 1.04eV for large Si, S, Zn, Cd, ZnS, and CdS clusters, respectively. Also, the MAEs of oeINDO and INDO/s absorption spectra maxima relative to those from TDDFT were 0.41eV and 1.49eV, respectively. The results showed that oeINDO agreed reasonably well with the benchmarks and it was more accurate than INDO/s. The time of computing with oeINDO (0.08 minutes) was found to be less than a hundredth of the time utilised for EOM-CCSD (2946.51 minutes). The oeINDO predicted a *red-shift* in the quantum dots absorption spectra with an increase in dot size. It also predicted Si, Zn and Cd dots to be metallic. The 1.2 nm and 1.4 nm spherical-like CdS and ZnS quantum dots, respectively, were found to be theoretically optimal for solar cell applications.

The improved INDO/s was computationally cheap and capable of producing more accurate excitation energies and absorption spectra for quantum dots.

Keywords: Cluster excitation energies, Cluster absorption spectra, Hamiltonian, High-level *ab-initio* Method, Nanomaterials

Word count: 500

DEDICATION

This work is dedicated to the Glory of God.

ACKNOWLEDGEMENTS

First and foremost, I appreciate God Almighty for life, wisdom, understanding, strength and help He gave me to complete this programme. To Him alone is all the glory, power, dominion and majesty.

My profound gratitude goes to my wonderful supervisors: Dr Oyebola O. Popoola and Dr O. Akin-Ojo. I appreciate Dr Oyebola O. Popoola for her kind supports, encouragement and for granting me the enabling environment to carry out this research. Her approachability and close work with me in this research are acknowledged and appreciated. I will ever be grateful to Dr O. Akin-Ojo for teaching me the art of research, providing me with an enabling environment and facilities to carry out this research. I acknowledge and appreciate his selfless and unwavering supports.

I appreciate the encouragement and supports I received from Profs. J.A. Adegoke, F. O. Ogundare, N.N. Jibiri, Janet A. Ademola, Drs O.M. Oshakuade, O.E. Oyewande, A.T. Otunla, Folashade L. Aderemi, E.O. Ogunshola and T.T. Ogunseye during the work.

Special thanks to the Head of Department, Prof. O.E. Awe, the postgraduate coordinator, Dr Mojisola O. Adeniyi and other member of staff of the Department of Physics for their contributions towards the success of this work.

I thank my dear wife, Oladunni Oyeniyi and my children, Rejoice and Temiloluwa Oyeniyi, for their love, understanding, encouragement, prayers and unalloyed supports.

I appreciate the helpful discussion with Dr Matteo Gatti (Ecole Polytechnique, France) on the research. I am grateful to Rev. Dr Wale Olajire, Bro. Johnson Aremu, Pastor Fisayo Olatunji and others for their concerns and prayers. My thanks also goes to Tolulope Falade for taking the pain to proofread this thesis. To all who have contributed in one way or the other to the success of this research, God bless you all.

CERTIFICATION

We certify that this work was carried out by Mr. E. Oyeniyi in the Department of Physics, University of Ibadan.

Supervisor

Dr O.O. Popoola

B.Sc., M.Sc., Ph.D. (Ibadan)

Senior Lecturer, Department of Physics,

University of Ibadan, Nigeria.

Co-supervisor

Dr O. Akin-Ojo

B.Sc., M.Sc. (Ibadan), Ph.D. (Delaware)

Senior Lecturer, Department of Physics,

University of Ibadan, Nigeria.

TABLE OF CONTENTS

LIST OF TABLES

LIST OF FIGURES

LIST OF ABBREVIATIONS

ALDA	Adiabatic Local-Density Approximation
AM1	Austin Model 1
B3LYP	Becke, 3-parameter, LeeYangParr
BSE	Bethe Selpeter Equation
CASPT2	Complete Active Space Perturbation Theory
CC	Coupled Cluster
CCSD	Coupled Cluster
CCSDT	Coupled Cluster
CIS	Configuration Interaction Singles
CISD	Configuration Interaction Singles Doubles
CNDO	Complete Neglect of Differential Overlap
CNDO/s	Complete Neglect of Differential Overlap for Spectroscopy
CASSCF	Complete Active Space Self-Consistent Field
DEF2-TZVPP	Valence triple-zeta with two sets of polarization functions
DFT	Density Functional Theory
DFTB	Density Functional Tight Binding
DOS	Density of States
EELS	Electron Energy Loss Spectroscopy
EMA	Effective Mass Approximation
EOM-CCSD	Equation-of-Motion Coupled Cluster Singles Doubles
EPM	Empirical Pseudopotential Method
GGA	Generalized Gradient Approximation

HF	Hartree-Fock
HOMO	Highest Occupied Molecular Orbital
INDO	Intermediate Neglect of Differential Overlap
INDO/s	Intermediate Neglect of Differential Overlap for Spectroscopy
LCAO	Linear Combination of Atomic Orbitals
LDA	Local Density Approximation
LUMO	Lowest Unoccupied Molecular Orbital
MOPAC	Molecular Orbital PACkage
MCSCF	Multi-configuration Self-consistent Field
oeINDO	Optimized for excitation Intermediate Neglect of Differential Overlap
PM3	Parametric Method 3
PM6	Parametric Method 6
PM7	Parametric Method 7
QMC	Quantum Monte Carlo
TDDFT	Time Dependent Density Functional Theory
UV-Vis	Ultra-violet-Visible
ZDO	Zero Differential Overlap
ZINDO/s	Zerner Intermediate Neglect of Differential Overlap for Spectroscopy

Chapter 1

INTRODUCTION

1.1 Introduction

Novel materials are crucial ingredients for the emerging and next-generation technologies that could impact human life positively. For instance, materials with combined features like cost-effectiveness, lightweight, environmental friendliness, high stability, abundance and energy-effectiveness are needed for photovoltaic devices, electric car batteries, portable electronic devices, high speed and large memory computers, medical devices for diagnosis and treatment of diseased cells, artificial intelligence etc. Nanotechnology offers a lot of possibilities to design new materials. It involves the manipulation and study of materials at the nanometer dimensions where unique phenomena enable novel application. Different nanosystems, such as quantum dots, have been discovered with several applications cutting across disciplines including physics, chemistry, biomedical sciences and engineering.

Quantum dot is a tiny man-made material with a size in the range of 1 - 100 nm (about ten-thousandth of the thickness of a hair strand). It is composed of hundreds to thousands of atoms. Quantum dot was discovered in the early 1980s independently by two researchers. Alexei Ekimov, a Russian Physicist, discovered a quantum dot in a glass matrix while Brus Louis in a separate work in the Bells Laboratory, discovered it in a colloidal solution (Brus, 1984, Ekimov et al., 1985). The nano-scale system (quantum dot) is called a zero-dimensional system because it restricts the motion of its particles (electrons and holes) in all spatial directions. Unlike its bulk counterpart, the quantum dot behaves like an atom or molecules with discrete energy levels and states and so, it

is sometimes called an 'artificial atom'. It has remarkably tunable properties such as size-dependent absorption and emission spectra and energy levels. A *red-shift* (decrease in energy) is observed in the quantum dot spectra and electronic gap as its size increases and a *blue-shift* (increase in energy) as its size decreases. Another fascinating feature of the quantum dot is the multiexciton generation. This is the ability of the dot to generate more than one excitons per incoming high-energy photon. In contrast, the bulk material generates only one exciton per incoming high-energy photon and loses its excess photon energy as heat. In addition, due to its high extinction coefficient, quantum dot shows descent stability (Soloviev et al., 2001, Nozik, 2008, Rühle et al., 2010, Suri et al., 2013). These unique and exciting features of quantum dots facilitate their wide applications.

Quantum dots are promising materials for cost-effective, portable, environmentally friendly and power-efficient solar cells. Their tunable electronic gap and multiexciton generation features could lead to an optimal harvest of sunlight and the generation of more electrons. Thus, a maximum theoretical conversion efficiency of 66%, twice that achievable by the conventional solar cells, is possible with quantum dot solar cell (Nozik, 2002, Zhou, 2015). Moreover, the dots tiny size and stability feature could lead to the production of inexpensive, portable and stable solar cells.

Quantum dots are novel materials in biomedical sciences. Their reduced size and tunability characteristics made them useful for the study of single molecules and thus, making them potential material for bio-imaging, diagnosis and treatment of tumours, drug delivery, bio-sensing etc. (Bae et al., 2011, Hubbell and Chilkoti, 2012, Nazir et al., 2014).

Nanodots are materials for more energy-efficient and brighter and purer colour television (TV) displays in the electronic industry. Unlike the conventional displays (organic light-emitting diode displays), which require a backlight to emit their colours, quantum dot TV displays are self-emissive, thus making them more cost-effective. The Sony electronic company in 2013, incorporated quantum dots in their TV displays and recently, the Samsung and LG electronic company researchers are working hard to incorporate dots in their TV displays (Bourzac, 2013).

Studies have shown that nano-sized materials like quantum dots exhibit quantum en-

tanglement, which makes them relevant for the next generation high speed and high computing-power computers (quantum computers) (Predojević, 2016). More efficient, miniaturized and cost-effective detectors, lasers, sensors can be produced with quantum dots. The future high power density (lighter, cheaper, and more efficient) and stable lithium-ion batteries can be realized by incorporating nano-sized materials in the batteries (Zhou, 2015). The list of the potential applications of quantum dots is 'endless' cutting across various disciplines.

Spectroscopy and excitation energies are important tools for the investigation of the properties of low-dimensional materials, such as quantum dots. Spectroscopy is a technique that is concerned with the study of the response of a system when perturbed with a probe (electron, neutron, or electromagnetic radiation). The plot of the system response against the probe wavelength is called a spectrum. Spectroscopy grants one access and insight into the microscopic nature of the system, which avail one a great deal of information about the properties of the system (Gatti, 2007, Marques et al., 2012, Delerue and Lannoo, 2013). Spectroscopy can provide information about the system structure, electronic gap, dielectric, susceptibility, fluorescence, molecular dynamics, geometry, chemical composition and other properties of a material. Most of the properties of molecular systems known today were obtained from spectroscopic studies.

Generally, in spectroscopy, a probe impinges on an electronic system and the system responds by moving from one state to another state (transition). Information about the electronic transition can be accessed from the determination of the energies of the probe and the outgoing particles (photon, electron, etc). Transition in electronic systems, W can be expressed using the Fermi Golden Rule given as

$$W = 2\pi|\langle\psi_f|H_{int}|\psi_i\rangle|^2\delta(\varepsilon_f - \varepsilon_i - \hbar\omega), \tag{1.1}$$

where H_{int} is the perturbation and $\hbar\omega$ is the photon energy. ψ_i and ψ_f are the initial and the final orbitals (wavefunctions), respectively. The ε_i and ε_f are the initial and final orbital energies, respectively. The Fermi Golden Rule expression is a fundamental formula for all spectroscopy techniques.

Numerous spectroscopy techniques have been developed and they are categorized according to the probe employed, the outgoing particles and the conservation or non-conservation of the total number of particles. The different categories are namely, photo-emission, inverse photo-emission, photo-absorption and electron loss spectroscopy. In the photoemission spectroscopy technique, the system absorbs a photon (probe) and its electron is excited above the vacuum level. The photo-emission spectrum is specified by the distribution of the photoelectron kinetic energy. Conversely, in the inverse photoemission spectroscopy, the system absorbs electrons (addition of electrons) and emits photons. In both techniques, the total number of electrons is not conserved. In the case of photo-emission, electrons are removed from the system while for inverse photoemission, they are added to the system. For photo-absorption spectroscopy, the system absorbs a photon, which results in electron excitations from a lower energy state to a higher energy state. However, in electron energy loss spectroscopy, electrons are excited in the system, when it is perturbed by an electron. In both photo-absorption and electron energy loss spectroscopy, the total number of electrons is conserved.

The absorption and emission spectroscopy are the first set of techniques developed and are still very relevant to study the properties of systems like nano-particles (Marques et al., 2012). In absorption spectroscopy, different transitions (excitations) are possible depending on the energy range of the electromagnetic radiation absorbed by the electronic system. If the system absorbs radiation in the ultraviolet-visible (UV-VIS) region, an electronic transition (excitation) from a lower energy state to a higher energy state is observed. Absorption in the infra-red region of the electromagnetic radiation spectrum results in the vibrational transition while absorption in the microwave region results in rotational transition.

In UV-VIS absorption spectroscopy, if the photon energy, $E = h\nu$, matches a difference in electron energy levels, $\Delta E = E_2 - E_1$ of the system, the system absorbs the photon and its electron is excited from the lower energy level E_1 to higher energy level E_2 (Fig.1.1). Absorption spectra are usually plots of the fraction of the unabsorbed photon (absorbance or absorption coefficient) against the incidence photon energy (Fig. 1.1).

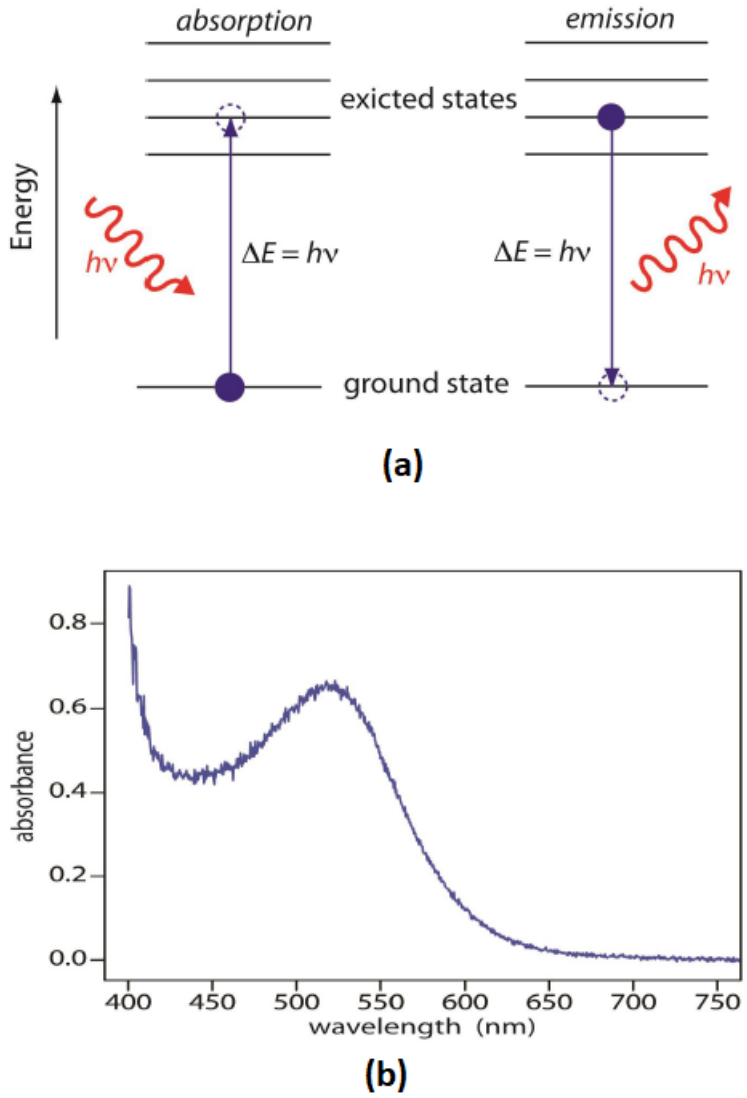

Figure 1.1: (a) Electronic excitation and de-excitation (b) Absorption spectrum - absorbance of a system against wavelength of incident photon (Harvey, 2011).

Both theoretical and experimental approaches have been employed for the determination of the electronic excitations and absorption spectra of materials. Although experiment is the most accurate and reliable approach, it sometimes poses some challenges, especially in large atomic clusters and nanostructure materials (Delerue and Lannoo, 2013). On one hand, the cost of infrastructure used in carrying out experiments is high and this could limit their acquisition and usage. On the other hand, experiments could be time-consuming and sometimes involve a high degree of complexity in their procedures. These make it difficult for individual researchers and research groups to carry out cutting-edge research within a short period of time. Consequently, material researchers have sometimes relied on efficient theoretical approaches to the study properties of materials. This approach serves to confirm and complement experimental results. They are useful for making predictions for experimentalists and sometimes help to describe some processes that are intractable in experiments (Gatti, 2007, Barone, 2011, Voityuk, 2013). One of the commonly used theoretical approaches in the study of the properties of materials are those based on quantum mechanical models.

Quantum mechanical modelling of ground-state, excited state and spectra of atomic systems continues to be an active area of research. The modelling method is based on seeking a solution to the Schrödinger equation to obtain state functions and their corresponding energies, which are useful in describing the atomic systems. Quantum mechanical models are basically divided into the *ab-initio* and semi-empirical model.

The *ab-initio* methods, also referred to as first principle methods, are methods that do not incorporate adjustable parameters in their model but calculate every term (including all integrals) in the model exactly. Several *ab-initio* methods based on a different level of theories have been developed. Some of the theories are the density functional theory, Hartree Fock theory, configuration interaction theory, perturbation theory, coupled-cluster theory, etc. (Jurs et al., 1990). Density functional theory and the Hartree Fock method have been successfully applied for ground-state calculations. Within a large basis set, they give good results, which are comparable to experiments. They have been employed for the calculations of system structural properties, bond properties, the heat of formation, etc. However, these methods fail in prediction of the electronic gaps, excitation energies and spectra properties of systems. Conversely, *ab-initio* methods like

equation-of-motion coupled-cluster singles doubles (EOM-CCSD), configuration interactions (CI), configuration interaction singles (CIS), complete active-space second-order perturbation theory (CASPT2), time-dependent density functional theory (TDDFT), etc. have been developed and applied successfully for the calculation of excitation energies and spectroscopy. However, these methods are limited by system size. They are *compute-intensive* and sometimes prohibitive for large atomic clusters and nanostructure materials. Due to the limitations of these methods, semi-empirical methods have been widely adopted for studying large clusters and nanostructure materials.

Semi-empirical methods are methods built from *ab-initio* models but some terms in the models, which make calculations expensive are omitted or replaced with simple expressions or adjustable parameters. In most cases, the one-center and two-center (e.g exchange and coulomb interaction) integrals are replaced with adjustable parameters or simple expressions while the higher-center integrals, which are assumed to have insignificant effects, are omitted. The values of adjustable parameters are then obtained from fits to experiments or high-level *ab-initio* methods. If the calibration of the parameters were accurately carried out, the obtained optimised parameters are capable of correcting errors introduced into the semi-empirical model due to the drastic approximations to the *ab-initio* model. Another drastic approximation in the semi-empirical methods is the expansion of their wave functions with minimal basis sets (the valence orbitals only) and the use of only valence electrons. Several semi-empirical methods have been developed, which include Empirical Pseudopotential Method (EPM), Effective Mass Approximation (EMA), Huckel model, extended Huckel model, intermediate neglect of differential overlap (INDO) based methods, neglect of diatomic of differential overlap (NDDO) based methods, and complete neglect of differential overlap (CNDO) based methods, Tight binding, Density Functional Tight Binding (DFTB), etc. Most of these semi-empirical methods were developed for ground-state calculations but a few including INDO/s have been developed uniquely for excitations and spectra calculations.

1.2 Statement of Problem

Theoretical modelling and determination of excitation energies and absorption spectra play important roles in the study and development of novel materials like quantum dots (Delerue and Lannoo, 2013, Voityuk, 2013). The recent powerful computing resources and high-level algorithm, have made it possible for the theoretical approaches to reproduce experimental results with good accuracy and less effort. Moreover, while the results from theoretical approaches normally complement the information obtained by experiment, it can in some cases enable prediction of hitherto unobserved chemical phenomena.

Both *ab-initio* and semi-empirical theoretical approaches have been developed for excitation energy and absorption spectra calculations. However, despite the available powerful computing resources, high-level and accurate *ab-initio* methods like GW/BSE, EOM-CCSD, CASPT2, Quantum Monte Carlo (QMC) are restricted to small systems (Delerue and Lannoo, 2013). As the system grows bigger, these methods become computationally expensive and sometimes prohibitive. In particular, they are prohibitive for large atomic clusters and quantum dots. Alternative methods to the high-level methods are the TDDFT and configuration interaction singles with perturbative doubles (CIS(D)). They could handle moderate-sized systems ($\leq$ 100 atoms) but are *compute-intensive* for larger clusters and quantum dots (Voityuk, 2013, Gieseking et al., 2016).

Due to the limitation of the accurate *ab-initio* methods, researchers have adopted semi-empirical methods for calculations in large clusters and quantum dots. Although semi-empirical methods are computationally cheap, they are generally less accurate and less transferable compared to the high-level *ab-initio* methods. In particular, INDO/s, a Hartree Fock based semi-empirical method, has been uniquely developed and widely applied for excitations and spectra calculations. However, due to drastic approximations and poor parametrization, INDO/s like any other semi-empirical approach, is generally less accurate and less transferable. (Jelski and George, 1999, Bredow and Jug, 2005, Thiel, 2014, Husch et al., 2018).

Reports have shown that, with the recent powerful computing resources and reliable data, improvement of the semi-empirical models could produce new models capable

of giving results comparable to those from experiments or high-level methods. While the NDDO, a ground-state semi-empirical model, has received significant improvement since its development in 1977 (Silva-Junior and Thiel, 2010, Stewart, 2013, Dral et al., 2016), INDO/s has not been significantly improved upon. The INDO/s parameters for several elements, especially the transition metal ones, are considered unreliable due to insufficient and inaccurate training data sets used during its parameterisation (Voityuk, 2013).

There is a need to develop computationally cheap theoretical methods for the accurate calculation of excitation energies and absorption spectra of large systems such as quantum dots.

1.3 Research Justification

Quantum dot is a novel material with a lot of untapped potentials. It is a promising candidate for a cost-effective, stable and more efficient solar cell. Reports have shown that quantum dot solar cells could convert sunlight to electricity with an efficiency greater than 65% (Nozik, 2002, Service, 2008). The quantum dot solar cells appeared as new technology on the National Renewable Energy Laboratory (NREL) chart in 2010 with a starting conversion efficiency of less than 4% and by 2019, the conversion efficiency has reached 16.6% (NREL, 2019). Evidently, with continuous and intense research into the quantum dot solar cell, an efficiency above 65% may be achieved in a short period of time. Quantum dot is a useful material for energy-efficient, cost-effective and excellent colour quality large displays (e.g TV display). However, a major setback is the use of cadmium-based and non-self-emissive phosphor quantum dots in the displays. Currently, researchers are working hard for new dot materials, that are heavy metal (cadmium) free and self-emissive (Brazis, 2017, Won et al., 2019). Quantum dots are potential materials for the next-generation quantum computers (fast and high storage powerful computing system) because they exhibit a phenomenon called quantum entanglement (an ability to localize single electron and give single-photon pulses) (Imamoglu, 2003, Predojević, 2016). Neuroscientists and biomedical scientists have discovered the novelty in quantum dots and are exploring them for possible applications in vivo and in vitro imaging, bio-

sensing, diagnosis and therapy of cancer and drug delivery (Saadeh et al., 2014, Abbasi et al., 2016). The list of potential applications of quantum dots is 'inexhaustible', cutting across various disciplines.

To harness the numerous potentials of quantum dots, access to and studies of their microscopic nature are required. To achieve these, accurate theoretical investigation of excitation energies and absorption spectra of these nanosystems are crucial (Varsano, 2006, Gatti, 2007, Delerue and Lannoo, 2013).

The existing high-level *ab-initio* methods like EOM-CCSD, CASPT2, GW/BSE for obtaining accurate excitation energies and absorption spectra are computationally expensive for quantum dots (Jin and Yang, 2019). For instance, the EOM-CCSD is known to compare very well with the experiment but is restricted to a few atom-systems ($\leq$ 10 atoms). The semi-empirical methods, however, are computationally cheap but are generally less accurate and less transferable as compared to the high-level methods (Jelski and George, 1999, Bredow and Jug, 2005, Thiel, 2014, Husch et al., 2018).

Thus, there is a need to develop a computationally cheap, reliable and accurate semi-empirical approach for the computation of excitation energies and absorption spectra of large atomic clusters and quantum dots.

1.4 Aim and Objectives

The aim of the research was to develop a computationally cheap method capable of yielding accurate excited state energies and ultra-violet-visible (UV-Vis) absorption spectra of quantum dots.

The objectives are to:

1. parameterise a semi-empirical Hamiltonian model with diatomic data from a high-level *ab-initio* method and to validate it.

2. predict excited state energies and UV-Vis absorption spectra of large atomic clusters and quantum dots using the newly obtained Hamiltonian model.

3. predict a theoretical optimal quantum dot size/shape for solar cell applications.

1.5 Outline of Thesis

The thesis is organized as follows. The next chapter presents the literature review, which covers the basics of nanomaterials and theoretical spectroscopy. It also contains the review of different approaches for the calculation of electronic excitations and absorption spectra of different systems including quantum dots. Chapter three gives detail of the tools used and steps followed in carrying out the present work. In chapter four, the results of the work are presented in graphical and tabular form and discussed in details. Conclusion and recommendations were presented in chapter five.

Chapter 2

THEORETICAL BACKGROUND AND LITERATURE REVIEW

2.1 Nanomaterials

Nanomaterials are materials with length scale in the range 1-100 nm, which lies between bulk materials and molecules. Within this length scale, the quantum mechanical laws come to play and the materials experienced an effect called the quantum confinement. This effect is responsible for the unique and exciting features exhibited by the nanomaterials. In the nanomaterials, particles (electrons and holes) are restricted along the direction the confinement effect is experienced. The effect gives rise to the quantization of the energy levels and states along the direction of the confinement. A material that restricts its particles along one direction is a two-dimensional material referred to as quantum well. When particles are restricted along two directions, a one-dimensional material called nanowire or nanotube is obtained. The restriction of particles in a material along all direction gives rise to a zero-dimensional material called a quantum dot. Quantum dots are sometimes referred to as 'artificial atoms' because they possess atomic-like optical and electronic properties (discrete energy levels and states). Quantum dot is one of the most prominent among the nanomaterials with a lot of potential of applications that cut across various disciplines (Kuno, 2005).

2.1.1 Quantum Dot: Confinement effect and quantization of energy and state

Quantum dot was discovered in the early '80s by Brus and Ekimov (Ekimov and Onushchenko, 1982, Rossetti et al., 1983). Since then, it has attracted the attention of researchers be-

cause of its amazing features, which are different from those of its bulk counterpart. Due to the confinement effect (Yoffe, 1993), quantum dot exhibits atomic-like properties - its energy levels and states are quantized. So, a quantum dot is sometimes referred to as an 'artificial atoms'. In addition, the properties of quantum dot can be tuned by changing its size or shape. For instance, the electronic gap of the dot is *red-shifted* as its size increases and *blue-shifted* as its size decreases.

An important effect in low-dimensional materials like quantum dot is the quantum confinement effect. It is an effect observed in a material, when the physical size of the material is less than or equal to its bulk exciton Bohr radius (the length of the electron-hole pair bound) . The exciton Bohr radius, a_{ex} is expressed as (Yoffe, 1993)

$$a_{ex} = \frac{4\pi\varepsilon\hbar^2}{m_{eff}e^2}, \tag{2.1}$$

where $\frac{1}{m_{eff}} = \frac{1}{m_e} + \frac{1}{m_h}$ and m_{eff} is the effective mass, ε is the dielectric constant of the material, $\hbar$ is the Planck constant, e is the electronic charge, m_e is the mass of an electron and m_h is the mass of hole. Quantum confinement effect in material results in the quantization of the energies and states of the material. A qualitative description of the confinement effect will be explored using a particle in the box model (idealized quantum dot) and effective mass approximation. Considering an electron confined along the x-axis in an infinite square well, the potential, $V(x)$ in the different regions of the well (2.1) is defined as follows:

$$V(x) = \begin{cases} \infty, & \text{if } x \leq 0 \\ 0, & \text{if } 0 < x < L \\ \infty, & \text{if } x \geq L \end{cases} \tag{2.2}$$

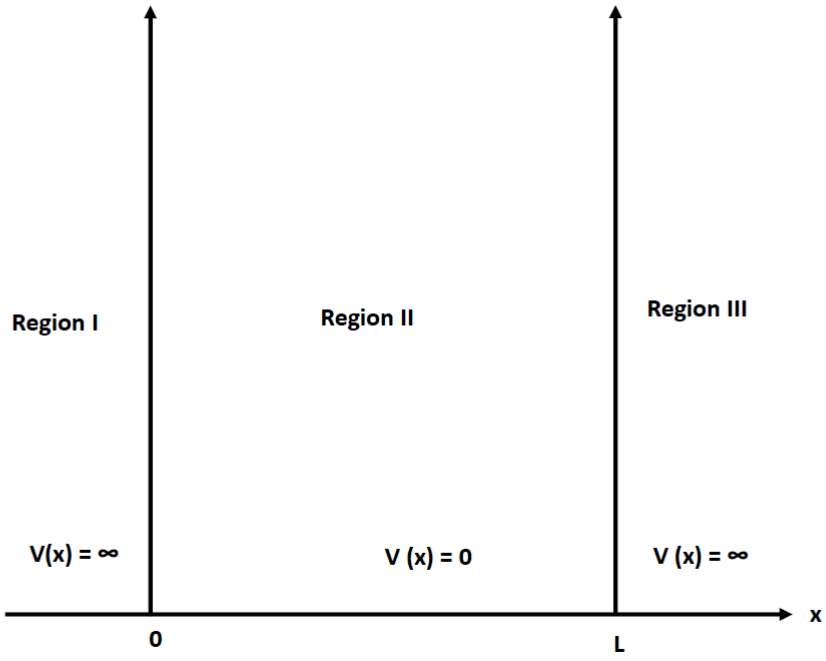

Figure 2.1: A one-dimensional infinite potential square well. The regions I and III are barriers with infinite potentials while the region II is a well with potential equal to zero.

The one-dimensional Schrödinger equation in equation 2.3 is solved for electron in each of the regions;

$$-\frac{\hbar^2}{2m}\nabla^2\psi(x)+V(x)\psi(x)=E\psi(x) \tag{2.3}$$

In the barrier regions, I and III ,

$$V(x)=\infty$$

$$\psi_I(x)=\psi_{II}(x)=0$$

Inside the well, region II, V(x)=0 and the Schrödinger equation becomes

$$(\nabla^2+k^2)\psi(x)=0, \tag{2.4}$$

where $k^2=\frac{2mE}{\hbar^2}$. The general solution is

$$\psi(x)=Acos(kx)+Bsin(kx). \tag{2.5}$$

Applying the boundary conditions, $\psi_I(0)=\psi_{II}(0)$ at $x=0$ and $\psi_I(L)=\psi_{II}(L)$ at $x=L$.

Then, the particular solution becomes

$$\psi_{n(x)}=\sqrt{\frac{2}{L}}\sin(\frac{n\pi x}{L}) \tag{2.6}$$

and

$$E_n=\frac{n^2\pi^2\hbar^2}{2mL^2}, \tag{2.7}$$

where $n=1,2,3,...m$ is index of the discretized energy levels and states.

For confinement along all three directions (ideal quantum dot),

$$\psi_{n(x,y,z)}=\sqrt{\frac{8}{L_xL_yL_z}}\sin(\frac{n_x\pi x}{L_x})\sin(\frac{n_y\pi y}{L_y})\sin(\frac{n_z\pi z}{L_z}) \tag{2.8}$$

$$E_{n_xn_yn_z}=\frac{n_x^2\pi^2\hbar^2}{2mL_x^2}+\frac{n_y^2\pi^2\hbar^2}{2mL_y^2}+\frac{n_z^2\pi^2\hbar^2}{2mL_z^2} \tag{2.9}$$

where $n_x,n_y,n_z=1,2,3,...$

The energy and state of the levels (Equations (2.8) and (2.9) are quantized since the quantum numbers, n_i are quantized. The lowest energy, E_{111} corresponds to the first s-orbital energy of an atom. The first excited states ($E_{211}, E_{121}, E_{112}$), which are degenerate (the different energy levels are described by the same state function) correspond to the 3 degenerate p-orbital energies in an atom. These show that the quantum dot behaves like an atom. In addition, the energy levels increase as the size of the quantum dot decreases.

The density of state of quantum dot states is a spike function expressed as:

$$DOS(E) = 2\delta(E - E_c). \tag{2.10}$$

Equation (2.10) and figure (2.2) show that the states of quantum dot exist only at discrete energies in contrast to the bulk system, which has a continuous energy state (Kuno, 2005, Delerue and Lannoo, 2013).

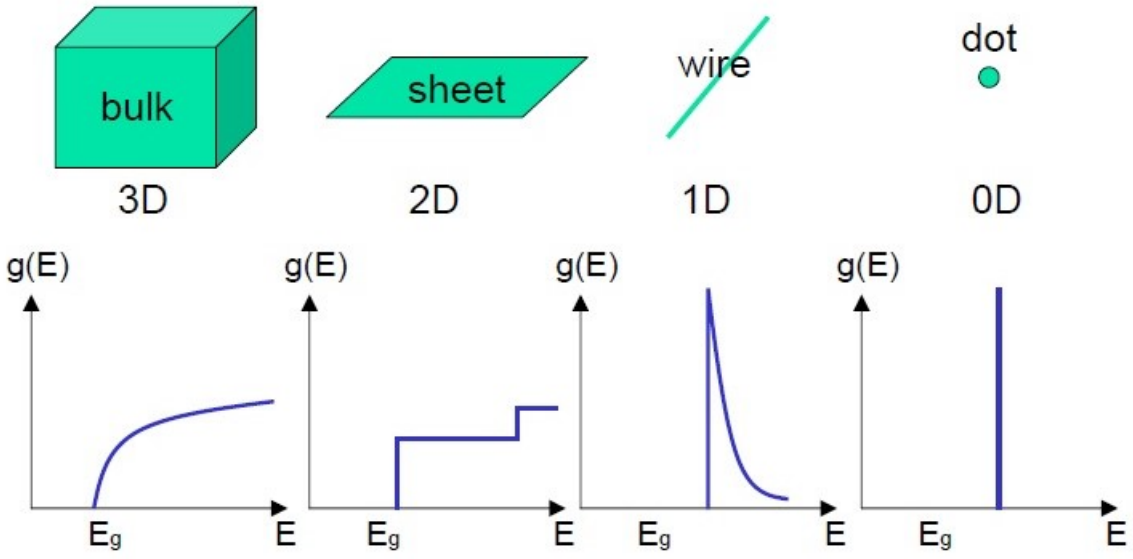

Figure 2.2: Electronic density of states of systems with 3, 2 , 1, and 0 degrees of freedom. These systems with 3, 2 , 1, and 0 degrees of freedom are referred to as bulk (3D), quantum well or sheet (2D), quantum wire (1D) and quantum dot, respectively (Kuno, 2005)

.

2.2 Theoretical spectroscopy

Spectroscopy is an essential tool for the study of electronic and optical properties of materials. It is a powerful tool that gives one access to the microscopic nature of the materials (Varsano, 2006, Delerue and Lannoo, 2013), from which information about the microscopic states, structures, bonds, conformation, chemical properties of the materials can be obtained. Within the spectroscopic measurements, a probe (e.g electron, electromagnetic, neutron) is impinged on a material. The response of the material to this probe is measured and plotted as a function of the probe frequency or wavelength. This plot is referred to as a spectrum. In particular, in absorption spectroscopy, the probe is an electromagnetic radiation and the system responds to the probe by moving from a lower energy state to a higher energy state.

Electromagnetic radiation is a wave composed of an electric and a magnetic field component whose directions are perpendicular to each other and mutually perpendicular to the direction of the propagation of the wave. If the electric field is along, the x-axis, E_x and the magnetic field is along the y-axis, H_y then,

$$E_x = E_0 \sin(\omega t - kz) \tag{2.1}$$

$$H_y = H_0 \sin(\omega t - kz) \tag{2.2}$$

$$\omega = 2\pi\nu$$

$$k = \frac{2\pi}{\lambda}$$

, where E_0 and H_0 are the electric field and magnetic amplitude respectively. λ and ν are the wavelength and frequency of the wave. The relationship between the energy, E, λ and ν is expressed given by

$$E = h\nu = \frac{hc}{\lambda}, \tag{2.3}$$

where h and c are the Planck constant and the speed of light, respectively. The radiations range from short wavelength gamma to the long wavelength, radio wave. However, for transition in a material, the most useful parts of the spectrum are the x-ray, ultraviolet, visible, infrared and microwave. When a material absorbs electromagnetic waves, three

important transitions are possible namely, electronic excitation or transition, vibrational transition and rotational transition (Marques et al., 2012).

The interest in this study is the electronic transitions or excitations. Electronic transitions are observed when a material absorbs electromagnetic radiation in the ultraviolet-visible region of the spectrum. This transition occurs when the energy difference of the states involved in the transition matches an energy ultraviolet-visible electromagnetic radiation range, defined by equation (2.3).

2.2.1 Time Dependent Perturbation Theory: Transition Probability and Absorption Coefficient

When system is given a small perturbation, the total Hamiltonian of the system can be expressed as

$$H = H_0 + W(t), \tag{2.4}$$

where H_0 is the Hamiltonian of the unperturbed system and $W(t)$ is the small time-dependent perturbation. The full time-dependent Schrödinger equation becomes

$$i\hbar\frac{\partial\Psi(r,t)}{\partial t} = H\Psi(r,t) = [H_0 + W(t)]\Psi(r,t). \tag{2.5}$$

The solution to equation (2.5) is written as

$$\Psi(r,t) = \sum_n C_n(t)\Phi_n^{(0)}(r,t), \tag{2.6}$$

where C_n is the linear combination constant. The $\Phi_n^{(0)}(r,t)$ is the solution to the time-dependent Schrödinger equation for the Zeroth- order Hamiltonian (unperturbed Hamiltonian), which is expressed as

$$\Phi_n^{(0)}(r,t) = \exp(\frac{-iE_n^{(0)}t}{\hbar})\phi_n^{(0)}(r,t). \tag{2.7}$$

Substituting 2.6 into 2.5 gives

$$i\hbar\sum_n \frac{\partial C_n(t)\Phi_n^{(0)}(r,t)}{\partial t} = \sum_n C_n(t)H_0\Phi_n^{(0)}(r,t) + \sum_n C_n(t)W(t)\Phi_n^{(0)}(r,t). \tag{2.8}$$

But, $H_0(r,t)\Phi_n^{(0)}(r,t) = E_n^{(0)}\Phi_n^{(0)}(r,t)$. Hence, equation (2.8) becomes

$$i\hbar\sum_n \frac{\partial C_n(t)\Phi_n^{(0)}(r,t)}{\partial t} = \sum_n C_n(t)E_n^{(0)}\Phi_n^{(0)}(r,t) + \sum_n C_n(t)W(t)\Phi_n^{(0)}(r,t). \tag{2.9}$$

Multiplying equation (2.9) through with $\Phi_m^{(0)}*$, integrating with respect to r and orthonormalising of $\phi_n^{(0)}$ gives

$$i\hbar\frac{\partial C_n(t)}{\partial t} = \sum_n C_n(t)\exp\{i\frac{E_m^{(0)} - E_n^{(0)}}{\hbar}\}W_{mn}(t), \tag{2.10}$$

where $W_{mn}(t) = \langle\Phi_m^{(0)}|W(t)|\Phi_n^{(0)}\rangle$.
For $|C_m| \ll |C_n|$, $|C_m| \approx 1$. Hence, equation (2.10) becomes

$$i\hbar\frac{\partial C_n(t)}{\partial t} = \exp(i\omega_{mn}t)W_{mn}(t), \tag{2.11}$$

where $\omega_{mn} = \frac{E_m^{(0)} - E_n^{(0)}}{\hbar}$. Re-arranging equation (2.11) gives

$$C_m(t) = \frac{1}{i\hbar}\int_{t_0}^{t} d\tau\ \exp(i\omega_{mn}\tau)W_{mn}(t). \tag{2.12}$$

$|C_m(t)|^2$ is the probability that the system at time, t moves from an initial state ϕ_n to final state ϕ_m. If a system is perturbed by weak electromagnetic radiation, the electric field component is responsible for the interaction and is expressed as

$$\vec{E} = E_0\hat{z}\cos(\omega t + kx), \tag{2.13}$$

where $\omega = 2\pi f$ and $k = \frac{2\pi}{\lambda}$. The field is assumed to be polarized along the z-axis and the E-M propagated along x-axis. The potential of the electromagnetic field is expressed as

$$V = -\sum_i Q_i z_i E_z = -\sum_i z_i Q_i E_0\cos(\omega t + kx_i). \tag{2.14}$$

Assuming $kx_i = 0$, then,

$$V(z,t) = W(z,t) = -E_0\sum_i z_i Q_i\cos(\omega t). \tag{2.15}$$

The transition probability due to weak interaction of electromagnetic wave with a system is

$$C_m(t) = -\frac{1}{i\hbar}E_0\langle\ \phi_m|\sum_i z_i Q_i|\phi_n\rangle \int_{t_0}^{t} d\tau\ \exp(i\omega_{mn}\tau)\cos(\omega\tau). \tag{2.16}$$

If electronic transition dipole is defined as

$$d_{mn} = \langle\ \phi_m|\sum_i z_i Q_i|\phi_n\rangle, \tag{2.17}$$

Then, equation (2.16) can be expressed as (Atkins and Friedman, 2011)

$$C_m(t) = -\frac{1}{i\hbar}E_0 d_{mn}\int_{t_0}^{t} d\tau\ \exp(i\omega_{mn}\tau)\cos(\omega\tau) \tag{2.18}$$

$|C_m(t)|^2$ can be reduced to (Atkins and Friedman, 2011);

$$|C_m(t)|^2 = \frac{2t\pi E_0}{\hbar^2}|d_{mn}|^2\delta(\omega_{nm}-\omega) \tag{2.19}$$

Transition probability rate:

$$P_{n\to m} = \frac{2\pi E_0^2}{\hbar^2}|d_{mn}|^2\delta(\omega_{nm}-\omega) \tag{2.20}$$

Equation (2.20) is the well known Golden rule formula (Griffiths, 1995, Schiff, 1995). Radiation field energy loss per unit time due to the absorption of a single photon is expressed as

$$-\frac{\partial E}{\partial t} = \sum_{nm}\hbar P_{n\to m} \tag{2.21}$$

and

$$E = \frac{\varepsilon_0\vec{E}_0}{2}$$

The optical absorption coefficient is proportional to (Struve, 1989)

$$\varepsilon(\omega) = -\frac{\frac{\partial E}{\partial t}}{\omega\vec{E}} = \frac{4\pi^2}{\hbar c}\omega(1-e^{-\beta\hbar\omega})\sum_{nm}P_n|d_{nm}|^2\delta(\omega_{nm}-\omega) \tag{2.22}$$

Integrated absorption coefficient, A is expressed in terms of molar extinction coefficient, $\varepsilon(\nu)$ as (Atkins and Friedman, 2011)

$$A = \int_{\nu_n}^{\nu_m} \varepsilon(\nu) d\nu. \tag{2.23}$$

where ν, ν_n and ν_m are the frequencies of the photon, state n and state m, respectively. The dimensionless oscillator strength, f_{nm}, which is used to quantify the intensity of absorption is express as (Struve, 1989, Atkins and Friedman, 2011):

$$f_{nm} = \frac{4\pi m_e \nu_{nm}}{3\hbar e^2} |d_{nm}|^2, \tag{2.24}$$

The relation between f_{nm} and A can be obtained as (Atkins and Friedman, 2011)

$$f_{nm} = \frac{4\varepsilon_0 m_e c}{N_A e^2} \int_{\nu_n}^{\nu_m} \varepsilon(\nu) d\nu \tag{2.25}$$

In practice (Atkins and Friedman, 2011),

$$f_{nm} = 6.26 \times 10^{-19} \int_{\nu_n}^{\nu_m} \varepsilon(\nu) d\nu = 6.26 \times 10^{-19} A \tag{2.26}$$

A transition is forbidden if oscillator strength, f_{nm} is zero and allowed otherwise.

2.2.2 Polarizability and absorption coefficient

In the response theory, when a weak time-dependent electric field V_{ext} interacts with a system of electrons, the relationship between the change in electron density, $\delta n(r', \omega)$ (dynamic polarizability), dynamic susceptibility, $\chi(r, r', \omega)$ and the $V_{ext}(r, \omega)$ is given by

$$\delta n(r', \omega) = \int dr \chi(r, r', \omega) V_{ext}(r, \omega). \tag{2.27}$$

It can be shown that the polarizability, P, the complex function of the susceptibility, χ and complex function of the dielectric constant, ε are related by

$$P = 1 + \chi + i\chi' = \varepsilon_1 + i\varepsilon_2. \tag{2.28}$$

Equating the imaginary parts of equation (2.28), one obtains

$$\chi' = \varepsilon_2. \tag{2.29}$$

The absorption coefficient is written given by

$$\alpha(\omega) = \frac{\omega\varepsilon_2}{n_1 c}, \tag{2.30}$$

where n_1 is the real part of the complex refractive index, ω is the circular frequency, and the c is the speed of light. The quantity ε_2 is defined as

$$\varepsilon_2(\omega) \propto \sum_{i,j} \langle \psi_j | \mathbf{e} \cdot \mathbf{P} | \psi_i \rangle \delta(E_j - E_i - \hbar\omega), \tag{2.31}$$

where ω is the frequency of the electromagnetic and $\mathbf{e}$ is polarization. The ψ_i, ψ_j, E_i and E_j are state of the occupied orbital, state of the unoccupied orbital, energy of the occupied orbital and energy of the unoccupied orbital (Marques et al., 2012).

2.3 Theoretical approaches for excitation energies of atomic clusters

Excitation energies and their corresponding states are important tools in absorption spectrum calculation (Gatti, 2007). From the earlier discussion on absorption spectroscopy, it is evident that, the accuracy of the absorption spectrum of an electronic system depends on the accurate determination of its orbital energies and their corresponding states. These quantities can be obtained by solving exactly the many-body Schrödinger equation, which is expressed as (Martin, 2020)

$$H\Psi(r,R) = E\Psi(r,R), \tag{2.1}$$

where the many-body Hamiltonian, H is defined as

$$H = -\frac{1}{2}\sum_i \nabla^2 - \frac{1}{2}\sum_I \nabla^2 - \sum_I \sum_i \frac{1}{|r_i - R_I|} + \sum_i \sum_j \frac{1}{|r_i - r_j|} + \sum_I \sum_J \frac{1}{|R_I - R_J|}. \tag{2.2}$$

The first term on the R.H.S of equation (2.2) is the total kinetic energy of the electrons. The second term is the total kinetic energy of the nuclei, third term defines the nuclear-electron interactions, fourth term is the electron-electron interactions and the fifth is the nucleus-nucleus repulsion interactions. $\Psi(r,R)$ is the many body wave function or the eigenfunction and E the eigenvalue (total energy). r and R are the position vectors of the electron and the nucleus, respectively. The solution to the many-body equation (equation (2.1)) for a system of atoms is intractable and this led to the introduction of the Born Oppenheimer approximation (Born and Oppenheimer, 1927). In the Born approximation, it is assumed that the nuclei are stationary with reference to the motion of electrons and thus, kinetic energy of the nuclei are neglected and the nuclei-nuclei repulsions are treated as constants. With these approximations, the Hamiltonian in equation (2.2) reduces to (Martin, 2020)

$$H_e = -\frac{1}{2}\sum_i \nabla^2 - \sum_I \sum_i \frac{1}{|r_i - R_I|} + \sum_i \sum_j \frac{1}{|r_i - r_j|}, \tag{2.3}$$

where H_e is the electronic Hamiltonian. Thus, the electronic eigenvalue problem is

$$H_e \Psi(r,R) = E_e \Psi(r,R). \tag{2.4}$$

Also, the total energy, E for a particular nuclei configuration, is written as

$$E = E_e + \sum_I \sum_J \frac{1}{|R_I - R_J|}, \tag{2.5}$$

where E_e is the electronic eigenvalues (orbital energies). Unfortunately, obtaining the solution to the electronic eigenvalue problem (equation (2.4)) is still a difficult task because of the electron-electron interaction term in the electronic Hamiltonian and the many-body wave-function. Hence, further approximations were introduced, which led to the development of different approximate methods. The key and fundamental among these approximate methods are the wave function methods and Density Functional methods.

2.3.1 Wave function methods: Hartree Fock and Post Hatree Fock methods

The Hartree Fock (HF) is a single particle approximation method, which assumes each electron in a system is moving in the mean-field of the other electrons in the system. The HF wave-function for N electrons is expressed as a Slater determinant in order to ensure that the antisymmetric principle for fermions(e.g electrons) is obeyed. The HF wave-function, Ψ is then expressed as

$$\Psi = \frac{1}{\sqrt{N!}} \begin{vmatrix} \chi_1(x_1) & \chi_1(x_2) & \chi_1(x_3) & ... & \chi_1(x_N) \\ \chi_2(x_1) & \chi_2(x_2) & \chi_2(x_3) & ... & \chi_2(x_N) \\ \chi_3(x_1) & \chi_3(x_2) & \chi_3(x_3) & ... & \chi_3(x_N) \\ \chi_4(x_1) & \chi_4(x_2) & \chi_4(x_3) & ... & \chi_4(x_N) \\ . & & & & \\ . & & & & \\ . & & & & \\ \chi_N(x_1) & \chi_N(x_2) & \chi_N(x_3) & ... & \chi_N(x_N) \end{vmatrix} \tag{2.6}$$

Compactly, Ψ can be written as

$$\Psi = |\chi_1(x_1)\chi_2(x_2)\chi_3(x_3)...\chi_N(x_N)\rangle, \tag{2.7}$$

where $\chi(x)$ are spin orbitals and x represent both the electron space and spin coordinates. The spin orbitals also called the molecular orbitals are expressed as a linear combination of atomic orbitals, given by

$$\chi_i(x_i) = \sum_m C_{i,m}\phi_m(x_i), \tag{2.8}$$

where ϕ_m is the atomic orbitals and C_{im} are the molecular orbital coefficient. If the wave-function is normalized, the expectation value of the energy (Hartree Fock energy) is

$$E = \langle\Psi|H|\Psi\rangle = \sum_i H_{ii} + \frac{1}{2}\sum_{ij}(J_{ij} - K_{ij}) \tag{2.9}$$

where H_{ii} is defined by

$$H_{ii} = \langle\chi(1)| - \frac{1}{2}\nabla^2 - \sum_R \frac{1}{|r_i - R|}|\chi(1)\rangle, \tag{2.10}$$

J_{ij} is the coulomb interaction between two electrons with spin orbitals χ_i and χ_j is expressed as

$$J_{ij} = \langle \chi_i(1)\chi_j(2)| \frac{1}{|r_1 - r_2|} |\chi_i(1)\chi_j(2)\rangle \tag{2.11}$$

and K_{ij}, the exchange interaction is expressed as

$$K_{ij} = \langle \chi_i(1)\chi_j(2)| \frac{1}{|r_1 - r_2|} |\chi_i(2)\chi_j(1)\rangle. \tag{2.12}$$

The variational principle is applied to equation 2.3.1 in order to obtain the best wave function that minimizes the HF Energy, E. The minimization of energy, E with respect to spin orbital give rise to an eigenvalue equation known as the Hartree Fock equation. The equation is expressed as (Magnasco, 2009, Szabo and Ostlund, 2012)

$$F(i)\chi_i(1) = \varepsilon_i \chi_i(1), \tag{2.13}$$

where $F(i)$, the one-particle operator called the Fock operator, is defined by

$$F(i) = -\frac{1}{2}\nabla_i^2 - \sum_R \frac{1}{|r_i - R|} + \sum_{i \neq j} \langle \chi_j(2)| \frac{1}{|r_1 - r_2|} |\chi_i(2)\rangle - \sum_{i \neq j} \langle \chi_j(2)| \frac{1}{|r_1 - r_2|} |\chi_i(2)\rangle, \tag{2.14}$$

ε_i and $\chi_i(1)$ are the orbital energies and orbitals, respectively. Hartree Fock equation is a self-consistent field theory (SCF) since it is non-linear and needed to be solved iteratively. It solution gives rise to orbitals and their corresponding energies.

The energy obtained from Hartree Fock equation is an upper bound of the exact energy because of some missing correlation (an effect whereby electrons try to avoid each) in the wave function (the single Slater determinant) used. In the Hartree Fock formalism, the parallel spin electrons are well correlated while anti-parallel spin electrons are uncorrelated. The correlation energy is define as

$$E_{corr} = E_{\text{exact}} - E_{HF}, \tag{2.15}$$

where E_{exact} and E_{HF} are the exact and Hartree Fock energies, respectively. The correlation energy is always negative since HF energy is greater than the Exact energy. Although, Hartree Fock has been applied successfully for some ground-state calculations including modelling and calculation of equilibrium structures, bonds, dissociation

energies etc, However, due to the non-inclusion of some correlations, HF overestimates electronic gaps and excitation energies (the difference between the energy of the occupied and unoccupied orbital) (Anisimov, 2010, Szabo and Ostlund, 2012).

A variety of post-Hartree Fock methods like configuration interaction (CI), multi-configuration self-consistent field, couple cluster sets, etc have been developed to improve the accuracy of Hartree Fock total energy, orbitals, orbital energies and excitation energies. These methods seek to recover some correlation energies that are not included in the Hartree Fock method.

2.3.1.1 Configuration Interaction and Configuration Interaction Singles

In the configuration interaction approach, the many-body wave function is expressed as follows:

$$\Psi = l_0\Psi_0 + \sum_{i,a} l_i^a \Psi_i^a + \sum_{i<j,a<b} l_{ij}^{ab}\Psi_{ij}^{ab} + \sum_{i<j<k,a<b<c} l_{ijk}^{abc}\Psi_{ijk}^{abc} + ... \tag{2.16}$$

where Ψ_0 is obtained from a solution to the Hartree Fock equation. Ψ_i^a, Ψ_{ij}^{ab}, Ψ_{ijk}^{abc} etc are slater determinants of different configuration obtained from Ψ_0 by replacing one or more of its occupied spin-orbital by the unoccupied. $l's$ are the slater determinant coefficients, which are determined from the variational principle. The Full configuration interaction is an accurate method for electronic excitations. However, it is computationally expensive and restricted to a small system of atoms. In practice, the full CI is truncated to obtain different approximate methods namely configuration interaction singles (only single excitation determinants are included in the basis sets +HF slater determinant), configuration interaction doubles (only double excitations wave functions are included in the basis sets + HF slater determinant), configuration interaction singles and doubles (both single and double excitations wave functions are included + HF slater determinant), etc (Sherrill and Schaefer III, 1999, Szabo and Ostlund, 2012).

In the configuration interaction singles (CIS), only the ground state (HF slater determinant) and the single substitution configurations slater determinants are utilized in the

basis sets. The CIS wave function is expressed as (Szabo and Ostlund, 2012)

$$\Psi_{CIS} = l_0\Psi_0 + \sum_{i,a} l_i^a \Psi_i^a \tag{2.17}$$

and the CIS eigenvalue problem is

$$H\Psi_{CIS} = E_{CIS}\Psi_{CIS}. \tag{2.18}$$

The ground and excited state energies obtained at the CIS level are upper bounds to the exact energies since Ψ_{CIS} is obtained using a variational approach. According to the Brillouin theorem, $\langle\Psi_0|H|\Psi_i^a\rangle = 0$. That is, there are no interactions between single excitations and the ground state Hartree Fock. So, the CIS ground state energy is not different from that of Hartree Fock and so, it is size-extensive (that is, the energy of the many-body system is proportional to the number of particles in the system) because Hartree Fock is also size-extensive. But there is also $\langle\Psi_i^a|H|\Psi_i^a\rangle \neq 0$. The CIS method is computationally less expensive as compare to other truncated CI methods and could handle moderately large atomic systems. Unfortunately, It overestimates excitation energies by an error that ranges from 0.5 eV to 2.0 eV when compared to experiment. It also gives only qualitative transition dipole moment. Thus, calculations performed with this method including INDO/CIS, produce qualitative spectra intensities when compare with experiments or high-level methods like EOM-CCSD (Dreuw and Head-Gordon, 2005).

Generally, the truncated CI methods except methods with doubly-excitation configurations, do not treat electron correlation properly. Even though CISD recovers some correlation, it still overestimates excitations. Also, the truncated CI methods except for CIS, are not size-extensive and are also computationally intensive as the system grows bigger. For instance, the configuration interaction singles doubles (CISD) scales N^6 computationally (Sherrill and Schaefer III, 1999).

The multi-configuration self-consistent field (MCSCF) is another post-Hartree Fock method which is based on truncated CI. The wave function, in this case, is expressed as in equation (2.16), but both the coefficient l_k and the atomic orbital coefficients are optimised to minimize the total energy. Examples of MCSCF are the complete active space self-consistent field (CASSCF), CASPT2, etc. The MCSCF is cumbersome and computa-

tionally expensive. Optimization of the active and virtual orbitals is tedious and not straightforward. Hence, this method is restricted to small atomic clusters (Szalay et al., 2011).

2.3.1.2 Couple Cluster (CC) and EOM-CCSD Method

A good alternative to the approximate full CI is couple cluster (CC) method. It describes the full CI (the 'exact' method) wave function as

$$\Psi_{cc} = exp(T)\Psi_0, \tag{2.19}$$

where Ψ_0 is the reference wavefuntion and T is the cluster operator. T is defined by

$$T = \sum_{n=1} T_n, \tag{2.20}$$

where T_n (n is the number of electrons) is the nth excitation operator. The T_1 (single excitation operator) is written as

$$T_1\Psi_0 = \sum_{a,i} t_a^i \Psi_a^i \tag{2.21}$$

and the T_1 (double excitation operator) as

$$T_2\Psi_0 = \sum_{a>b,i>j} t_{ab}^{ij} \Psi_{ab}^{ij}, \tag{2.22}$$

where t_a^i and t_{ab}^{ij} are linear combination coefficients. Truncating T in Eq. (2.20), the following approximate coupled cluster methods could be obtained:

1. Couple cluster single (CCS) (T=T_1)

$$\Psi_{cc} = (1 + T_1 + \frac{T_1^2}{2!} + \frac{T_1^3}{3!} + ...)\Psi_0$$

2. Couple cluster doubles (CCD) (T=T_2)

$$\Psi_{cc} = (1 + T_2 + \frac{T_2^2}{2!} + \frac{T_2^3}{3!} + ...)\Psi_0$$

3. Couple cluster singles and doubles (CCSD) ($T = T_1 + T_2$)

$$\Psi_{cc} = (1 + T_1 + \frac{T_1^2}{2!} + \frac{T_1^3}{3!} + ...)(1 + T_2 + \frac{T_2^2}{2!} + \frac{T_2^3}{3!} + ...)\Psi_0$$

4. Couple cluster singles doubles and triples (CCSDT) ($T = T_1 + T_2 + T_3$)

$$\Psi_{cc} = (1 + T_1 + \frac{T_1^2}{2!} + \frac{T_1^3}{3!} + ...)(1 + T_2 + \frac{T_2^2}{2!} + \frac{T_2^3}{3!} + ...)(1 + T_3 + \frac{T_3^2}{2!} + \frac{T_3^3}{3!} + ...)\Psi_0$$

Total energy is obtained by evaluating (Bartlett, 2012)

$$E_{cc} = \langle \Psi_0 | H | e^T \Psi_0 \rangle. \tag{2.23}$$

Generally, CC methods are size extensive (energy scales linearly with size of system) and accurate (Dutta et al., 2018, Bartlett, 2012). The CCSDT is a very accurate method, which is referred to as 'gold standard' in computational chemistry (Rezac and Hobza, 2013). Unfortunately, CC methods including CCSDT are computational intensive and limited to small-sized systems. For instance, CCSD scales as N^6, CCSD(T) as N^7 and CCSDT as N^8 (Christiansen et al., 1995, Ochsenfeld et al., 2007, Evarestov, 2007).

A variant of the CC method employed for the excitation state calculations is the equation-of-motion coupled-cluster singles and doubles (EOM-CCSD) method. In EOM-CC, the excited state wave function Ψ_{ex} is created from the couple cluster wave function Ψ_{cc} by using the excitation operator, B_k. Thus,

$$\Psi_{ex} = B_k \Psi_{cc} = B_k e^T \Psi_0 \tag{2.24}$$

B_k is the sum of singles B_0, doubles B_1, triples B_2 etc excitation operator terms.

$$B_k = B_0 + B_1 + B_2 + ... \tag{2.25}$$

$$B_0 = b_0 \tag{2.26}$$

$$B_1 = \sum_{a,i} b_a^i S_a^i \tag{2.27}$$

$$B_2 = \frac{1}{4} \sum_{a>b,i>j} b_{ab}^{ij} S_{ab}^{ij} \ldots \tag{2.28}$$

The Schrödinger equation for the excited state is written as

$$H B_k e^T \Psi_0 = E_{exc} B_k e^T \Psi_0. \tag{2.29}$$

It can be shown that

$$[\bar{H}, B_k] \Psi_0 = \triangle E_{exc} \Psi_0, \tag{2.30}$$

where $\bar{H} = e^{-T} H e^T$ and ΔE_{exc} is the excitation energy (Stanton and Bartlett, 1993, Watts, 2008).

EOM-CCSD excitation energies are known to be comparable with experiments. It is a benchmark method for both *ab-initio* and semi-empirical methods. However, it is computationally intensive and prohibitive for large atomic clusters . It scales equivalently to CCSD and requires large computation memory for its computations. (Caricato et al., 2011, Bennie et al., 2017).

2.3.2 Density Functional Theory

The density functional theory (DFT) is an electronic structure method that utilizes the electron density as its major variable. While the wave function of an N-electron system, ignoring the spin variable, has 3N dimensions, its electronic density n($\vec{(r)}$) has 3-dimensions. For a particular electronic system, more integrals are evaluated within the wave function theory than with the density functional theory. Thus, DFT is much less computationally intensive than the wave function theory methods.

In 1964, Hohenberg and Kohn (Hohenberg and Kohn, 1964) proposed the basic theorem of the DFT method, although the idea was earlier conceived by Thomas and Fermi. The theorems are as follows (Burke et al., 2007):

1. The external potential of a system of interacting electrons is determined uniquely by the electron density which in turn, determines the Hamiltonian, the wave function and other observables of the system.

2. The lowest energy can be obtained by optimising the electron density using the

variational principle.

3. The functional F[n]= exact kinetic energy functional(T[n]) + exact electron-electron interaction(V_{ee}[n]) is the same for all-electronic systems. That is, F[n] is a universal functional.

The ground-state energy is given by

$$E = min_n(F[n] + V_{ext}) \tag{2.31}$$

$$F[n] = min_{\Psi \to n}\langle \Psi | T + V_{ee} | \Psi \rangle, \tag{2.32}$$

where Ψ is the ground-state wave function that minimizes F[n]. Kohn and Sham proposed an elegant approximation for the functional, F[n] (Kohn and Sham, 1965). They assumed the electronic system subjected to the Kohn-Sham potential (V_{ks}) to be non-interacting but has the same density as the real system (interacting system). This approximation results to the single-particle Schrödinger equation (Burke et al., 2007, Koch and Holthausen, 2015),

$$(-\frac{1}{2}\nabla^2 + V_{ks}[n(r)])\phi_i(r) = \varepsilon_i \phi_i(r), \tag{2.33}$$

where $n(r) = \sum_i |\phi_i(r)|^2$ and $V_{ks} = V_{ext} + V_H + Vxc$. The $\phi_i(r)$ is the Kohn-Sham orbital. The external potential, V_{ext} is defined by

$$V_{ext} = \int dr \frac{Z}{|r - R|}. \tag{2.34}$$

The V_H is the Hartree or coulomb potential expressed as

$$V_H = \int dr' \frac{n(r')}{|r - r'|}. \tag{2.35}$$

The V_{xc} is the exchange correlation, which is composed of the correction to the kinetic energy and the non-classical electron-electron interaction. It is expressed as

$$V_{xc} = \frac{\delta E_{xc}}{\delta n(r)}, \tag{2.36}$$

where E_{xc} is the exchange-correlation energy. The Kohn-Sham equation will give exact

ground-state energies provided the exchange-correlation potential for which analytical solution is not available, is well defined. In other words, the accuracy of the Kohn-Sham equation depends on the exchange-correlation functional since every other term in the equations are defined exactly. Different approximate methods have been developed to calculate exchange-correlation functionals. Prominent among these methods are the local density approximation (LDA) (Miehlich et al., 1989) and generalized-gradient approximation (GGA) (Perdew et al., 1996). In the LDA approximation, the system is assumed to be a homogeneous uniform electron gas and the exchange-correlation energy expressed by (Burke et al., 2007)

$$E_{xc}^{LDA}[n] = \int dr\, n(r)\varepsilon_{xc}(n(r)), \tag{2.37}$$

where ε_{xc} is the called the energy density, which is the sum of the individual exchange and correlation contribution. It can be calculated exactly using the Quantum Monte Carlo method. Although LDA works well for homogeneous systems and systems with slow varying densities, it fails for inhomogeneous systems (Burke et al., 2007). The GGA functional was developed in order to extend the exchange-correlation functional to inhomogeneous systems. In GGA formalism, the ε_{xc} varies with density. The gradient of density parameters could be obtained by fit to experiments.

$$E_{xc}^{GGA}[n] = \int dr\, n(r)\varepsilon_{xc}(n(r), \nabla(n(r))). \tag{2.38}$$

Generally, DFT has been applied successfully for ground-state calculations. However, they are known to poorly predict the optical properties of a system. They underestimate excitation energies and electronic gaps. The time-dependent density functional theory (TDDFT), a post-DFT method, has been developed and employed for excitation energies and spectra calculations.

2.3.2.1 Time-Dependent Density Functional Theory (TDDFT)

TDDFT is an extension of DFT. Runge and Gross generalized Kohn and Hohenberg theorems to time-dependent DFT (Runge and Gross, 1984). The theorem states that

there is a one-one correspondence between the time-dependent density $n(r,t)$ and the time-dependent external potential $V(r,t)$. That is, $V(r,t)$ is uniquely defined by $n(r,t)$. Thus, time-dependent Hamiltonian and other time-dependent observables are defined by $n(r,t)$. The expectation values of observables are unique functionals of $n(r,t)$ and the initial state (the ground state). This leads to generalizing the Kohn-Sham non-interacting ground state equation to a time-dependent Kohn-Sham equation (Marques et al., 2006, Burke et al., 2007):

$$\left[-\frac{1}{2}\nabla^2 + V_{ks}[n(r,t)]\right]\phi_i(r,t) = i\frac{\partial}{\partial t}\phi_i(r,t). \tag{2.39}$$

$n(r,t)$ is the time-dependent density expressed as

$$n(r,t) = \sum_{i=1}^{N} |\phi_i(r,t)|^2 \tag{2.40}$$

where $\phi_i(r,t)$ is the time-dependent orbital. The $V_{ks}(r,t)$ is the time-dependent Kohn-Sham effective potential expressed as

$$V_{ks}(r,t) = V_{ext}(r,t) + V_H(r,t) + V_{xc}(r,t), \tag{2.41}$$

$V_{ext}(r,t)$, $V_H(r,t)$, and $V_{xc}(r,t)$ are the time-dependent external potential, time-dependent Coulomb potential and time-dependent exchange-correlation, respectively. The time-dependent exchange-correlation is defined by

$$V_{xc} = \frac{\partial A}{\partial n(r,\tau)}|_{n(r,t)}, \tag{2.42}$$

where A is the action, which is analogous to total energy. τ is the Keldish pseudo time. Just as in the case of V_{xc} for ground-state, the $V_{xc}(x,t)$ has no exact form. The simplest approximate form of $V_{xc}(x,t)$ is the adiabatic local density approximation (ALDA) written as

$$V_{xc}^{ALDA}(r,t) = V_{xc}^{LDA}(n(r,t)). \tag{2.43}$$

The TDDFT within the ALDA does well for slowly varying densities and gives good predicts for low-lying excited states.

Excitation energies could be extracted from TDDFT through linear response calculations

(Marques et al., 2012, Maitra, 2016). When a system is perturbed by a weak electric field, $V_{ext}(r,\omega)$, the change in density of the system, $\delta n(r,\omega)$ can be expressed as:

$$\delta n(r,t) = \int dt' \int dr' \chi[n](r,r',t-t')\delta V_{ext}(r,t') \tag{2.44}$$

Where χ is the density-density response function that measures the change in density of the system due to the external potential from the weak electric field. Equivalently, the change in density can be obtained for the time-dependent Kohn-Sham effective potential:

$$\delta n(r,t) = \int dt' \int dr' \chi[n](r,r',t-t')\delta V_{ks}(r,t') \tag{2.45}$$

Equating (2.44) and (2.45) to have

$$\begin{aligned}\delta n(r,t) = \int dt' \int dr' \chi[n](r,r',t-t')\delta V_{ext}(r,t') = \\ \int dt' \int dr' \chi[n](r,r',t-t')\delta V_{ks}(r,t')\end{aligned} \tag{2.46}$$

and

$$\frac{\delta V_{ks}(r,t')}{\delta V_{ext}(r,t')} = \frac{\delta V_{ext}(r,t')}{\delta V_{ext}(r,t')} + \frac{\delta V_H(r,t')}{\delta V_{ext}(r,t')} + \frac{\delta V_{xc}(r,t')}{\delta V_{ext}(r,t')}. \tag{2.47}$$

Introducing equation (2.47) into equation (2.46), the TDDFT linear response equation called the Dyson-like equation is obtained and is given as

$$\begin{aligned}\chi(r,r',\omega) = &\chi_{ks}(r,r',\omega) + \int dr_1 \int dr_2 \chi_{ks}(r,r1,\omega)\{\frac{1}{|r_1-r_2|} + \\ &f_{xc}(r_1,r_2,\omega)\}\chi_{ks}(r_2,r',\omega),\end{aligned} \tag{2.48}$$

where the exchange-correlation kernel, f_{xc} is written as

$$f_{xc}(r_1,r_2,\omega) = \frac{\delta V_{xc}(r,\omega)}{\delta n(r,t)}$$

and the Kohn-Sham response function, $\chi_{ks}(r,r',\omega)$ as

$$\chi_{ks}(r,r',\omega) \propto \sum_i \sum_j \frac{|\phi_i|^2 \, |\phi_j|^2}{\omega - (\varepsilon_i - \varepsilon_j)}. \tag{2.49}$$

ϕ and ε are the orbital and orbital energy from the time-independent Kohn-Sham equa-

tion. The summations are over all occupied and unoccupied Kohn-Sham orbital and orbital energies. The poles of $\chi_{ks}(r,r',\omega)$ correspond to Kohn-Sham excitations while the poles of $\chi(r,r',\omega)$ correspond to the true excitation energies.

Casida provided another means of solving equation (2.48). He recasted the equation as an eigenvalue problem, which is expressed as follows (Casida, 1995, 2009, Maitra, 2016):

$$\sum_{p}[\delta_{pp'}\xi_p + 2\sqrt{\omega_p\omega'_p}\langle p|\{\frac{1}{|r_1-r_2|}+f_{xc}(r_1,r_2,\omega)\}|p\rangle]\mu_p = \xi\mu_p, \tag{2.50}$$

where $\xi = \omega^2$ and

$$\langle p|\{\frac{1}{|r_1-r_2|}+f_{xc}(r_1,r_2,\omega)\}|p\rangle = \int dr \int dr'\ \phi_i(r)^*\phi_j(r)\ \{\frac{1}{|r_1-r_2|}+ f_{xc}(r_1,r_2,\omega)\}\ \phi_i(r')^*\phi_j(r'). \tag{2.51}$$

$\omega_p = \varepsilon_i - \varepsilon_j$ is the excitation energy and μ_p is the eigenvector from which the oscillator strength is calculated. ε_i and ε_j are the Kohn-Sham unoccupied and occupied orbital energies, respectively. ϕ_i and ϕ_j are the Kohn-Sham unoccupied and occupied orbital respectively (Marques et al., 2006, Burke et al., 2007, Maitra, 2016). TDDFT is known to handle moderate-sized systems but is computationally expensive for large atomic clusters like quantum dots (Gabay et al., 2017).

2.3.3 Semi-empirical approaches

Semi-empirical methods are obtained from drastic approximation to first principle wave function theory or density functional theory. They involve omitting or replacing with parametric expressions some terms (most times integrals) in the methods that make computation intensive. Thereafter, the parameters are calibrated with experiments or high-level *ab-initio* results. If the calibration is carried out correctly with reliable data, it is possible to correct for the errors introduced into semi-empirical approaches due to the approximations. Although the semi-empirical methods could handle large atomic clusters and nano-systems with less computational cost and effort, they are often less accurate and less transferable than the high-level first principle methods. Different semi-

empirical methods have been developed. An overview of the Huckel, extended Huckel, Neglect of differential overlap (NDO), empirical pseudopotential method (EPM) and density functional tight binding (DFTB) semi-empirical methods will be given.

2.3.3.1 The Tight Binding Model

The Tight Binding Model (Harrison, 1989) involves solving the eigenvalue equation,

$$H\psi_i(r) = \varepsilon_i\psi_i. \tag{2.52}$$

The i^{th} molecular orbital, $\psi_i(r)$ is expressed as a linear combination of the valence atomic orbitals and is expressed as

$$\psi_i(r) = \sum_n \sum_\alpha C^n_{i\alpha}\phi^n_\alpha \tag{2.53}$$

where n and α are atoms and their corresponding orbitals, respectively. C is the basis set expansion coefficient. Substitute equation 2.53 into equation 2.52, multiply by orbital ϕ^*_β and integrate over all space to have

$$\sum_n \sum_\alpha C^n_{i\alpha}\langle\phi_\beta|H|\phi_\alpha\rangle = \varepsilon_i \sum_n \sum_\alpha C^n_{i\alpha}\langle\phi_\beta|\phi_\alpha\rangle \tag{2.54}$$

$$\sum_n \sum_\alpha C^n_{i\alpha}H_{\beta\alpha} = \varepsilon_i \sum_n \sum_\alpha C^n_{i\alpha}S_{\beta\alpha}, \tag{2.55}$$

where $S_{\beta\alpha}$ is the overlap matrix, which is expressed as a unit matrix since the orbitals are assumed to be orthogonal. $H_{\beta\alpha}$ is the Hamiltonian matrix whose diagonal matrix elements, $H_{\beta\beta}$ and $H_{\alpha\alpha}$ are the free atomic orbital energies. The off-diagonal elements are obtained using the two center Slater Koster approximations (Slater and Koster, 1954) while the adjustable parameters therein, are obtained from fits to experimental or *ab-initio* data. Within the Slater Koster approximations, the off-diagonal Hamiltonian matrix elements are reduced to the following for sp basis set (Harrison, 2012):

$$H_{\beta\alpha} = H_{ss\sigma}, H_{sp\sigma}, H_{pp\sigma}, H_{pp\pi}$$

. The off-diagonal Hamiltonian elements obtained by Harrison are defined by (Harrison, 2012)

$$H_{abc} = -\frac{n_{abc}}{d^2}, \tag{2.56}$$

where a, b=s or p, c=σ or π and n_{abc} is an adjustable parameter that can be obtained from a fit. The variable d is the separation between atomic orbitals. Other adjustable expressions for Hamiltonian matrix elements have been proposed (Papaconstantopoulos and Mehl, 2003, Shi and Papaconstantopoulos, 2004). After fixing the Hamiltonian and overlap matrix elements, the eigenvalue equation can be solved to obtain the orbital energies, ε_i and the orbital coefficients, C. However, calculation of absorption spectra with the tight-binding is not straightforward because wave functions are not explicitly defined.

2.3.3.2 Density Functional Tight Binding (DFTB)

DFTB is a variant of tight binding, which is obtained from a drastic approximation of DFT. Its theoretical framework is given in the following (Seifert, 2007, Koskinen and Mäkinen, 2009, Seifert and Joswig, 2012). The total energy of a system within the DFT scheme is written as

$$E[n] = \sum_{i}^{occ} \langle \psi_i | -\frac{1}{2}\nabla^2 + \int d^3r\, V_{ext} n(r) | \psi_i \rangle + \frac{1}{2}\int d^3r\, \frac{nn'}{|r-r'|} + E_{xc} + E_{nuc}. \tag{2.57}$$

If the true density that minimizes E[n] is given as $n = n_0 + \delta n$, expanding E[n] up to second order in the density fluctuation, δn:

$$\begin{aligned} E[n_0+\delta n] = &\sum_{i}^{occ} \langle \psi_i | -\frac{1}{2}\nabla^2 + V_{eff}[n_0] | \psi_i \rangle + \frac{1}{2}\int d^3r \int d^3r'\, \frac{\delta^2 E_{xc}[n_0]}{\delta n \delta n'} + \\ &\frac{1}{|r-r'|}\,\delta n \delta n' - \frac{1}{2}\int d^3r\, V_H[n_0] n_0(r) - E_{xc}[n_0] - E_{nuc} \\ &- \int d^3r\, V_{xc} E_{xc}[n_0] n_0(r) \end{aligned} \tag{2.58}$$

The band structure energy is expressed as

$$E_{bs} = \sum_{i}^{occ} \langle \psi_i | -\frac{1}{2}\nabla^2 + V_{eff}[n_0] | \psi_i \rangle = \sum_{i}^{occ} \langle \psi_i | H_0[n_0] | \psi_i \rangle, \tag{2.59}$$

where

$$V_{eff} = V_{ext} + V_{xc} + V_H. \tag{2.60}$$

The energy from charge fluctuation, $E_{coulomb}$:

$$E_{coulomb} = \frac{1}{2}\int d^3r \int d^3r' \, (\frac{\delta^2 E_{xc}[n_0]}{\delta n \delta n'} + \frac{1}{|r-r'|}) \, \delta n \delta n'. \tag{2.61}$$

The repulsive energy (E_{rep}) is written as

$$E_{rep} = -\frac{1}{2}\int d^3r \, V_H[n_0]n_0(r) - E_{xc}[n_0] - E_{nuc} - \int d^3r \, V_{xc}E_{xc}[n_0]n_0(r). \tag{2.62}$$

Hence, equation (2.58) becomes

$$E[n_0 + \delta n] = E_{bs} + E_{coulomb} + E_{rep}. \tag{2.63}$$

The following approximations are made for terms in equation (2.63):

$$E_{rep} = \sum_{Y>Z} V_{rep}^{YZ}(R), \tag{2.64}$$

where $V_{rep}^{YZ}(R)$ represents the repulsive function for each atom pair separated by distance R and can be obtained from fit to accurate theoretical data.

$$E_{coulomb} = \sum_{YZ} \gamma_{YZ} \, (R_{YZ}) \, \Delta q_a \Delta q_b \tag{2.65}$$

Minimizing $E[n_0 + \delta n]$ with the variational principle approach, one obtains an equivalent single particle Kohn-Sham equation. The wave function ψ_i is expressed in the basis of the atomic valence orbitals and given by

$$\psi_i(r) = \sum_{a=1}^{n} C_{ai}\phi_a(r). \tag{2.66}$$

Just as observed in the DFT, the DFTB underestimates electronic gap (Marutaphan and Wongchoosuk, 2017). Also, it is not straightforward to calculate absorption spectra within the DFTB formalism because its wavefunction is not explicitly defined.

2.3.3.3 Empirical pseudopotential based model

Zunger and Co-worker developed a model based empirical pseudopotential method(EPM) for nanostructure calculations. The method is described as follows (Harrison and Valavanis, 2016, Wang and Zunger, 1994): Solution to the eigenvalue problem, equation (2.67) is sought for.

$$H\psi_{n,k}(r) = \varepsilon_n \psi_{n,k}(r). \tag{2.67}$$

The wave function, $\psi_{n,k}(r)$ is expanded in plane wave basis sets.

$$\psi_{n,k}(r) = \sum_G C_G \exp(i|\mathbf{G}+\mathbf{k}|\cdot\mathbf{r}) \tag{2.68}$$

The Hamiltonian, H is written as

$$H = -\frac{1}{2}\nabla^2 + V(r). \tag{2.69}$$

Substituting equations (2.68) and (2.69) into equation (2.67), multiply by $\exp(-i|\mathbf{G'}+\mathbf{k}|\cdot\mathbf{r})$ and integrating over all space, gives

$$\sum_G H_{\mathbf{G'},\mathbf{G}} C_{\mathbf{G}} = \varepsilon_n \sum_G S_{\mathbf{G'},\mathbf{G}} C_{\mathbf{G}}, \tag{2.70}$$

where

$$H_{\mathbf{G'},\mathbf{G}} = |\mathbf{G}+\mathbf{k}|\delta_{\mathbf{G'},\mathbf{G}} + V, \tag{2.71}$$

$$S_{\mathbf{G'},\mathbf{G}} = \delta_{\mathbf{G'},\mathbf{G}}, \tag{2.72}$$

$$V = \sum_t \exp(i\mathbf{q}.\mathbf{t}) V_f(q), \tag{2.73}$$

$$\mathbf{q} = \mathbf{G'} - \mathbf{G}. \tag{2.74}$$

$V_f(q)$ is an adjustable parameter. It is chosen at a few discrete q points for a bulk semiconductor (Cohen and Bergstresser, 1966) while for nanostructures, $V_f(q)$ is continuous and dense(Wang and Zunger, 1994). The $V_f(q)$ for nanostructure material can be expressed as

$$V_f(q) = \frac{a_1(q^2 - a_2)}{a_3 \exp(a_4 q^2) - 1} \tag{2.75}$$

or

$$V_f(q) = a_i \exp(-c_i(q-b_i)^2), \tag{2.76}$$

where a_n n=1, 2, 3, 4 and $a_i,\ b_i,\ c_i$ are empirical parameters obtained from fits to experimental or *ab-initio* data. Although computation cost due to different center-integrals has been drastically reduced, one is faced with the problem of diagonalizing the Hamiltonian matrix resulting from the dense plane waves employed in the nanostructure computations. The huge Hamiltonian matrix requires large computational memory to store them(Harrison and Valavanis, 2016). Zunger and co-workers proposed a method called the Folded spectrum method (FDM) to solve the huge matrix problem. Their method seeks to solve the matrix equation around the electronic gap of the nanostructure. (Wang and Zunger, 1994, 1996, Harrison and Valavanis, 2016).

2.3.3.4 Huckel and Extended Huckel model

The Huckel model is an approximate molecular orbital theory developed in 1931 (Hückel, 1931). Its molecular orbitals are expanded with basis sets of only pi orbitals. Thus, the model is restricted to only pi molecules e.g Benzene. The model is described as follows (Andrew, 2001, Magnasco, 2013). The model seeks to solve the eigenvalue equation,

$$H\psi_i(r) = \varepsilon_i \psi_i(r). \tag{2.77}$$

The molecular orbital is expressed in terms of pi atomic orbitals only as follows:

$$\psi_i = \sum_a C^i_{a,\pi} \phi_{a,\pi}, \tag{2.78}$$

where ψ_i is the molecular orbital, C is the expansion coefficient, and $\phi_{a,\pi}$ is the pi orbital centered on atom a. The eigenvalue problem can be reduced to the secular equation,

$$\sum_a H_{ab,\pi} C^i_{a,\pi} = \varepsilon_i \sum_a S_{ab,\pi} C^i_{a,\pi}. \tag{2.79}$$

The Hamiltonian matrix element, $H_{ab,\pi}$ is defined as

$$H_{ab,\pi} = \langle \phi_{b,\pi} | H | \phi_{a,\pi} \rangle. \tag{2.80}$$

The diagonals element of the Hamiltonian matrix are defined by

$$H_{aa,\pi} = H_{bb,\pi} = \alpha. \tag{2.81}$$

The off-diagonal Hamiltonian matrix elements, $a \neq b$ (resonance integral) are expressed for nearest neighbor interaction as

$$H_{ab,\pi} = \beta. \tag{2.82}$$

Otherwise,

$$H_{ab,\pi} = 0. \tag{2.83}$$

The overlap matrix element:

$$S_{ab,\pi} = \langle \phi_{b,\pi} \phi_{a,\pi} \rangle = I, \tag{2.84}$$

where I is a unit matrix. The extended Huckel method was proposed by Hoffman (Hoffman, 1964) to extend the application of the Huckel model to other systems other than pi molecules only. In this model, the molecular orbital is written in the basis of the valence orbitals as

$$\psi_i = \sum_a \sum_k C^i_{a,k} \phi_{a,k}. \tag{2.85}$$

The valence atomic orbital, ϕ_k can be expressed in terms of a Gaussian function as

$$\phi_k = d_k \exp(-\gamma_k r^2). \tag{2.86}$$

The Fock secular equation to be solved is expressed as

$$FC = SCE. \tag{2.87}$$

F is a Fock matrix with its elements, $F_{\nu\mu}$, which can be expressed in diagonal and off-diagonal form. The diagonal matrix element,

$$F_{\nu\nu} = I_{\nu\nu}, \tag{2.88}$$

where $I_{\nu\nu}$ is the ionization energy for orbital ν.
The off-diagonal matrix element,

$$F_{\nu\mu} = KS_{\nu\mu}\frac{I_{\mu\mu}+\nu\nu}{2}, \tag{2.89}$$

where K is an empirical parameter and $S_{\nu\mu}$ is the overlap matrix element. Other expressions for off-diagonal Fock matrix elements, $F_{\nu\mu}$ have been published (Wolfsberg and Helmholz, 1952, Hoffmann and Lipscomb, 1962).

With the Fock matrix and overlap matrix fixed, the eigenvalue problem can be solved to obtain the molecular energies, the transition energies and transition orbitals. The Huckel and extended Huckel models are rarely used for any meaningful calculation because they give only qualitative results (Wolfsberg and Helmholz, 1952, Hoffmann and Lipscomb, 1962, Magnasco, 2013).

2.3.3.5 Neglect of Differential Overlap (NDO)

The Neglect of Differential Overlap (NDO) methods are the most widely applied and successful semi-empirical methods (Zerner, 1991, Bredow and Jug, 2005, Christensen et al., 2016). They are approximate methods to the Hartree Fock formalism, which start from the Roothaan equation (a simplified and matrix form of the Hartree Fock equation). Within this formalism, one seeks to solve the secular equation,

$$FC = SCE, \tag{2.90}$$

where F is a Fock matrix with Fock elements F_{ab}. C is the molecular basis coefficient vector with vector elements c_{ka}, E is a set of orbital energies $\{\varepsilon_a\}$ and S is the overlap matrix with matrix elements S_{ab}. Using Roothan HF formalism,

$$F_{ab} = H_{ab} + \sum_{c=1}^{n}\sum_{d=1}^{n}[P_{ab}\langle ab|cd\rangle + \frac{1}{2}\langle ac|bd\rangle], \tag{2.91}$$

where

$$H_{ab} = \langle a| - \frac{1}{2}\nabla^2 - \sum_{A}^{N}\frac{Z}{|r-R_A|}|b\rangle. \tag{2.92}$$

The density matrix, P_{ab} is written as

$$P_{ab} = 2\sum_{i=1}^{N/2} c_{ai}c_{bi}, \tag{2.93}$$

where a, b, c, and d refer to atomic orbitals ϕ_a, ϕ_b, ϕ_c, and ϕ_d respectively. The variables n and N are the numbers of atomic orbitals and electrons, respectively. Within the NDO approximation, the basic approximations applied to the Roothaan equation are the zero differential overlap approximations (ZDO). These approximations are as follows (Andrew, 2001):

1. $\phi_a\phi_b\, d^3r = 0$
2. The overlap matrix is the unit matrix: $S_{ab} = \delta_{ab}$
3. The different centre integrals $\langle ab|cd\rangle = \langle aa|dd\rangle\delta_{ab}\delta_{cd}$. Consequently, all the three- and four-centre integrals are omitted.

Applying the ZDO approximations to the Roothaan secular equation, the equation reduces to (Andrew, 2001, Segal, 2012)

$$FC = CE, \tag{2.94}$$

with the diagonal matrix elements define by

$$F_{aa} = H_{aa} + \sum_{c=1}^{n} P_{cc}\langle aa|cc\rangle - \frac{1}{2}P_{aa}\langle aa|aa\rangle \tag{2.95}$$

and the off-diagonal matrix elements by

$$F_{ab} = H_{ab} - \frac{1}{2}P_{ab}\langle aa|bb\rangle. \tag{2.96}$$

2.3.3.6 Complete Neglect of Differential Overlap (CNDO)

The ZDO approximation was first implemented by Pople and Segal (1965) in the complete neglect of differential overlap. The Fock matrix elements of the CNDO are expressed as follows (Pople and Segal, 1965, Andrew, 2001, Magnasco, 2013):

For diagonal matrix elements,

$$F_{aa} = H_{aa} + \left(P_{YY} - \frac{1}{2} P_{aa} \right) \gamma_{aa} + \sum_{Y \neq Z} P_{ZZ} \gamma_{ab}, \tag{2.97}$$

where

$$H_{aa} = U_{aa} + \sum_{Y \neq Z} V_{YZ}, \tag{2.98}$$

$$U_{aa} = \langle a | - \frac{1}{2} \nabla^2 - \frac{Z A_Y}{|r - R_Y|} | a \rangle, \tag{2.99}$$

and

$$V_{YZ} = \langle a | - \sum_{Z \neq Y}^{N} - \frac{Z A_Z}{|r - R_Z|} | a \rangle. \tag{2.100}$$

For off-diagonal matrix elements ($a \neq b$, both a and b are on the same atom, say Y),

$$F_{ab} = -\frac{1}{2} P_{ab} \gamma_{YY}. \tag{2.101}$$

For off-diagonal matrix elements ($a \neq b$, a and b different atoms , say Y and Z),

$$F_{ab} = \beta_{YZ} S_{ab} - \frac{1}{2} P_{ab} \gamma_{YZ} \tag{2.102}$$

The total electron density, P_{YY} on an atom is define as

$$P_{YY} = \sum_{d \ on \ Y}^{Y} P_{dd}. \tag{2.103}$$

The two-electron repulsion integral with both orbitals a and d on atom Y, is

$$\gamma_{YY} = \langle aa | dd \rangle = \langle s_Y s_Y | s_Y s_Y \rangle. \tag{2.104}$$

The two-electron repulsion integral with orbitals a and d on different atoms, Y an Z is

$$\gamma_{YZ} = \langle aa | dd \rangle = \langle s_Y s_Y | s_Z s_Z \rangle. \tag{2.105}$$

In order to deal with the problem of orbital invariance experienced in the Huckel and extended Huckel models, the electron interactions are approximated as interactions be-

tween the s-orbitals. s_Y and s_Z are s-orbitals on atoms Y and Z, respectively (Zerner, 1991). U_{aa} is the one-centre electron integral obtained from the experimental ionization potential. V_{YZ} is the attraction interaction between electrons on atom Y and nuclei of atom Z. It is calculated over s-orbitals representing the valence orbitals. β is the resonance integral responsible for bonding and is obtained from a fit to *ab-initio* results (Zerner, 1991, Andrew, 2001). Different CNDO methods have been developed which include CNDO/1, CNDO/2 and CNDO/s. In CNDO also known as CNDO/1, equilibrium bond distances are underestimated and energies are overestimated due a penetration effect of the valence electrons. The CNDO/2 was developed in 1966 as an improvement over CNDO/1. It was developed in order to remove the electron penetration effects found in CNDO/1, by adjusting the expression for V_{YZ}. Also, U_{aa} in CNDO/2 is obtained in a slightly different way from CNDO/1 (Segal, 2012). While the CNDO/1 and CNDO/2 are implemented for ground state calculations, the CNDO/s developed by Bene and Jeffe, was uniquely developed for excitations and spectroscopy calculations (Bene and Jaffe, 1968).

2.3.3.7 Intermediate Neglect of Differential Overlap(INDO)

INDO was developed by Pople and co-workers in 1967 as an improvement over CNDO . Unlike the CNDO method, electron spin effect was included in the INDO method (Pople et al., 1967). In contrast to the ZDO approximation and CNDO, the electron-electron repulsion integrals on one-center are non-zero in the INDO model. These integrals are calculated using the Slater-Condon parameters obtained from spectroscopic data. The INDO Fock matrix is define by both diagonal and off-diagonal matrix elements (Pople et al., 1967, Andrew, 2001).

For the diagonal matrix elements ($a = b$),

$$F_{aa} = U_{aa} + \sum_{b\ on\ Y} [P_{bb}\langle aa|bb\rangle - \frac{1}{2}P_{bb}\langle ab|ab\rangle] + \sum_{Y\neq Z} (P_{ZZ} - ZA_Z)\gamma_{ab}. \tag{2.106}$$

For off-diagonal matrix elements ($a \neq b$, both a and b are on the same atom, say Y),

$$f_{ab} = \frac{3}{2}P_{ab}\langle ab|ab\rangle - \frac{1}{2}P_{ab}\langle aa|bb\rangle. \tag{2.107}$$

For off-diagonal matrix elements ($a \neq b$, a and b different atoms , say Y and Z),

$$F_{ab} = \frac{1}{2}(\beta_Y + \beta_Z)S_{ab} - \frac{1}{2}P_{ab}\gamma_{YZ}. \tag{2.108}$$

An important variant of the INDO is INDO/CI, which was developed in 1971 to calculate lower excitation states for hydrocarbons (Van Catledge, 1971). Zerner and co-workers in 1976, developed the Zerner intermediate neglect of differential overlap for spectroscopy (ZINDO/s), sometimes known as intermediate neglect of differential overlap for spectroscopy (INDO/s). It is an INDO method followed by CIS and it is widely employed for excitations and spectroscopy in organic molecules and transition metal complexes (Ridley and Zerner, 1976, Zerner et al., 1980b). Within the ZINDO/s approximation, the one-centre two-electron repulsion integrals were obtained from spectroscopic data through the Slater-Condon parameters and the resonance integrals β by fits to experiments. The electron- nuclear attraction γ_{YZ} is define using the modified Mataga Nishimoto parametric expression (Mataga and Nishimoto, 1957):

$$\gamma_{YZ} = \frac{f(\gamma_{YY} + \gamma_{ZZ})}{2f + R_{YZ}(\gamma_{YY} + \gamma_{ZZ})}, \tag{2.109}$$

where f is and R_{YZ} is the separation between the centers of atoms Y and Z.

2.3.3.8 Neglect of Diatomics of Differential Overlap (NDDO)

The most sophisticated neglect of differential overlap method is the NDDO. It includes all one center electron-electron repulsion integrals as INDO but retains the two center integrals of the form $\langle ab|cd\rangle$, where a and b are centered on the same atom and c and d also on the same atom. Hence, more terms are evaluated in the NDDO formalism than in the INDO and CNDO (Pople and Segal, 1965). The Fock matrix in NDDO is defined by both diagonal and off-diagonal matrix elements(Andrew, 2001).
For diagonal matrix elements ($a = b$, $F_{ab} = F_{aa}$),

$$F_{aa} = H_{aa} + \sum_{c\ on\ Y}\sum_{d\ on\ Y} P_{cd}[\langle aa|cd\rangle - \frac{1}{2}\langle ac|ad\rangle] + \sum_{Z\neq Y}\sum_{c\ on\ Z}\sum_{d\ on\ Z} P_{cd}\langle aa|cd\rangle. \tag{2.110}$$

For off-diagonal matrix elements ($a \neq b$, both a and b are on the same atom, say Y),

$$F_{ab} = H_{ab} + \sum_{c\ on\ Y} \sum_{d\ on\ Y} P_{cd}[\langle ab|cd\rangle - \frac{1}{2}\langle ac|bd\rangle] + \sum_{Z\neq Y} \sum_{c\ on\ Z} \sum_{d\ on\ Z} P_{cd}\langle ab|cd\rangle. \quad (2.111)$$

For off-diagonal matrix elements ($a \neq b$, a and b different atoms, say Y and Z),

$$f_{ab} = H_{ab} - \frac{1}{2} \sum_{c\ on\ Y} \sum_{d\ on\ Z} P_{cd}\langle ac|bd\rangle. \quad (2.112)$$

Various methods based on NDDO have been developed. The first method based on NDDO is the modified neglect of differential overlap (MNDO) introduced in 1976 (Dewar and Thiel, 1977). In the MNDO,
the diagonal matrix elements,

$$H_{aa} = U_{aa} - \sum_{Z\neq Y} -Z_\alpha \langle a_Y a_Y | s_Z s_Z\rangle. \quad (2.113)$$

For off-diagonal matrix elements ($a \neq b$, both a and b are on the same atom, say Y),

$$H_{ab} = -\sum_{Z\neq Y} -Z_\alpha \langle a_Y b_Y | s_Z s_Z\rangle. \quad (2.114)$$

For off-diagonal matrix elements ($a \neq b$, a and b different atoms , say Y and Z),

$$H_{ab} = \frac{1}{2} S_{ab}(\beta_a^Y + \beta_b^Z), \quad (2.115)$$

where Z_α is the atomic number of atom Z, s_Z is s-orbital on atom Z, S_{ab} is the overlap integral and β_a^Y is a parameter for atomic orbital a centered on atom Y.
Other NDDO based methods like the AM1, PM3, MNDO/d, PM6, PM7 are improvements over MNDO and have been applied successfully for ground-state calculations (Silva-Junior and Thiel, 2010).

2.4 INDO/s formalism and parametrization

INDO/s is a variant of INDO approximation (Ridley and Zerner, 1973). It is an INDO formalism followed by configuration interaction singles (CIS) calculations. It was uniquely

developed and parameterised for excited states and spectroscopic studies. Its parameters were determined for organic molecules (Ridley and Zerner, 1973, 1976), transition metals (Bacon and Zerner, 1979, Zerner et al., 1980a) and lanthanide complexes (Kotzian et al., 1992).

2.4.1 INDO/s formalism and parameterisation for organic molecules

The INDO/S Fock matrix elements follow from those of the INDO approximations(Ridley and Zerner, 1973). See detail of the description of INDO matrix elements in section 2.3.3.7. Definition and determination of parameters within the INDO/S formalism are given as follows:

Considering s,p basis set, the one center integrals U_{ss} and U_{pp} are written as follows:

$$U_{ss} = -(Z_I - 1)F^0_{ss} + \frac{1}{6}mG^1(sp) + I_s \tag{2.1}$$

$$U_{pp} = -(Z_I - 1)F^0_{ss} + \frac{2}{25}(m-1)F^2_{pp} + \frac{1}{6}lG^1(sp) + I_p \tag{2.2}$$

where Z_I is the atomic number of atom I, F^2 and G^1 are Slater-Condon factors and I_s and I_p are ionization potentials for electron in s and p orbital, respectively. The values of F^2 and G^1, I_μ are obtained from atomic spectra table (Moore, 1949).

The nuclear attraction integral is written as

$$V_{IJ} = Z_J\gamma_{IJ}, \tag{2.3}$$

where γ_{IJ} is a two-center Coulomb integral and defined using the modified Mataga Nishimoto parametric expression (Mataga and Nishimoto, 1957),

$$\gamma_{IJ} = \frac{f(\gamma_{II} + \gamma_{JJ})}{2f + R_{IJ}(\gamma_{II} + \gamma_{JJ})}. \tag{2.4}$$

R_{IJ} is the separation between atomic centers I and J and

$$\gamma_{JJ} = F^0(JJ) = I_J - A_J, \tag{2.5}$$

where I_J and A_J are ionization potential and electron affinity, respectively, obtained from atomic spectra data given by Moore. The one-center two-electron repulsion integrals are defined from Slater-Condon factors (Moore, 1949) as follows:

$$\langle ss|ss\rangle = F^0(ss) \tag{2.6}$$

$$\langle sp|sp\rangle = 0.3333G^1(sp) \tag{2.7}$$

$$\langle p_x p_x|p_x p_x\rangle = F^0(pp) + 0.16F^2(pp) \tag{2.8}$$

$$\langle p_x p_x|p_y p_y\rangle = F^0(pp) - 0.08F^2(pp) \tag{2.9}$$

$$\langle p_x p_y|p_x p_y\rangle = 0.12F^2(pp) \tag{2.10}$$

The f factors and β parameters for C, H, O, and N of the two-center two-electron repulsion were optimised to reproduce the spectra from benzene and pyridine geometries. $f_{\sigma\sigma}$ and $f_{\pi\pi}$ were set as 1.267 and 0.585, respectively. The bonding parameters were set as $\beta_s = \beta_p = \beta_I$ and β_I was obtained from a fit to spectral data (Voityuk, 2013). Without any re-parametrization, calculations of spectra of different organic molecules including naphthalene, pyrazine, pyrimidine, etc were carried out using the model.

2.4.2 INDO/s formalism and parametrization for transition metals

Unlike the parametrization of INDO/s for organic molecular that mostly involves the valence sp basis, the transition metal includes the d orbitals also. As such, a bit of modification is introduced into the INDO Hamiltonian as follows (Zerner et al., 1980a, Bacon and Zerner, 1979): The diagonal matrix element (one centre one-electron Fock matrix) is

$$F_{aa} = U_{aa} - \sum_{J\neq I}\gamma_{\bar{\mu}B}\{(n_s+n_p)+(n_d)_J\} + \sum_{cd}p_{cd}\left[\langle\mu\mu|cd\rangle - \frac{1}{2}\langle\mu c|\mu d\rangle\right] + \sum_{c\notin I}P_{cc}\gamma_{ca}. \tag{2.11}$$

The off-diagonal matrix element (one-centre two-electrons Fock matrix) is given by

$$F_{ab} = \sum_{cd}p_{cd}\left[\langle\mu\mu|cd\rangle - \frac{1}{4}\langle\mu c|\mu d\rangle\right]. \tag{2.12}$$

The off-diagonal matrix element (two-centre two electron Fock matrix) is

$$F_{ab} = \beta_{ab} - \frac{1}{2} P_{ab} \gamma_{\bar{ab}}. \tag{2.13}$$

The one-electron core, U_{aa} are calculated from ionization processes.
The bonding integral, $\beta_{ab} = \frac{1}{2}(\beta_a^A + \beta_b^B)\bar{S}_{ab}$,
where β_a^A and β_b^B are bonding parameters for orbital a centered on atom A and b centered on atom B, respectively. The weighted overlap $\bar{S}_{ab}$ for spd basis are expressed as follows:

$$\bar{S}_{ss} = S_{ss}$$

$$\bar{S}_{sp} = S_{sp}$$

$$\bar{S}_{pp} = g_\pi f_{p\pi} S_{p\pi p\pi} + g_\sigma f_{p\sigma} S_{p\sigma p\sigma}$$

$$\bar{S}_{sd} = S_{sd}$$

$$\bar{S}_{dd} = g f_{d\delta} S_{d\delta d\delta} + g_\pi f_{d\pi} S_{p\pi d\pi} + g_0 f_{d\sigma} S_{p\sigma d\sigma}$$

g_a and f_a are geometric factors and interaction weighing factors respectively. $f_{p\pi}$ and $f_{p\sigma}$ are set to 0.64 and 1.267, respectively (Ridley and Zerner, 1973, 1976). $f_{d\pi}$ and $f_{d\sigma}$ are set to one. The parameters $\beta_s = \beta_p$ and β_d were obtained empirically from spectra. The two-electron Coulomb integral, γ_{IJ} were in some cases evaluated from the Mataga Nishimoto expression (Zerner et al., 1980a) and in other cases evaluated over Slater-type orbitals (Bacon and Zerner, 1979, Zerner et al., 1980a). The one-centre two electron integrals were obtained from the Slater-Condon parameters.

2.4.3 Determination of electronic and optical properties with INDO/s

INDO/s was developed for calculations of ionization potentials, electronic excited states and spectra. It fails for geometry optimisation and some ground state calculations (Voityuk, 2013). INDO/s is employed for predicting low-lying vertical excitation energies and oscillator strength. These are carried out by first, performing a self-consistent field ground state calculation and thereafter, a CIS calculation is performed in order to obtain excita-

tion energies. The oscillator strength, f_{os} is then calculated with the expression,

$$f_{os} = \frac{2}{3}\Delta E|\vec{D_{tr}}|^2, \tag{2.14}$$

where ΔE is the excitation energy in eV, and $\vec{D_{tr}}$ is the transition dipole moment (in Debye)) defined by

$$\vec{D_{tr}} = \langle \psi_f|\vec{\mu}|\psi_i\rangle. \tag{2.15}$$

INDO/s, when benchmarked with the well known Thiel data set for electronically excited energies of 28 small organic molecules, gave a mean absolute error $\approx 0.5eV$ but was found to overestimate oscillator strength (Silva-Junior and Thiel, 2010, Voityuk, 2013). The accuracy of INDO/s calculation for transition metals has not been reliably verified due to a lack of reliable data and a need for further parameterisation (Voityuk, 2013). Higher excitation energies are poorly predicted in INDO/s since calibrations were performed with low-lying excited state reference data (Silva-Junior and Thiel, 2010). INDO/s is also employed for the calculation of ionization potential (I_P) and electron affinity (E_A) in the following way:

$$I_P = -\varepsilon_{HOMO} \tag{2.16}$$

and

$$E_A = -\varepsilon_{LUMO}, \tag{2.17}$$

where ε_{HOMO} is the energy of the highest occupied molecular orbital (HOMO) while ε_{LUMO} is the energy of the lowest unoccupied molecular orbital (LUMO). INDO/s predicts I_p for molecules with a typical error $\approx 0.40eV$ but fails for transition metal complexes (Voityuk et al., 1999). Furthermore, INDO/s can be applied for calculating polarizability, charge distribution and excitation energy transfer (Voityuk, 2013).

2.4.4 Applications of INDO/s Methods

A lot of studies have been performed with INDO/s but here we discuss a few examples. Electronically excited states and UV-vis spectra of carbon nanostructures and their complexes have been largely studied with INDO/s. The results obtained compare well

with experiments (Feng et al., 1990, Tian et al., 2006). In particular, Zerner and co-worker reported a low-lying band of $27,300cm^{-1}$ from INDO/s which compare well with $25,900cm^{-1}$ from experiment for C_{60} (Feng et al., 1990). A mean error of 0.38 eV was reported from the calculation of the electronic gap with INDO/s for 60 different organic molecules (Hutchison et al., 2002). INDO/s has also been employed to study complex systems like carbon nanotubes (Kilina et al., 2012). It has also been applied in the study of excitation and charge transfer in DNA (Voityuk, 2006). Prediction of the structure of the material with desired electronic properties with the INDO/s method has been reported (Di Bella et al., 1993, Quarti et al., 2011).

2.4.5 Limitations and improvement in INDO/s

INDO/s, no doubt plays a significant role in the study of electronic and optical properties of large systems and nanoparticles. However, it is limited in some ways. First, while its accuracy for predicting the low-lying excited energies still needs improvement, it gives a poor prediction for higher excited states. Moreover, the parameterisation for transition metals are not reliable (Voityuk, 2013). With available powerful computing tools, significant improvement in the performance of INDO/s can be achieved by re-parameterising it with reliable data from experiment and a high-level *ab-initio* calculations. However, Only little improvements have been achieved in INDO/s since its development in the 70s. Voityuk modified and parameterised INDO/s for C, H, N, and O with the theoretical best-estimated data (electronic excitation energies and oscillator strength) (Silva-Junior and Thiel, 2010). The newly obtained model which is called INDO/x performed better than INDO/s. The mean absolute deviate was obtained from INDO/x as 0.26 eV for singlet vertical excitation energies and 0.33 eV for triplets vertical excitation energies. The corresponding deviations for INDO/s are 0.56 eV and 0.64 eV, respectively. INDO/s was parameterised to reproduce spectrum from TDDFT for silver nanoclusters (Gieseking et al., 2016). To the best of our knowledge, re-parametrisation of INDO/s for a lot of elements including transition metals, sulphur and silicon have not been performed.

2.5 Quantum Mechanical Methods for Determination of Excitations Energies and Absorption Spectra

Arguably, experiments are generally the best and most accurate methods for the determination of electronic excitations energies and absorption spectra. The spectrophotometer has been extensively employed to determine the UV-Vis absorption spectra even for large systems such as biological molecules (Nilapwar et al., 2011). It has been used to estimate protein concentration(Aitken and Learmonth, 2009), DNA melting point(Nilapwar et al., 2011). Results from experiments have been applied reliably for benchmarking empirical and semi-empirical methods (Winget et al., 2003, Winget and Clark, 2005, Kayi and Clark, 2007, Stewart, 2007, Voityuk, 2014).However, experiments pose some challenges, which include high infrastructure costs, complexity in their procedures, and difficulties in describing vertical excitations (Schreiber et al., 2008, Silva-Junior et al., 2008, Voityuk, 2013). With the advent of powerful computing resources, high-level quantum mechanical methods have demonstrated the ability to yield results that are comparable to experiments (Barone, 2011). Some of the high-level methods for excitation energies and absorption spectra calculations include EOM-CCSD (Christiansen et al., 1995, Caricato et al., 2010), GW (van Setten et al., 2012, Leng et al., 2016), solution of the Bethe Salpeter Equation (BSE) (Nakanishi, 1969, Leng et al., 2016, Blase et al., 2018), Quantum Monte Carlo (QMC) method (Schautz et al., 2004), the CASPT2 (Andersson et al., 1990) and others.

The EOM-CCSD approach is known as the gold-standard for excitation energies and absorption spectra calculations. It is highly accurate with typical errors within 0.1 eV of experimental energies (Caricato et al., 2010, 2011, Bennie et al., 2017). It has been applied to a wide range of problems related to electronic excitations including excitation state vibrionic coupling. Also, the EOM-CCSD method contains no adjustable parameter and one does not have to deal with the problem of choice of active space as is the case in multi-reference reference methods such as CASPT2. It is a benchmark method for other molecular orbital theory methods like TDDFT (Caricato et al., 2011). However, EOM-CCSD is computationally prohibitive for large systems like nano-scale materials (e.g quantum dots) . It is restricted to systems with less than 20 atoms or so, within a moderate basis set (Caricato et al., 2010, Bennie et al., 2017).

Complete Active Space Perturbative Theory (CASPT2) method is a multi-reference approach that successfully describes electron correlations (Andersson et al., 1990). It was employed alongside the coupled-cluster (CC2, CC3, CCSD) approaches in the well known Thiel's benchmark set for excitation states of 28 molecules (Schreiber et al., 2008, Silva-Junior et al., 2008). Reports have shown that CASPT2 compares well with EOM-CCSD with typical error within 0.2 - 0.3 eV(Schreiber et al., 2008). CASPT2 has been applied for validation of *ab-initio* methods (Silva-Junior et al., 2008, Sauri et al., 2010) and calibration of semi-empirical methods (Silva-Junior and Thiel, 2010). However, like the EOM-CCSD, in practice CASPT2 is restricted to small atomic systems. The accuracy of BSE and QMC for excitation calculations have also been reported for small-sized systems.

Good alternative to the accurate methods discussed so far are the TDDFT and CIS(D) (Runge and Gross, 1984, Barone, 2011). They can handle moderate-sized molecules. Report have shown that excitation energies from TDDFT compare with Thiel's benchmark (data from CASPT2, CC methods etc) for 28 medium-sized organic molecules with a typical error of 0.27 eV (Silva-Junior et al., 2008). Also, valence states excitation obtained with TDDFT compare well with experiment with a mean absolute error of 0.23 eV (Leang et al., 2012). Gieseking and co-workers applied TDDFT to benchmark INDO/s absorption spectrum for silver nanoclusters (Gieseking et al., 2016). Hartree Fock followed by configuration interaction singles doubles (CISD) gives roughly comparable results with TDDFT. Nonetheless, TDDFT and CIS(D) are *compute-intensive* for large atomic clusters ($N > 60$ atoms) and nano-sized materials.

Generally, semi-empirical quantum mechanical methods have been widely adopted for the studies of excitations and spectroscopy of large atomic clusters and molecules. These methods are computationally cheap but generally less accurate compared with accurate *ab-initio* methods. The most common, reliable and straight forward semi-empirical quantum mechanical methods are those based on the Hartree Fock formalism or molecular orbital theory. In particular, INDO/S was uniquely developed and parameterised for excitations and spectroscopy. It is still widely applied to study organic molecules and some transition complexes (Voityuk, 2013).

2.6 Development and Improvement in Semi-empirical Molecular Orbital Theory

The semi-empirical molecular orbital theory dates as far back as the early 1930s when Huckel proposed the Huckel theory applied, which is uniquely applied to π molecular systems only. The molecular orbital is expressed in the basis sets of only the π electrons. The method gives only a qualitative description of the electronic structure of planar conjugated systems and is useful for teaching in class (Hückel, 1931, Andrew, 2001). In the 1950s, the Pariser-Parr-Pople (PPP) model was developed as an improvement over the Huckel theory though, still applicable only to π molecules. It includes the effect of electron-electron repulsion which is not well represented in the Huckel formalism. The PPP method is useful in spectroscopic calculations and for periodic systems (Pariser and Parr, 1953, Zerner, 1991). In 1963, Hoffman extended the Huckel theory to other molecules other than the conjugated(π) molecules. The method, which is known as the Extended Huckel Theory (EHT) includes all valence electrons in its calculations. EHT has found application in band structure calculations and is suitable for the study of metallic systems. However, it fails for geometry optimisations (Hoffmann, 1963, Zerner, 1991, Andrew, 2001).

Pople and Co-workers in the 1960s proposed some methods based on zero differential overlap (ZDO) approximations, namely Complete Neglect of Differential Overlap (CNDO), Intermediate Neglect of Differential Overlap (INDO) and Neglect Diatomic of Differential Overlap(NDDO). The CNDO developed in 1965, was the first model to implement ZDO approximation (Pople et al., 1967, Andrew, 2001). The CNDO (also known as CNDO/1) has been fairly successful in predicting some physical properties of a molecular system and sometimes used to generate initial guess in *ab-initio* methods. However, it predicts equilibrium bonding and heat of formation poorly. Pople and co-workers (1966) proposed CNDO/2(Pople, 1965, Pople et al., 1967), an improved formalism over CNDO/1. In contrast to CNDO/1, penetrating integral effect in CNDO/2 is well defined and, thus, it predicts better equilibrium bond lengths, bond angles and dipole moments. For instance, CNDO/2 predicts the bond length of carbon monoxide(CO) to be 1.190 a.u which compares well with the experiment value of 1.128 a.u. Unfortunately, CNDO/2 predicts the heat of formation poorly (Andrew, 2001, Segal, 2012). Another variant of CNDO is the CNDO/S, which is developed to calculate electronic spectra.

Here, the resonance integral was redefined and spectroscopic data were included for the optimisation of its parameters (Bene and Jaffe, 1968). However, its shortcomings have been reported (Hata et al., 2006). INDO approximation is a more sophisticated method than CNDO. It was proposed by Pople and co-workers to overcome some problems in the CNDO approximation. In the INDO approximation, in contrast to the CNDO approximation, the one-center two-electron repulsion integrals are not neglected and by this, spin effects are taken into account. While the CNDO formalism does not distinguish between the energy of a singlet and triplet states, INDO does. INDO was found to reproduce similar results as in CNDO/2. For instance, the dipole moment of CH_2 calculated with INDO and CNDO/2 are 2.17 Debye and 2.26 Debye, respectively. The bond angle of CH_2 from INDO and CNDO/2 are 107.2° and 108.6°, respectively (Segal, 2012).

Important variants of INDO are the INDO/1, INDO/s, SINDO, and SINDO/1. Zener and co-workers (1973) developed INDO/1 employed for geometry optimisation calculations and INDO/s for electronic spectroscopy calculations (Ridley and Zerner, 1973). INDO/s was parameterised at the CIS level with spectroscopic data. It has been widely employed for calculation electronic transition in organic molecules and transition metal complexes (Voityuk, 2013). It does predict well $d \rightarrow d^*$ orbital transition and oscillator strengths for weak transitions. However, INDO/s is inaccurate for charge transfer and Rydberg state calculations (Zerner, 1991, Voityuk, 2013).

The NDDO is the most sophisticated and widely employed semi-empirical method. It has received significant improvement since its development. The modified neglect of differential overlap (MNDO), the first method to implement the NDDO approximation, was developed by Dewar and Thiel in 1977 (Dewar and Thiel, 1977). It has been parameterised for a lot of elements (Zerner, 1991). MNDO is successful in predicting, polarizabilities, hyperpolarizabilities, and other properties. Although it has advantages over the MINDO methods, it has the challenge of poor prediction of the hydrogen bond, underestimation of rotational barriers, hypervalent molecules are unstable, underestimation of electronic excitations among other issues (Zerner, 1991, Andrew, 2001). The problems associated with MNDO are partly due to overestimation atom-atom repulsion for the sum of vander Waals equivalent distance (Andrew, 2001). To overcome this problem, the

Dewar group developed the Austin Model 1 (AM1) in 1985. AM1 employs Gaussian functions to describe the atom-atom repulsion (Dewar et al., 1985) thereby increasing the number of parameters in AM1 as compared to MNDO. However, the computation time in both MNDO and AM1 is about the same (Andrew, 2001, Kayi, 2009). Also, in AM1, the reparameterisation of MNDO parameters was performed. This was necessary because MNDO parameterisation was considered unreliable since it was performed in the 1970s when computational resources were limited.(Kayi, 2009). AM1 has been parameterised for main group elements. It performs well for hydrogen bonds and activation energy predictions. However, some hypervalent systems e.g alkyl and peroxide compounds are poorly described within the AM1 model (Kayi, 2009). The parametric model 3 (PM3) (Stewart, 1989) was introduced in 1989. It was parameterised for more elements than AM1 (Zerner, 1991) and was also obtained by modifying the core-core term of MNDO and reparameterising. While AM1 parameters were derived by intuition and chemical knowledge, PM3 parameters , on the other hand were obtained from parameter optimisation. Although AM1 and PM3 have some of their parameters different, they both predict well some molecular structure properties with the same level of accuracy (Andrew, 2001). However, PM3 predicts hydrogen bond to be too short and poorly predicts the amide bond rotations.

Generally, MNDO, AM1, and PM3 are faced with the problem of poor prediction of weakly bonded molecules and parameters of metals in these models are unreliable. MNDO/d was introduced to describe metals and transition metals. It involves the inclusion of the d orbitals into MNDO. Thus, MNDO/d is applied for hypervalent molecules, transition elements and it is helpful in describing the polarization of the second-row elements. MNDO/d performs better than PM3, AM1, MNDO, especially in predicting some properties like the heat of formation for hypervalent compounds and transition metals (Thiel and Voityuk, 1996, Jensen, 2017, Chatfield and Christopher, 2002). MNDO/d has been parameterised for Cd, Zr, Zn, Mg, and Na. Nonetheless, just like the original MNDO, it performs poorly in predictions of hydrogen bonding (Thiel and Voityuk, 1996, Chatfield and Christopher, 2002). Henre and co-worker also added d functions to PM3 to obtain a model called PM3(tm). Its parametrization was based on geometries of systems and as such, it is applied for molecular geometry generations. However, this method seems unreliable since the method is very scarce in literature (Børve et al., 1997,

Chatfield and Christopher, 2002). There is also the AM1(d) model in which d functions were added to AM1 and its core-core interaction term modified. It was first parametrized for molybdenum in the year 2000 by Voityuk and Rosch (Voityuk and Rösch, 2000) and latter optimised for potassium by Lopez and York (Lopez and York, 2003). PM5 was developed by reparametrization of PM3 and the core-core repulsion term replaced with "pure" parameters. It shows a slight improvement over PM3 and has been parameterised for many elements (Kayi, 2009). In 2003, Clark and co-workers introduced the AM1* (Winget et al., 2003) which is based on AM1. With d functions added and the core interaction redefined for some elements other than O, F, N, C, H. Hence, AM1* reproduces the same result as AM1 for O, F, N, C, H (Winget and Clark, 2005, Winget et al., 2003, Kayi and Clark, 2007). Without a need for a change to AM1 formalism, AM1 was parametrized in 2006 to obtain RM1 the model. The reparametrization was performed for ten elements only, namely, I, Br, Cl, F, P, S, O, N, C, H (Rocha et al., 2006).

PM6 was developed in 2007 by Stewart by modifying the NDDO core-core repulsion, including d function and reparametering. Parametrization was performed for seventy elements. Report has shown the improvement of PM6 over the NDDO methods discussed so far. The heats of formation and bond length are better predicted within PM6 than PM3 and AM1 (Stewart, 2007). Some variants of PM6 have also been introduced which include PM6-DH (Rezac et al., 2009), PM6-DH2 (Fanfrlik et al., 2010) and PM6-D3H4X. They are improvements over PM6 for non-covalent interactions (Hostavs et al., 2013). The most recent PM series is the PM7 developed in 2013 by Stewart. It is an improvement over PM6 and includes terms to describe non-covalent interactions. It performs better than PM6 in predicting bond length and heat of formation (Stewart, 2013). Recently, Voityuk improved upon INDO/S for C, H, N and O to obtain a model called INDO/x which reproduces the excitation energies of the TBE-2 organic molecules with typical error of 0.26 eV against 0.56 eV from INDO/S (Voityuk, 2014).

2.7 Parameterization scheme in NDO semi-empirical methods

The goal of any semi-empirical molecular orbital methods is to reproduce experimental or high-level *ab-initio* results with less computational effort and resources. In *ab-initio*

molecular orbital methods, the different center-integrals are responsible for the computation expense. In the semi-empirical scheme, however, the less important integrals like three and four-centered integrals are omitted while the one and two-centered integrals are replaced with parameters or parametric expressions. These parameters are then calibrated to reproduce experimental or high-level *ab-initio* data. The accuracy of a semi-empirical method depends strongly on the accuracy of their optimised parameters. Provided the essential physics are retained, the optimised parameters can correct for the error introduced by the drastic approximations and make the semi-empirical methods even more comparable to experiments than the *ab-initio* counterparts (Zerner, 1991).

In parameterisation, the collection of reliable data, application of weighting factors and the parameterisation procedure are important steps in obtaining reliable parameters. (Thiel et al., 2000, Kayi, 2009)

2.7.1 Reference Data

Molecular reference data is a set of accurate data comprising the chemical and structural properties of molecular or atomic systems obtained from experiments or high-level *ab-initio* methods. The data are sometimes from experiments or high-level ab-initio (CC, CASPT2, GW/BSE, QMC, B3LYP) calculations or both. These data are expected to represent the main features of their potential applications (Thiel et al., 2000, Kayi, 2009). Some of the important properties captured in the reference data are dipole moments, geometrical structures, the heat of formation, ionization potential and reaction energies. For instance, parametrization for geometrical properties is obtained from fits to reference bond lengths, bond angles, and dihedrals. For spectra and optical properties, calibrations are done using transition dipole moments, oscillator strength, excitation energies. Experimental data and high-level data databases are available from different sources including the Cambridge database (Groom et al., 2016), the NIST Webbook (Linstrom and Mallard, 2001), and Theoretical best estimate(Silva-Junior and Thiel, 2010).

2.7.2 Parametrization procedure

Parametrization has to do with optimisation or determination of the parameters of semi-empirical methods in order to reproduce experimental or high-level *ab-initio* data. Optimisations are carried out by varying the model parameters in order to minimize an error function such as (Kayi, 2009, Govender et al., 2014)

$$f = \sum_a \omega_a [\eta_a^c - \eta_a^{ref}]^2, \tag{2.1}$$

where, η_a^{ref} and η_a^c are the values of the experiment/*ab-initio* and computed a_{th} property of interest,respectively and ω_a is the a_{th} weighing factor. The optimised parameters are obtained when the following conditions are fulfilled (Govender et al., 2014, Kayi, 2009):

$$\frac{df}{dP_a} = 0 \tag{2.2}$$

$$\frac{d^2 f}{dP_a^2} > 0 \tag{2.3}$$

Where P_a is the a_{th} parameter. In the parameterisation procedure, the guess of the starting parameter can be very challenging. Starting parameters sometimes are obtained from the existing parameters of other methods.

A trial and error approach is not a good option to carry out a successful parametrization. Rather, various algorithms like the steepest descent and non-linear square-least which have been developed, can be employed. Another important aspect of parameterisation is to verify the transferability of the parameters/model obtained. That is, can the optimised parameters produce accurate results for geometries not included in the training set? Usually, not all different set of optimised parameters of a model are transferable. Hence, parameterisations must be performed carefully, rigorously and a constant check of the transferability of each set optimised parameters must be carried out.

2.8 Theoretical studies of quantum dots

There are different methods in literature for the studies of large atomic systems and quantum dots. The one-band effective mass approximation method (EMA) is a simple

method that has been extensively employed for the study of nanostructure systems, including quantum dots. The approach assumes holes and electrons in the quantum dot are confined by an effective potential (potential barrier). Although qualitative results are obtained with this method, it has helped to gain some insights into some characteristics features of the nanostructure systems. EMA has been extensively deployed to study the quantum confinement effect in nanostructures (Borah et al., 2018). Reports have shown that EMA describes the electronic gap well for large nanoparticles but deviates largely from the experiment for small nanoparticles (Vatankhah and Ebadi, 2013). EMA has also been employed to study the dependence of the electronic gap and the binding energy of the dot on some physical properties (Baskoutas et al., 2004). EMA fails for medium-sized and smaller quantum dots because it does not account for atomistic effects.(Fu et al., 1998). Also, within this method, the study of the structural, electronic, and optical properties of a system is not straight forward. (Borah et al., 2018).

The k.p method is an improvement over EMA. It is comprised of multiple bands but still limited by the non-inclusion of atomistic effect. As in the EMA case, the k.p methods fail for intermediate and small nanostructures. The empirical pseudopotential method (EPM) (Wang and Zunger, 1994) is a significant advancement over EMA and k.p methods. It was developed in 1960, originally for bulk material calculations but has been modified for nanostructure calculations. Within the EPM frame, atomistic effects are accounted for using empirically determined pseudopotentials (Wang and Zunger, 1994, Galli et al., 2002). EPM has been successfully applied for the determination of the electronic and optical properties of nanostructures. Zunger and co-workers in their work-study employed EPM to determine the electronic and optical properties of silicon quantum dots (Wang and Zunger, 1994, 1997) and CdSe quantum dots (Wang and Zunger, 1996). Bester employed the EPM followed by CIS to study the electronic excitations of nanostructures.(Bester, 2008). However, EPM involves a huge number of plane-wave basis sets for large systems like quantum dots. Solving the corresponding huge matrix requires a lot of computational time and resources. However, Zunger and co-workers developed a method to address this problem in the EPM method (Wang and Zunger, 1996).

Tight binding (TB) method is another semi-empirical method which includes the atomistic effect in its descriptions of electronic structure (see section 2.3.3.1 for a description

of TB). TB methods have been successfully applied for ground state properties of bulk materials. Also, significant improvements of the method has been achieved and it is being employed in the study of finite systems like quantum dots. Suman and co-workers reported a qualitative result of the electronic state of the quantum dots using the tight-binding framework (Dhayal et al., 2014). The method has also been applied to study the optical properties and effect of strain on the electronic state of the quantum dots (Ramaniah and Nair, 1993, Santoprete et al., 2003, Schulz, 2007). A variant of the tight-binding method is the density functional tight binding (DFTB), a method based on DFT (see section 2.3.3.2 for description DFTB). DFTB has been employed for nanostructure optimisations (Zonias et al., 2009, Fedorov et al., 2016),to and study electronic and optical properties of atomic system (Wilson et al., 2014, Darghouth et al., 2015). Despite the vast application of the TB and DFTB, they are limited due to the challenges of transferability. Though, the calculation of excitation energies and spectra have been reported within these methods (Nishimoto, 2015), the calculations are not straight forward because their wavefunctions are not explicitly defined. In addition, DFTB are inaccurate in predictions of properties like the electronic gap, ionization potential and electron affinity. (Darghouth et al., 2015).

Quantum dots can also be studied using methods based on the Hartree Fock formalism. Paramount among these methods are the NDDO, INDO, and CNDO based methods described earlier. These methods are a drastic approximation to Hartree Fock and carry out their calculations with minimal basis sets. They differ from the TB and EPM discussed above in that, their procedure includes self-consistent fields which aids transferability. The advent of powerful computational resources and high-level data have caused a significant improvement in these methods and thus, have been adopted for large atomic clusters and nanocluster calculations. PM3 and AM1, methods based on NDDO, have been applied for the study nanoparticle structure, electronic and optical properties (Robles et al., 1999, Wang et al., 2008). The most recent improvement in NDDO based method, PM6 and PM7, have been employed to compute polarizabilities for molecules and nanoparticles. The accuracy was found to reduce moving from molecules of small size to nanoparticles (Praveen et al., 2015). MSINDO, a method based on INDO, has also been applied for nanoparticle calculations (Jug and Wichmann, 2000, Wahab, 2012). INDO/s, a method widely applied for excitation energies and spectroscopy calculation,

has been employed to study electronic properties (Reimers and Hush, 2001), optical properties of silver nanoclusters (Gieseking et al., 2016), carbon nanotube (Furmanchuk et al., 2012) and absorption spectra of TiO_2 nanoparticles (Persson et al., 2000).

2.9 Software Packages for quantum molecular structure calculations

Several computer software packages for *ab-initio* and semi-empirical quantum electronic structures calculations have been developed and implemented. These packages include GAMESS (Guest* et al., 2005), Gaussian, NW-CHEM (Valiev et al., 2010), Q-CHEM (Shao et al., 2015), ORCA (Neese, 2012, 2018), MOPAC (Stewart, 1990), MOLPRO, and so on. While some of these packages are open sources others are not. In particular, the ORCA (Neese, 2012, 2018), a close-source but free code package, has been widely employed for the implementation of DFT, Hartree Fock and post-Hartree Fock methods, and semi-empirical methods. Many semi-empirical methods including AM1, MNDO, PM3, and ZINDO codes have been implemented in ORCA. ORCA implements the ZINDO/1 and ZINDO/2 methods for geometry optimisation and ZINDO/s (also known as INDO/s) for electronic excitations and spectroscopy calculations.

The ZINDO/s executed in the ORCA software has a semi-empirical Hamiltonian which as presented in equations 2.11, 2.12, and 2.13 have the following adjustable Hamiltonian parameters for each atom, where applicable:

1. Interaction factors: $f_{ss\sigma}$, $f_{sp\sigma}$, $f_{sd\sigma}$, $f_{pp\sigma}$, $f_{pd\sigma}$, $f_{dd\sigma}$, $f_{pp\pi}$, $f_{pd\pi}$, $f_{dd\pi}$, and $f_{dd\delta}$
2. Core integral: U_{ss}, U_{pp}, U_{dd} and U_{ff}
3. Basis set parameters:
   (a) Number of Slater type orbitals: N_s, N_p, N_d, and N_f for s, p, d, and f orbitals, respectively.
   (b) Exponents: ζ_{s1}, ζ_{s2}, ζ_{p1}, ζ_{p2}, ζ_{d1}, ζ_{d2}, ζ_{f1} and ζ_{f2} for s, p, d, and f orbitals.
4. Resonance integrals: β_s, β_p, β_d and β_f for s, p, d, and f orbitals, respectively.
5. Number of electrons: N_{el}

6. Gamma parameters(one-center, two electron integrals): γ_{ss}, γ_{sp}, γ_{sd}, γ_{sf}, γ_{pp}, γ_{pd}, γ_{pf}, γ_{dd}, γ_{df}, and γ_{ff}.

7. Slater-Condon parameters: $F2_{pp}$, $F2_{pd}$, $F2_{dd}$, $F4_{dd}$, $G1_{sp}$, $G1_{pd}$, $G2_{sd}$, $G3_{pd}$, $R1_{sppd}$, $R2_{sdpp}$ and $R2_{sddd}$

8. Nuclear interaction parameters: NR_n (n=1, 2, 3, ..., 13)

9. Parameters for spin orbit coupling: SOC_p, SOC_d and SOC_f

Chapter 3

MATERIALS AND METHOD

This chapter gives a detailed report on how the research work was carried out. The materials used for the work include high performance computing (HPC) devices, ORCA 4.0 (Neese, 2012), Amoeba Optimizer (Press et al., 2007), MOPAC 7 (Stewart, 1990), Avogadro, QuantumATK (Stradi et al., 2017), Gnuplot 4.6 (Racine, 2006) and Gabedit 2.5.0 (Allouche, 2008, 2011). For more information on these materials, the reader is referred to appendix A.

In this work, a new method capable of producing accurate excitation energies and absorption spectra for large clusters and quantum dots was developed. It involves parameterising the Intermediate Neglect of Differential Overlap for spectroscopy (INDO/s) Hamiltonian model to reproduce excitation energies for homogeneous diatomics. This new method was tested on silicon, zinc, cadmium, sulphur, zinc sulphide and cadmium sulphide clusters. In the new method which is presented in this thesis:

(i) for a given diatomics e.g Si_2, determine V_e EOM-CCSD excitation energies for different atom-atom separations of the system. We need V_e=8 lowest vertical excitations. We note that, in principle, the EOM-CCSD excitation energies can be replaced by energies from any high-level *ab-initio* method such as GW, BSE, MRCI. While these methods are prohibitive for large systems, the computational resources required for small systems such as diatomics is affordable.

(ii) Parameterise the model Hamiltonian (in this case, INDO/S) to reproduce the *ab-initio* excitation energies calculated in (i) above.

(iii) The one-electron terms U_{ss}, U_{pp}, U_{dd} are shifted in order to reproduce accurate first ionization potential for each atom. This does not change the excitation energies since these are differences in energies and, thus, are not affected by a constant shift of all the energies. However, this shift is important in ensuring transferability when inhomogeneous diatomics (e.g CdS) are being investigated.

Note that:

(i) Since only diatomics are involved, only one and two-center integrals feature in this approach. This is perfectly consistent with the NDDO Hamitonian (sect. 2.3.3.8) which contain terms involving one and two-center integrals (with no three- and four-center integrals in the approximation). Thus, the approach presented captures all the integrals present in NDDO. This is in contrast to common methods which parameterise using data from systems containing more than two atoms. The *ab-initio* data for systems with more than two atoms contain effects from three-center and more (if more than three atoms are in the systems). Thus, parameterising NDDO Hamiltonian to reproduce properties of systems with more than two atoms would force the one and two-center integrals become 'effective parameter' capturing the effect of three- and four-center integrals in an effective or average way. It is clear that this approach would lead to parameters which change with the surrounding atomic configurations i.e. these parameters/models will not typically be transferable. New parameters will be required for different atomic environments.

(ii) As far as we know, this is the first work that parameterises semi-empirical Hamiltonians to the energies of only one and two-atom systems.

(iii) Since the new method presented in this work completely neglects the three- and four-center integrals, when used for clusters with more than two atoms, new terms beyond the NDDO formalism need to be included. This will be the topic for future work (see chapter 5).

(iv) Having obtained the parameters for diatomics, without any changes, these parameters are used for the calculations of properties of clusters with more than two atoms. The performance of these parameters for these kind of clusters shows the extent to which they are transferable parameters.

3.1 Calculation of benchmark excited state energies and UV-Vis absorption spectra from *ab-initio* methods

The semi-empirical Hamiltonian model training (parameterisations) and validation data sets are composed of benchmark excitation energies and absorption spectra from high-level *ab-initio* methods. The high-level *ab-initio* methods employed were EOM-CCSD, for the training on diatomics and TDDFT, and CIS(D) for validation. All calculations were done with a large basis set namely, DEF2-TZVPP basis set (see Ref. (Weigend and Ahlrichs, 2005)). The calculations were performed using the ORCA 4.0 package.

3.1.1 Calculation of excited state energies for dimer geometries

The training data sets used for parameterisations in this work are vertical excitation energies from EOM-CCSD calculations for homogeneous diatomics. The vertical excitation energies calculations were carried out for Si_2, S_2, Cd_2 and Zn_2 of different separations at the EOM-CCSD/DEF2-TZVPP level. (i) For Si_2, the calculations were performed at different separations between 1.8 and 3.0 Å in steps of 0.2 Å with the triplet state of the ground state configurations. Eight lowest vertical excitation energies were obtained for each separation, giving a total of 64 excitations for all eight separations considered. (ii) For S_2, a total of 20 excitation energies were calculated at five different separations from 1.8 and 2.6 Åin steps 0.2 Å. The S_2 excitations were also performed from the triplet ground state configurations. (iii) Cd_2 vertical excitation energies were obtained from singlet ground-state configurations at different separations from 2.0 and 4.0 Å in steps of 0.25 Å. A total of 88 vertical excited state energies were obtained for Cd_2. (iv) For Zn_2, the configurations used are the same as for Cd_2 described above.

3.2 Parameterisation of the ZINDO/s (INDO/s) Hamiltonian model

Using the amoeba optimisation algorithm, the Hamiltonian matrix, H of the Zerner Intermediate Neglect of Differential Overlap for spectroscopy (ZINDO/s) also known as INDO/s (Intermediate Neglect of Differential Overlap for spectroscopy) was parameterised. The ORCA 4.0 software was then used to solve the Fock secular equation fol-

lowed by diagonalisation of the CIS matrix.

The secular equation is given as

$$HC = C\varepsilon, \tag{3.1}$$

where H is the Hamiltonian matrix, C is the orbital coefficient and ε is the orbital energy.

The elements of the Hamiltonian matrix H as detailed in sect. 2.3.3.7 are expressed as:

- H_{aa}: diagonal elements

$$H_{aa} = U_{aa} + \sum_{c} P_{cc}[\langle aa|cc\rangle - \frac{1}{2}\langle ac|ac\rangle] + \sum_{B\neq A}(P_{BB}\gamma_{AB} - Z_B\gamma_{AB}), \tag{3.2}$$

  where U_{aa} is the one center integral, P_{cc} is the density matrix, $\langle aa|cc\rangle$ and $\langle ac|ac\rangle$ are the Coulomb and exchange integrals, respectively. γ_{AB} is the two-center two-electron repulsion integral and Z_B is the atom B effective atomic number.

  P_{BB} is expressed as

$$P_{BB} = \sum_{b\in B} P_{bb} \tag{3.3}$$

$$P_{ab} = 2\sum_{i} C_{ai}C_{bi}, \tag{3.4}$$

  where a, b, and c are atomic orbitals. C_{ai} and C_{bi} are orbital coefficients.

- H_{ab}: where both a and b are on the same atom

$$H_{ab} = \frac{1}{2}P_{ab}[3\langle ab|ab\rangle - \langle aa|bb\rangle] \tag{3.5}$$

- H_{ab}: where a and b are on different atoms A and B, respectively

$$H_{ab} = \frac{1}{2}(\beta_a + \beta_b)S_{ab} - \frac{1}{2}P_{ab}\gamma_{AB}, \tag{3.6}$$

  where β_a and β_b are resonance integrals for atoms A and B, respectively. S_{ab} is the overlap integral calculated using atomic orbitals with exponents, ζ_a and ζ_b for orbitals ψ_a and ψ_b, respectively.

The Hamiltonian matrix adjustable parameters are namely:

1. One-center integral, U_{aa} (a = s, p, d ...)
2. One-center Coulomb integrals ($\langle aa|bb\rangle$ and $\langle aa|cc\rangle$), γ_{ab}
3. Slater Condon parameters (F^0, G^1, F^1, F^2 etc) used in defining one-center exchange integrals ($\langle ab|ab\rangle$ and $\langle ac|ac\rangle$).
4. Bonding parameters, β_a and β_b
5. The gammas (γ_{AA} and γ_{BB}) parameters upon which two-center coulomb integral (γ_{AB}) depend (Mataga and Nishimoto, 1957):

$$\gamma_{AB} = \frac{f(\gamma_{AA} + \gamma_{BB})}{2f + R_{AB}(\gamma_{AA} + \gamma_{BB})} \tag{3.7}$$

   R_{AB} is the separation between atomic centers A and B.
6. Exponents (ζ) of the atomic orbital ($\phi(r) \propto e^{-\zeta r}$)

After solving Eq. 3.1, a CIS calculation is carried out. The CIS is a post-Hartree Fock method whose wavefunction, Ψ is given as

$$\Psi_{CIS} = l_0\Phi_0 + \sum_{i,a} l_i^a \Phi_i^a, \tag{3.8}$$

where Φ_0 and Φ_i^a are the Hartree Fock groundstate wavefunction and singly-excited configuration Slater determinants, respectively Szabo and Ostlund (2012). Excited states are obtained by diagonalizing the CIS matrix, $\mathbf{A}$=$\langle\Psi_{CIS}|\hat{H}|\Psi_{CIS}\rangle$, whose matrix elements for a closed-shell system are given by

$$\mathbf{A}_{ij}^{ab} = \langle\Phi_i^a|\hat{H}|\Phi_j^b\rangle = \delta_{ij}\delta_{ab}(\varepsilon_a - \varepsilon_i) - J_{ia} + 2K_{ia}, \tag{3.9}$$

where ε_j and ε_i are the orbital energies and J_{ij} and K_{ij} are the Coulomb and exchange integrals.

The ZINDO/s Hamiltonian matrix was parameterised with benchmark excitation energies obtained from EOM-CCSD for Si, S, Zn, and Cd diatomics of different separations

(section 3.1.1). The parameters were adjusted to minimize the error function χ^2 given as

$$\chi^2 = \frac{1}{N}\sum_{j=1}^{N}\left|\left|E_j^{\mathrm{f}} - E_j^{\mathrm{a}}\right| - \varepsilon\right|. \tag{3.10}$$

The set of parameters that minimizes χ^2 were chosen as the optimised parameters and the mean absolute errors were calculated using

$$MAE = \frac{1}{N}\sum_{j=1}^{N}\left|E_j^{\mathrm{f}} - E_j^{\mathrm{a}}\right|, \tag{3.11}$$

where $E_j^f and E_j^a$ are the jth excitation energies from the fit and *ab-initio* calculations, respectively, N is the total number of *j*th excitation energies and ε gives the extent of the accuracy to be achieved.

For Si_2 and S_2, eleven parameters each were optimised, namely U_{ss}, Upp, ζ_s, ζ_p , β_s, β_p, γ_{ss}, γ_{sp}, γ_{pp}, G_{sp} and F_s. N=64 for Si_2 and 20 for S_2. The value of ε was set equal to 0.1 eV for both Si_2 and S_2 .

Twenty-four and twenty-five parameters were optimised for Zn_2 and Cd_2, respectively. The parameters include U_{ss}, U_{pp}, U_{dd}, ζ_s, ζ_p, ζ_d, β_s, β_p, β_d, γ_{ss}, γ_{sp}, γ_{pp}, γ_{sd}, γ_{pd}, γ_{dd}, $G1_{sp}$, $G1_{pd}$, $G2_{sd}$, $G3_{pd}$, $F2_{pp}$, $F2_{pd}$, $F2_{dd}$ and $F4_{dd}$. N=88 excitations and ε =0.0 eV for each of Zn_2 and Cd_2.

As mentioned in sect. 2.9, the third and final step of this new method is to shift U_{ii} (i =s, p, d) in order to reproduce first ionization potentials. During the parameterisation, the U_{ii} (i=s,p,d) were not directly optimised but their differences, U_{pp} -U_{ss} and U_{dd} -U_{ss} were. Keeping the differences constant ($U_{pp} - U_{ss}$ and $U_{dd} - U_{ss}$), U_{ii} (i=s, p, d) were optimised to reproduce the first ionization potential (IP) obtained with Coupled-Cluster Singles and Doubles (CCSD)/DEF2-TZVPP for Si, S, Zn, and Cd. Ionization potential (IP) was obtained as follows:

$$IP = E(M) - E(M-1) \tag{3.12}$$

Where $E(Y)$ is the energy of the atom/ion with Y electrons.

Following the parameterisations and shifting of the U_{ii} (i=s,p,d) parameters of the ZINDO/s (INDO/s) Hamiltonian, the newly obtained model was called optimised for excitation Intermediate Neglect of Differential Overlap (oeINDO). The parameters for all the systems studied in this work are listed in chapter four. However, more importantly, the method used is described in this thesis and can be engaged for developing parameters for other atoms.

3.3 Validation of the oeINDO

An important question to ask is, is the newly obtained Hamiltonian model (i.e oeINDO model) transferable? That is, can the new model give accurate results for geometries that were not used during the parameterisation? To verify the transferability of the oeINDO, calculation of the excitation energies and absorption spectra were carried out with the oeINDO model for complex homo-nuclear and hetero-nuclear geometries not included in the training geometry sets. The geometries considered were Si_n (n=3, 4, 5, 19, 40), S_n (n=3, 5, 6, 10, 20), Zn_n (n=3, 4, 6, 8, 16, 24), Cd_n (n=3, 4, 6, 8, 16), $(ZnS)_n$ (n=2, 3, 4, 10), $(CdS)_n$ (n=2, 3, 4, 10) and $Cd_xZn_yS_{19}$ (x=5, 10, 15; y=14, 9, 4). (See next section 3.3.1 below for how the structures were obtained) The same calculations were performed with the original ZINDO/s model. The oeINDO and ZINDO/s results obtained were compared with those obtained from EOM-CCSD. For larger atomic clusters for which EOM-CCSD is expensive, oeINDO and ZINDO/s results were compared with those from TDDFT and CIS(D). MAEs (equation 3.11) were computed to compare results. Gnuplot and Gabedit were employed to visualize and plot excitation energies and UV-VIS absorption spectra.

3.3.1 Calculation of excited state energies and Ultraviolet-Visible (UV-Vis) absorption spectra for complex structures

To obtain the semi-empirical Hamiltonian validation data sets, excitations and absorption spectra were computed with high-level methods for complex structures outside the training structures (diatomics). The calculations were performed both for homo-nuclear and hetero-nuclear complex structures using EOM-CCSD, B3LYP/TDDFT and CIS(D)

with large basis set DEF2-TZVPP. The homo-nuclear structures include Si_n (n=3, 4, 5, 19, 40), S_n (n=3, 5, 6, 10, 20), Zn_n (n=3, 4, 6, 8, 16, 24) and Cd_n (n=3, 4, 6, 8, 16) while the hetero-nuclear structure considered were $(ZnS)_n$ (n=2, 3, 4, 10) and $(CdS)_n$ (n=2, 3, 4,10). For large structures, EOM-CCSD is prohibitively expensive and so, only TDDFT and CIS(D) were employed for their calculations. EOM-CCSD calculations were performed only for Si_n (n=3, 4, 5), S_n (n=3, 5), Zn_n (n=3, 4) and Cd_4. The structures chosen were the equilibrium structures for these complexes. The equilibrium structures of some of the atomic clusters were sourced from Literature while others were obtained by carrying out geometry optimisation using *ab-initio* or semi-empirical methods. The equilibrium structure of Si_n n=3, 4, 5, 19, 40, 148 and S_n n= 3,4, 5, 6, 10, 20 (where n is the number of atoms) were sourced from literatures (Raghavachari, 1986, Raghavachari and Rohlfing, 1988, Tam et al., 2015, Jin et al., 2015, Jackson and Jellinek, 2016). The equilibrium structures of Zn, Cd, ZnS, and CdS clusters and quantum dots were obtained by performing geometry optimisation calculations.

3.3.2 Geometry Optimisation

The geometry optimisation for Zn_n (n= 3, 4, 6, 8, 16, 24) and Cd_n (n= 3, 4, 6, 8, 16, 20) clusters were carried out by first generating their starting geometry coordinates using the Avogadro software. The geometries obtained were then optimised using the three-parameters functional of Becke, Lee Yang and Parr (B3LYP) (Becke, 1993) and the valence triple-zeta with two sets of polarization functions (DEF2-TZVPP) basis sets (Weigend and Ahlrichs, 2005). The vibrational frequencies of each optimised structure were computed to ascertain that the structure obtained was a global minimum. These calculations were performed using ORCA 4.0. For quantum dots of Si, Zn, Cd, S, ZnS, and Cds, the starting geometries were built from the builder Wulff constructor in quantumATK software. For large atomic clusters like quantum dots, geometry optimisations with *ab-initio* (e.g B3LYP/TZVPP or even with smaller basis sets) are computationally expensive. Hence, the computationally cheap and moderately accurate semi-empirical, PM7 (Hostavs et al., 2013), was employed in carrying out geometry optimisation calculations for quantum dots. These calculations were performed using PM7 as executed in the MOPAC7 package.

3.4 Study of large atomic clusters and quantum dots using the oeINDO model

After the validation of the oeINDO model, it was employed to calculate and predict excitation energies and UV-VIS absorption spectra for Si, S, Zn, Cd, ZnS, CdS and CdZnS large clusters and quantum dots. Also, it was employed to predict theoretical optimal size and shape of ZnS and CdS quantum dots for solar cell applications. The Gnuplot and Gabedit were used to visualize and plot absorption spectra plots.

Chapter 4

RESULTS and DISCUSSION

4.1 Results of Parameterization

The results of the parameterisations of the INDO/s Hamiltonian model using excitation energies obtained from EOM-CCSD/DEF2-TZVPP for diatomics are presented in Figures 4.1, 4.2, 4.3, and 4.4. The figures are scatter plots of excitation energies obtained from the optimised INDO/s (oeINDO) and unoptimised INDO/s (ZINDO/s) in comparison with EOM-CCSD (the benchmark) for Si_2, S_2, Zn_2 and Cd_2. The blue circles in these figures represent excitation energies from oeINDO while the red plus signs represent ZINDO/s excitations. The straight green line represents excitation energies from EOM-CCSD.

The Mean Absolute Error (MAE) was computed for sets of points (excitation energies). So that, if the MAE of a particular set of points is zero relative to the benchmark, then, the points lie exactly on the straight green line in the figure.

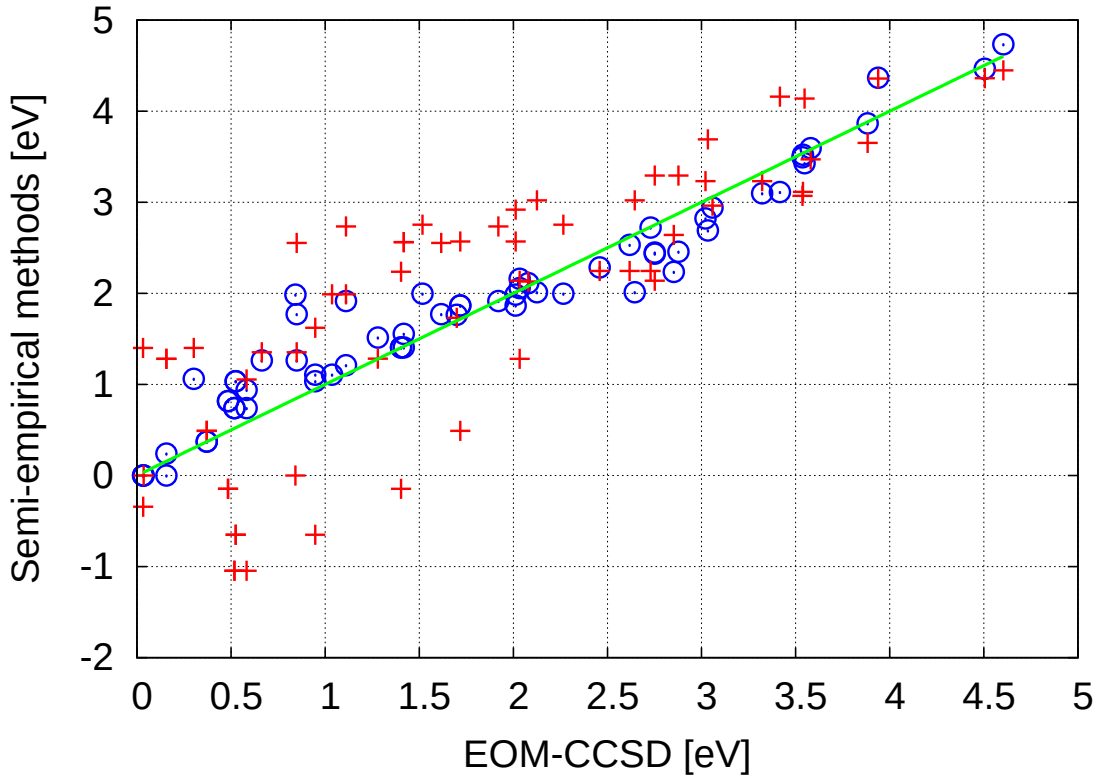

Figure 4.1: A scatter plot of Si_2 excitation energies obtained using ZINDO/s and oeINDO against those from EOM-CCSD (the benchmark). The blue circles are the oeINDO excitation energies while the red plus signs are the ZINDO/s excitation energies. The straight green line represent the benchmark.

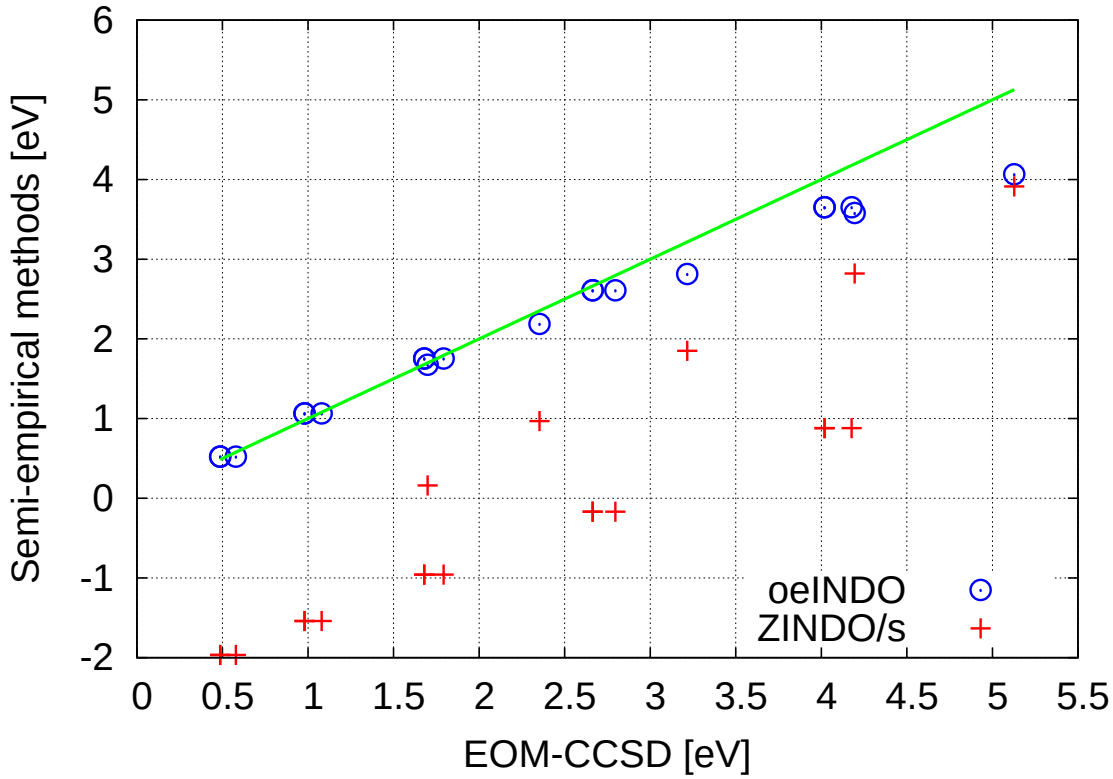

Figure 4.2: Scatter plot of S_2 excitation energies obtained using ZINDO/s and oeINDO against those from EOM-CCSD (the benchmark). The blue circles are the oeINDO excitation energies while the red plus signs are the ZINDO/s excitation energies. The straight green line represents the benchmark.

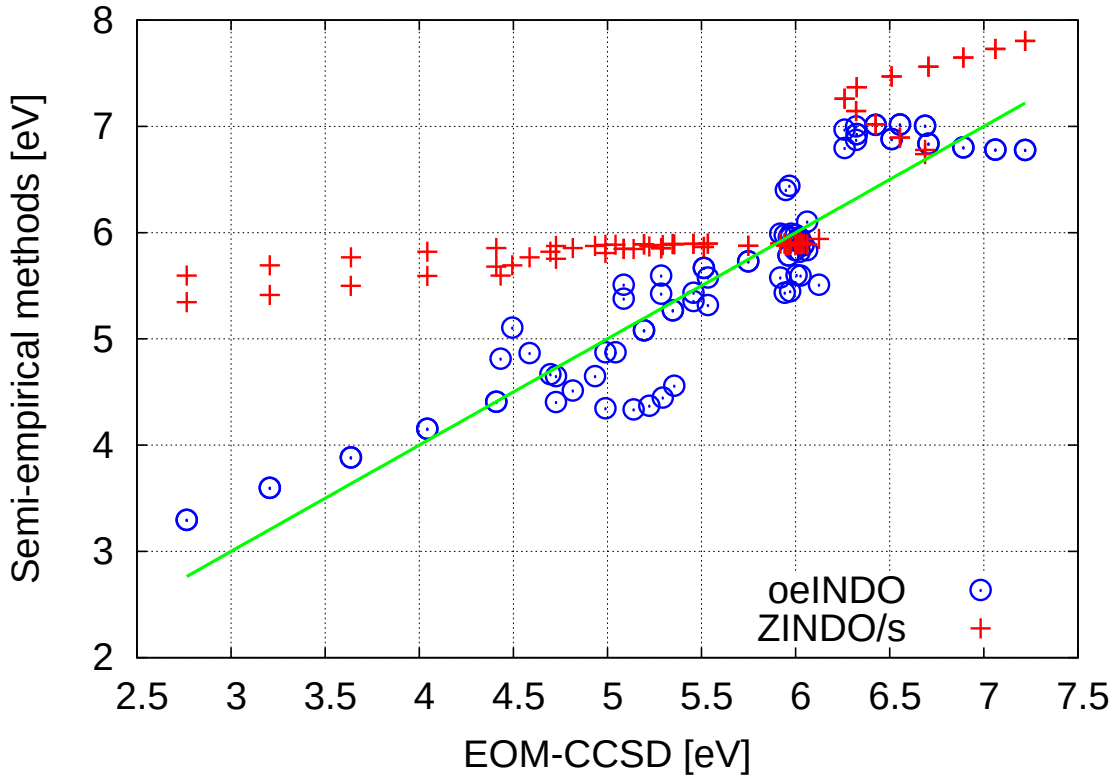

Figure 4.3: Scatter plot of Cd_2 excitation energies obtained using ZINDO/s and oeINDO against those from EOM-CCSD (the benchmark). The blue circles are the oeINDO excitation energies while the red plus signs are the ZINDO/s excitation energies. The straight green line represents the benchmark.

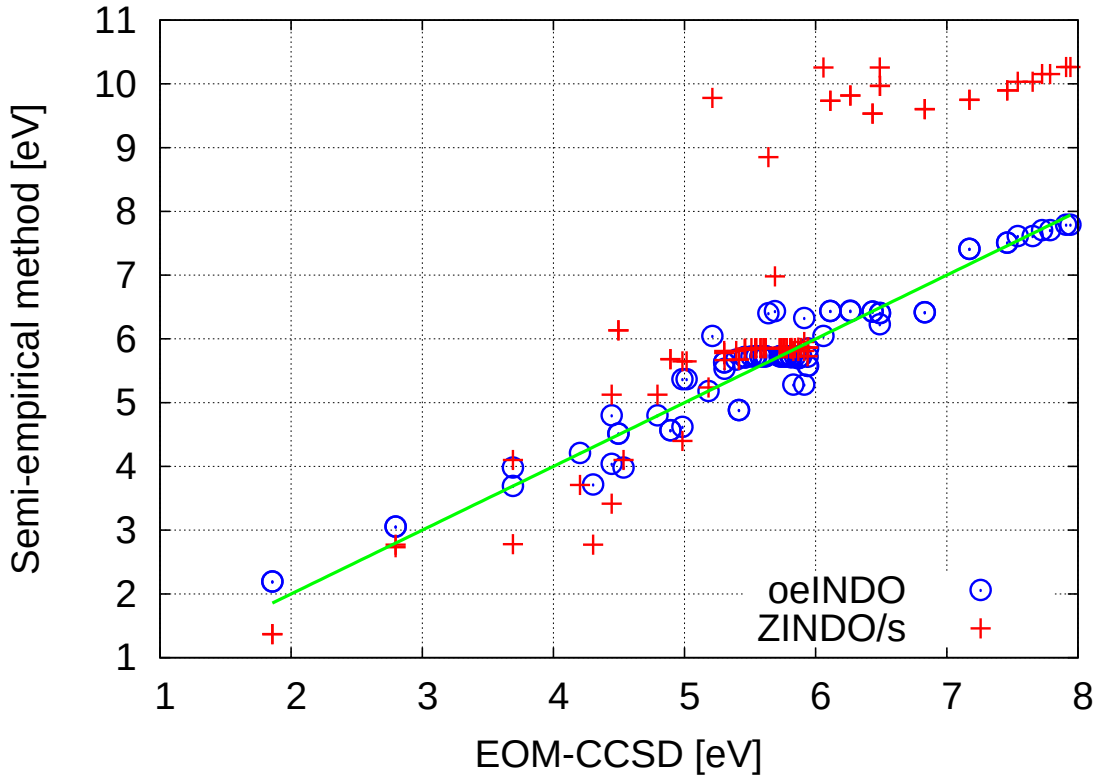

Figure 4.4: Scatter plot of Zn_2 excitation energies obtained using ZINDO/s and oeINDO against those from EOM-CCSD (the benchmark). The blue circles are the oeINDO excitation energies while the red plus signs are the ZINDO/s excitation energies. The straight green line represents the benchmark.

Figure 4.1 is a scatter plot of 64 excitation energies each obtained using oeINDO and ZINDO/s against those from EOM-CCSD for Si_2. It can be observed from the figure that the oeINDO energies (blue circles) agree reasonably well with the EOM-CCSD energies (the straight green line). Also, the oeINDO energies are closely matched than the ZINDO/s energies (red plus signs) to the EOM-CCSD energies. The MAE of the oeINDO energies as compared with those from EOM-CCSD was computed to be 0.21 eV while that for ZINDO/s was computed to be 0.87 eV (about four times the error observed in oeINDO). Also, ZINDO/s produced some negative excitation energies which are not acceptable because excitation energy is the difference between the energy of the unoccupied electronic state (higher energy) and the occupied electronic state (lower energy).

Figure 4.2 is a scatter plot of excitation energies of sulphur diatomics produced with oeINDO and ZINDO/s and compared with EOM-CCSD excitation energies. The figure shows that excitation energies calculated with oeINDO matched well and better than ZINDO/s excitation energies to the EOM-CCSD ones. The MAE of the oeINDO excitation energies relative to those from EOM-CCSD is calculated to be 0.19 eV. The ZINDO/s excitation energies, however, deviate from those of EOM-CCSD with a large error of 2.38 eV. It can also be observed that ZINDO/s gave negative excitations at some dimer separations, which are unacceptable.

For Cd_2 geometries (Figure 4.3), oeINDO excitation energies (blue circles) were also found to align more closer than ZINDO/s energies (red plus signs) to the EOM-CCSD energies (straight green line). The MAE of oeINDO energies relative to those of EOM-CCSD is 0.29 eV. However, ZINDO/s energies deviate more with MAE 0.67 eV (over twice the error noticed for oeINDO).

Figure 4.4 presents a total of 88 excitation energies each obtained with oeINDO and ZINDO/s for Zn_2 geometries and compared with those from EOM-CCSD (benchmark). From the figure, the blue circles (oeINDO energies) are found to match closer to the straight green line (EOM-CCSD energies) than the red plus signs (ZINDO/s energies). The oeINDO matches with MAE 0.22 eV while ZINDO/s matches with a larger error of MAE 1.09 eV.

Table 4.1: MAEs of excitation energies (eV) from ZINDO/s and oeINDO relative to EOM-CCSD energies for various diatomics

Diatomics	oeINDO	ZINDO/s
Si_2	0.21	0.87
S_2	0.19	2.38
Zn_2	0.22	1.09
Cd_2	0.29	0.67

A summary of the MAEs of oeINDO and original INDO/s excited state energies relative to EOM-CCSD excited state energies for the different diatomic systems are given in Table 4.1. On the average, the oeINDO energies compare with EOM-CCSD energies with a typical error of 0.23 eV while ZINDO/s energies deviate with a larger MAE of 1.25 eV.

After the parameterisations, the one center integrals, U_{ii} were shifted to reproduce first ionization potential (IP) at CCSD/DEF2-TZVPP level. First ionization potentials of silicon, zinc, cadmium and sulphur calculated at CCSD/DEF2-TZVPP level are 8.069, 8.8971, 8.665, and 12.363 eV, respectively. The shift of U_{ss} and U_{pp} produced silicon atom first IP of value 8.069 eV which compares well with the experimental value of 8.1517 eV. However, for Zn and Cd atoms, the shift in U_{ss}, U_{pp} and U_{dd} produced IPs with the error of about 1.1 eV relative to IPs calculated with CCSD/DEF2-TZVPP.

The parameters of ZINDO/s and the one obtained from the parameterisations of INDO/s (oeINDO) are presented in the following Tables 4.2- 4.5 and discussed.

Table 4.2: ZINDO/s and oeINDO parameters for Si_2

Parameters	ZINDO/s	oeINDO
ζ_s	1.52 bohrs	1.430753 bohrs
ζ_p	1.52 bohrs	1.411963 bohrs
U_{ss}	-36.235929 eV	-25.4244 eV
U_{pp}	-28.594917 eV	-13.6400 eV
β_s	13.0 eV	29.06189 eV
β_p	13.0 eV	9.052134 eV
γ_{ss}	7.57 eV	2.311795 eV
γ_{sp}	7.57 eV	2.311795 eV
γ_{pp}	7.57 eV	2.311795 eV
F^2_{pp}	2.2627 eV	1.750264 eV
G_{sp}	4.8122 eV	3.132682 eV

Table 4.3: oeINDO and ZINDO/s parameters for S_2

Parameters	oeINDO	ZINDO/s
U_{ss}	-39.7751 eV	-36.235929 eV
U_{pp}	-33.2246 eV	-28.594917 eV
ζ_s	2.169004 bohrs	1.52 bohrs
ζ_p	1.586553 bohrs	1.52 bohrs
β_s	11.524900 eV	13.0 eV
β_p	12.301215 eV	13.0 eV
γ_{ss}	6.013544 eV	7.57 eV
γ_{sp}	6.013544 eV	7.57 eV
γ_{pp}	6.013544 eV	7.57 eV
F^2_{pp}	6.431554 eV	2.2627 eV
G_{sp}	3.455990 eV	4.8122 eV

Table 4.4: oeINDO and ZINDO/s parameters for Zn_2

Parameters	oeINDO	ZINDO/s
U_{ss}	-111.667 eV	-110.620093 eV
U_{pp}	-105.918 eV	-105.224805 eV
U_{dd}	-159.416 eV	-161.738551 eV
ζ_s	1.561604 bohrs	1.5090 bohrs
ζ_p	1.417918 bohrs	1.5090 bohrs
ζ_d	3.645080 bohrs	4.6261 bohrs
β_s	10.184300 eV	10.0 eV
β_p	4.392070 eV	10.0 eV
β_d	33.844518 eV	34.0 eV
γ_{ss}	5.172389 eV	7.98 eV
γ_{sp}	5.172389 eV	7.98 eV
γ_{pp}	5.172389 eV	7.98 eV
γ_{sd}	9.930301 eV	9.39 eV
γ_{pd}	9.930301 eV	9.39 eV
γ_{dd}	14.589140 eV	14.55 V
F^2_{pp}	1.386388 eV	1.1778 eV
F^2_{pd}	1.497962 eV	1.4878 eV
F^2_{dd}	10.747871 eV	11.4063 eV
F^4_{dd}	10.088581 eV	7.6249 eV
$G1_{sp}$	2.159041 eV	2.5292 eV
$G1_{pd}$	1.091506 eV	0.8679 eV
$G2_{sd}$	0.533253 eV	0.6199 eV
$G3_{pd}$	1.275683 eV	0.9919 eV

Table 4.5: oeINDO and ZINDO/s parameters for Cd_2

Parameters	oeINDO	ZINDO/s
U_{ss}	-88.9433 eV	-110.620093 eV
U_{pp}	-83.5324 eV	-105.224805 eV
U_{dd}	-117.034 eV	-161.738551 eV
ζ_s	1.784273 bohrs	1.5090 bohrs
ζ_p	1.586890 bohrs	1.5090 bohrs
ζ_{d1}	5.565263 bohrs	4.6261 bohrs
ζ_{d2}	2.818233 bohrs	4.6261 bohrs
β_s	8.743760 eV	10.0 eV
β_p	5.270200 eV	10.0 eV
β_d	32.520550 eV	34.0 eV
γ_{ss}	5.820365 eV	7.98 eV
γ_{sp}	5.820365 eV	7.98 eV
γ_{pp}	5.820365 eV	7.98 eV
γ_{sd}	7.632756 eV	9.39 eV
γ_{pd}	7.632756 eV	9.39 eV
γ_{dd}	10.301339 eV	14.55 eV
F^2_{pp}	2.848384 eV	1.1778 eV
F^2_{pd}	1.338146 eV	1.4878 eV
F^2_{dd}	6.415983 eV	11.4063 eV
F^4_{dd}	4.067983 eV	7.6249 eV
$G1_{sp}$	3.630364 eV	2.5292 eV
$G1_{pd}$	0.769576 eV	0.8679 eV
$G2_{sd}$	0.561897 eV	0.6199 eV
$G3_{pd}$	0.463479 eV	0.9919 eV

The oeINDO and the original ZINDO/s parameters for silicon, sulphur, zinc and cadmium are presented in Tables 4.2, 4.3, 4.4, and 4.5, respectively. A total of 11 parameters each were optimised for Si_2 and S_2 , 23 parameters for Zn_2 and 24 parameters for Cd_2.

The new set of parameters (oeINDO) for silicon atoms are different from those of the original ZINDO/s (see Table 4.2). For the ZINDO/s, the exponents, ζ_s and ζ_p are equal. Also, the bonding parameters, β_s and β_p have equal values. However, for oeINDO, ζ_s and ζ_p are slightly different while the β_s and β_p largely differ in values. The values of γ parameters (parameters upon which the two center one electron integrals depend) for oeINDO are less than those of original ZINDO/s. The difference between U_{ss} and U_{pp} is $\approx 12\ eV$ for oeINDO and $\approx 8\ eV$ for ZINDO/s. The difference between the F^2 parameters of oeINDO and ZINDO/s is $\approx 0.5\ eV$ and between their G^1 parameters is $\approx 1.7\ eV$, respectively .

Significant differences were also observed in oeINDO and ZINDO/s parameters for sulphur atom (see Table 4.3). The difference between the U_{ss} and U_{pp} is $\approx 6\ eV$ for oeINDO and $\approx 8\ eV$ for ZINDO/s. The values exponents (ζ) are equal for ZINDO/s but differ significantly for oeINDO. The bonding parameters (βs) differ by $\approx 0.7\ eV$ for oeINDO but are equal for ZINDO/s. The values of γs for oeINDO are less than those of ZINDO/s by $\approx 1.5\ eV$

For a zinc atom, a significant difference of about 5.6 eV was observed between oeINDO and ZINDO/s p-orbital bonding parameters. Also, their *gamma* parameters differ by about 2.8 eV.

For cadmium, the oeINDO β, γ, and ζ_d deviate significantly from those of ZINDO/s. The differences between the one center electron integral U_{ss} and U_{dd} are $\approx 28\ eV$ for oeINDO and $\approx 51\ eV$ for ZINDO/s.

Significant deviations were observed in the values of oeINDO parameters from the original ZINDO/s ones and this is responsible for the good performance of oeINDO in reproducing the EOM-CCSD energies for diatomics with a minimal error.

4.2 Validation of the oeINDO model

The parameters obtained for the oeINDO model as presented in Tables 4.3, 4.4, 4.5 and 4.2 were validated by verifying their transferability and accuracy for complex geometries not included in training geometry sets. To achieve these, excitation energies and absorption spectra obtained for complex equilibrium geometries/structures using oeINDO and ZINDO/s were compared with excitation energies and spectra from *ab-initio* methods (EOM-CCSD, TDDFT and CIS(D)).

4.2.1 Equilibrium Structures

This subsection gives information about the complex structures employed for the new model validation and predictions. Both homogeneous and heterogeneous structures were considered. The small- and medium-sized homogeneous equilibrium structures include Si_n (n= 148, 40, 19, 5, 4, 3,), S_n (n= 20, 10, 6, 5, 4, 3), Zn_n (n=3, 4, 6, 8, 16, 24), and Cd_n (n=3, 4, 6, 8, 16). The small- and medium-sized heterogeneous equilibrium structures are $(ZnS)_n$, $(CdS)_n$ (n=2, 3, 4, 10) and $Cd_xZn_yS_{19}$. For nano-sized systems (quantum dots), the homogeneous and heterogeneous structures used for predictions with the new model have sizes ranging from 0.8-3.0 nm (38-779 atoms).

The Si_n (n= 148, 40, 19, 5, 4, 3,) and S_n (n= 20, 10, 6, 5, 4, 3) equilibrium geometries and ground-state configurations were sourced from Literature (Tam et al., 2015, Raghavachari, 1986, Raghavachari and Rohlfing, 1988, Jin et al., 2015, Jackson and Jellinek, 2016). The equilibrium silicon nano-sized structures were obtained from geometry optimisation calculations using PM 7 and presented in Figure B.5 in the appendix. The structure sizes are 1.6 nm (a structure with 128 silicon atoms), 1.8 nm (190 silicon atoms), 2.0 nm (244 silicon atoms) and 3.0 nm (779 silicon atoms).

Equilibrium structures obtained for Zn_n (n=3, 4, 6, 8, 16 24) clusters at the b3lyp/def2-tzvpp level are presented in the appendix in Figure B.1. Equilibrium Zn_3 and Zn_4 clusters were observed to be equilateral and tetragonal in shape, respectively. The optimised zinc nano-clusters (quantum dots) obtained at the PM7 level are namely 1.0 nm zinc cluster (containing 38 zinc atoms), 1.2 nm (62 zinc atoms), 1.4 nm (104 zinc atoms), 1.6 nm (128 zinc atoms), 1.8 nm (190 zinc atoms) and 2.0 nm (244 zinc atoms), and are

presented in Figure B.3.

The Cd_n (n=3, 4, 6, 8, 16) equilibrium structures obtained, are shown in Figure B.2 in the appendix. The equilibrium Cd_3 and Cd_4 clusters assumed equilateral and tetragonal shapes, respectively. The sizes of the optimised Cd nano-clusters at the level of PM7 are in the range of 1.0 - 2.0 nm.

Different nano-sized structures obtained at the PM7 level for sulphur, cadmium sulphide and zinc sulphide are shown in Figures B.4, B.7 and B.6, respectively. The sizes of sulphur quantum dots range from 1.0 to 2.0 nm. For cadmium sulphide, the range of the dot sizes is 1.0 to 2.2 nm while for zinc sulphide quantum dots, the sizes are 1.0, 1.2, 1.4, 1.8, 2.0 and 2.2 nm.

4.2.2 Transferability of oeINDO silicon parameters

In order to verify how accurate the oeINDO silicon parameters were, its eight lowest excited state energies were compared with benchmark for Si_n (n = 3, 4, 5, 19, 40). The first eight lowest excited state energies of Si_n (n = 3, 4, 5, 19, 40) were computed with EOM-CCSD, TDDFT, CIS(D), oeINDO and ZINDO/s and presented in Tables 4.6, 4.8, 4.9, 4.10 and 4.11. The values from these Tables were presented as scatter plots in Figure 4.11 and the mean absolute errors (MAEs) were computed and summarized in Tables 4.7 and 4.12 . Also, UV-vis absorption spectra, which are displayed in Figures 4.5, 4.6, 4.7, 4.8, and 4.9 were used to further validate the oeINDO model.

Table 4.6: First Eight Lowest Excited State Energies (eV) for Si_3

EOM-CCSD	oeINDO	INDO/s	TDDFT	CIS(D)
1.406	1.310	−0.047	1.267	1.447
1.478	1.342	2.258	1.343	1.653
1.981	1.497	2.797	1.896	2.118
2.197	2.316	3.292	2.142	2.307
2.583	2.458	3.630	2.475	2.787
2.998	2.538	3.875	3.026	3.230
3.494	3.211	4.274	3.364	3.965
3.619	3.342	4.341	3.535	3.995

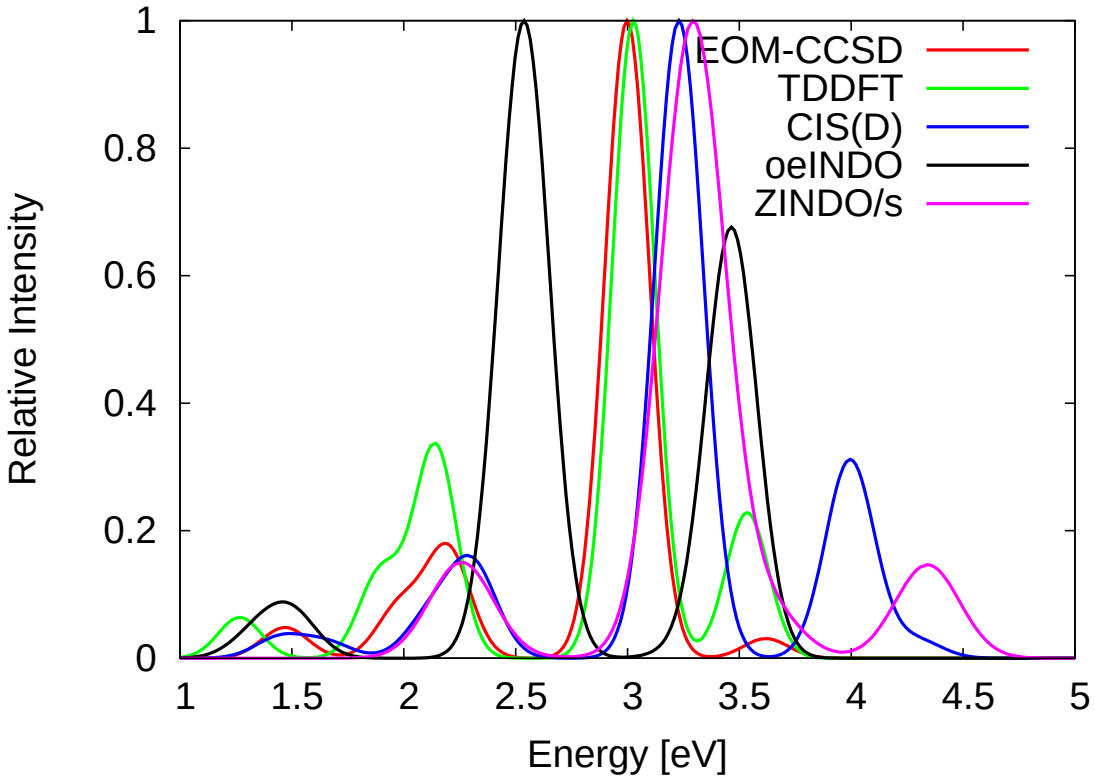

Figure 4.5: Absorption spectra for Si_3 equilibrium geometry obtained from different methods. The intensities have been scaled so that the highest intensity is equal to unity.

Table 4.7: MAEs in eV of semi-empirical methods, CIS(D) and TDDFT from *ab-initio* methods for Si equilibrium geometries

Methods	EOM-CCSD	TDDFT	CIS(D)
	Si_3		
oeINDO	0.22	0.17	0.39
ZINDO/s	0.92	0.98	0.74
TDDFT	0.07	-	-
CIS(D)	0.20	-	-
	Si_4		
oeINDO	0.18	0.24	0.31
ZINDO/S	1.38	1.71	1.25
TDDFT	0.12	-	-
CIS(D)	0.29	-	-
	Si_5		
oeINDO	0.09	0.04	0.16
ZINDO/S	1.47	1.52	1.39
TDDFT	0.09	-	-
CIS(D)	0.05	-	-
	Si_{19}		
oeINDO	-	0.32	0.36
ZINDO/S	-	1.42	1.46
	Si_{40}		
oeINDO	-	0.12	0.03
ZINDO/S	-	0.68	0.80

Table 4.8: First Eight Lowest Excited State Energies (eV) for Si_4

EOM-CCSD	oeINDO	INDO/s	TDDFT	CIS(D)
1.580	1.451	2.722	1.499	1.622
1.836	1.514	3.423	1.579	1.882
2.300	2.257	3.937	2.184	2.450
2.958	2.520	3.980	2.716	3.187
3.047	2.894	4.204	2.905	3.307
3.179	3.057	4.526	2.976	3.311
3.197	3.113	4.581	3.152	3.873
3.539	3.185	5.516	3.448	4.518

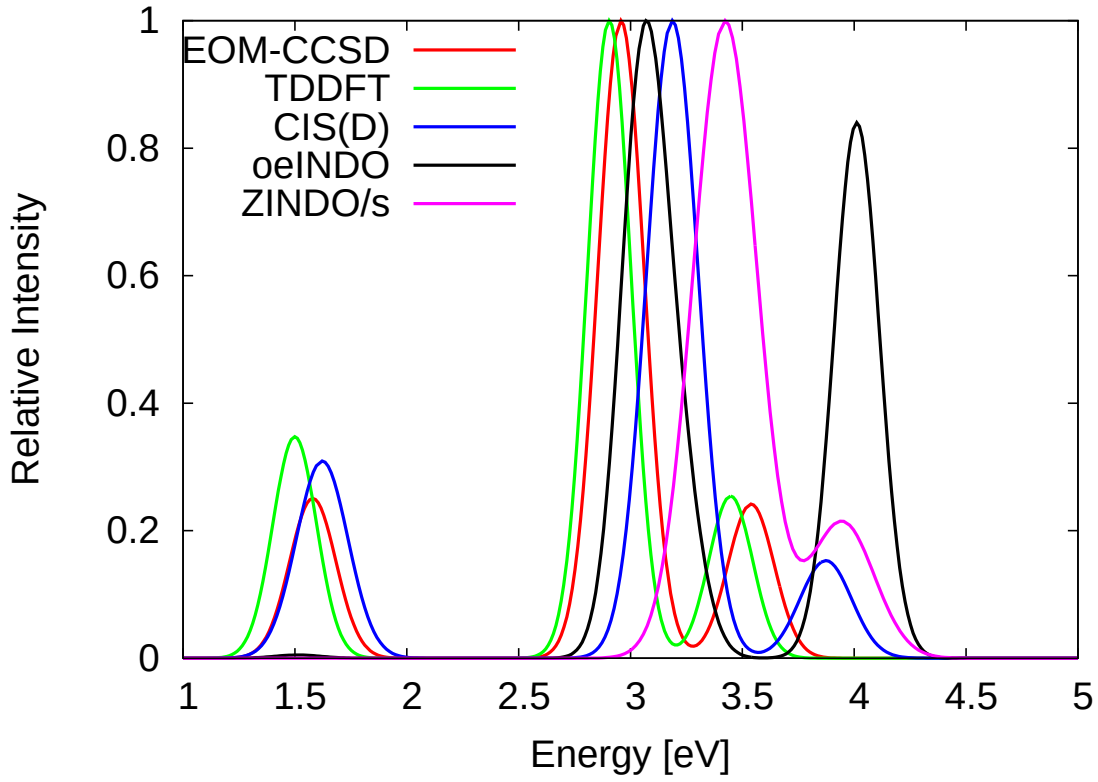

Figure 4.6: Absorption spectra of Si_4 equilibrium geometry obtained from different methods. The intensities have been scaled so that the highest intensity is equal to unity.

Considering the first eight lowest vertical excited energies for Si_3 equilibrium structure presented in Table 4.6, the first lowest excited state energy of oeINDO (1.31 eV) as well as those from TDDFT (1.27 eV) and CIS(D)(1.45 eV) compared well with the 1.40 eV, first excited state from EOM-CCSD (the benchmark). The ZINDO/s energy is however much deviated and gives negative excitation energy value of -0.047 eV, which is unacceptable. The MAE (see Table 4.7) calculated for the eight excitation energies from oeINDO compared to the EOM-CCSD ones was 0.22 eV. The ZINDO/s excitations, however, compared with EOM-CCSD excitations with a large MAE of 0.98 eV. Table 4.7 shows that *ab-initio* methods (TDDFT and CIS(D)) agree with EOM-CCSD with MAE 0.07 eV and 0.20 eV, respectively. In comparison with other *ab-initio* methods, oeINDO excitations compared with TDDFT and CIS(D) excitations with MAEs 0.17 eV and 0.39 eV, respectively. Figure 4.5 shows the absorption spectra from EOM-CCSD, oeINDO, CIS(D), TDDFT and ZINDO/s for Si_3 structure. The oeINDO spectrum agrees reasonably with that of EOM-CCSD. The highest peak of oeINDO is *red-shifted* by about 0.50 eV from that of EOM-CCSD.

The oeINDO reproduced the EOM-CCSD first eight lowest excitations energies (table 4.8) with MAE 0.18 eV (Table 4.7) for the Si_4 equilibrium structure. Relative to EOM-CCSD, although oeINDO error is slightly higher than that of TDDFT (MAE=0.12 eV), it performs better than the *ab-initio*, CIS(D) (MAE=0.29 eV). The excitation energies from the original ZINDO/S deviate much from those from EOM-CCSD with MAE of 1.38 eV. The first excited state energy (Table 4.8) from oeINDO (1.45eV) shows good agreement with that of the benchmark, EOM-CCSD (1.58 eV). The TDDFT and CIS(D) energies 1.50 and 1.62 eV, respectively are also in good agreement with the EOM-CCSD one. Absorption spectra plots for Si_4 equilibrium structure in Figure 4.6, show that oeINDO agrees better than CIS(D) (*ab-initio*) to EOM-CCSD. The highest peak of oeINDO is *blue-shifted* from that of EOM-CCSD by 0.11 eV while ZINDO/s and CIS(D) peaks are *blue-shifted* with a larger error of 0.46 eV and 0.22 eV, respectively. TDDFT spectrum shows a good match with the EOM-CCSD one with error < 0.1 eV.

Table 4.9: First Eight Lowest Excited State Energies (eV) for Si_5

EOM-CCSD	oeINDO	INDO/s	TDDFT	CIS(D)
2.535	2.465	3.445	2.470	2.557
2.575	2.466	3.445	2.622	2.619
2.794	2.657	4.097	2.655	2.844
2.844	2.687	4.380	2.749	2.905
2.844	2.770	4.380	2.749	2.905
2.859	2.770	4.666	2.759	2.988
2.859	2.835	4.983	2.759	2.988
3.097	2.835	4.983	2.824	3.209

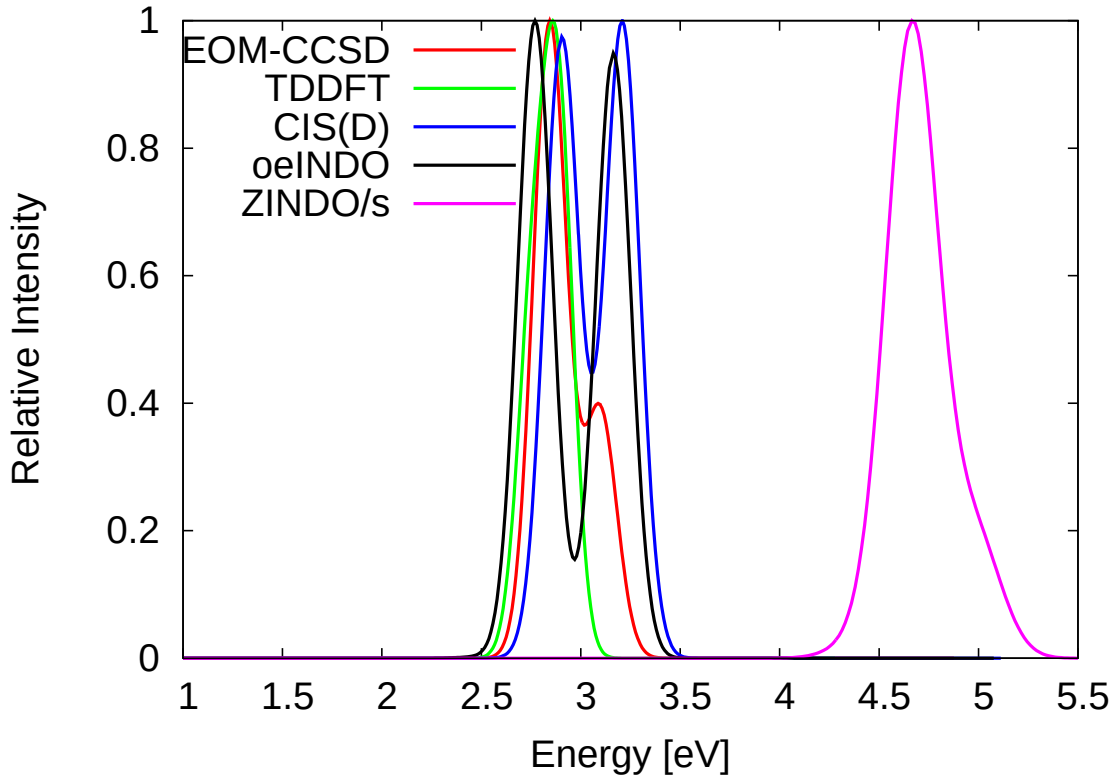

Figure 4.7: Absorption spectra for Si_5 equilibrium geometry obtained from different methods.. The intensities have been scaled so that the highest intensity is equal to unity.

Table 4.10: First Eight Lowest Excited State Energies (eV) for Si_{19}

oeINDO	INDO/s	TDDFT	CIS(D)
1.649	2.447	1.773	1.761
1.731	2.769	1.927	1.830
2.390	3.452	1.993	1.931
2.482	3.639	2.100	2.021
2.613	3.861	2.108	2.077
2.638	3.948	2.175	2.081
2.670	3.979	2.234	2.272
2.703	4.026	2.265	2.322

Table 4.11: First Eight Lowest Excited State Energies (eV) for Si_{40}

oeINDO	INDO/s	TDDFT	CIS(D)
0.394	1.221	0.722	0.318
0.420	1.348	0.848	0.540
0.581	1.384	0.932	0.587
0.614	1.434	1.072	0.694
0.689	1.491	1.089	0.707
0.754	1.641	1.126	0.767
0.802	1.649	1.133	0.839
0.818	1.740	1.189	0.877

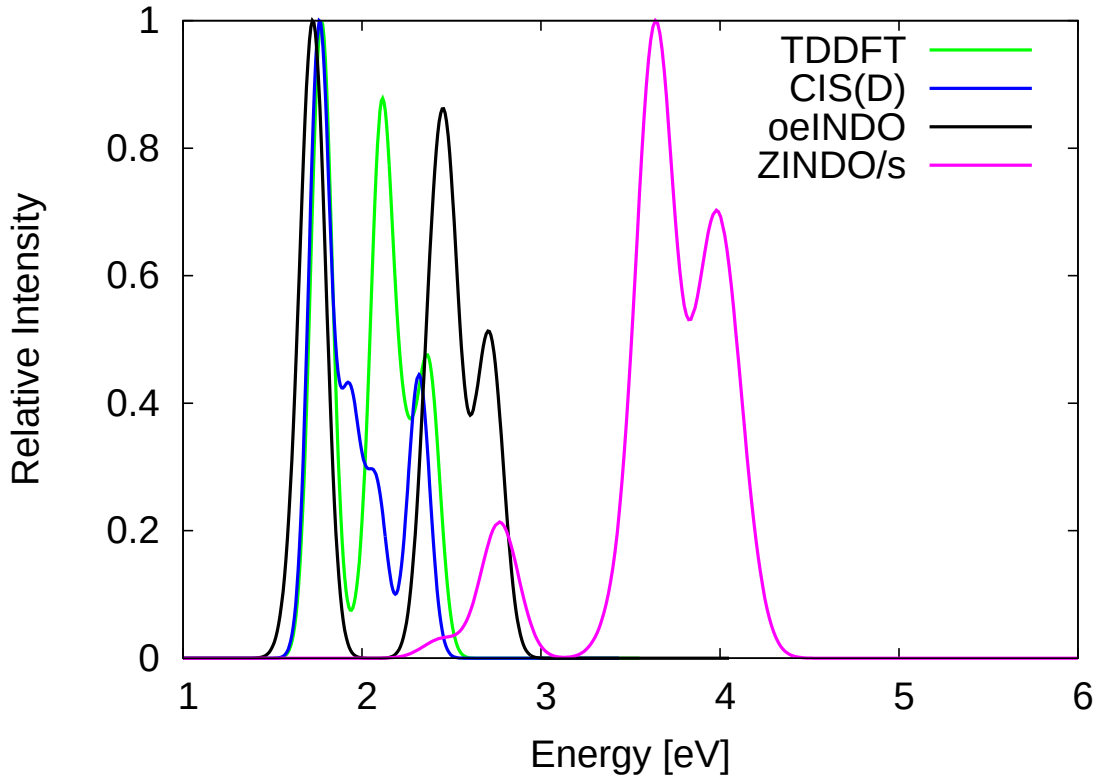

Figure 4.8: Absorption spectra for Si_{19} equilibrium geometry obtained from different methods.. The intensities have been scaled so that the highest intensity is equal to unity.

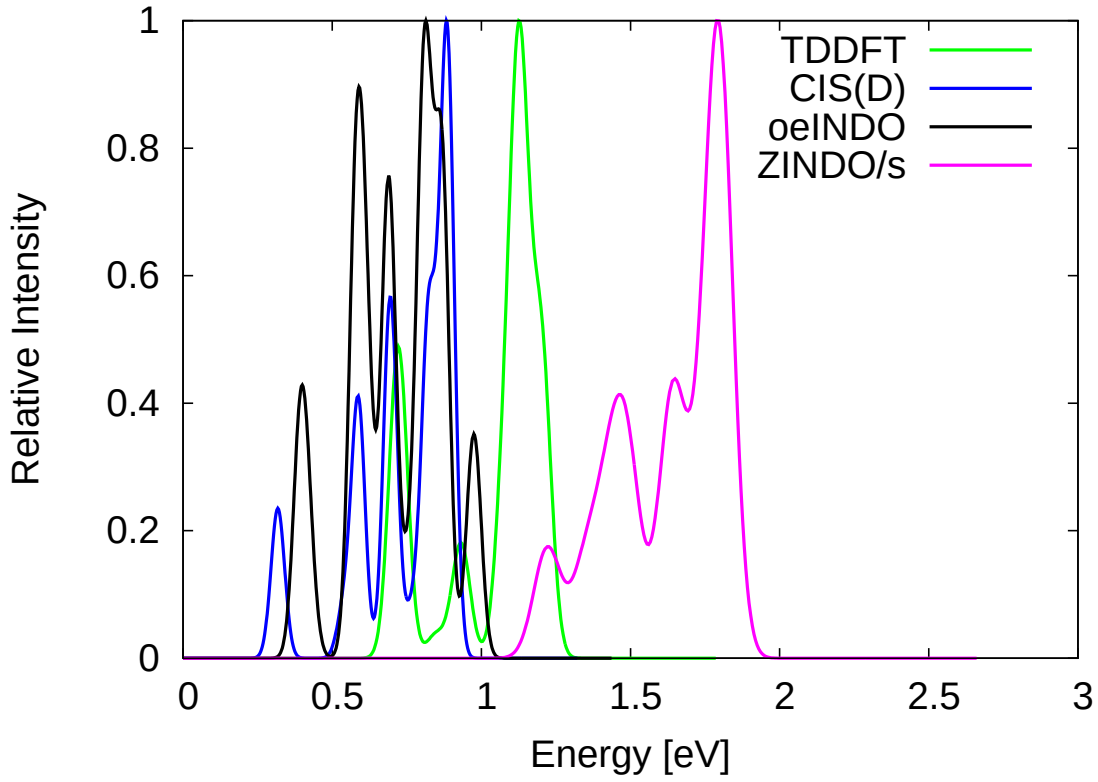

Figure 4.9: Absorption spectra for Si_{40} equilibrium geometry obtained from different methods.. The intensities have been scaled so that the highest intensity is equal to unity.

For the Si_5 equilibrium cluster (Figure 4.7), oeINDO also showed a good performance. Its absorption spectra (Figure 4.7) and excitations (Table 4.9) are in good agreement with those from EOM-CCSD. The oeINDO spectrum and those from other *ab-initio* methods including the benchmark method are found in the same energy range (2.5-3.5 eV) but ZINDO/s one is much shifted from this range. The oeINDO spectrum maximum is shifted from the EOM-CCSD maximum with a slight error of 0.07 eV while ZINDO/s peak is shifted with a larger error $>$ 1.7 eV. From Table 4.9, it can be seen that the first and second excited state energies from oeINDO (2.47 and 2.47 eV) as well as those from TDDFT (2.47 and 2.62 eV) and CIS(D) (2.56 and 2.62 eV) are in good agreement with the EOM-CCSD ones (2.54 and 2.58 eV). However, the corresponding ZINDO/s energies (3.45 and 3.45 eV) deviate more. The first eight excited state energies from oeINDO match with those from EOM-CCSD with a small error of MAE 0.09 eV while the ZINDO/s ones deviate much more with 1.47 eV.

For larger structures, Si_{19} and Si_{40}, EOM-CCSD computations are prohibitively expensive. Hence, oeINDO results for these structures were compared to TDDFT and CIS(D) results. For the Si_{19} equilibrium structure, the Table 4.10 shows that the first excited energy from oeINDO ($\approx$ 1.7 eV) match better than ZINDO/s ($\approx$ 2.5 eV) one to *ab-initios* ($\approx$ 1.8 eV). The MAEs (Table 4.7) of the first eight lowest excitations from oeINDO relative to CIS(D) and TDDFT are 0.36 eV and 0.32 eV, respectively. For Si_{40}, oeINDO excitation energies agree with those obtained with TDDFT and CIS(D) with small MAEs of 0.12 eV and 0.03 eV, respectively. As seen earlier Table 4.7, TDDFT agrees with EOM-CCSD with a typical error of about 0.09 eV. Hence, oeINDO excitations for Si_{40} compared with EOM-CCSD with a typical error of about 0.21 eV. The absorption spectra of Si_{19} and Si_{40} are presented in Figure 4.8 and Figure 4.9, respectively. The figures show that the oeINDO spectra are comparable with TDDFT spectra. For Si_{19}, the spectrum from oeINDO is comparable with the TDDFT spectrum pattern and its spectrum highest peak agrees well with those from CIS(D) and TDDFT with an error of 0.05 eV. For Si_{40} (Figure 4.9), oeINDO gives similar spectrum pattern as that of CIS(D) in the same energy range.

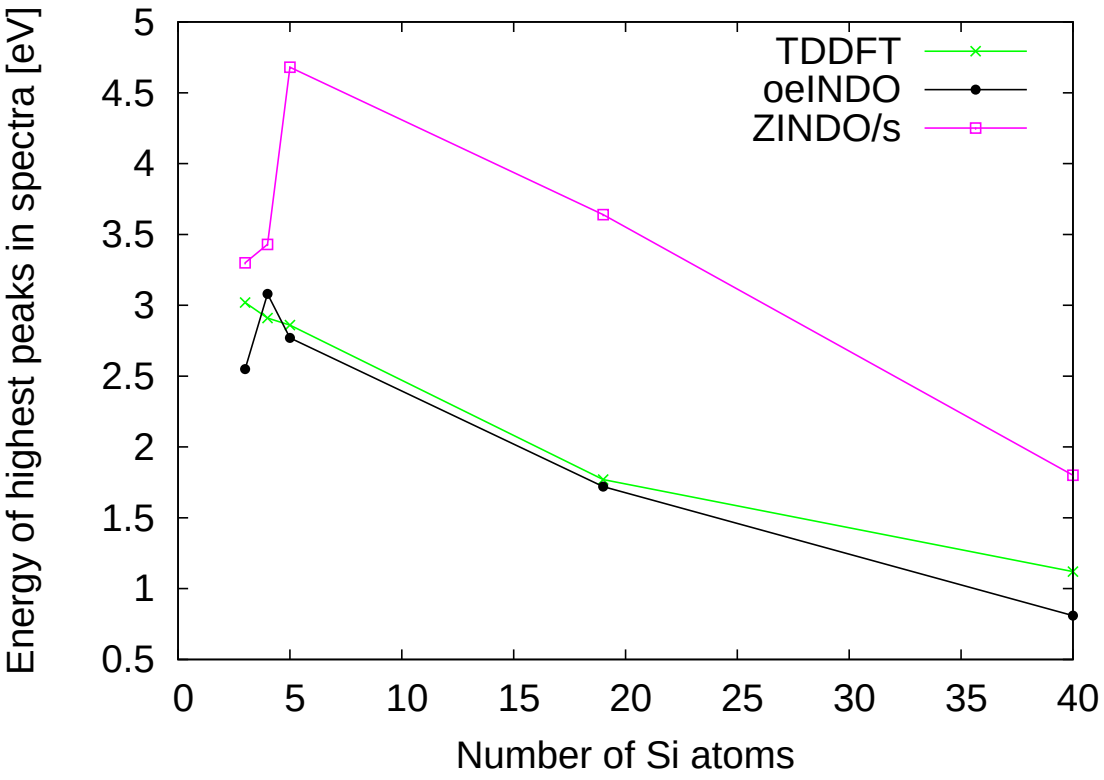

Figure 4.10: Highest peaks against number of units n in equilibrium Si_n structures.

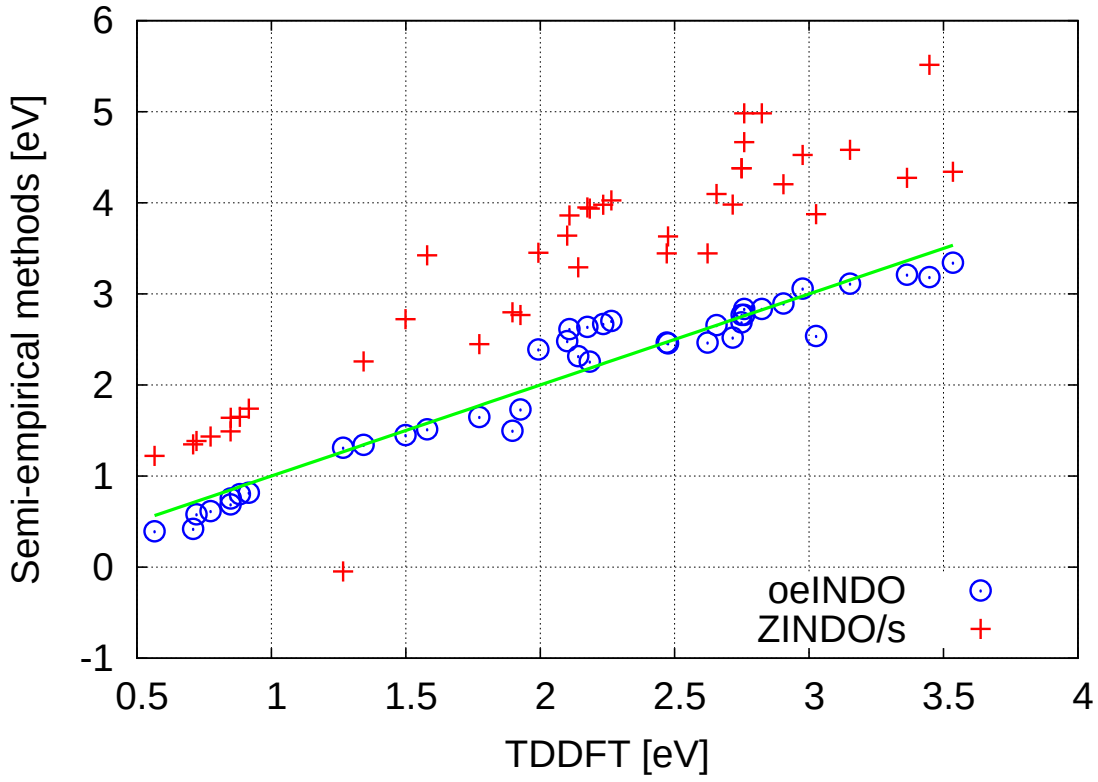

Figure 4.11: Semi-empirical energies against TDDFT energies for Si_n $(n = 3,4,5,19,40)$ equilibrium. structures.

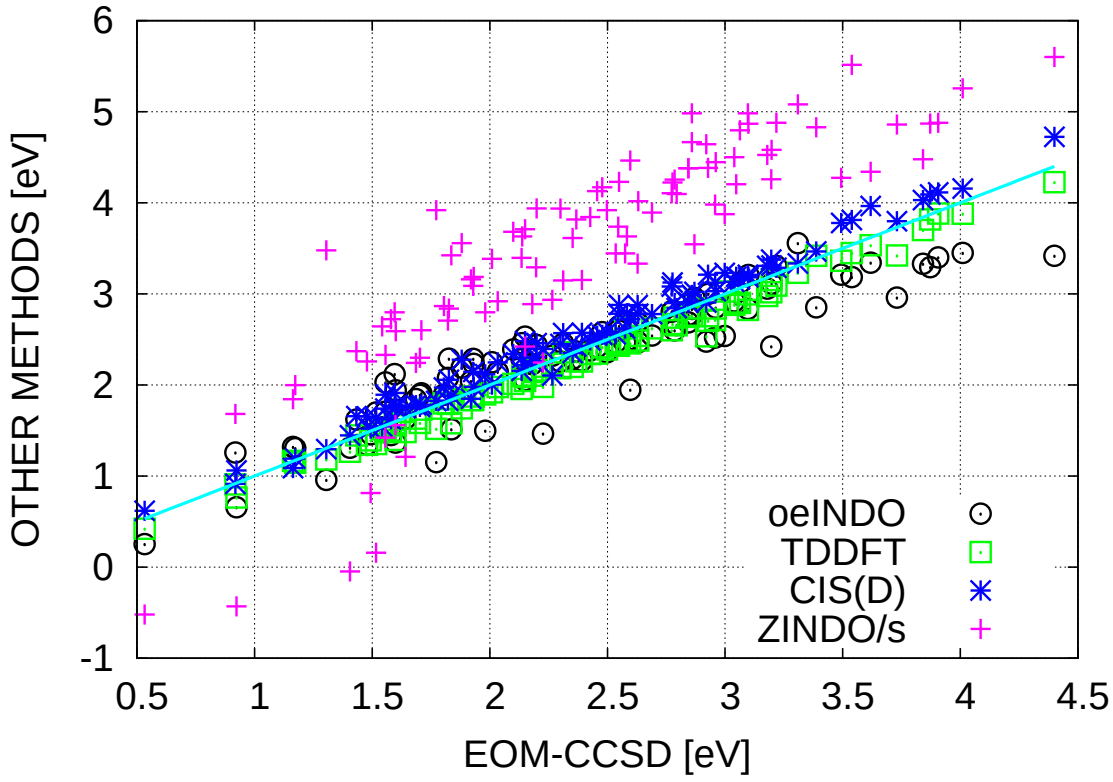

Figure 4.12: Scatter plot of different (non-equilibrium and equilibrium) Si_n (n= 5, 4, 3) clusters.

Table 4.12: MAEs (eV) of excitations from various methods as compared to EOM-CCSD excitations for different (non-equilibrium and equilibrium) Si clusters

Methods	Si_5	Si_4	Si_3
oeINDO	0.11	0.27	0.25
ZINDO/S	1.31	1.32	0.87
TDDFT	0.08	0.11	0.06
CIS(D)	0.06	0.15	0.13

The plot of absorption spectra of the highest peaks as a function of the number of Si atoms is presented in Figure 4.10. It shows that the oeINDO peak positions compare reasonably well with TDDFT peaks with a typical error of 0.22 eV. The positions of the ZINDO/S peaks deviate much with a typical error of 1.03 eV.

Table 4.7 summarizes the MAEs of excitations energies from oeINDO and ZINDO/s as compared with EOM-CCSD, CIS(D), and TDDFT for the $Si_n(n = 3,4,5,19,40)$ equilibrium geometries. Evidently, oeINDO is more accurate than ZINDO/s. Also, the scatter plot of a total of 40 excitation energies from all the Si equilibrium geometries presented in Figure 4.11, is a further proof that oeINDO agrees better than ZINDO/s with *ab-initio* methods. The MAE of oeINDO excitations as compared to TDDFT is 0.15 eV (that is, about 0.24 eV relative to EOM-CCSD) while for ZINDO/s, the MAE is 1.23 eV relative to TDDFT.

Calculations were also performed with non-equilibrium silicon cluster structures. A total of 12 silicon structures were obtained by perturbing the $Si_n(n = 3,4,5)$ equilibrium structures with scale factors 0.9, 1.0, 1.1 and 1.2. The scatter plots of 48 excitation energies each from different methods for these structures are presented in Figure 4.12. The summary of the MAEs of excitation energies from the 12 equilibrium and non-equilibrium structures are displayed in Table 4.12. Obviously, the results from the table and the figure show that oeINDO is also gives good result for non-equilibrium structures. Table 4.7 shows, on the average, that oeINDO excitations agree with those from EOM-CCSD with MAE of 0.27 eV. However, the ZINDO/s deviates from EOM-CCSD with an MAE of 1.17 eV, much larger than for oeINDO. On the other hand, TDDFT and CIS(D) compare with EOM-CCSD with 0.08 eV and 0.12 eV, respectively.

4.2.3 Transferability of oeINDO Zinc Parameters

The validity of oeINDO model for zinc was verified by comparing its first eight excited state energies with those from EOM-CCSD, TDDFT and CIS(D). The energies for Zn_3 are presented in Table 4.13 while for other Zn cluster structures are given in Tables C.2-C.6 in the appendix. The scatter plots comparing excitations from other methods (including oeINDO) with benchmark (EOM-CCSD), semi-empirical methods with TDDFT and semi-empirical methods with CIS(D) are presented in Figures 4.13, 4.14 and 4.15, respectively. Absorption spectra for Zn cluster structures obtained with different methods and presented in Figures 4.16 - 4.21, were also employed for model validation.

Table 4.13: First Eight Lowest Excited State Energies (eV) for Zn_3

EOM-CCSD	oeINDO	INDO/s	TDDFT	CIS(D)
3.942	3.803	2.837	3.831	3.979
3.946	3.808	2.843	3.833	3.983
4.225	4.012	3.430	4.034	4.251
4.259	4.260	4.071	4.036	4.340
4.262	4.373	4.147	4.213	4.344
4.608	4.373	4.148	4.279	4.662
5.105	4.654	4.894	5.126	5.117
5.105	4.660	4.901	5.134	5.118

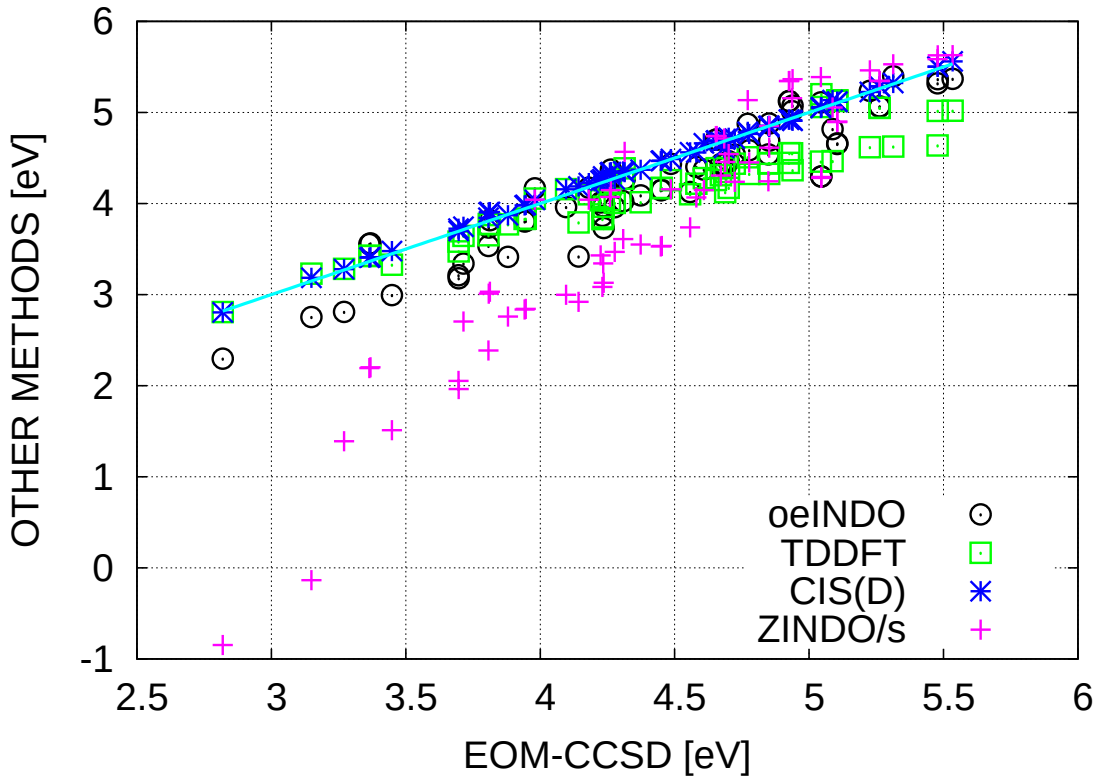

Figure 4.13: Comparing excitation energies obtained using different methods with those calculated at EOM-CCSD/TZVPP level for different Zn_n ($n = 3,4$) equilibrium and non-equilibrium structures.

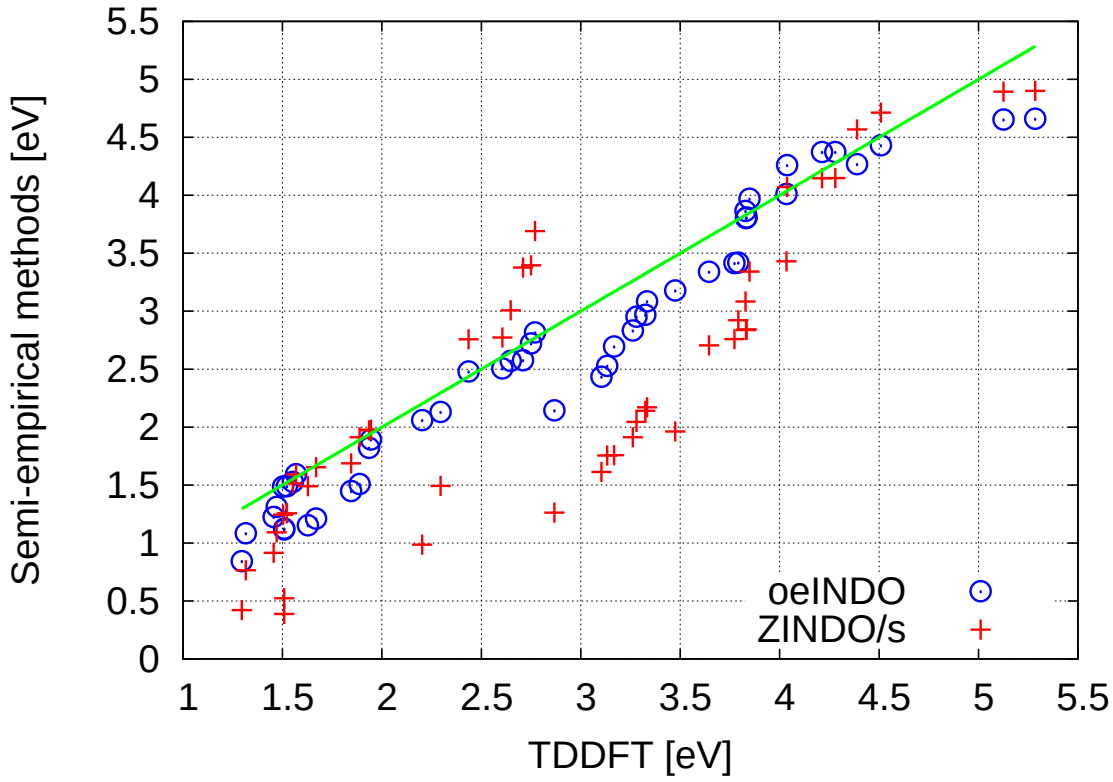

Figure 4.14: Excitation energies obtained using semi-empirical methods (oeINDO (blue circles) and ZINDO/s (red plus signs) against TDDFT energies for Zn_n ($n = 3,4,6,8,16,24$) equilibrium structures

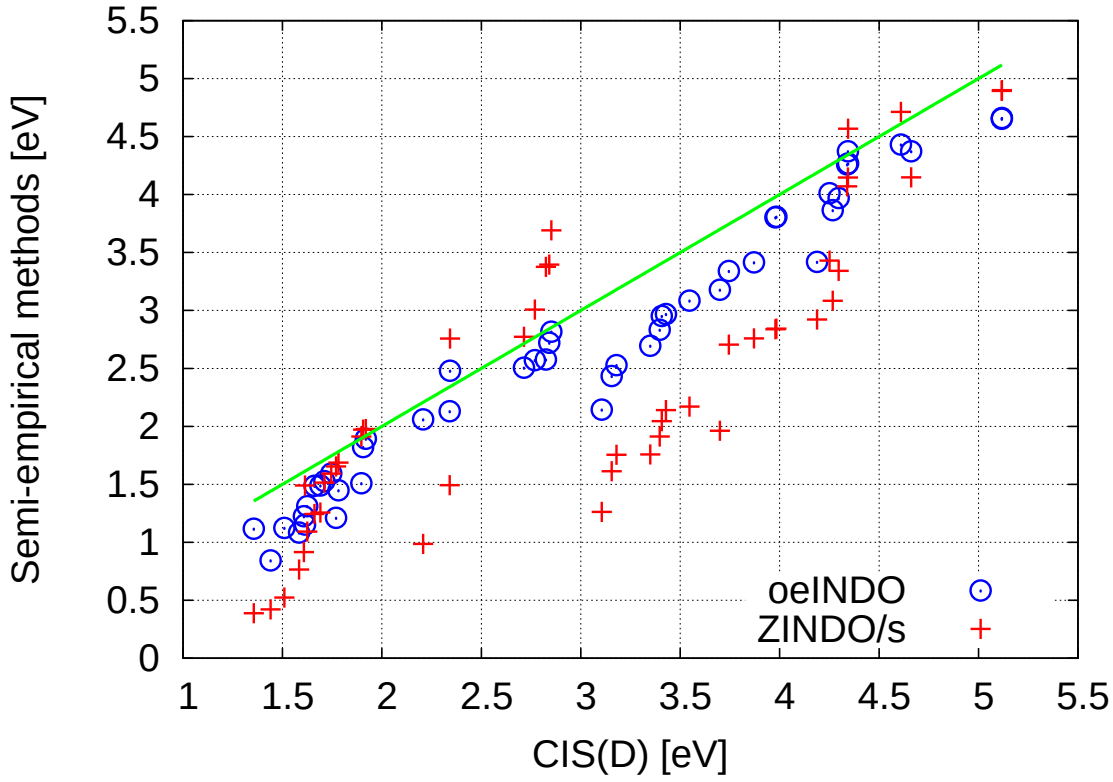

Figure 4.15: Excitation energies obtained using semi-empirical methods against CIS(D) energies for Zn_n $(n = 3,4,6,8,16,24)$ equilibrium structures.

From Table 4.13, it can be seen that excited state energies from oeINDO as well as those from TDDFT and CIS(D) are close to the EOM-CCSD ones. For instance, oeINDO and EOM-CCSD first excited state energies, $\approx$ 3.8 and $\approx$ 3.9 eV, respectively differ by only 0.1 eV. However ZINDO/s first excited state energy, $\approx$ 2.8, differ from that of EOM-CCSD by a larger error of 1.1 eV. Figure 4.13 is a scatter plot of 32 excitation energies each obtained using different methods for eight different Zn_n (n=3, 4) equilibrium and non-equilibrium structures. The plot compares the excitation energies from semi-empirical methods and other *ab-initio* methods with those from EOM-CCSD. It can be observed that oeINDO excitations have a better match than TDDFT and ZINDO/s excitations to EOM-CCSD excitations. The oeINDO excitations match the EOM-CCSD excitations with MAE 0.25 eV while the TDDFT and ZINDO/s excitations match with 0.28 and 0.70 eV, respectively. The CIS(D)results compare with the EOM-CCSD ones with a smaller MAE of 0.03 eV. It can also be observed that the ZINDO/s model gave some negative excitation energy values, which indicate bad predictions by the model; excitation energy is defined as the difference between the lowest unoccupied molecular orbital (higher energy level) and the highest occupied molecular orbital (lower energy level).

For larger Zn_n ($n > 4$) clusters, EOM-CCSD is compute intensive. Thus, results from other *ab-initio* methods (TDDFT and CIS(D)) were used for the validation of the oeINDO model. Calculation of excitations and absorption spectra were carried for Zn_n (n=3, 4, 6, 8, 16, 24) equilibrium structures using oeINDO, ZINDO/s, TDDFT and CIS(D). A scatter plot comparing the excitation energies from the semi-empirical methods (oeINDO and ZINDO/s) with those from TDDFT for all the equilibrium structures are shown in Figure 4.14. The figure shows that oeINDO excitation energies (blue circles) are much closer than ZINDO/s ones (red plus signs) to TDDFT excitation energies (the straight line). The excitations from oeINDO agree well with TDDFT with MAE 0.24 eV while ZINDO/s excitations deviate with a larger MAE of 0.63 eV.

Despite the fact that UV-Vis absorption spectra of Zn diatomics were not included in the training data sets, oeINDO produced spectra that qualitatively agree with those from the benchmark. The absorption spectra for Zn_n (n=3, 4, 6, 8, 16, 24) equilibrium clusters are well predicted by oeINDO as shown in Figures 4.16, 4.17, 4.18, 4.19, 4.20 and 4.21.

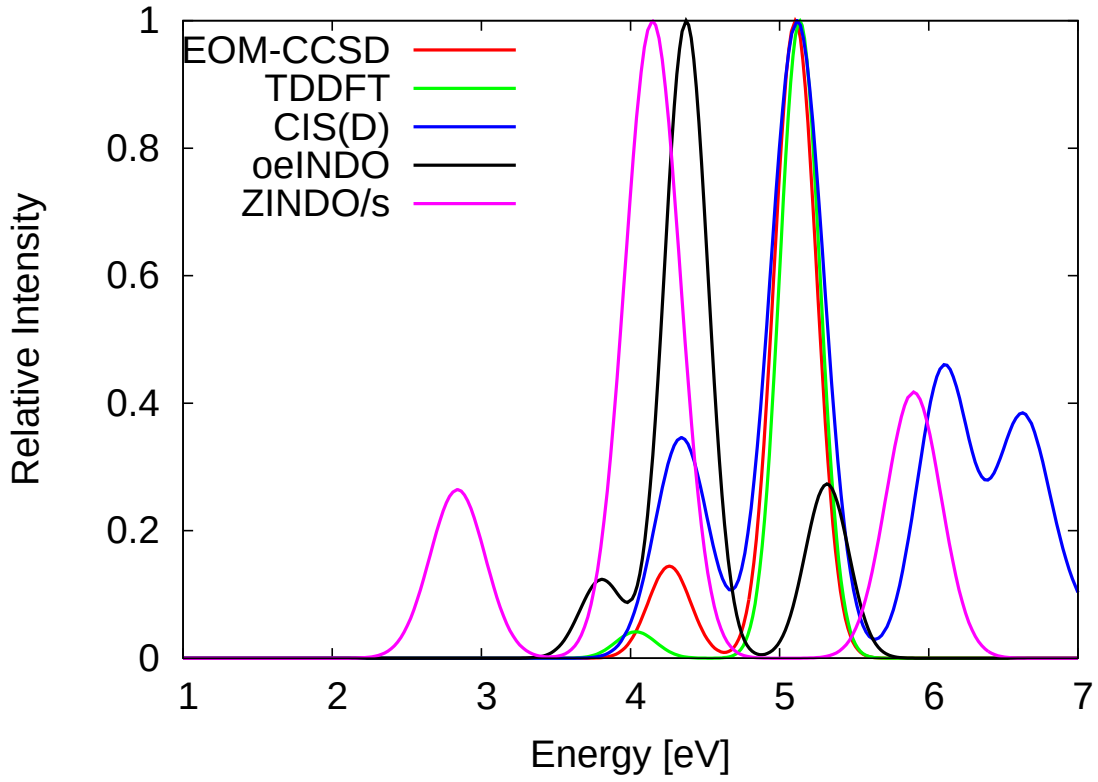

Figure 4.16: Absorption spectra for Zn_3 equilibrium geometry obtained using different methods.The intensities have been scaled so that the highest intensity is equal to unity.

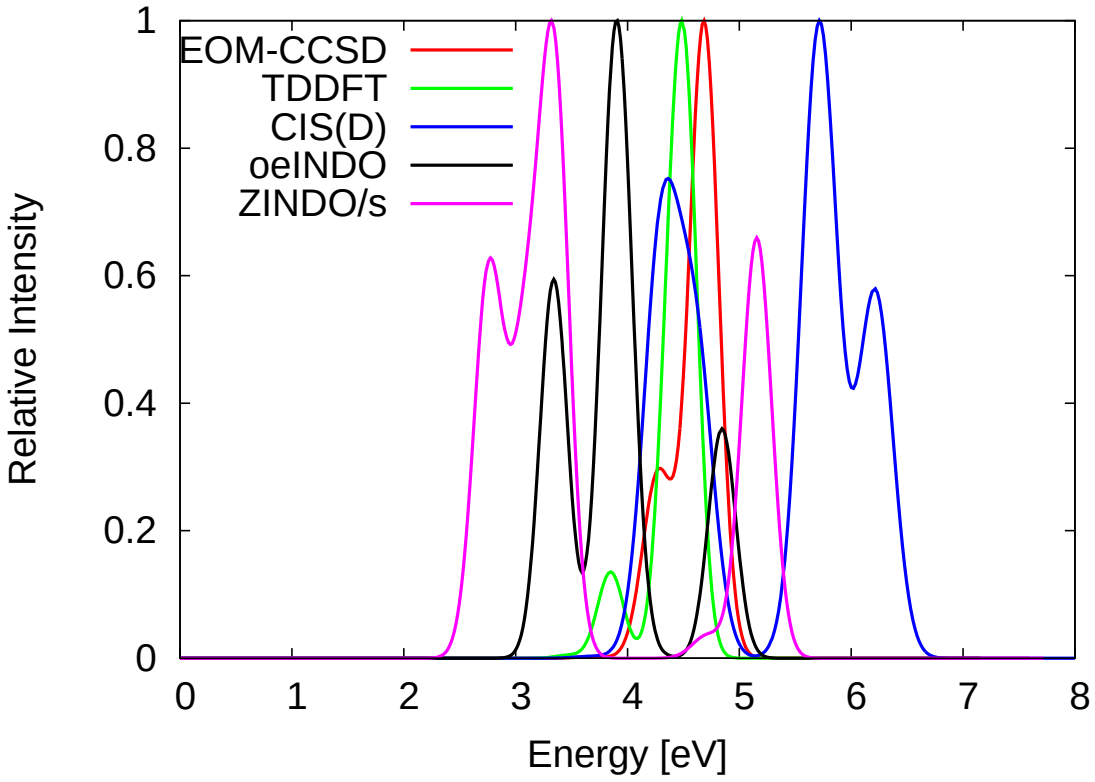

Figure 4.17: Absorption spectra for Zn_4 equilibrium geometry obtained using different methods.The intensities have been scaled so that the highest intensity is equal to unity.

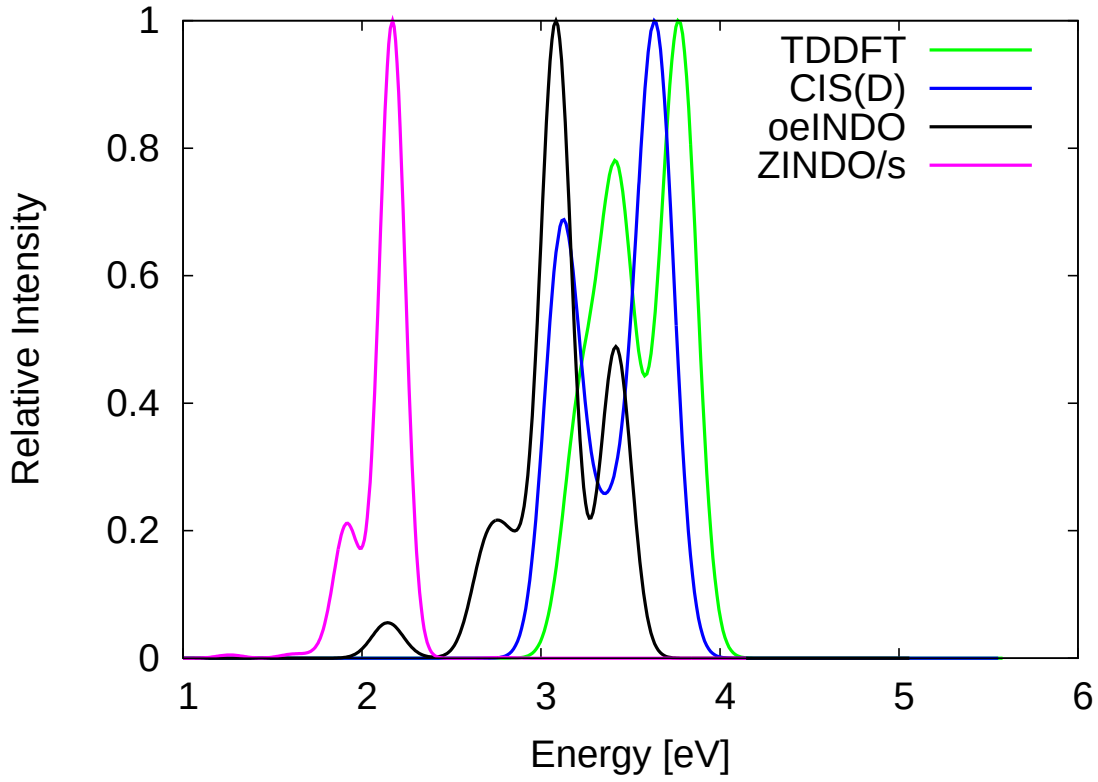

Figure 4.18: Absorption spectra for Zn_6 equilibrium geometry obtained using different methods.The intensities have been scaled so that the highest intensity is equal to unity.

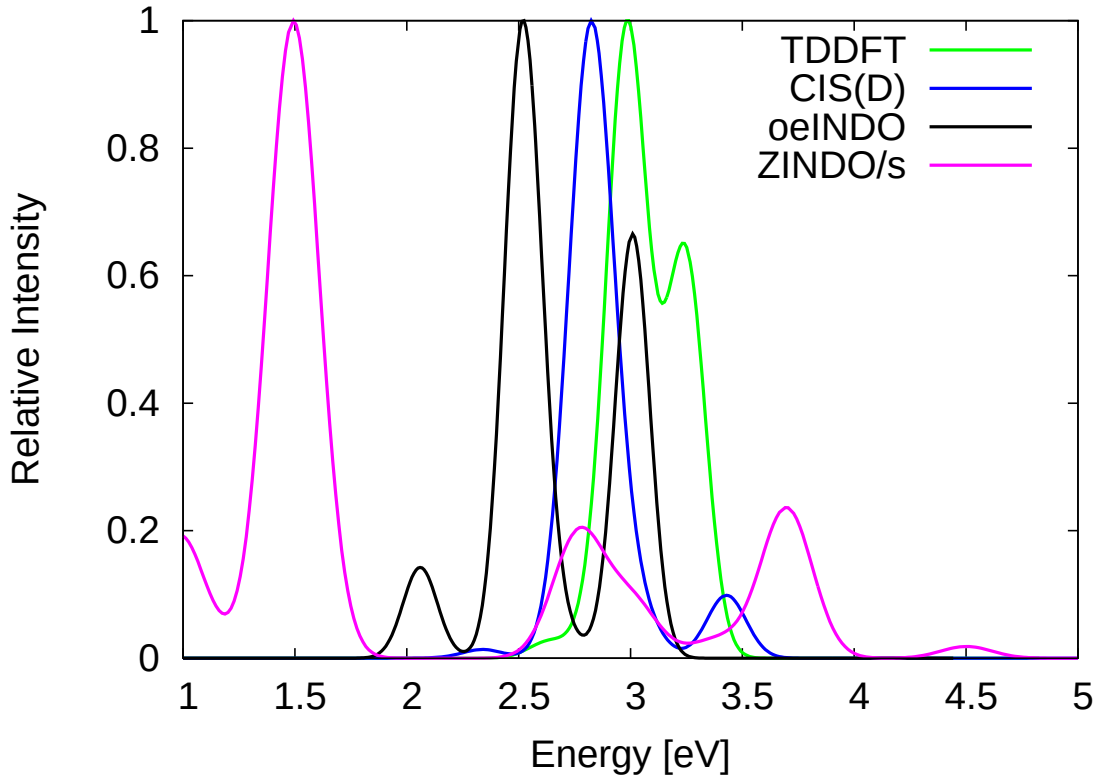

Figure 4.19: Absorption spectra for Zn_8 equilibrium geometry obtained using different methods.The intensities have been scaled so that the highest intensity is equal to unity.

For Zn_3 absorption spectra (Figure 4.16), the absorption bands of the spectra from the different methods are prominent within the ultraviolet region (3.0 - 30.0 eV). The highest peak of the oeINDO spectrum is *red-shifted* from the EOM-CCSD (the benchmark) by about 0.5 eV while ZINDO/s is *red-shifted* by a larger error of about 1.0 eV. The peaks of the spectra from the *ab-initio* methods (CIS(D) and TDDFT), however, have good match with that of EOM-CCSD.

The absorption spectra of Zn_4 equilibrium structure presented in Figure 4.17 show that it absorbs in the ultraviolet region (3.0 - 30.0 eV) for all methods except ZINDO/s, which shows absorption partly in the visible region (1.5 -3.0 eV) and partly in the ultraviolet region. The highest peak of the oeINDO spectrum compared better with the EOM-CCSD one than does ZINDO/s and CIS(D), although, in general, intensities from CIS based methods are expected to compare only qualitatively with accurate *ab-initio* or experimental results.

For Zn_n ($n > 4$) clusters, the semi-empirical model results were compared with only the TDDFT and CIS(D) results since EOM-CCSD is expensive for these clusters. In the spectra for Zn_6 equilibrium structure (Figure 4.18), the absorption band of the *ab-initio* methods as well as that of oeINDO occur at about the same range. The peak relative intensity of oeINDO is *red-shifted* from TDDFT by about 0.70 eV while that from ZINDO/s is shifted by 1.60 eV which is more than twice that of oeINDO.

For Zn_8 (Figure 4.19), oeINDO matches *ab-initio* results better than do ZINDO/s. The highest peak of the oeINDO is *red-shifted* from TDDFT and CIS(D) spectra by about 0.5 eV and 0.3 eV, respectively while ZINDO/s, on the other hand, is *red-shifted* by larger errors of about 2.5 eV and 2.2 eV from TDDFT and CIS(D), respectively.

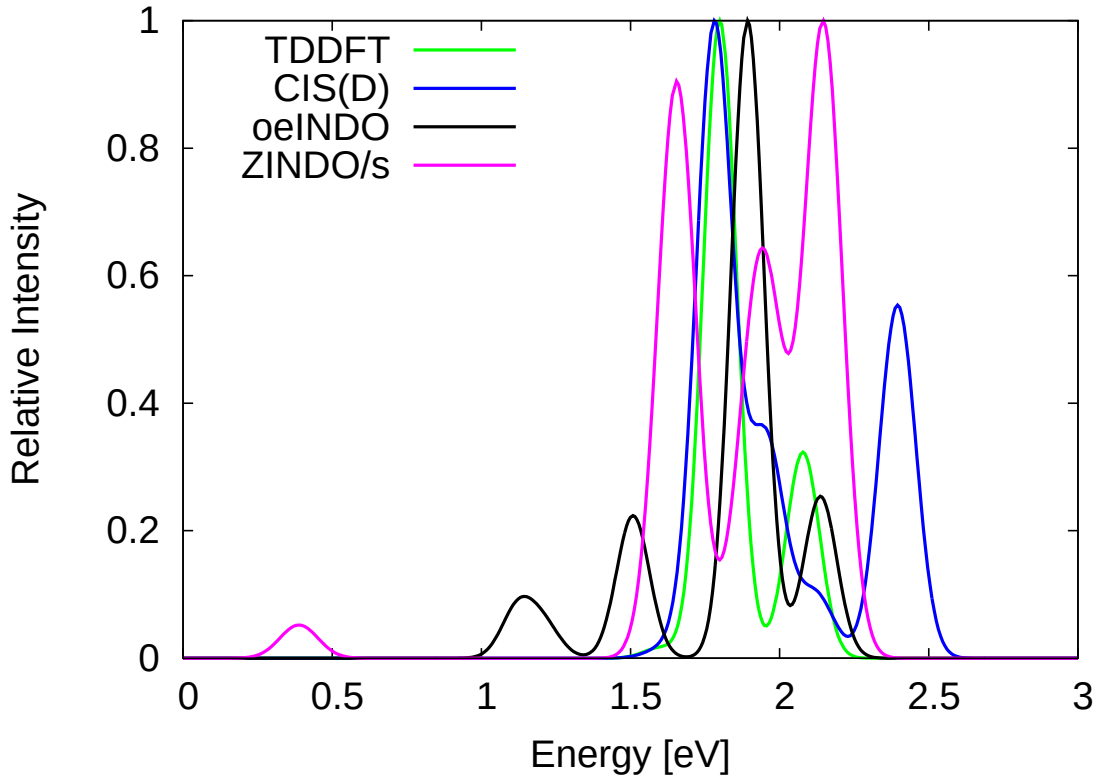

Figure 4.20: Absorption spectra for Zn_{16} equilibrium geometry obtained using different methods.The intensities have been scaled so that the highest intensity is equal to unity.

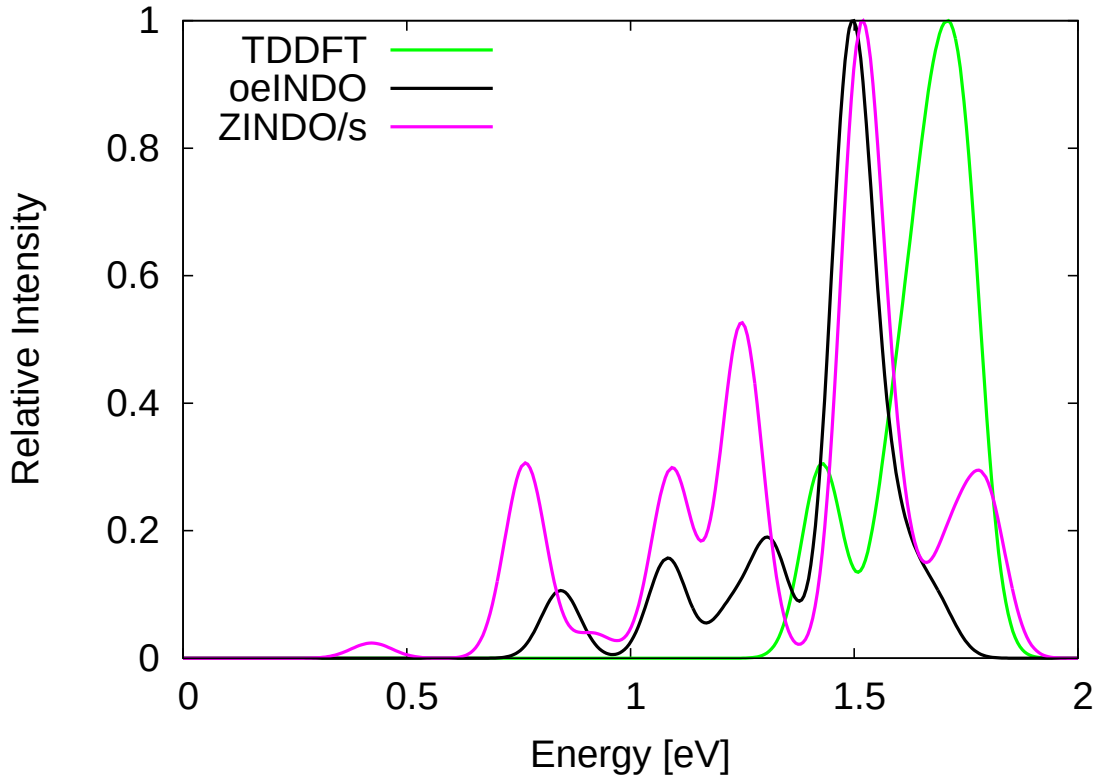

Figure 4.21: Absorption spectra for Zn_{24} equilibrium geometry obtained using different methods.The intensities have been scaled so that the highest intensity is equal to unity.

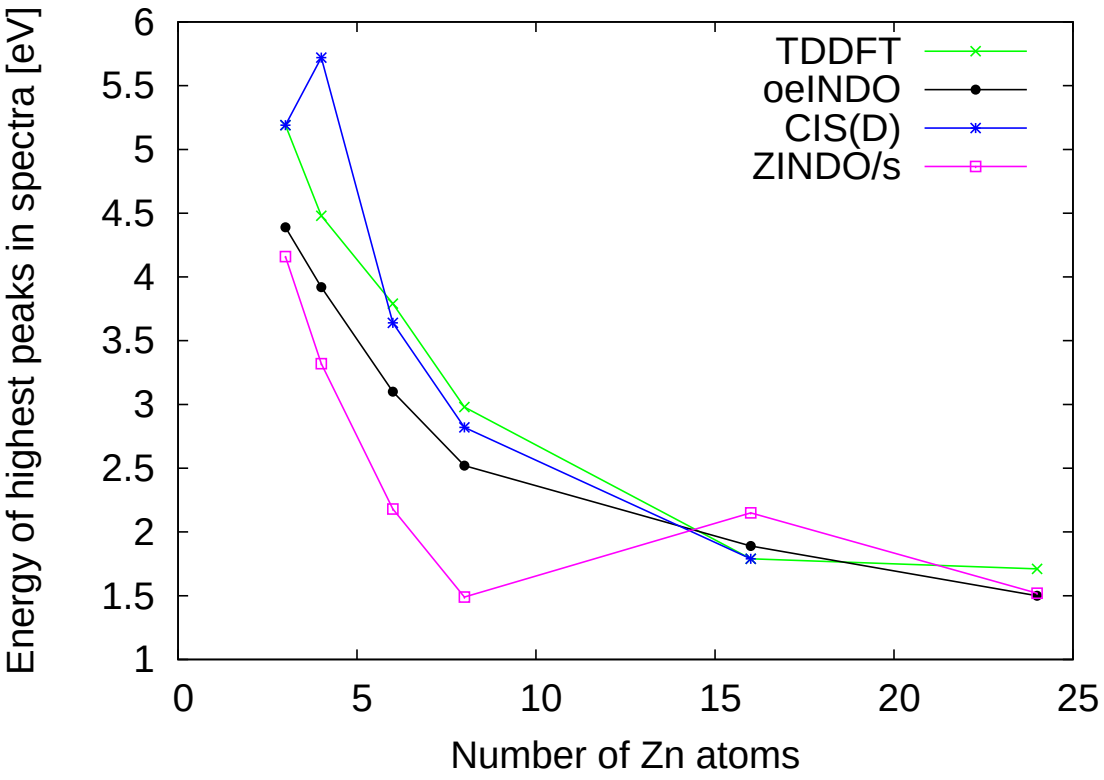

Figure 4.22: Highest peaks against number of units n in equilibrium Zn_n structures

The absorption spectra for Zn_{16} and Zn_{24} from oeINDO displayed in Figures 4.20 and 4.21, respectively agree reasonably with those from TDDFT and CIS(D). For Zn_{16}, the highest peak of the oeINDO absorption spectrum is *blue-shifted* with a small error of about 0.1 eV from TDDFT but the ZINDO/s peak is *blue-shifted* by about 0.80 eV, which is eight times larger. Absorption spectra of Zn_{24} (Figure 4.21) shows that the position of the oeINDO highest peak matches that from TDDFT with a typical error of about 0.25 eV.

Plots of the energy of highest peaks of the absorption spectra as a function of the number of atoms is shown in Figure 4.22 for different methods. The oeINDO method reproduced the same trend as observed for TDDFT; the peaks are *red-shifted* (decreased in peak energies) with increase in the number of atoms. However, for ZINDO/s the trend broke for the sixteen atoms Zn cluster. The MAEs of the peak energies from oeINDO and ZINDO/s as compared to TDDFT are 0.40 eV and 0.83 eV respectively, with the latter being roughly two times less accurate than the former in this case.

From the results discussed so far, oeINDO is transferable and compares favourably well with accurate *ab-initio* methods.

4.2.4 Transferability of oeINDO Cadmium parameters

The accuracy of the oeINDO parameters for cadmium was also checked. The oeINDO cadmium parameters were tested with cadmium complex structures, Cd_n (n = 3, 4, 6, 8, 16, 20, 25, 30). Eight lowest excited state energies for each of these structures were calculated using various methods including oeINDO. The results are presented in Tables (Tables 4.14, C.7, C.8, C.9 and C.10) and given in form of scatter plots for comparison. Absorption spectra computed using different methods for the same set of structures were also used for the test, even though spectra were not part of the parameterisation data.

Table 4.14: First Eight Lowest Excited State Energies (eV) for Cd_3

EOM-CCSD	oeINDO	INDO/s	TDDFT	CIS(D)
4.077	3.970	5.615	3.691	4.225
4.091	3.981	5.618	3.702	4.241
4.339	4.028	5.739	3.895	4.468
4.367	4.045	5.833	3.905	4.524
4.379	4.488	5.833	4.077	4.538
4.720	4.512	5.834	4.125	4.834
5.189	4.907	5.835	4.965	5.309
5.191	4.913	5.860	4.970	5.312

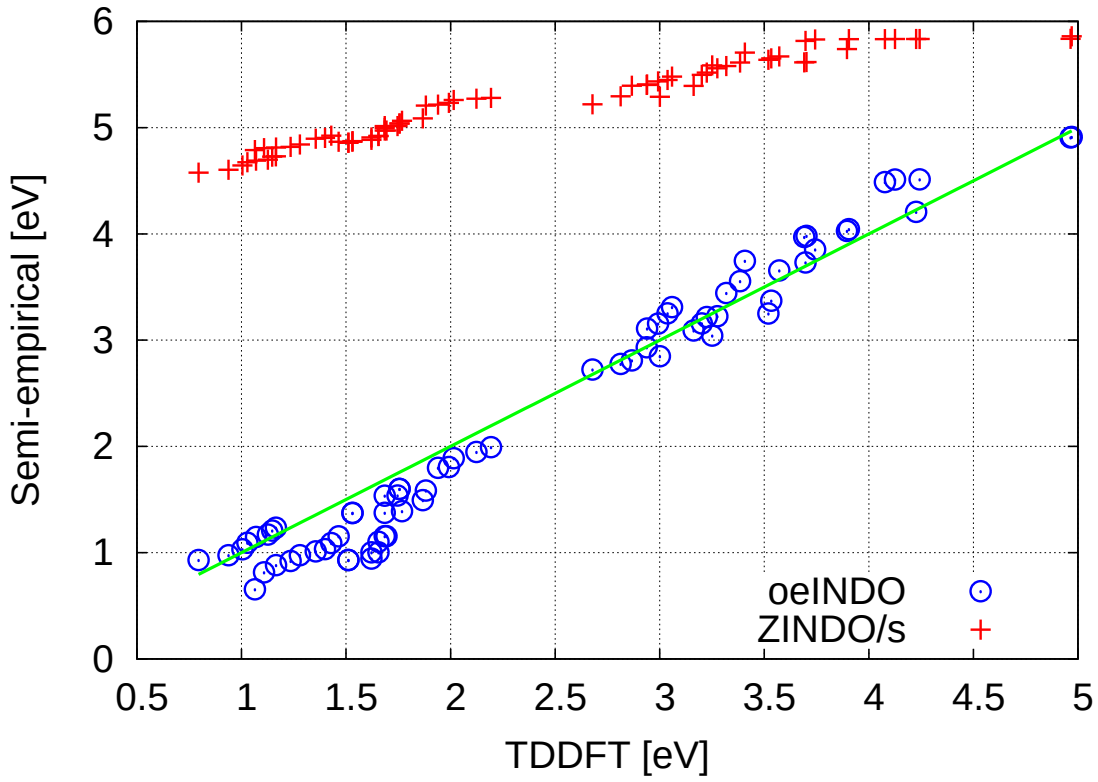

Figure 4.23: Semi-empirical methods against TDDFT energies for Cd_n (n=3, 4, 6, 8, 16, 20, 25, 30) equilibrium structures. The straight green line represents energies obtained using TDDFT.

Table 4.14 shows the excited state energies obtained for Cd_3 equilibrium structure using oeINDO, EOM-CCSD, ZINDO/s, TDDFT, and CIS(D). The table shows that oeINDO produced first and second excited state energies of 3.970 and 3.981 eV, respectively, which in close agreement with corresponding energies of 4.077 and 4.091 eV from EOM-CCSD. The MAE of the eight lowest excited state energies from oeINDO relative to the EOM-CCSD ones is 0.21 eV. It can be observed that, relative to EOM-CCSD, oeINDO performed better than TDDFT (MAE=0.37 eV) and ZINDO/s (MAE=1.22 eV). However, CIS(D) appreciably out performs oeINDO with the MAE of its energies relative to the EOM-CCSD energies being 0.13 eV. The tables displaying the excitation energies of other Cd_n structures can be found in the appendices C.7 - C.10.

Seventy-two (72) excitation energies each were obtained from calculations with oeINDO and ZINDO/s for Cd_n (n=3, 4, 6, 8, 16, 20, 25, 30) equilibrium structures. These energies were compared with those from TDDFT as shown in Figure 4.23. The figure shows that the excitation energies (blue circles) from oeINDO match closely with TDDFT (the straight green line). However, the ZINDO/s excitations (red plus signs) are much deviated from the straight line. The MAE of the oeINDO energies relative to those of the TDDFT is 0.22 eV. The ZINDO/s energies however, deviated much more from TDDFT with MAE of 2.83 eV, more than ten times the size of the MAE from oeINDO.

Although the UV-Vis absorption spectra were not used as reference data during the parameterisation, oeINDO produced absorption spectra that are qualitatively comparable to spectra from accurate *ab-initio* approaches for Cd_n (n = 3, 4, 6, 8, 16, 20, 25, 30) equilibrium structures.

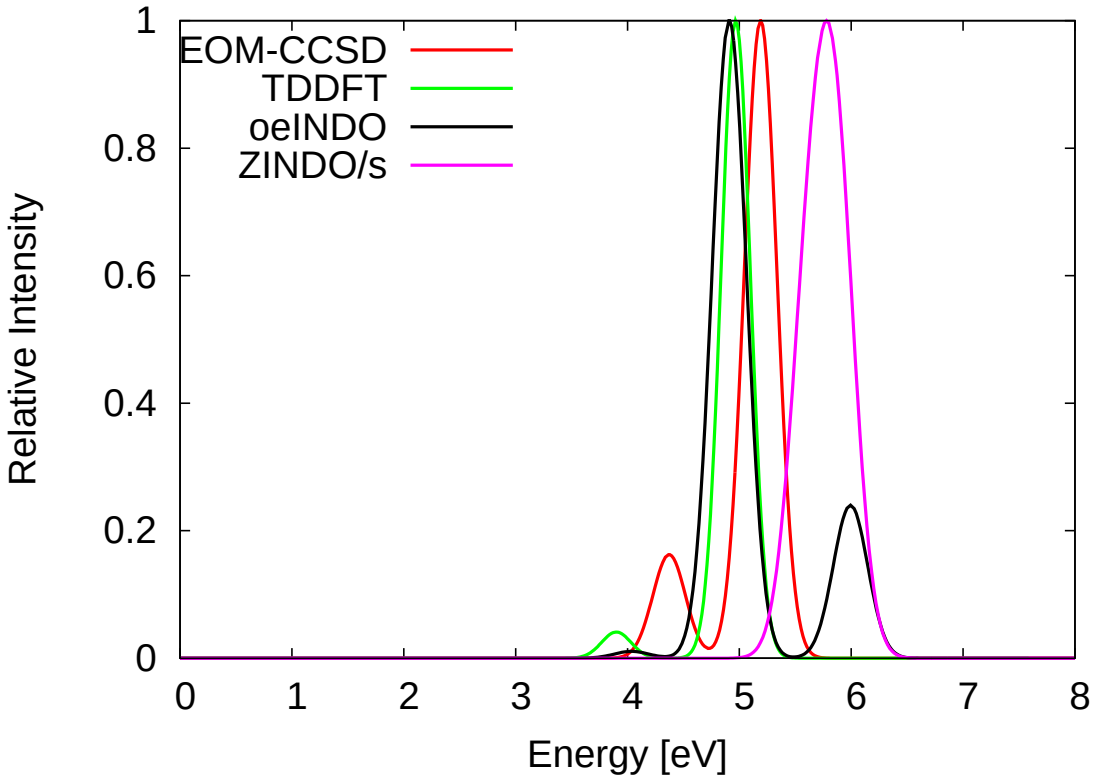

Figure 4.24: Absorption spectra for Cd_3 equilibrium geometry obtained from different methods.The intensities have been scaled so that the highest intensity is equal to unity.

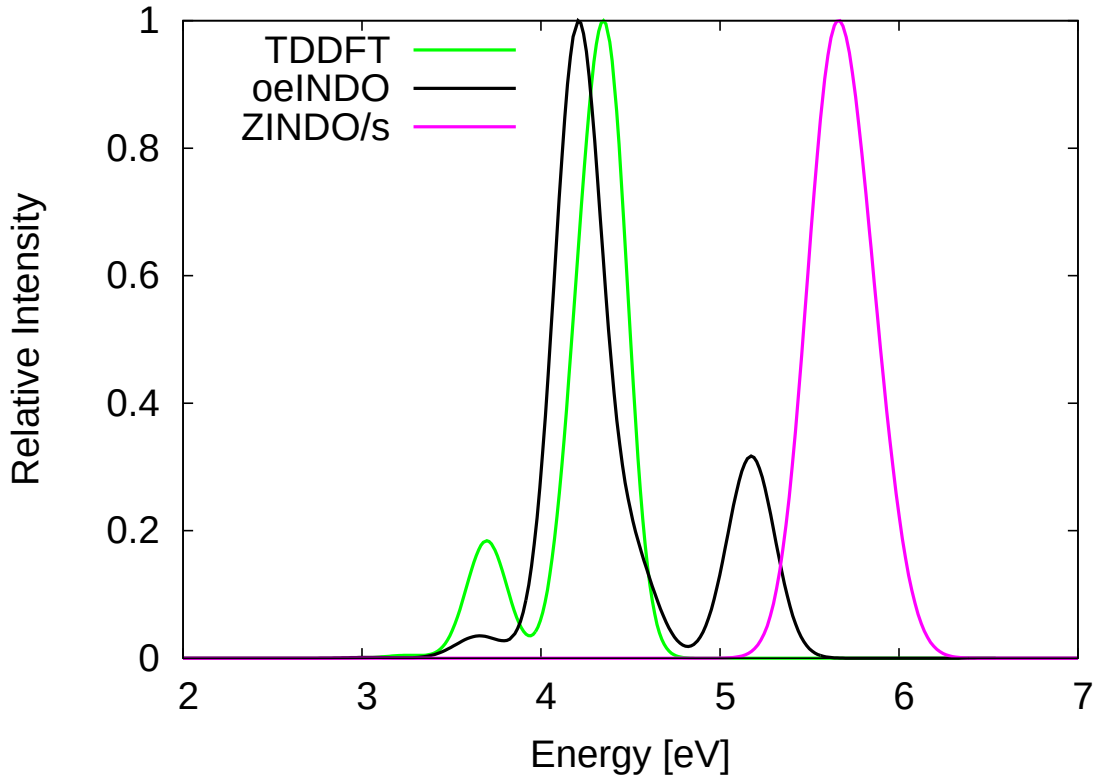

Figure 4.25: Absorption spectra for Cd_4 equilibrium geometry obtained from different methods.The intensities have been scaled so that the highest intensity is equal to unity.

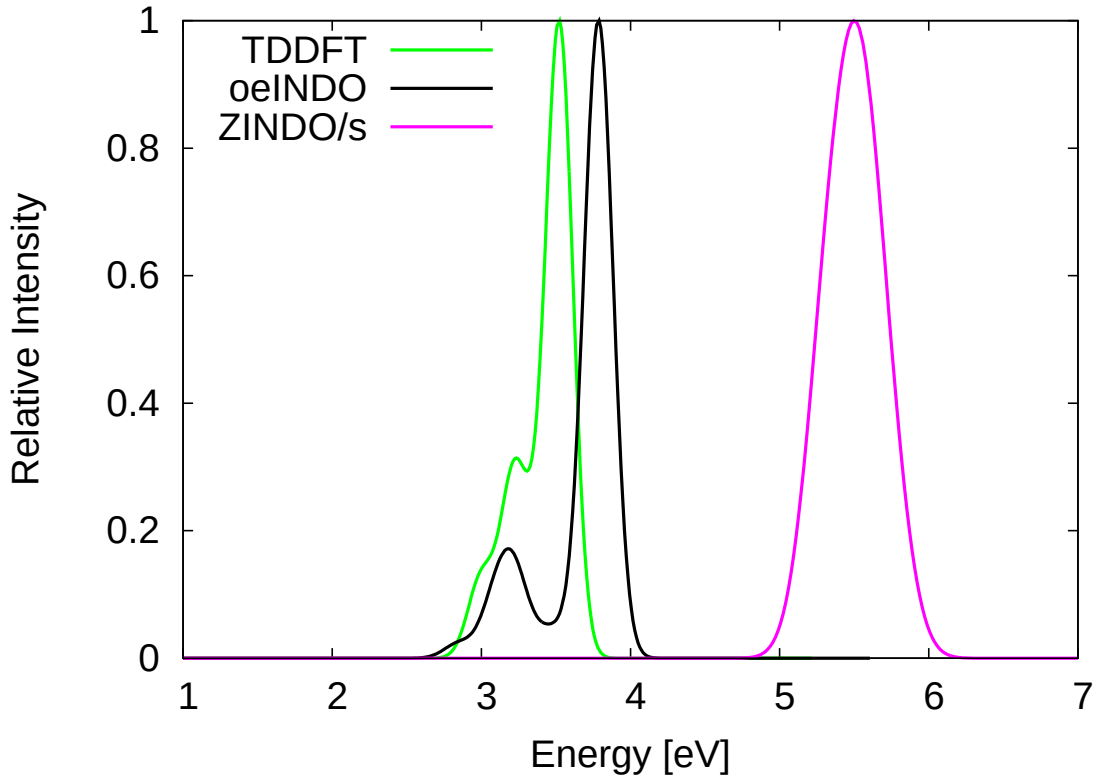

Figure 4.26: Absorption spectra for Cd_6 equilibrium geometry obtained from different methods.The intensities have been scaled so that the highest intensity is equal to unity.

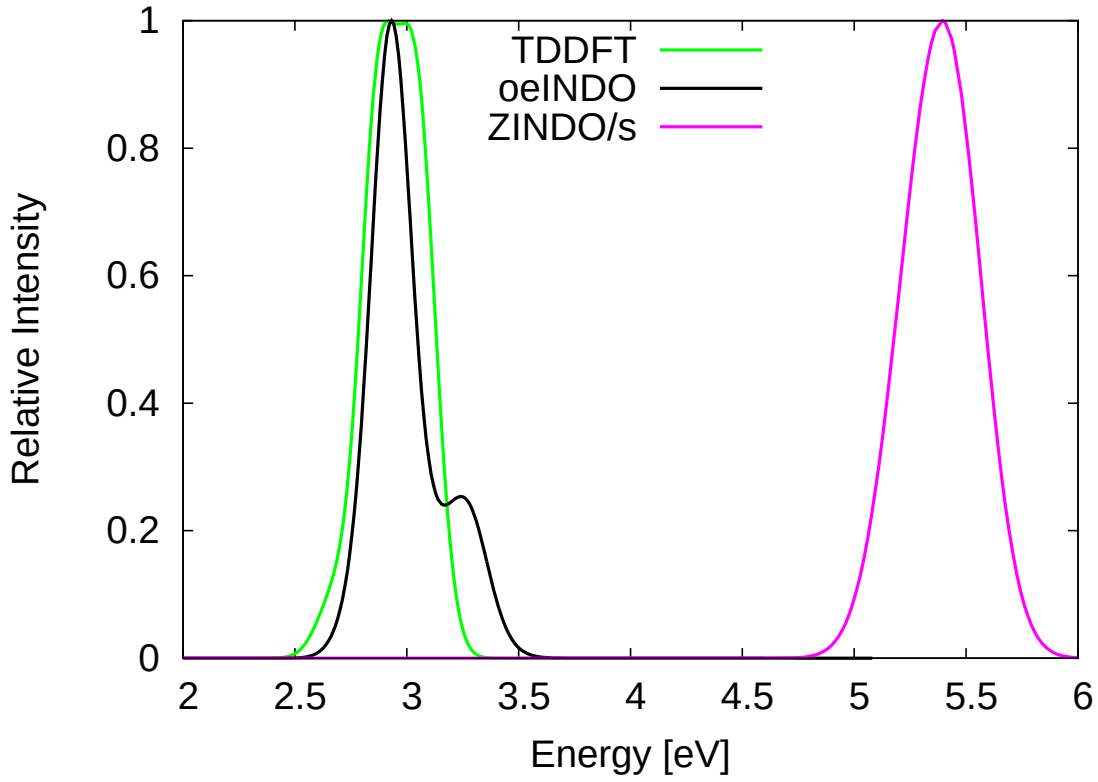

Figure 4.27: Absorption spectra for Cd_8 equilibrium geometry obtained from different methods.The intensities have been scaled so that the highest intensity is equal to unity.

The absorption spectra of Cd_3 obtained using the EOM-CCSD, TDDFT, oeINDO and ZINDO/s methods are presented in Figure 4.24. The absorption bands of the spectra from all the different methods lie in the ultraviolet region. The oeINDO band matches well with that of the TDDFT; the highest absorption peaks of TDDFT and oeINDO are both *red-shifted* (decreased in energy) by about 0.10 eV from EOM-CCSD. However, the ZINDO/s peak is *blue-shifted* (increased in energy) by about 0.50 eV from EOM-CCSD or five times more than the oeINDO error.

Figure 4.25 shows absorption spectra from TDDFT, oeINDO and ZINDO/s for Cd_4. Because of the limited computational resources, the spectrum from EOM-CCSD was not computed. All the methods predict Cd_4 equilibrium structure to absorb electromagnetic radiation within the ultraviolet energy range. The oeINDO absorption energy range and the spectrum highest peak agrees well with those from TDDFT. Its peak is shifted from that of the TDDFT by a small error, less than 0.10 eV. The peak of the ZINDO/s, however, is *blue-shifted* by a larger error of about 1.50 eV.

The absorption spectra for Cd_6 in Figure 4.26, further reveal that oeINDO spectra compare well with the *ab-initio* ones. The TDDFT and oeINDO both predict absorption spectra in the same energy range (2.60 eV - 4.0 eV). The oeINDO spectrum highest peak is *blue-shifted* from TDDFT by a small error of 0.30 eV while the ZINDO/s one is shifted by error of about 2.0 eV, which is roughly seven times more.

For Cd_8, the oeINDO spectrum matches almost exactly with that from TDDFT as shown in Figure 4.27. The ZINDO/s spectrum, on the other hand, deviates from TDDFT by about 2.40 eV.

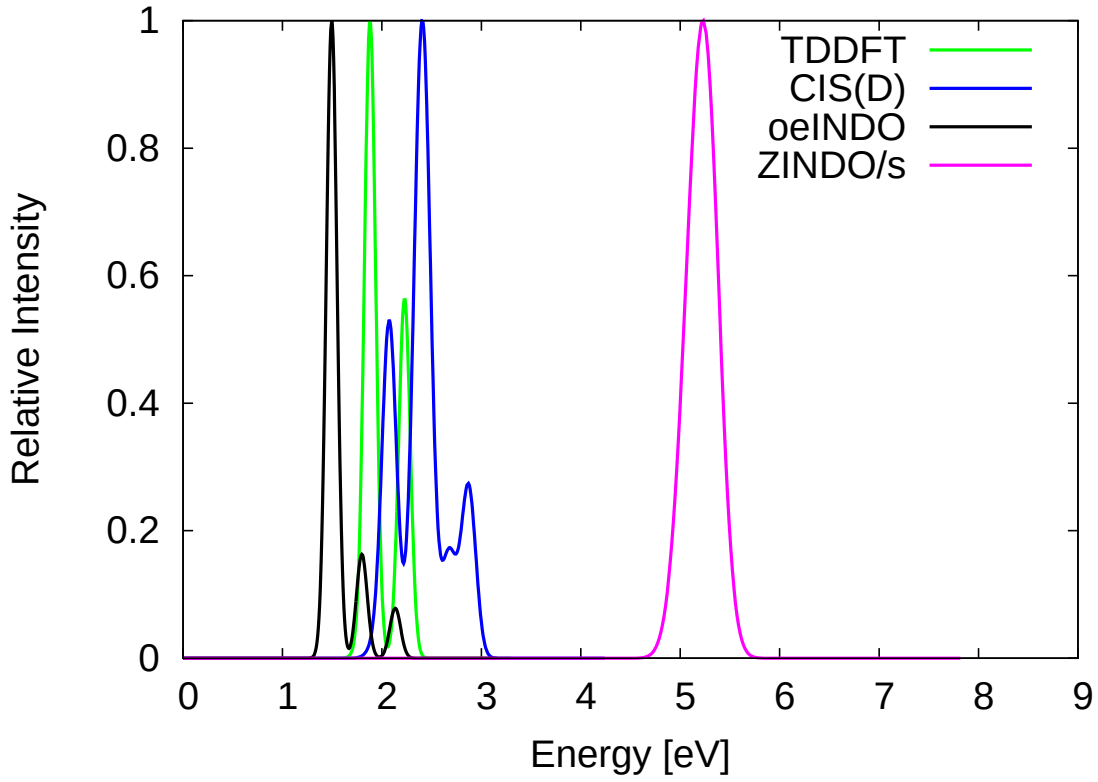

Figure 4.28: Absorption spectra of Cd_{16} equilibrium geometry obtained from different methods.The intensities have been scaled so that the highest intensity is equal to unity.

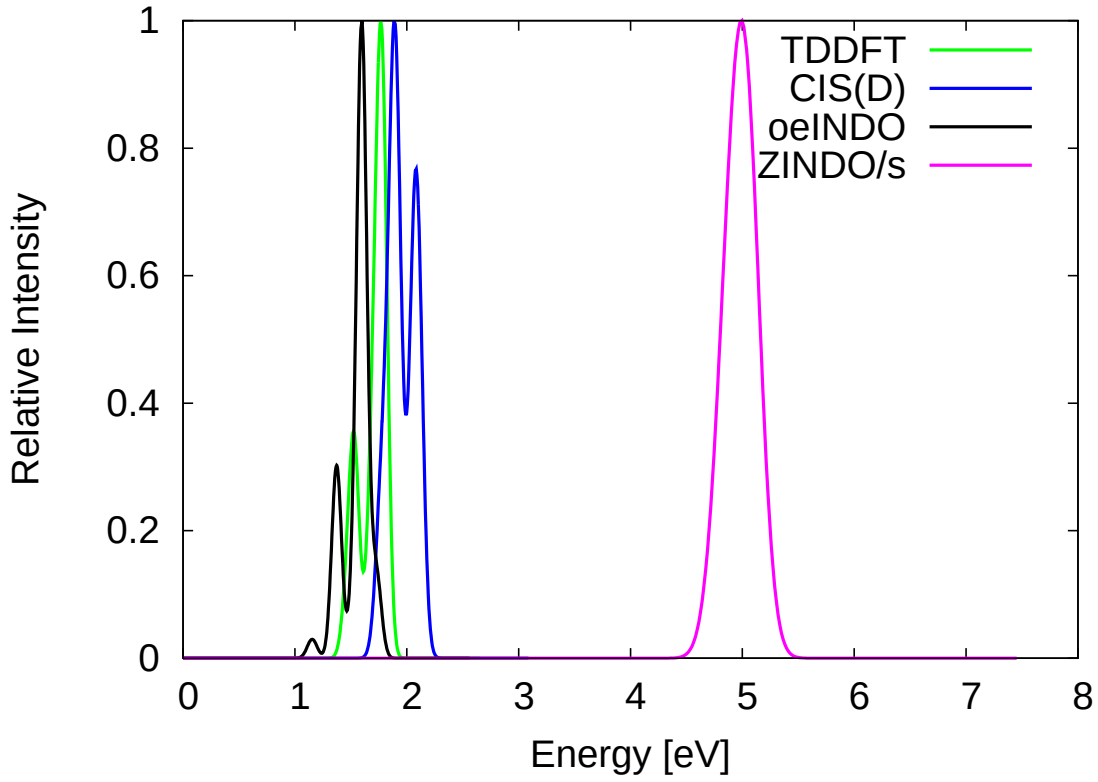

Figure 4.29: Absorption spectra for Cd_{20} equilibrium geometry obtained from different methods.The intensities have been scaled so that the highest intensity is equal to unity.

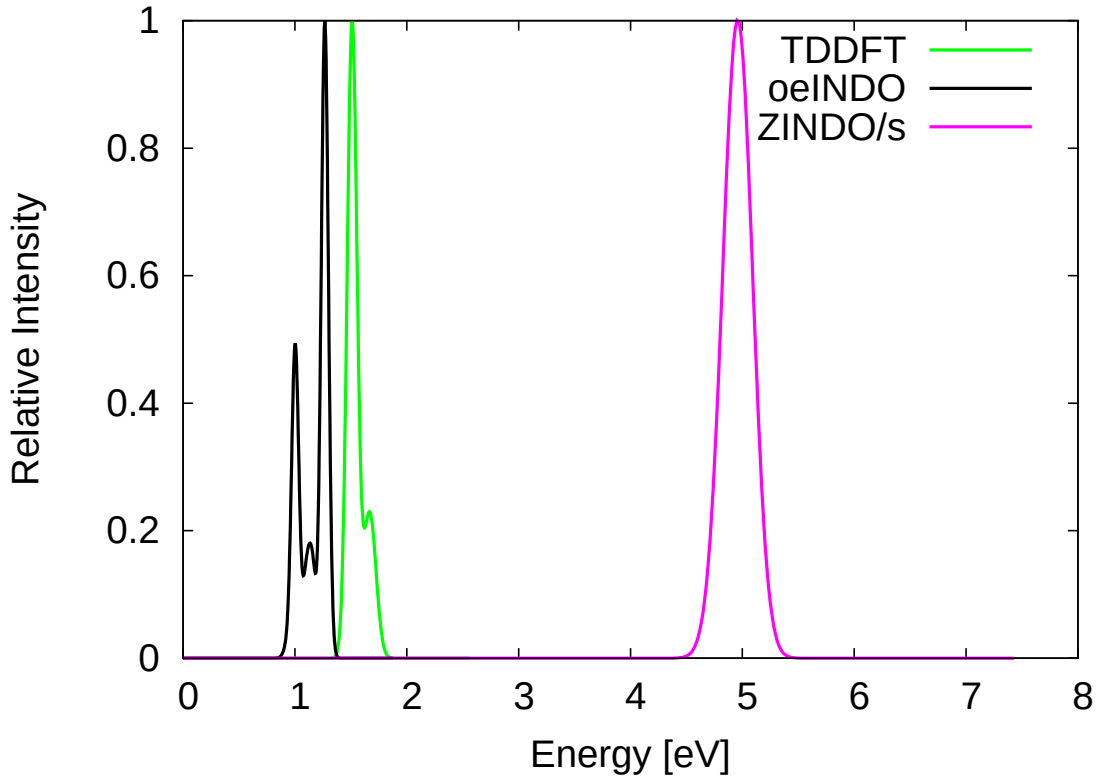

Figure 4.30: Absorption spectra for Cd_{25} equilibrium geometry obtained from different methods.The intensities have been scaled so that the highest intensity is equal to unity.

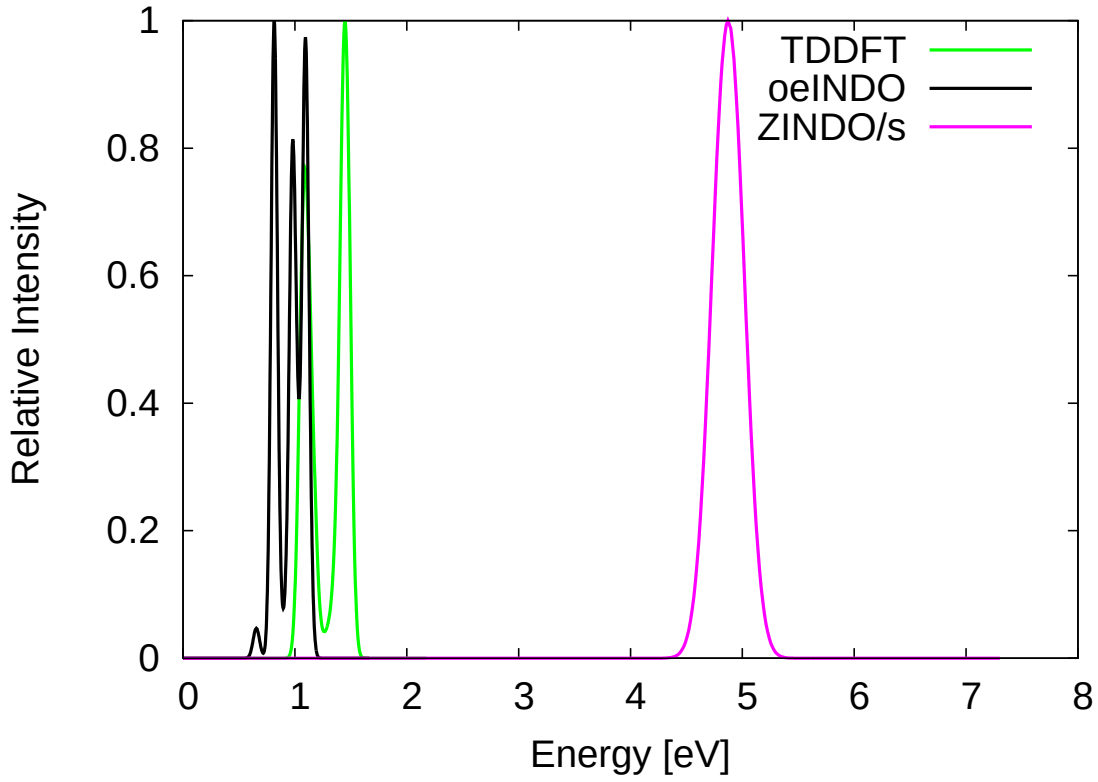

Figure 4.31: Absorption spectra for Cd_{30} equilibrium geometry obtained from different methods.The intensities have been scaled so that the highest intensity is equal to unity.

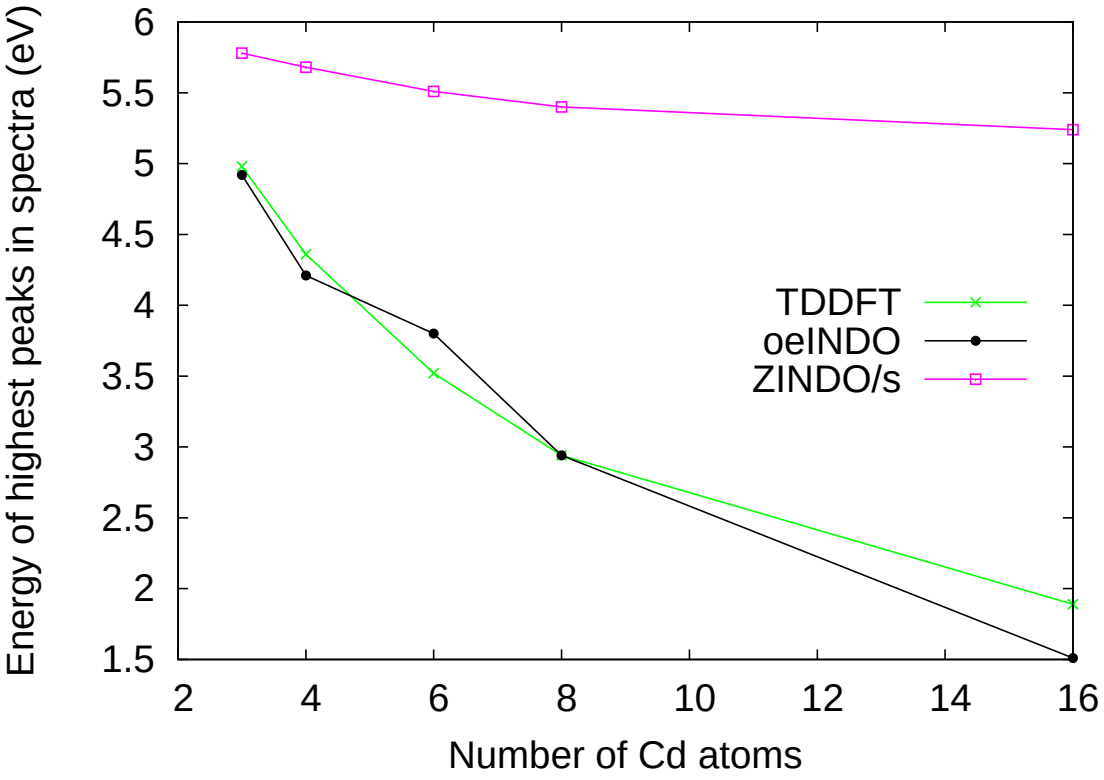

Figure 4.32: Highest peaks against number of units n in equilibrium Cd_n structures

The spectra of the Cd_{16} cluster as shown in Figure 4.28 corroborates the good performance of oeINDO. Both oeINDO and TDDFT showed that the cluster absorbs is in the visible region of the electromagnetic spectrum. In contrast, ZINDO/s showed absorption the ultraviolet region for the same cluster. The positions of the peaks of the oeINDO and ZINDO/s spectra intensity relative to that of TDDFT are about 0.30 eV and 3.30 eV, respectively. The absorption spectra for Cd_{20}, Cd_{25} and Cd_{30} in Figures 4.29, 4.30, and 4.29, respectively, also show that the oeINDO spectra agree well with those from the *ab-initio* TDDFT and CIS(D) method. The ZINDO/s spectra, however, deviate much more up to $\approx 3.3\ eV$

Figure 4.32 summarizes how the peak maxima from the oeINDO and ZINDO/s absorption spectra compare with those from TDDFT. It can be observed for all methods that the energies of the peaks decrease with the number of atoms. The peaks of oeINDO agree well with those from TDDFT with MAE of 0.17 eV while ZINDO/s peaks deviate from TDDFT with a larger MAE of 1.98 eV.

4.2.5 Transferability of oeINDO Sulphur Parameters

The oeINDO method was also validated by verifying its accuracy for complex sulphur structures that were not included in the training geometries. Excitation energies and absorption spectra were computed with different methods for S_n (n=3, 5, 6, 10, 20) equilibrium structures and their results are presented in Figures 4.33, 4.34, 4.35, 4.36, 4.37, and 4.37.

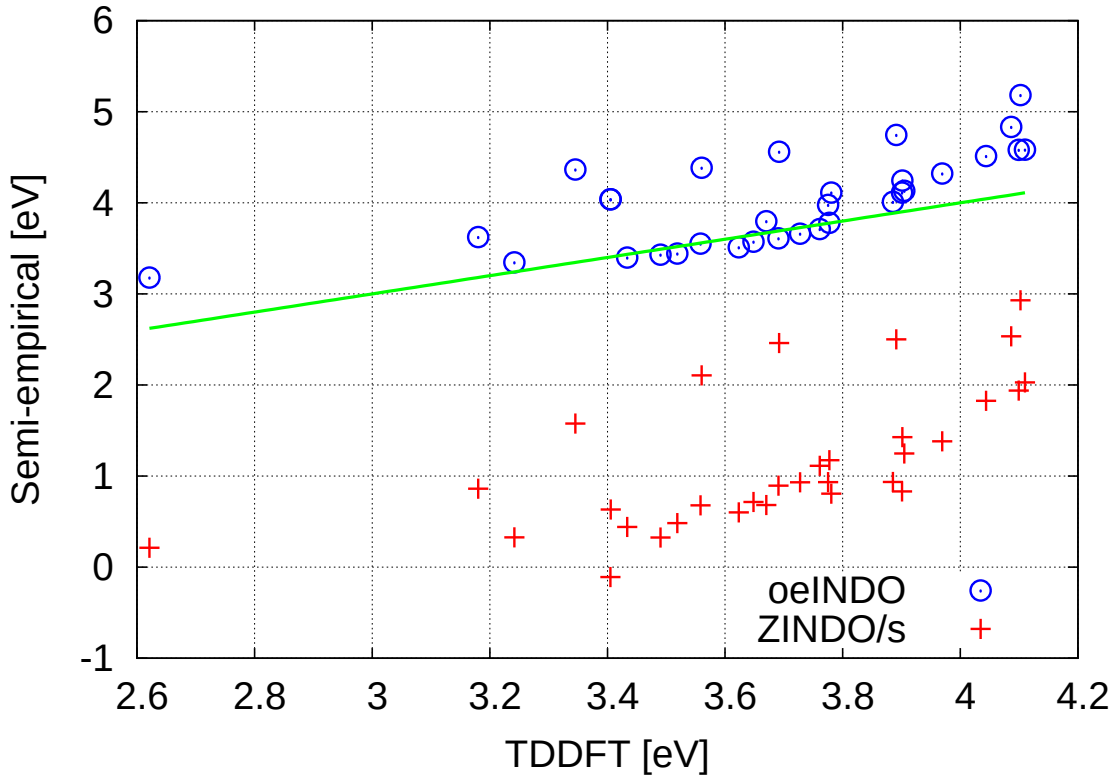

Figure 4.33: Semi-empirical methods against TDDFT energies for S_n $(n = 5, 6, 10, 20)$ equilibrium structures

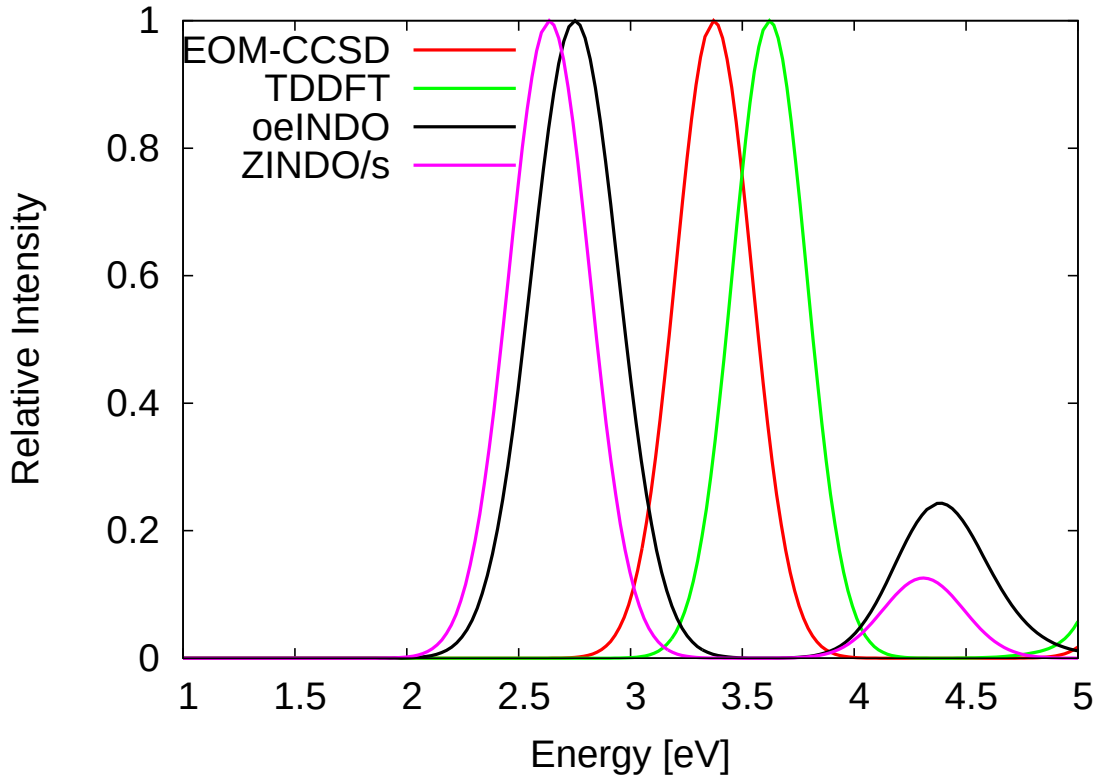

Figure 4.34: Absorption spectra for S_3 equilibrium geometry obtained from different methods.The intensities have been scaled so that the highest intensity is equal to unity.

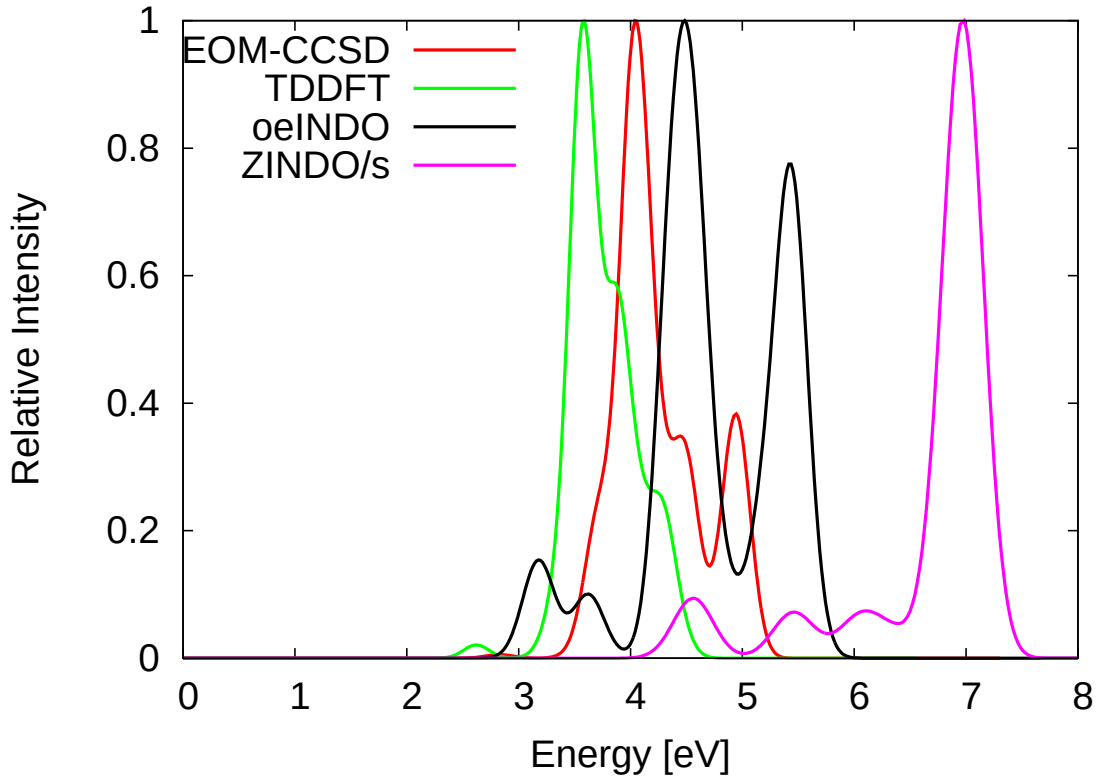

Figure 4.35: Absorption spectra for S_5 equilibrium geometry obtained from different methods.The intensities have been scaled so that the highest intensity is equal to unity.

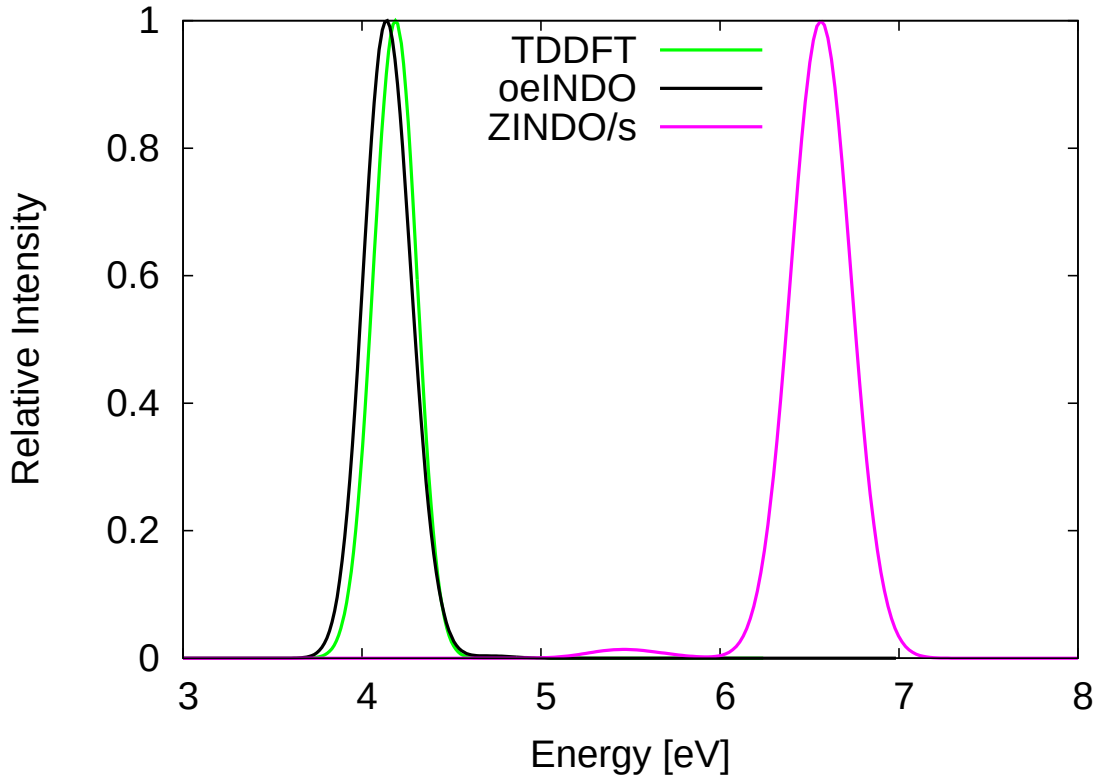

Figure 4.36: Absorption spectra for S_6 equilibrium geometry obtained from different methods.The intensities have been scaled so that the highest intensity is equal to unity.

Figure 4.33 is a scatter plot that shows how the excitation energies from oeINDO and ZINDO/s compare with those from TDDFT for S_n (n=5, 6, 10, 20) structures. A total of thirty-two excitation energies were obtained with of this each method. The plot shows that oeINDO excitation energies (blue circles) are reasonably close to the *ab-initio* TDDFT excitations while ZINDO/s energies (red plus signs) deviate more. The oeINDO excitations compared favorably with the TDDFT ones with MAE of 0.36 eV while ZINDO/s excitations (red plus signs) compared with a larger MAE of 2.51 eV.

The absorption spectra of S_3 equilibrium structure obtained with different methods are presented in Figure 4.34. Similar spectra patterns are observed for all methods. The EOM-CCSD (benchmark), oeINDO and ZINDO/s absorption band appear in the visible and the ultra-violet energy regions but that of TDDFT is found only in the ultraviolet region. The highest peak of the spectra from TDDFT, oeINDO and ZINDO/s are shifted from EOM-CCSD by 0.26 eV (*blue-shifted*), 0.61 eV (red-shifted), and 0.70 eV (*red-shifted*), respectively. Relative to EOM-CCSD, the oeINDO performed better than the original ZINDO/s model.

The spectra for the S_5 equilibrium structure in Figure 4.35 show that oeINDO agrees well with EOM-CCSD. It reproduced the EOM-CCSD spectra pattern. The oeINDO has a comparable performance with TDDFT. Both oeINDO and TDDFT spectra highest peaks are shifted from EOM-CCSD by approximately 0.44 eV. While the oeINDO peak is *blue-shifted*, the TDDFT one is *red-shifted*. The spectrum peak from ZINDO/s however, is much deviated from EOM-CCSD spectrum highest peak with a larger error of 2.94 eV.

For the sulphur structures with six or more atoms, EOM-CCSD is computationally intensive and the available computational resources could not handle them. Thus, comparisons were made with TDDFT, a reasonable alternative to EOM-CCSD. In Figure 4.36, a very good agreement was observed between the oeINDO and TDDFT absorption spectra for the S_6 equilibrium structures. Both have similar spectra pattern and show absorption in the energy range 3.50 - 4.80 eV. However, ZINDO/s spectrum is far shifted (*blue-shifted*) from that of the TDDFT by 2.39 eV.

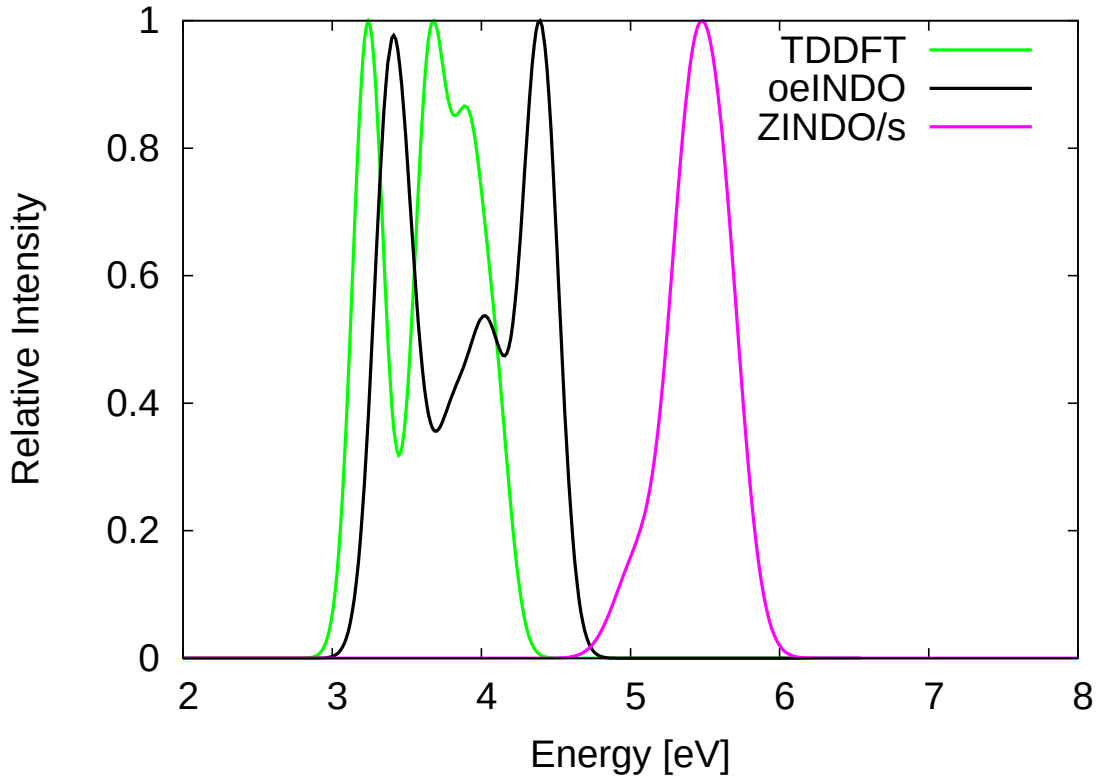

Figure 4.37: Absorption spectra for S_{10} equilibrium geometry obtained from different methods.The intensities have been scaled so that the highest intensity is equal to unity.

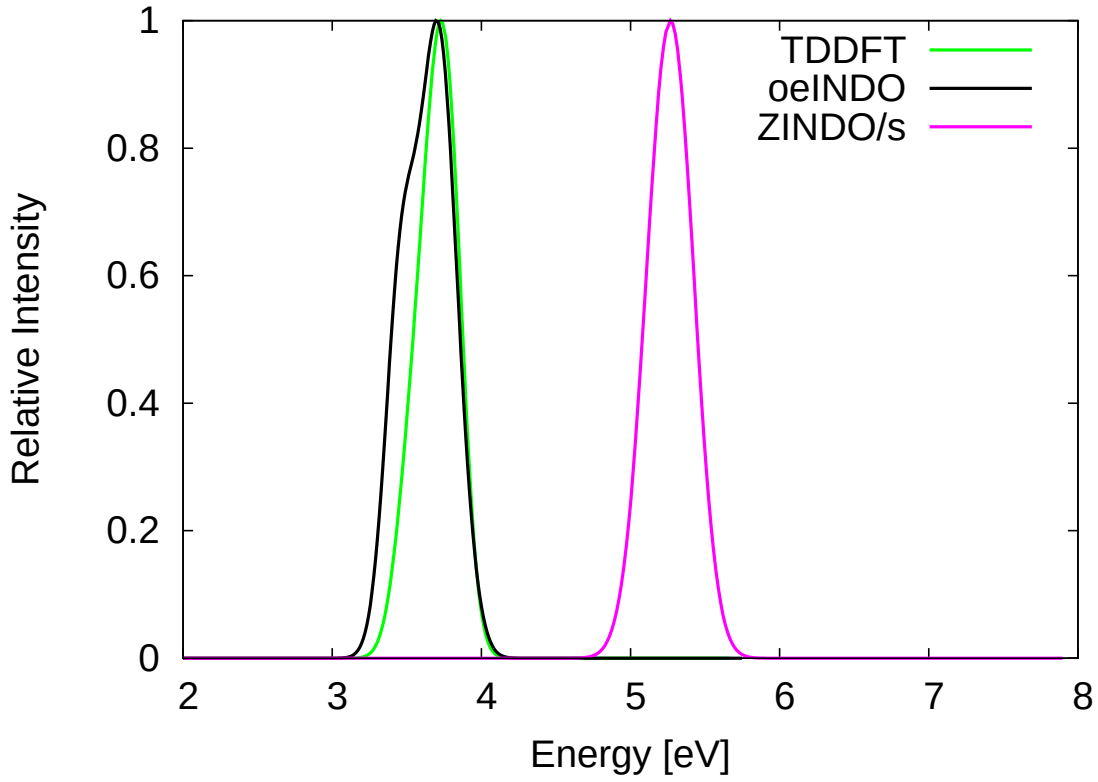

Figure 4.38: Absorption spectra for S_{20} equilibrium geometry obtained from different methods.The intensities have been scaled so that the highest intensity is equal to unity.

The performance of the oeINDO in favorably reproducing spectra from *ab-initio* calculations was also confirmed with the absorption spectra obtained for S_{10} and S_{20} structures as shown in Figures 4.37 and 4.38, respectively.

For S_{10} equilibrium structure, oeINDO reproduced the spectrum pattern observed in the TDDFT one. The first prominent peak from oeINDO is shifted from the first and second peak of the TDDFT spectrum by about 0.2 and 0.72 eV, respectively.

A good match of the spectra from oeINDO and TDDFT was also observed for S_{20} equilibrium structure (Figure 4.38). Both show that the S_{20} structure absorbs in the ultraviolet region with their highest peaks matching exactly. In contrast, the spectra from ZINDO/s is *blue-shifted* from TDDFT by a large amount: 1.56 eV.

The average absolute shift of oeINDO absorption spectra highest peaks from those of the TDDFT for all S_n (n=5, 6, 10, 20) equilibrium structures is 0.5 eV. The ZINDO/s is however shifted by a larger amount of 2.02 eV.

4.2.6 Transferability of oeINDO to ZnS clusters

Despite the fact that the Zn-S diatomics were not directly parameterised, the transferability and accuracy of the oeINDO model to complex ZnS clusters were also found to be good. Calculations for these clusters were carried out using the oeINDO Zn_2 and S_2 parameters.

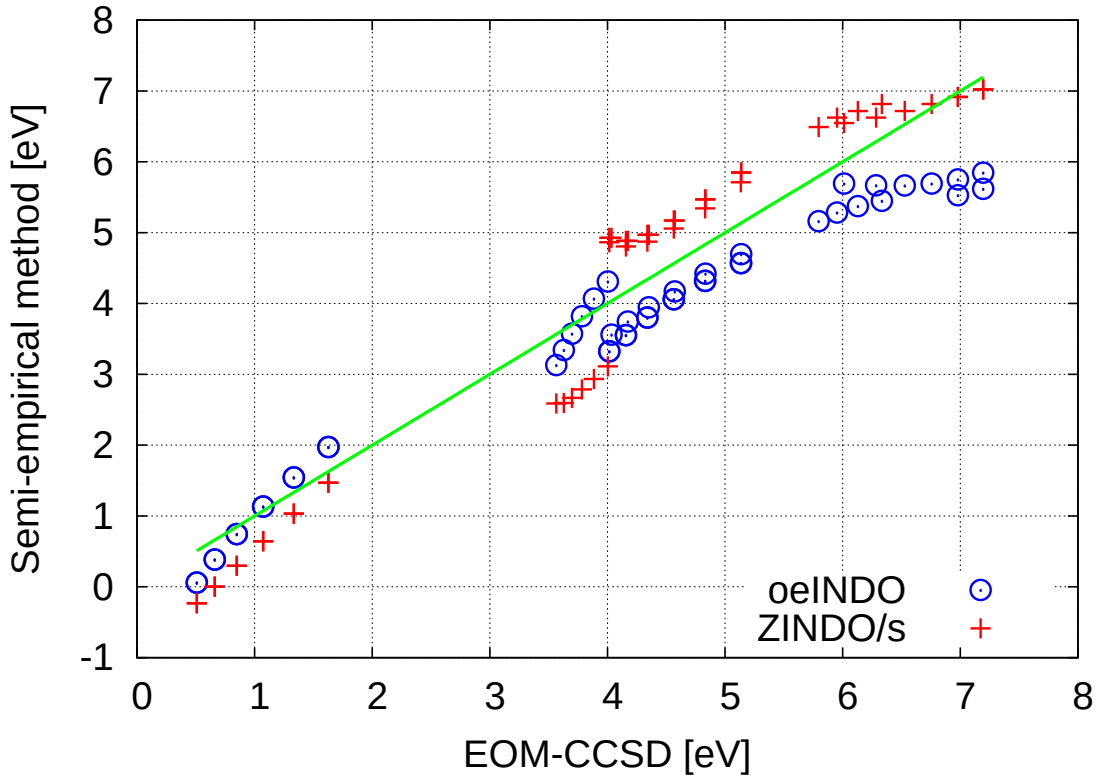

Figure 4.39: Scatter plot of Zn-S diatomics excitation energies from ZINDO/s and oeINDO against those from EOM-CCSD (the benchmark). The blue circles are the oeINDO excitation energies while the red plus signs are the ZINDO/s excitation energies. The straight green line represents the benchmark.

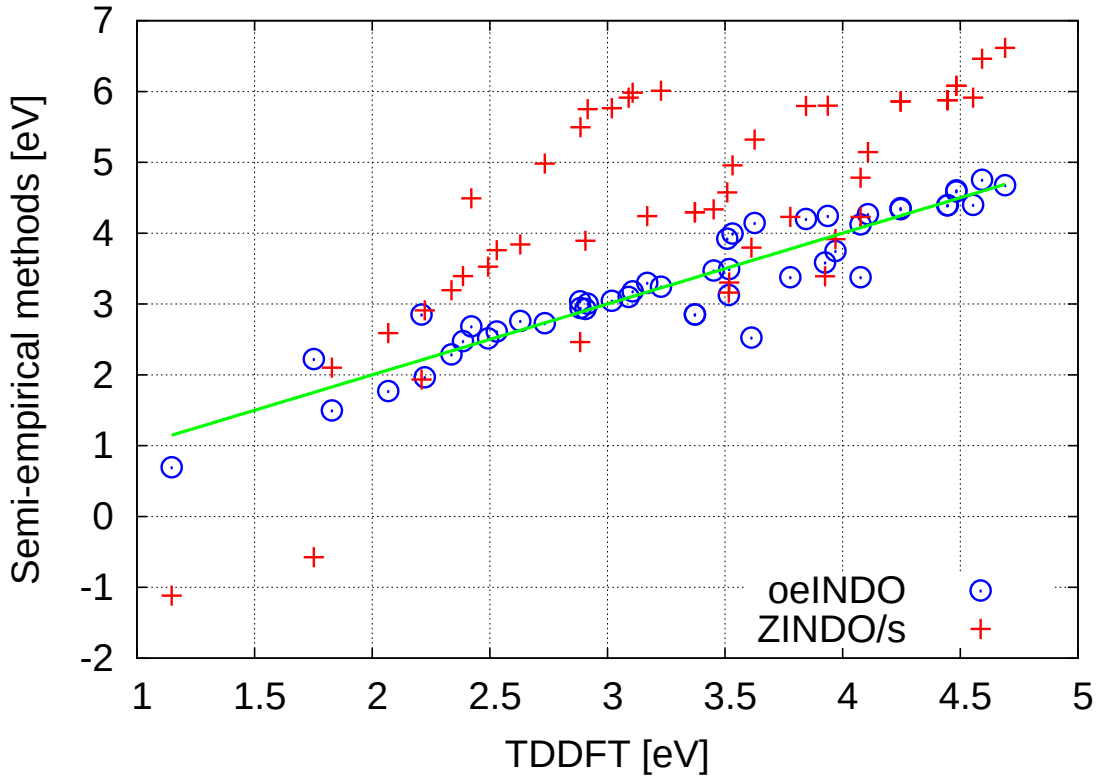

Figure 4.40: Semi-empirical methods against TDDFT energies for $(ZnS)_n$ $(n = 2,3,4,10,19)$ equilibrium structures.

Figure 4.39 is a scatter plot of 48 excitation energies each obtained using oeINDO and ZINDO/s against those obtained with EOM-CCSD for Zn-S diatomics. The oeINDO energies compared with the EOM-CCSD energies with MAE of 0.52 eV while ZINDO/s compared with a slightly larger error of 0.57 eV.

The excitation energies computed for $(ZnS)_n$ (n=2, 3, 4, 10, 19) equilibrium structure using the oeINDO, ZINDO/s and TDDFT method are presented in Tables C.17 - C.21. A scatter plot showing a total of 40 excitation energies obtained using oeINDO and ZINDO/s against those from TDDFT for all $(ZnS)_n$ (n=2, 3, 4, 10, 19) equilibrium structures are displayed in Figure 4.41. The plot shows that oeINDO agrees well with the TDDFT and performs better than ZINDO/s. The MAE of the excitations from oeINDO relative to those from TDDFT is 0.23 eV while MAE of the excitations from ZINDO/s relative to TDDFT is much larger: 1.33 eV. Also, it can be observed from Table C.17 and Figure 4.41 that ZINDO/s has its first and second-lowest excitation energies as negative values for the $(ZnS)_2$ structure.

The oeINDO transferability was further verified with the absorption spectra obtained for the different ZnS complex clusters. The oeINDO spectra as shown in Figures 4.41, 4.42, 4.43, 4.44, and 4.45 agree reasonably with those from TDDFT.

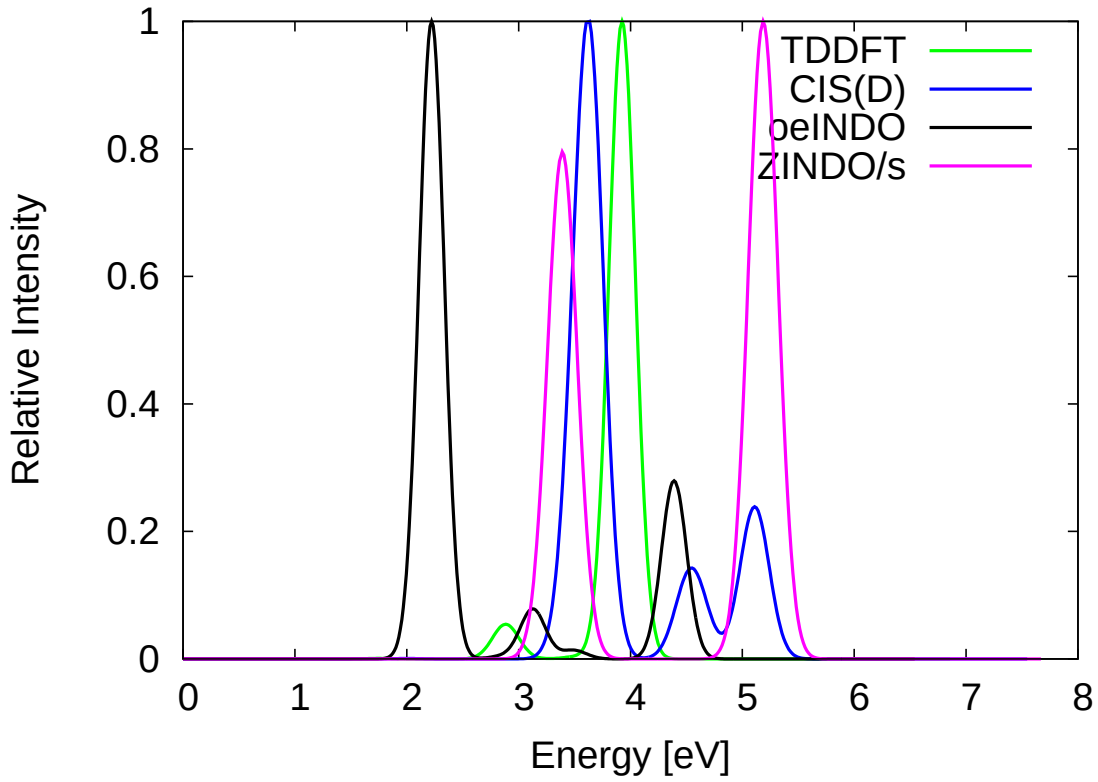

Figure 4.41: Absorption spectra for $(ZnS)_2$ equilibrium geometry obtained from different methods.The intensities have been scaled so that the highest intensity is equal to unity.

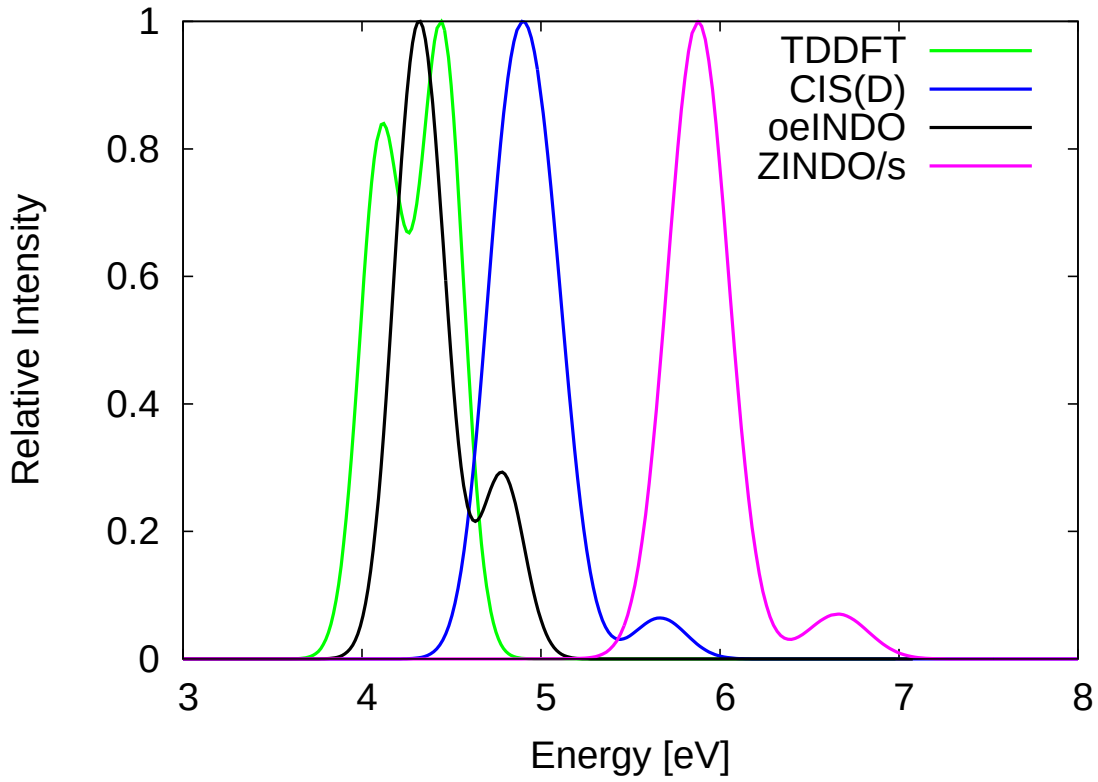

Figure 4.42: Absorption spectra for $(ZnS)_3$ equilibrium geometry obtained from different methods.The intensities have been scaled so that the highest intensity is equal to unity.

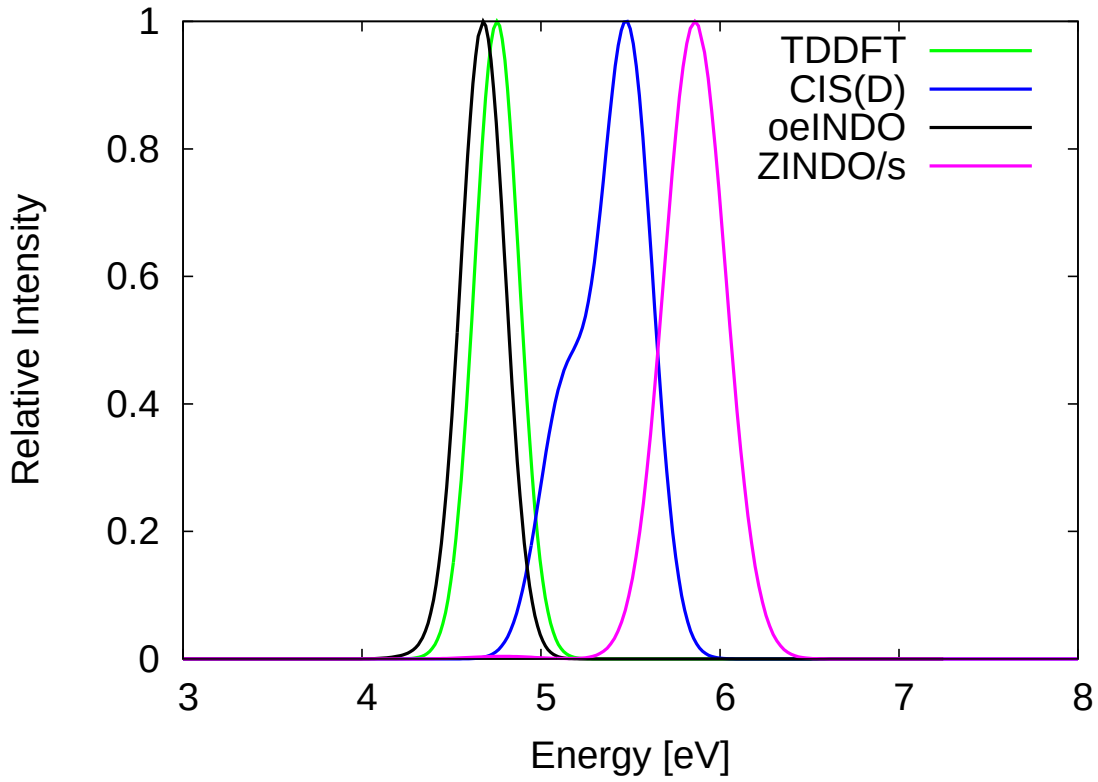

Figure 4.43: Absorption spectra for $(ZnS)_4$ equilibrium geometry obtained from different methods.The intensities have been scaled so that the highest intensity is equal to unity.

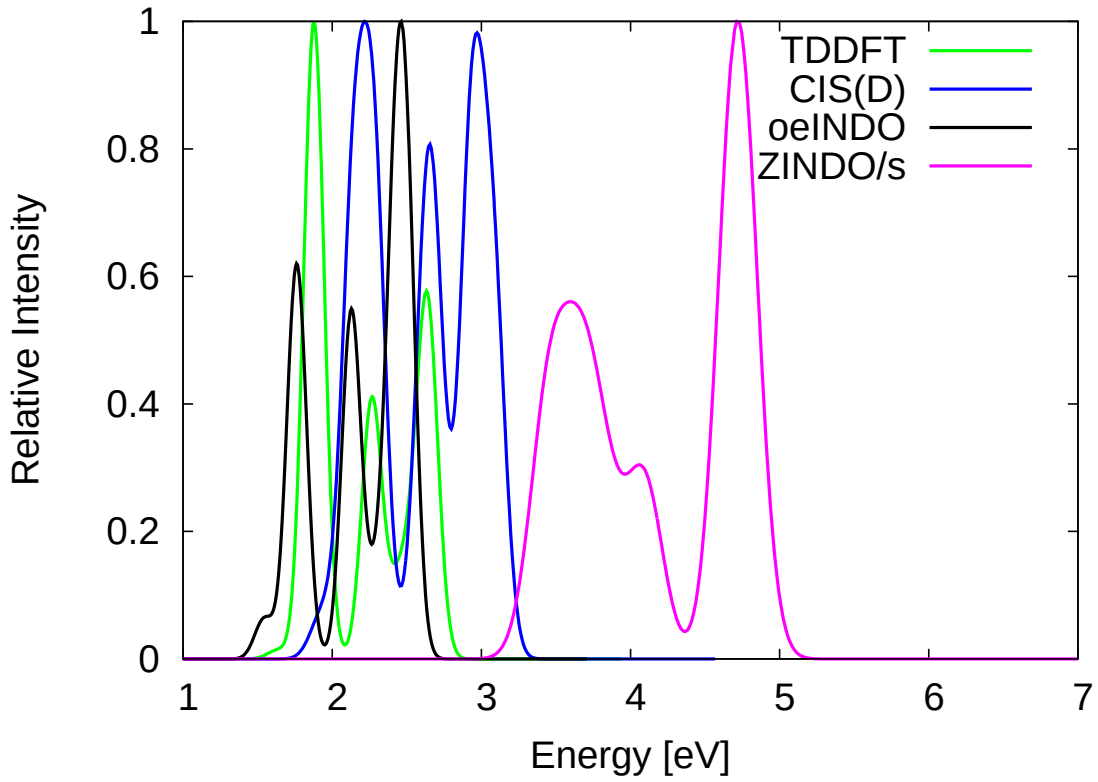

Figure 4.44: Absorption spectra for $Zn_{10}S_{10}$ equilibrium geometry obtained from different methods.The intensities have been scaled so that the highest intensity is equal to unity.

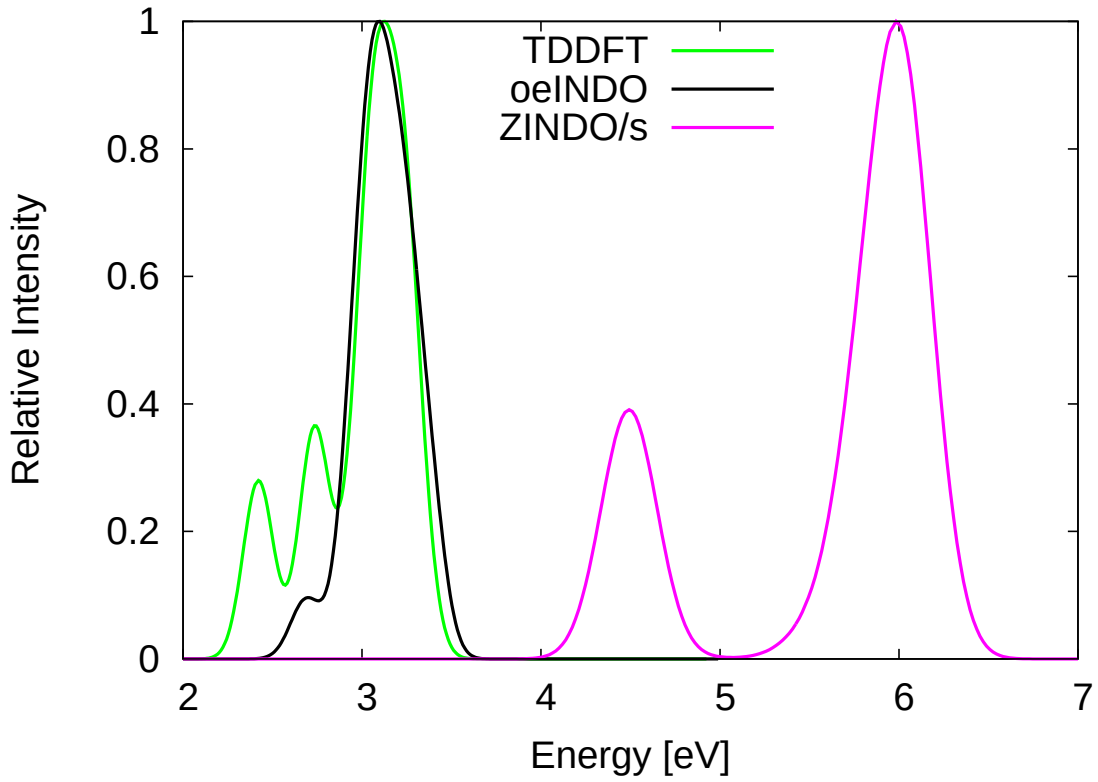

Figure 4.45: Absorption spectra for $Zn_{19}S_{19}$ equilibrium geometry obtained from different methods.The intensities have been scaled so that the highest intensity is equal to unity.

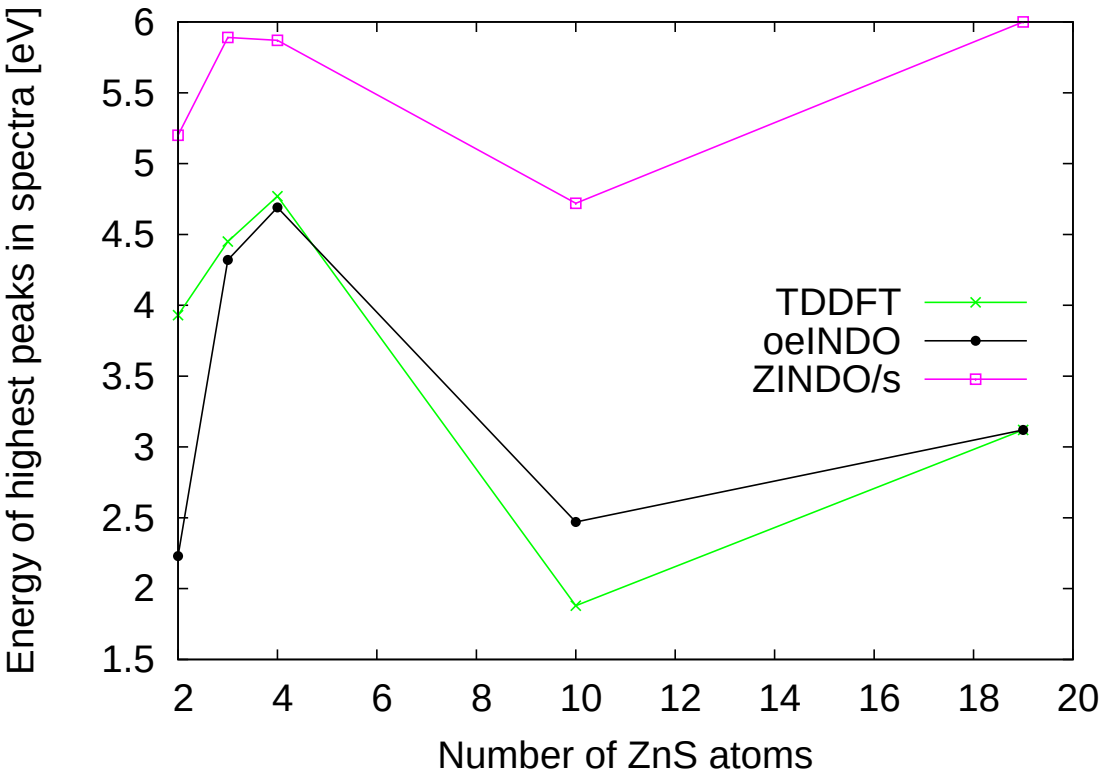

Figure 4.46: Highest peaks against number of units n in equilibrium $(ZnS)_n$ structures

The absorption spectra of $(ZnS)_2$ (Figure 4.41), from oeINDO, CIS(D), TDDFT and ZINDO/s peaks at about 2.23 eV (in visible region of the spectrum), 3.63 eV (ultraviolet region), 3.93 eV (ultraviolet region) and 5.20 eV (ultraviolet region), respectively. The oeINDO spectrum highest peak is *red-shifted* by 1.70 eV from that TDDFT while that of ZINDO/s is *blue-shifted* by 1.20 eV.

The spectra from different methods for the $(ZnS)_3$ cluster in Figure 4.16 show that the cluster absorbs in the ultraviolet region for all methods employed. oeINDO reproduced the TDDFT absorption spectrum with its highest peak shifted from TDDFT by 0.13 eV. However, the CIS(D) and ZINDO/s spectra peaks are shifted from TDDFT by 0.45 eV and 1.45 eV, respectively.

A very good match of the oeINDO and TDDFT was observed for $(ZnS)_4$ (Figure 4.43). The oeINDO spectrum highest peak matched that of TDDFT with a small error of 0.08 eV.

The absorption spectra from oeINDO in Figure 4.37 and Figure 4.45 for $(ZnS)_n$ (n=10, 19) support the transferability ability of the oeINDO parameters. For $(ZnS)_{10}$ cluster, the oeINDO, TDDFT and CIS(D) spectra have similar pattern and they all absorb in the visible region (1.50 - 3.0 eV). ZINDO/s however, absorb in the ultraviolet region (3.0 - 30.0 eV). oeINDO reproduces the spectrum from the TDDFT for $(ZnS)_{19}$ cluster with a good match in absorption spectra maxima.

Figure 4.46 shows how the spectra maxima from oeINDO and ZINDO/s compare with those from TDDFT. Obviously, the oeINDO compares better than ZINDO/s with TDDFT as the benchmark. The MAE of the spectra peaks from oeINDO relative to TDDFT is 0.50 eV while that for ZINDO/s relative to TDDFT is 1.90 eV.

4.2.7 Transferability of oeINDO to CdS clusters

Just as in the case of ZnS clusters, the Cd-S diatomics were not directly parameterised rather, the parameters obtained for Cd_2 and S_2 were employed to calculate the excitation energies and absorption spectra for the $(CdS)_n$ (n=2, 3, 4, 10) equilibrium structures.

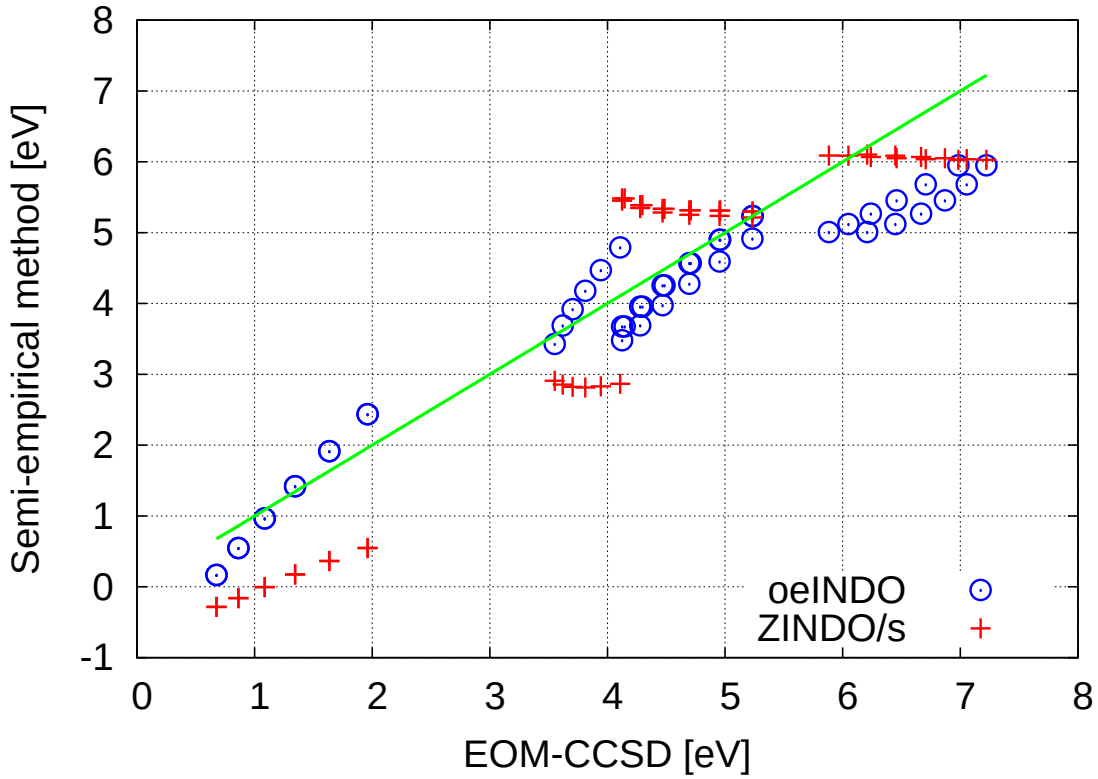

Figure 4.47: Scatter plot of Cd-S diatomics excitation energies from ZINDO/s and oeINDO against those from EOM-CCSD (the benchmark). The blue circles are the oeINDO excitation energies while the red plus signs are the ZINDO/s excitation energies. The straight green line represents the benchmark.

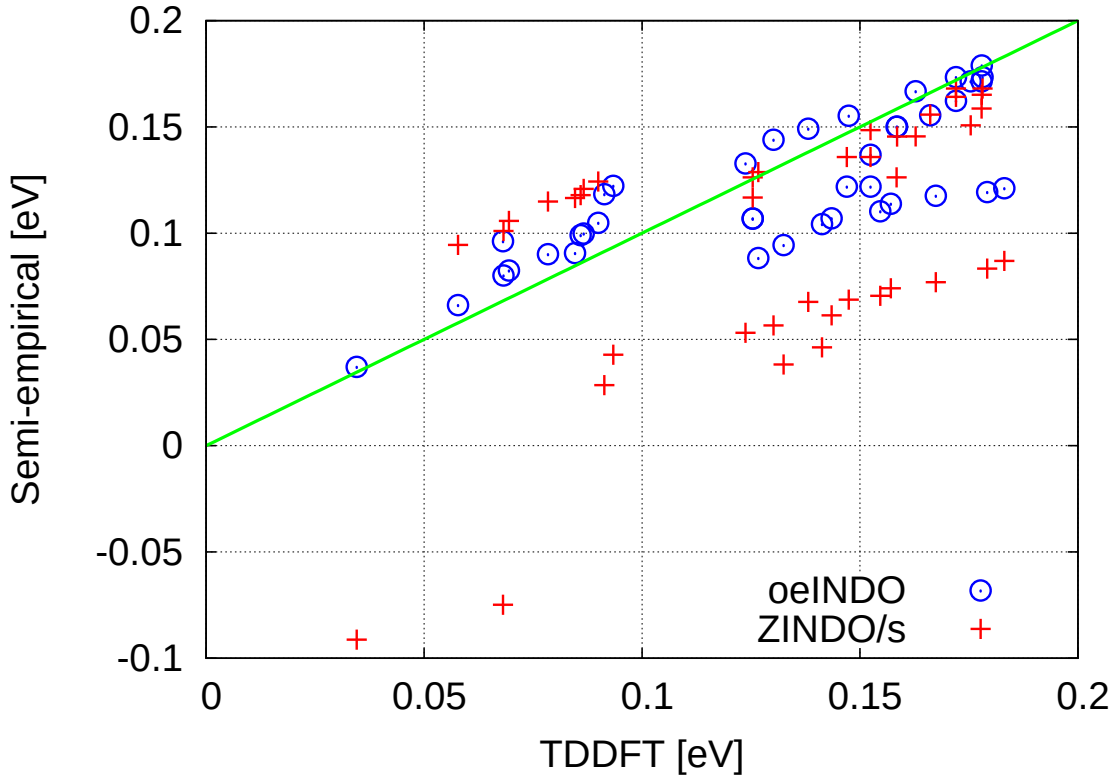

Figure 4.48: Semi-empirical methods against TDDFT energies for $(CdS)_n$ $(n = 2,3,4,10)$ equilibrium structures

Figure 4.47 shows the scatter plot of oeINDO and ZINDO/s excited state energies against the EOM-CCSD energies for Cd-S diatomic of different separations. A total of 48 excitation energies obtained with each method. The oeINDO compared better than ZINDO/s to EOM-CCSD. The MAE of oeINDO excited energies relative to EOM-CCSD energies is 0.51 eV. The MAE of ZINDO/s however, is much larger: 0.81 eV.

A total of thirty-two vertical excitation energies were computed each using oeINDO and ZINDO/s for $(CdS)_n$ (n=2, 3, 4, 10) equilibrium structures and compared with corresponding energies from TDDFT. Comparisons were not made with EOM-CCSD because the available computational resource is limited and cannot handle the huge calculations involved for these structures.

The scatter plot in Figure 4.48 shows the comparison of the excitation energies from oeINDO and ZINDO/s to those from TDDFT for $(CdS)_n$ (n=2, 3, 4, 10) equilibrium structures. The oeINDO excitation energies matched with the TDDFT ones with MAE of 0.36 eV. ZINDO/s performed poorly. Its excitation energies deviate from TDDFT energies with larger MAE of 0.96 eV. More so, it gave some negative excitations (Figure 4.48 and Table C.22), which are unacceptable because the excitation energy difference (HOMO -LUMO) cannot be a negative value.

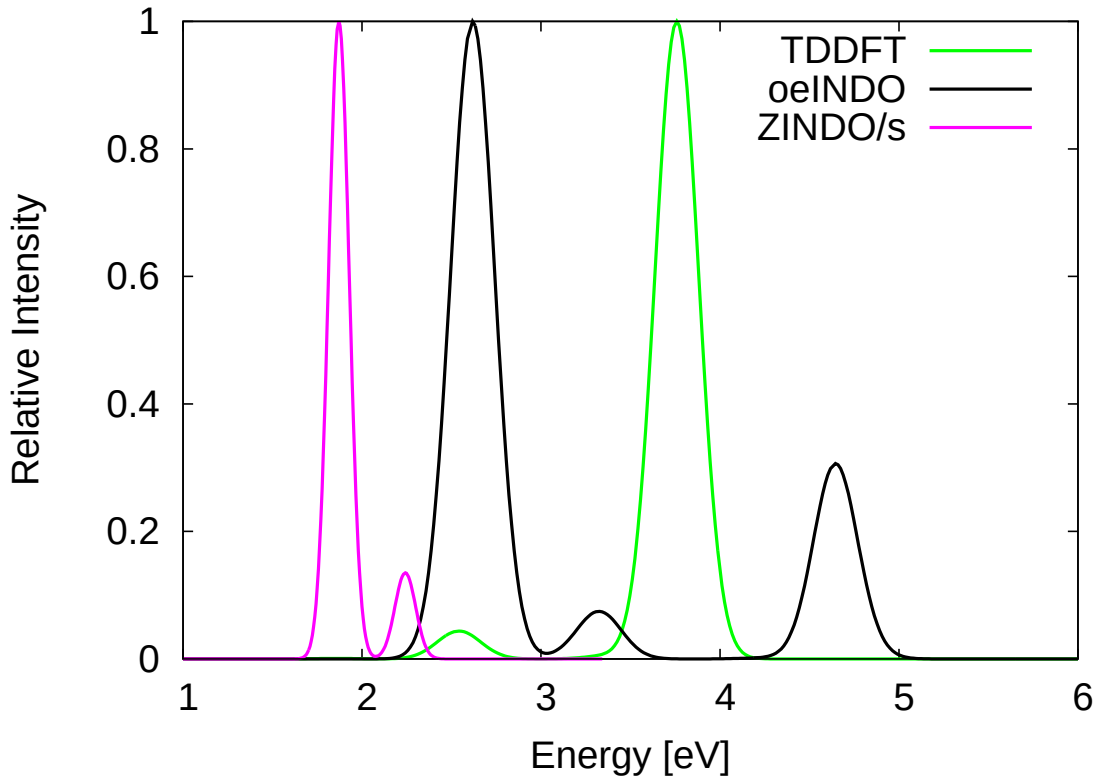

Figure 4.49: Absorption spectra for $(CdS)_2$ equilibrium geometry obtained from different methods.The intensities have been scaled so that the highest intensity is equal to unity.

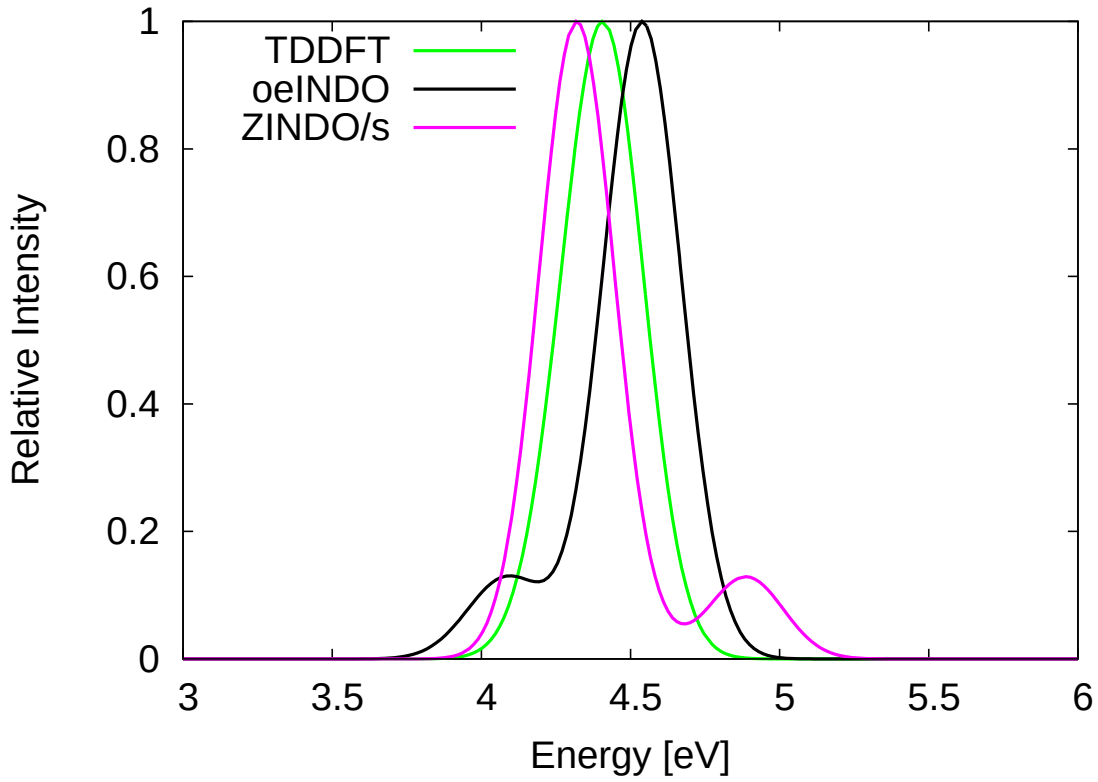

Figure 4.50: Absorption spectra for $(CdS)_3$ equilibrium geometry obtained from different methods.The intensities have been scaled so that the highest intensity is equal to unity.

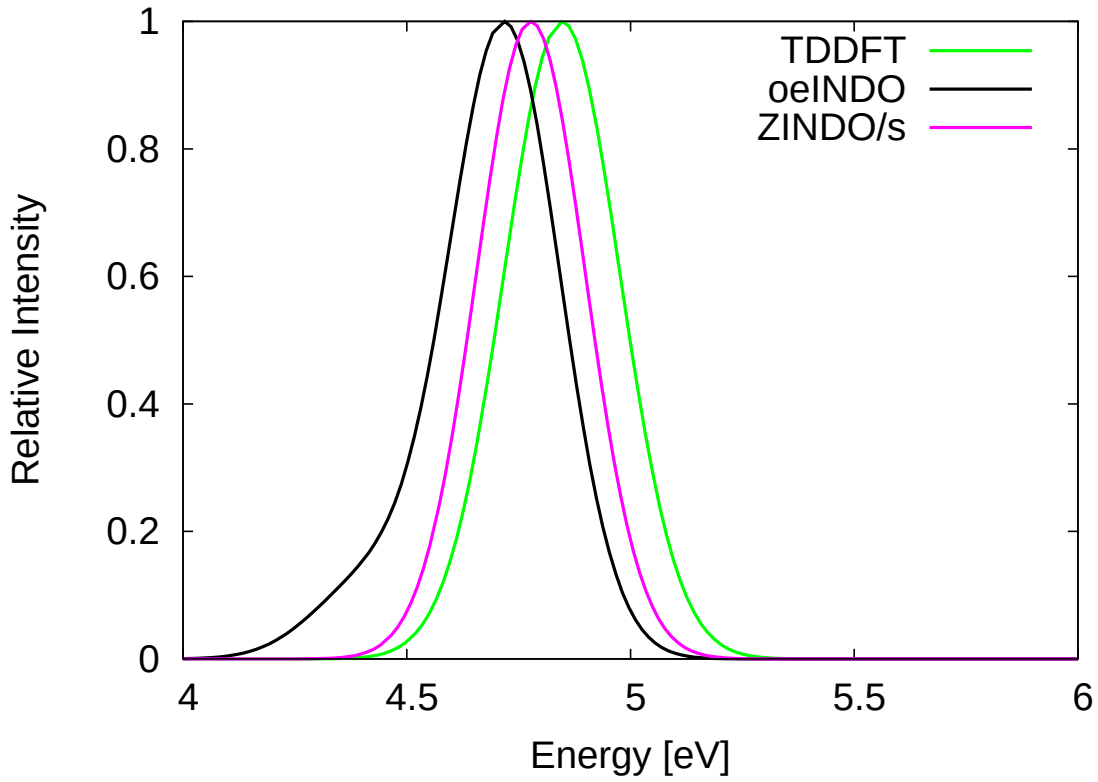

Figure 4.51: Absorption spectra for $(CdS)_4$ equilibrium geometry obtained from different methods.The intensities have been scaled so that the highest intensity is equal to unity.

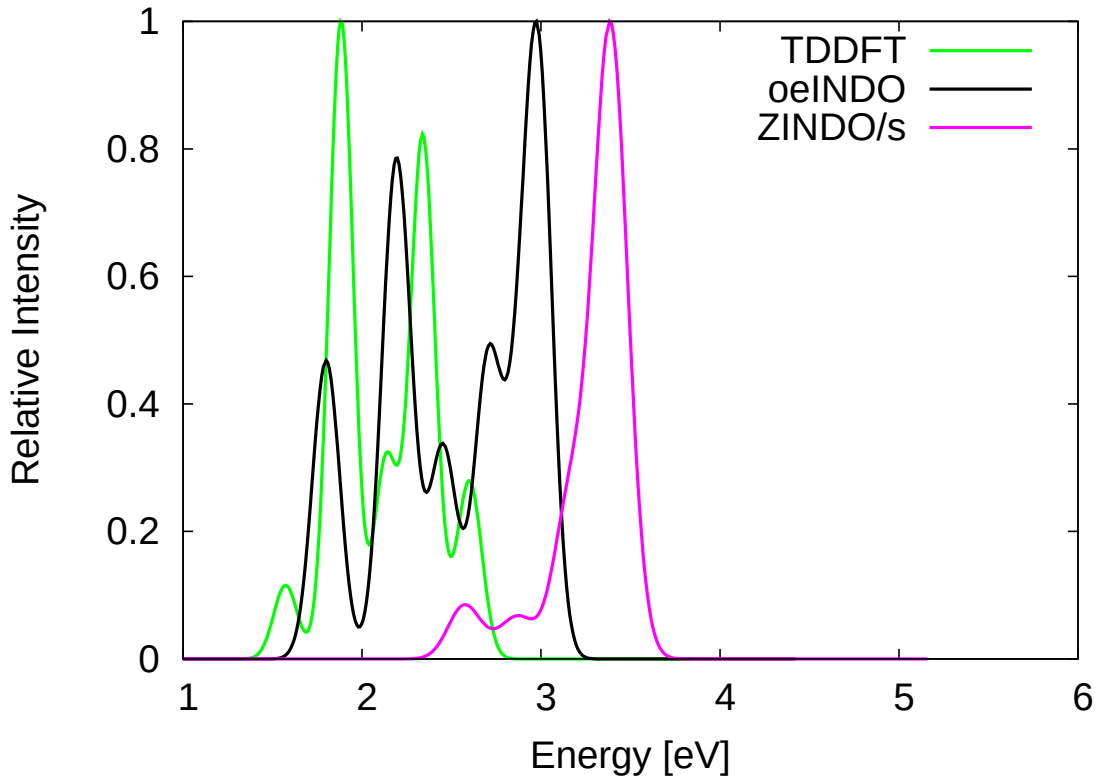

Figure 4.52: Absorption spectra for $(CdS)_{10}$ equilibrium geometry obtained from different methods.The intensities have been scaled so that the highest intensity is equal to unity.

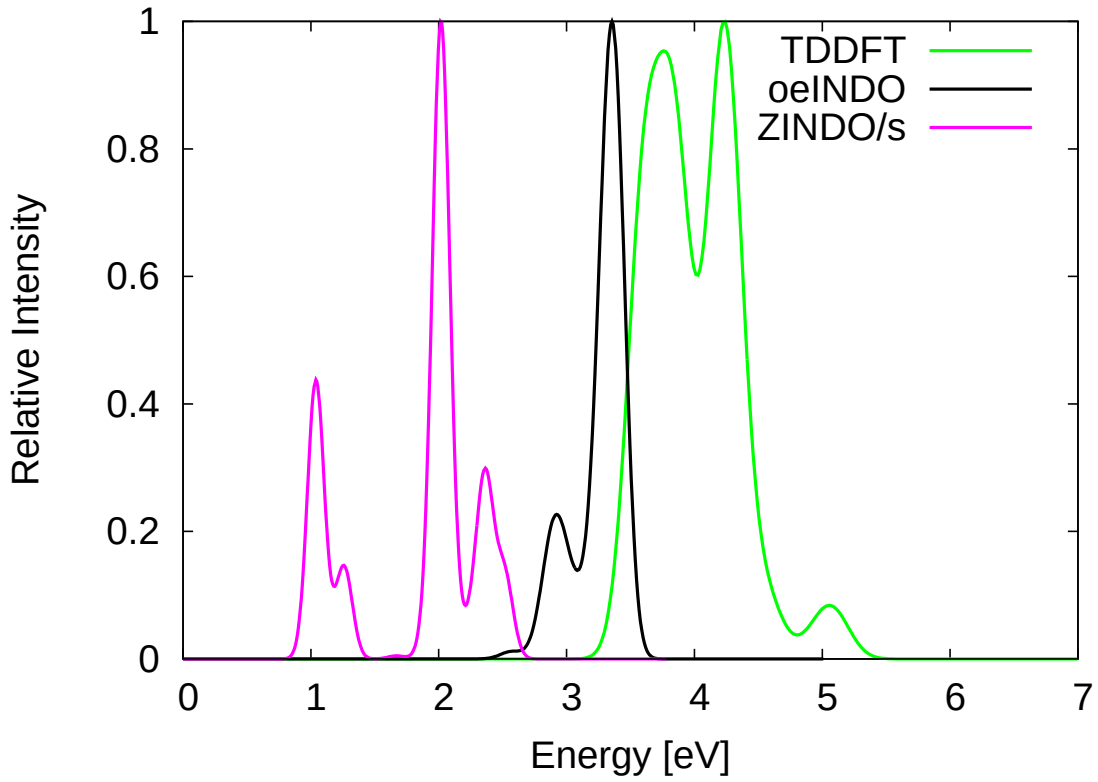

Figure 4.53: Absorption spectra for $(CdS)_{19}$ equilibrium geometry obtained from different methods.The intensities have been scaled so that the highest intensity is equal to unity.

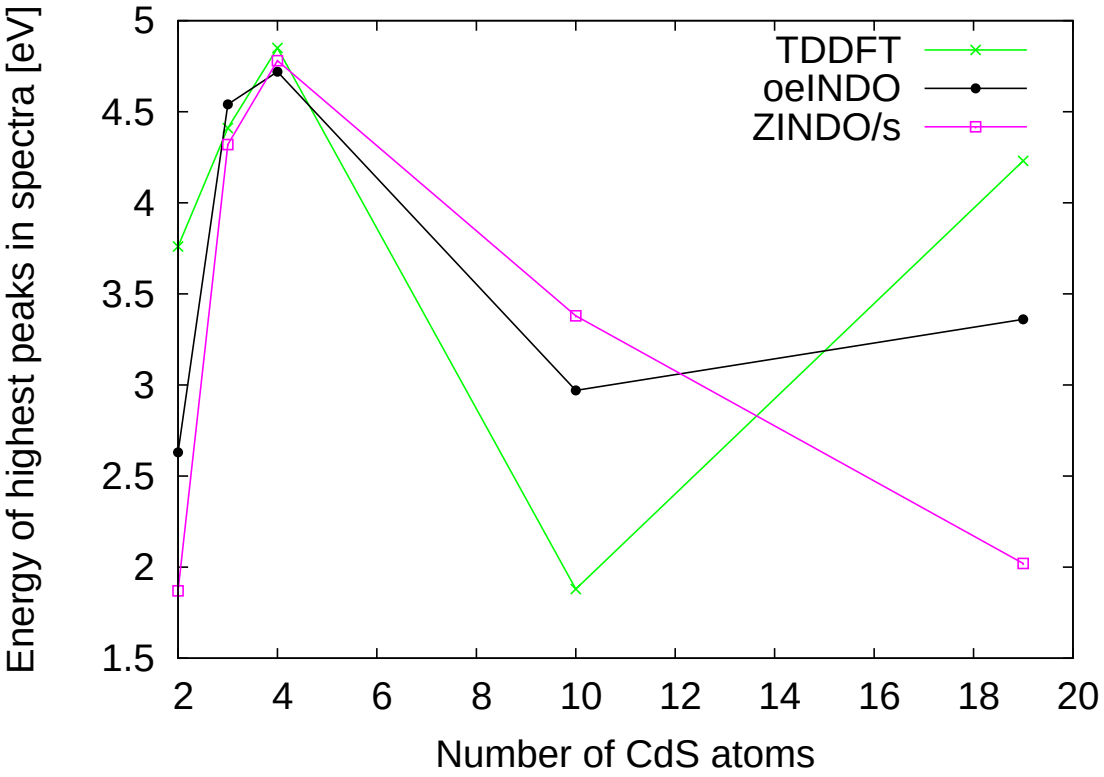

Figure 4.54: Highest peaks against number of units n in equilibrium $(CdS)_n$ structures. The oeINDO curve and not the ZINDO/s curve qualitatively reproduces the TDDFT one.

Figures 4.49, 4.50, 4.51, 4.52, and 4.53 further confirm the capability of oeINDO to give reasonably accurate results for structures not included in the parameterisation training sets.

For the $(CdS)_2$ equilibrium structure, the absorption spectra pattern is similar for all methods as shown in Figure 4.49. Although the highest peaks of the spectra from both oeINDO and ZINDO/s are *red-shifted* from that of TDDFT, the oeINDO peak is in better agreement with TDDFT results.

Both oeINDO and ZINDO/s methods reasonably reproduced the absorption spectrum from TDDFT for the $(CdS)_3$ equilibrium structure. The absorption bands for all three methods are within the ultraviolet energy range. The highest peaks of the absorption spectra from both oeINDO and ZINDO/s are shifted from TDDFT by about 0.1 eV.

The situation with spectra obtained for the $(CdS)_4$ equilibrium structure (Figure 4.51) are not different from those of the $(CdS)_3$ equilibrium structure. In Figure 4.51, it can be observed that the absorption patterns and bands from all methods are similar. The ZINDO/s and oeINDO spectra agree well with TDDFT. However, the spectrum highest peak from ZINDO/s is better compared to TDDFT than for oeINDO to TDDFT. The peaks of spectra from ZINDO/s and oeINDO are shifted from that of TDDFT by 0.07 eV and 0.13 eV, respectively.

The absorption spectra of the larger CdS clusters, ($(CdS)_n$ (n=10, 19)) in Figures 4.52 and 4.53, show that the oeINDO spectra compare qualitatively with TDDFT. The absorption bands and pattern of the oeINDO and TDDFT in Figure 4.52 are comparable. For $(CdS)_{19}$ spectra (Figure 4.53), both the oeINDO and TDDFT spectra peak were found in the ultraviolet region of the electromagnetic spectrum. The oeINDO spectrum peak is shifted from that of TDDFT by about 0.87 eV. The highest peak of the ZINDO/s spectrum is in the visible region and is shifted from TDDFT highest peak by 2.21 eV.

Figure 4.54 displays the plot of absorption highest peaks for $(CdS)_n$ against number of units n. It can be seen that oeINDO highest absorption peaks produced a similar trend observed in that for TDDFT. The average shift of the oeINDO peaks from TDDFT peaks is 0.67 eV while ZINDO/s spectra peaks shifted by 1.15 eV (almost double the error observed in oeINDO).

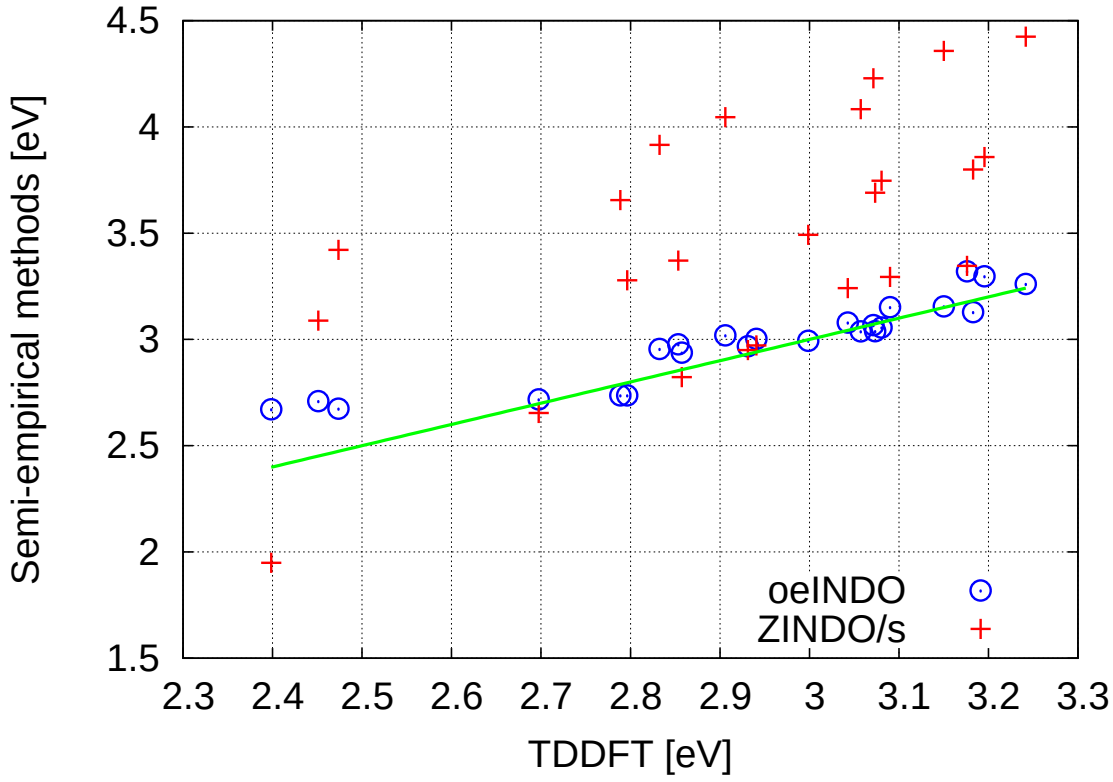

Figure 4.55: Plot comparing excitation energies from semi-empirical methods (ZINDO/s and oeINDO) with those from TDDFT for $Cd_5Zn_{14}S_{19}$, $Cd_{10}Zn_9S_{19}$ and $Cd_{15}Zn_4S_{19}$.

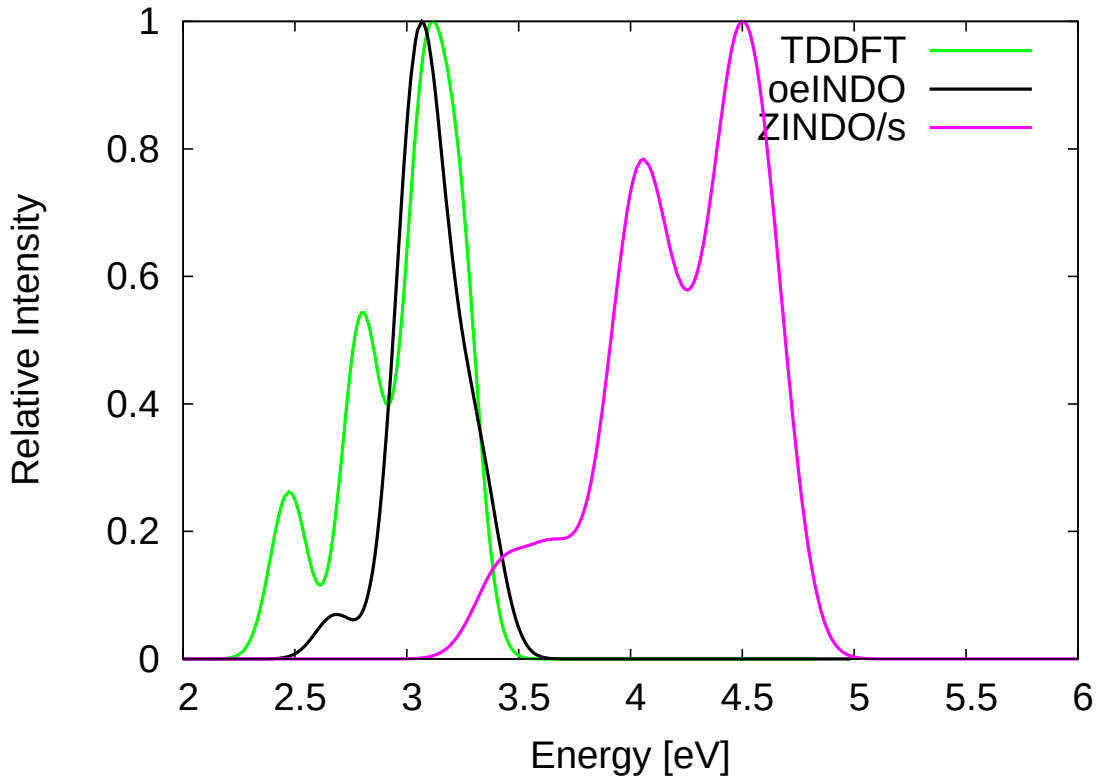

Figure 4.56: Absorption spectra for $Cd_5Zn_{14}S_{19}$ equilibrium structure obtained from different methods.The intensities have been scaled so that the highest intensity is equal to unity.

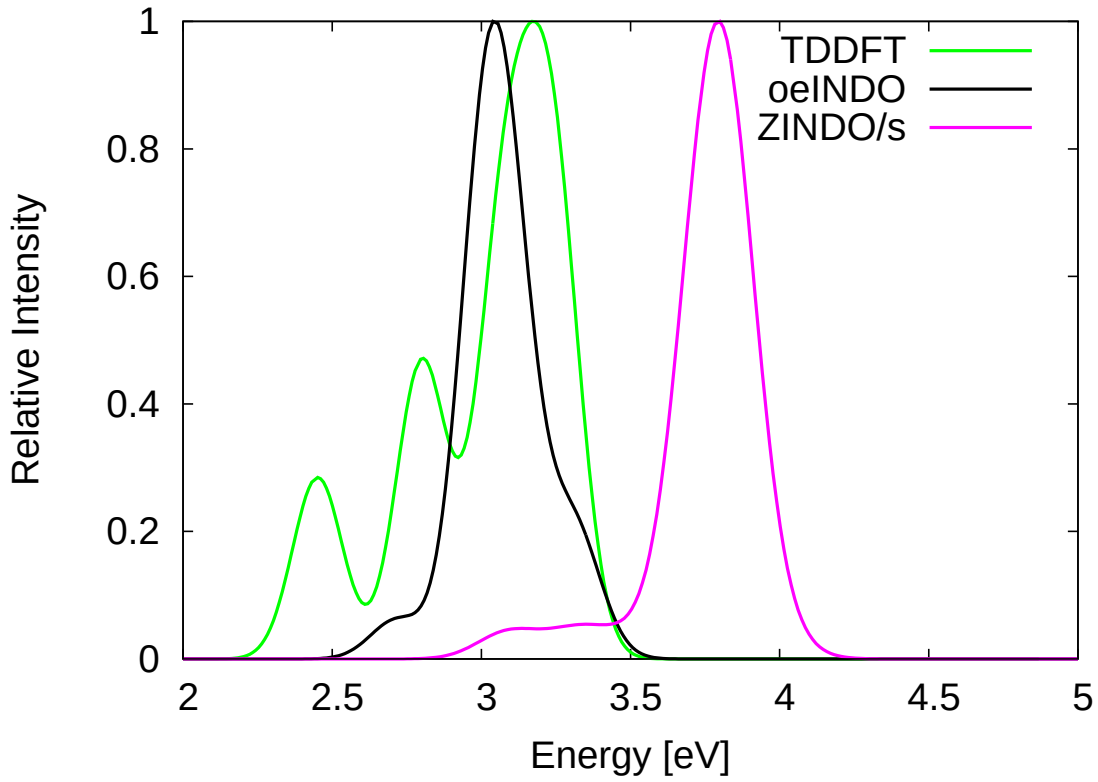

Figure 4.57: Absorption spectra for $Cd_{10}Zn_9S_{19}$ equilibrium structure obtained from different methods.The intensities have been scaled so that the highest intensity is equal to unity.

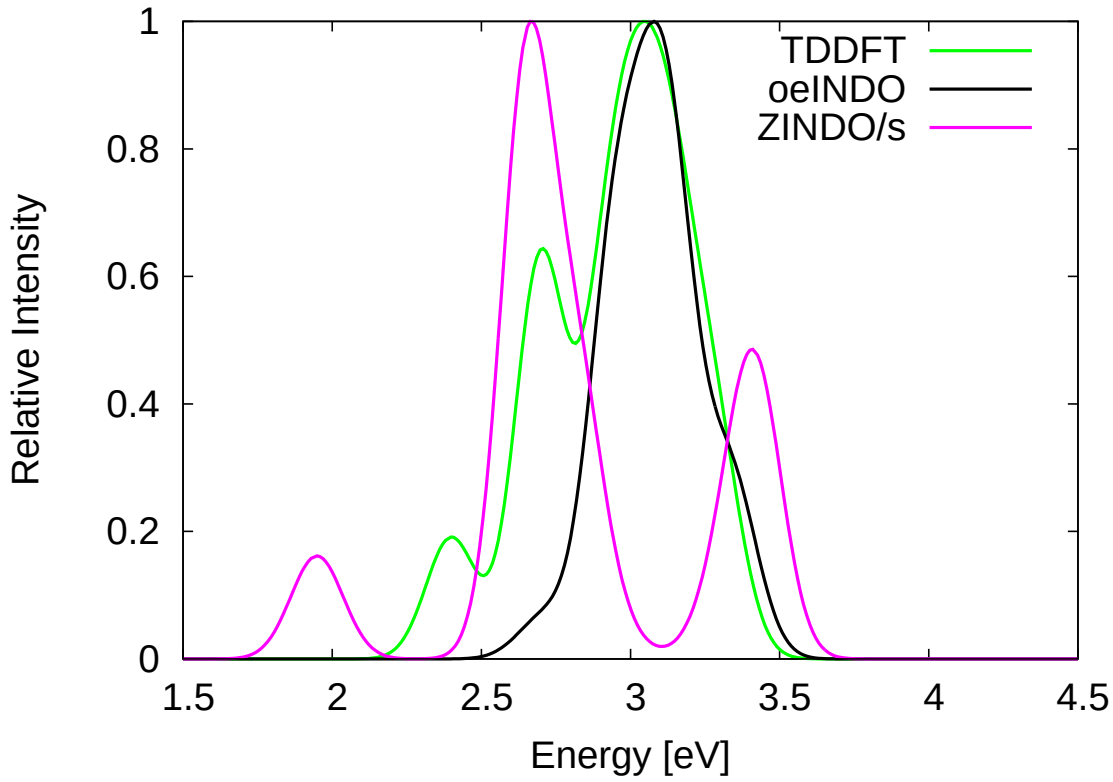

Figure 4.58: Absorption spectra for $Cd_{15}Zn_4S_{19}$ equilibrium structure obtained from different methods.The intensities have been scaled so that the highest intensity is equal to unity.

4.2.8 Transferability oeINDO parameters to $Cd_xZn_yS_{19}$ clusters

The transferability of oeINDO model was also verified with cadmium-zinc sulphide, $Cd_xZn_yS_{19}$ structures (where x, y are the number atoms), that is, how well did the model reproduce the *ab-initio* model (TDDFT) results. The accuracy of the model was discussed using scatter plot of excitation energies from oeINDO and ZINDO/s as compared to TDDFT for $Cd_5Zn_{14}S_{19}$, $Cd_{10}Zn_9S_{19}$ and $Cd_{15}Zn_4S_{19}$ equilibrium structures. UV-vis absorption spectra for the same set of structures were also employed for the discussion.

Figure 4.55 displays a plot comparing excitation energies from semi-empirical methods (ZINDO/s and oeINDO) with those from TDDFT for $Cd_5Zn_{14}S_{19}$, $Cd_{10}Zn_9S_{19}$ and $Cd_{15}Zn_4S_{19}$ structures. It can be observed that blue circles (oeINDO energies) are much more closely packed than the red plus signs (ZINDO/s energies) to the green line (representing the *ab-initio*, TDDFT energies). The oeINDO excitations match well with excitations from TDDFT with MAE of 0.08eV while ZINDO/s excitations deviate with a larger MAE: 0.60 eV.

The absorption spectra of $Cd_5Zn_{14}S_{19}$ structure obtained from TDDFT, oeINDO and ZINDO/s are presented in Figure 4.56. A good match of the absorption spectra from TDDFT and oeINDO methods can be observed with their prominent peaks matching with a small error of 0.04 eV. Also, the spectra are found in about the same energy range 2.3-3.5 eV. However, ZINDO/s spectrum energy is 3.2-5.0 eV (almost outside the benchmark energy range). Its highest peak located at 4.51 eV is *blue-shifted* from TDDFT one by a much larger error of 1.39 eV.

The absorption spectra of $Cd_{10}Zn_9S_{19}$ equilibrium structure from TDDFT and oeINDO match reasonably well (see fig. 4.57). The absolute difference in their highest peak is 0.14 eV. ZINDO/s spectrum maximum is, however, shifted from that of the TDDFT by 0.62 eV.

For the $Cd_{15}Zn_4S_{19}$ equilibrium structure, the absorption spectra obtained from TDDFT and oeINDO are also in good agreement. Their highest peaks, which are observed at 3.05 eV (TDDFT) and 3.07 eV (oeINDO), match with a small error of 0.02 eV. The ZINDO/s spectrum peak on the other hand is observed at 2.67 eV being shifted from that of TDDFT by 0.38 eV.

Table 4.15: First eight (8) lowest vertical excitation energies (eV) for large silicon clusters

S/N	Si_{124}	Si_{147}	Si_{172}	Si_{244}	Si_{779}
1	0.008	0.235	0.039	0.017	0.016
2	0.038	0.305	0.048	0.062	0.017
3	0.050	0.391	0.058	0.071	0.019
4	0.053	0.408	0.064	0.075	0.025
5	0.070	0.533	0.079	0.101	0.036
6	0.094	0.560	0.081	0.110	0.038
7	0.101	0.587	0.090	0.134	0.042
8	0.110	0.677	0.100	0.148	0.054

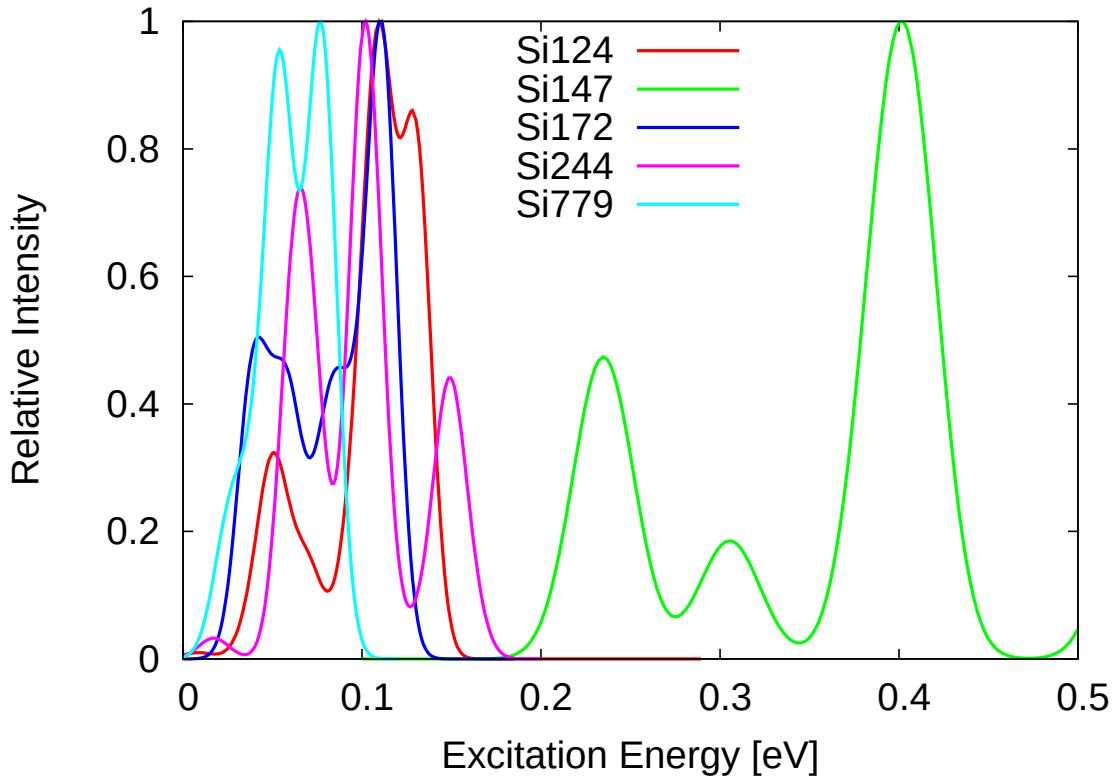

Figure 4.59: Absorption spectra of Si_n $(n = 124, 147, 172, 779)$ equilibrium geometries obtained from oeINDO.The intensities have been scaled so that the highest intensity is equal to unity.

Table 4.16: First eight (8) vertical excitation energies (eV) for Zn quantum dots of different sizes

S/N	Zn_{62} (1.2 nm)	Zn_{104} (1.4 nm)	Zn_{128}) (1.6 nm)	Zn_{190} (1.8 nm)	(Zn_{244}) 2.0nm
1	0.080	0.080	0.048	0.055	0.042
2	0.203	0.094	0.077	0.096	0.068
3	0.211	0.098	0.124	0.112	0.084
4	0.296	0.145	0.133	0.123	0.099
5	0.304	0.161	0.139	0.135	0.115
6	0.325	0.171	0.159	0.148	0.126
7	0.349	0.180	0.188	0.157	0.147
8	0.395	0.191	0.210	0.169	0.149

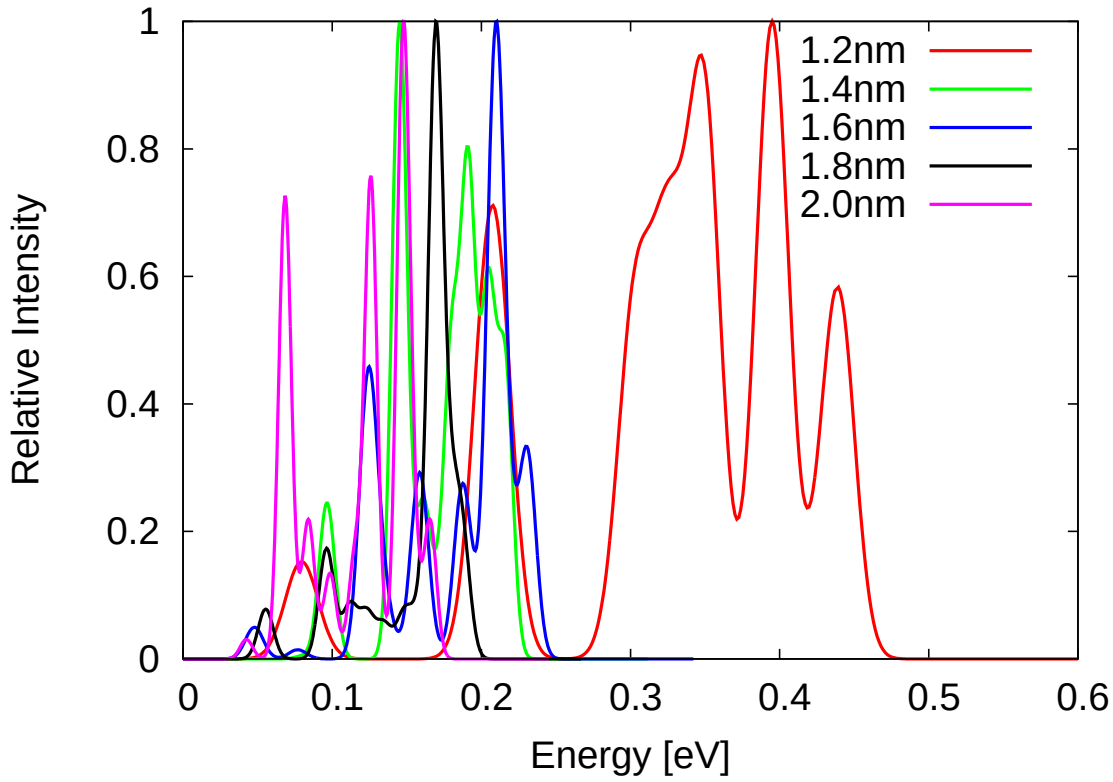

Figure 4.60: Absorption spectra of Zn quantum dots of different sizes (diameters) obtained from oeINDO.The intensities have been scaled so that the highest intensity is equal to unity.

4.3 Study of large clusters and quantum dots using the oeINDO model

Having validated the oeINDO model in the previous section, it was employed for the study of large clusters and quantum dots, for which accurate *ab-initio* methods (e.g EOM-CCSD, TDDFT) are computationally expensive or sometimes prohibitive. The oeINDO was used to compute excitation energies and absorption spectra of silicon, zinc, cadmium, sulphur, cadmium sulphide and zinc sulphide large clusters and quantum dots of various sizes. Results obtained are presented in Tables 4.15 -4.21 and Figures 4.59 -4.66 and discussed.

Table 4.15 and Figure 4.59 show the excitation energies and absorption spectra, respectively obtained for 124, 147, 172, 244, 779 Si atom clusters (ranging from 1.0 to 3.0 nm Si quantum dots) using the oeINDO method. It can be observed that the first excitation energy (4.15) and the absorption edge (4.59) of each silicon cluster are less than 0.04 eV except for Si_{147} which has a value of 0.23 eV. This indicates that large silicon clusters and quantum dots are metallic or 'near metallic' systems. This result is in agreement with the result obtained by Jacksons et al. (Jackson and Jellinek, 2016). Furthermore, the first lowest excitation energy (electronic gap) 4.59 of 0.24 eV determined for Si_{147} using oeINDO compares well with the electronic gap (of roughly 0.30 eV) obtained in the same report (Jackson and Jellinek, 2016).

The results of excitation energies and absorption spectra for zinc quantum dots of diameters 1.2, 1.4, 1.6, 1.8 and 2.0 nm obtained with oeINDO are presented in Table 4.16 and Figure 4.60. The first excitation energies and the absorption spectra edge of all the Zn quantum dots are < 0.1 eV which suggest that the systems are all metallic. This agrees with previous reports (Kostko et al., 2005, Aguado et al., 2018). An important feature of nano-sized systems, confinement effect, was also observed. It involves a *red-shift* (decrease in energy) in the absorption spectra maxima with an increase in the size of the dot and a *blue-shift* (increase in energy) as the size decreases. From the Zn dot spectra plot, one can readily observe that confinement effect set in at dot size 1.6 nm with maximum peak at 0.21 eV. The peak energy decreased to 0.17 eV for dot size 1.8 nm and 0.14 eV for size 2.0 nm.

Table 4.17: Vertical excitation energies for Cadmium quantum dots of different sizes

S/N	Cd_{38} (1.0 nm)	Cd_{62} (1.2 nm)	Cd_{104} (1.4 nm)	Cd_{128} (1.6 nm)	Cd_{190} (1.8 nm)
1	0.741	0.401	0.070	0.078	0.088
2	0.759	0.436	0.090	0.101	0.092
3	0.800	0.464	0.131	0.150	0.110
4	0.831	0.487	0.145	0.197	0.146
5	0.858	0.519	0.177	0.222	0.153
6	0.863	0.584	0.186	0.241	0.157
7	0.884	0.601	0.214	0.250	0.161
8	0.899	0.618	0.231	0.273	0.171

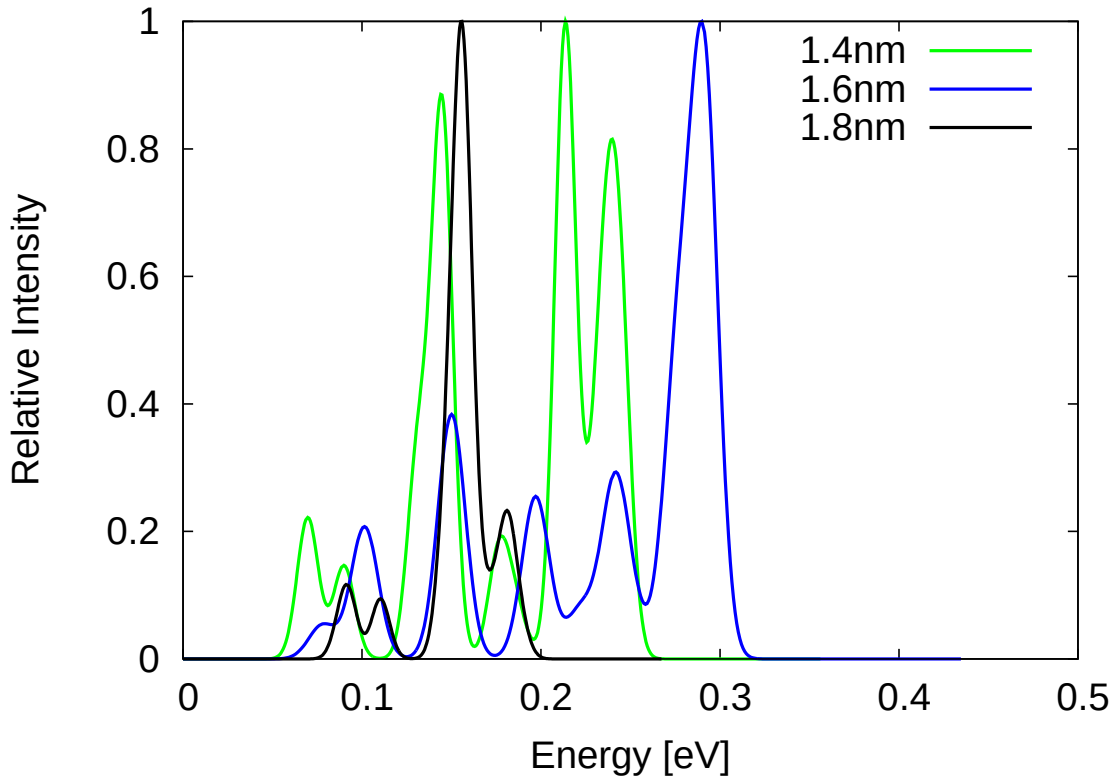

Figure 4.61: Absorption spectra of Cd quantum dots of different sizes (diameters) obtained from oeINDO.The intensities have been scaled so that the highest intensity is equal to unity.

Table 4.18: Lowest eight (8) vertical excitation energies(eV) for sulphur quantum dots of different sizes

S/N	S_{38} (1.0 nm)	S_{62} (1.2 nm)	S_{104} (1.4 nm)	S_{128} (1.6 nm)	S_{244} (2.0nm)
1	2.357	0.230	0.411	0.075	0.117
2	2.384	0.284	0.472	0.155	0.141
3	2.551	0.407	0.692	0.165	0.216
4	2.578	0.593	0.831	0.271	0.231
5	2.681	0.871	0.861	0.317	0.272
6	2.698	0.998	0.913	0.346	0.308
7	2.738	1.022	0.916	0.384	0.340
8	2.748	1.118	0.965	0.430	0.343

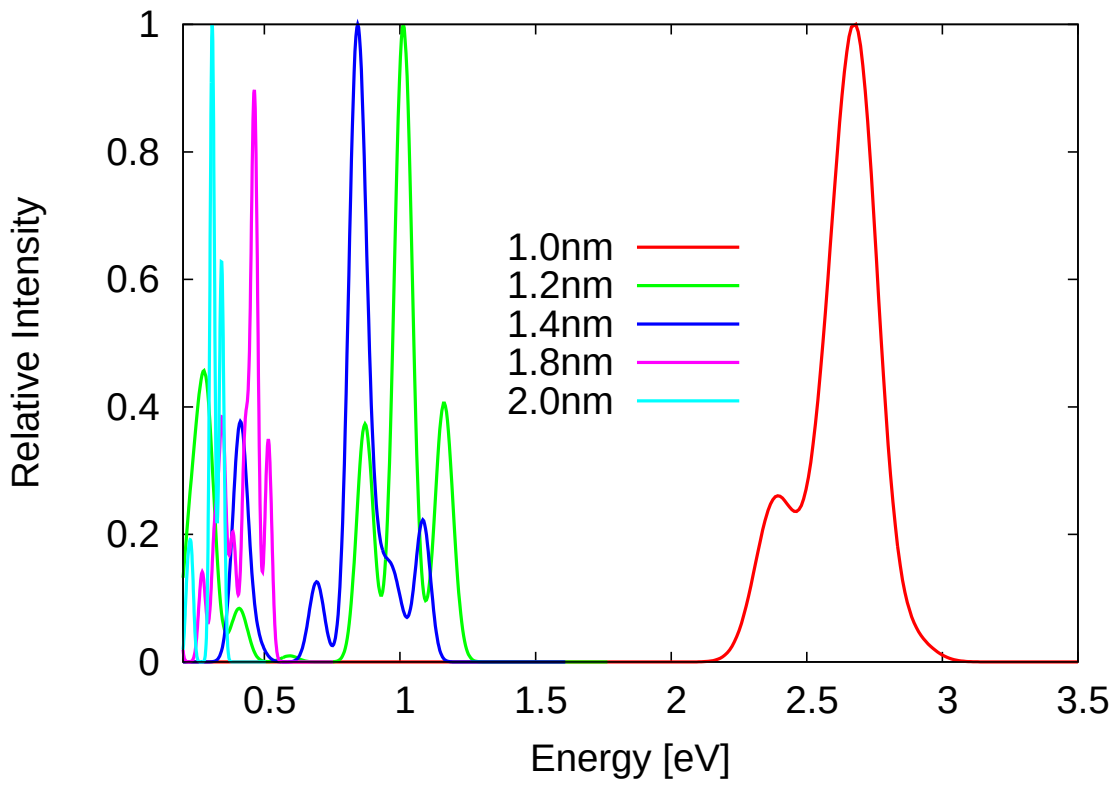

Figure 4.62: Absorption spectra of S quantum dots of different sizes (diameters) obtained from oeINDO.The intensities have been scaled so that the highest intensity is equal to unity.

Table 4.17 and Figure 4.61 show the results of the excitation energies and absorption spectra of nano-sized cadmium structures (1.0 -1.8 nm) obtained using oeINDO. It can be observed that the spectra maxima are *red-shifted* and become more metallic with an increase in the size of the Cd quantum dot. This agrees with earlier reports (Kohaut and Springborg, 2016, Kohaut, 2017). In the report by Kohaut and Springborg (Kohaut and Springborg, 2016), using DFT, the electronic gap of Cd_{38} (1.0 nm Cd dot) and Cd_{60} were computed to be 0.563 eV and 0.29 eV, respectively. Computation of gaps (first excitation energies) for the same structures (4.17) with oeINDO yielded results that are about ≈ 0.2 eV greater. But, DFT is known for typical underestimation of electronic gaps (Tran and Blaha, 2017). Hence, oeINDO prediction of the electronic gaps, which are higher than those from DFT, should be more accurate.

The oeINDO results of the calculation of excitation energies and absorption spectra for different sulphur quantum dots are presented in Table 4.18 and Figure 4.62. From spectra plot, absorption maximum peaks are located at 2.73 eV, 1.0 eV, 0.80 eV, 0.45 eV and 0.25 eV for the 1.0 nm, 1.2 nm, 1.4 nm, 1.8 nm and 2.0 nm sulphur dots, respectively. It can be observed that the spectra prominent peaks are *red-shifted* (decrease in energy) as the size of the cluster increases -confinement effect. In addition, the spectra and the first excitation energies from the Table 4.18 show a transition of the sulphur dots from non-metallic to metallic somewhere between 1.0 nm and 1.6 nm dot size.

Table 4.19: First eight lowest vertical excitation energies (eV) for ZnS quantum dots of different sizes

S/N	$Zn_{19}S_{19}$ (1.0nm)	$Zn_{25}S_{25}$ (1.2nm)	$Zn_{52}S_{52}$ (1.4nm)	$Zn_{95}S_{95}$ (1.8nm)	$Zn_{122}S_{122}$ (2.0nm)	Z
1	1.179	1.909	1.595	1.156	0.057	
2	1.352	1.994	1.769	1.270	0.085	
3	1.631	2.039	1.885	1.311	0.231	
4	1.811	2.188	1.904	1.343	0.307	
5	1.859	2.225	1.929	1.399	0.333	
6	1.974	2.363	2.005	1.475	0.376	
7	1.983	2.390	2.034	1.541	0.407	
8	2.078	2.424	2.070	1.614	0.456	

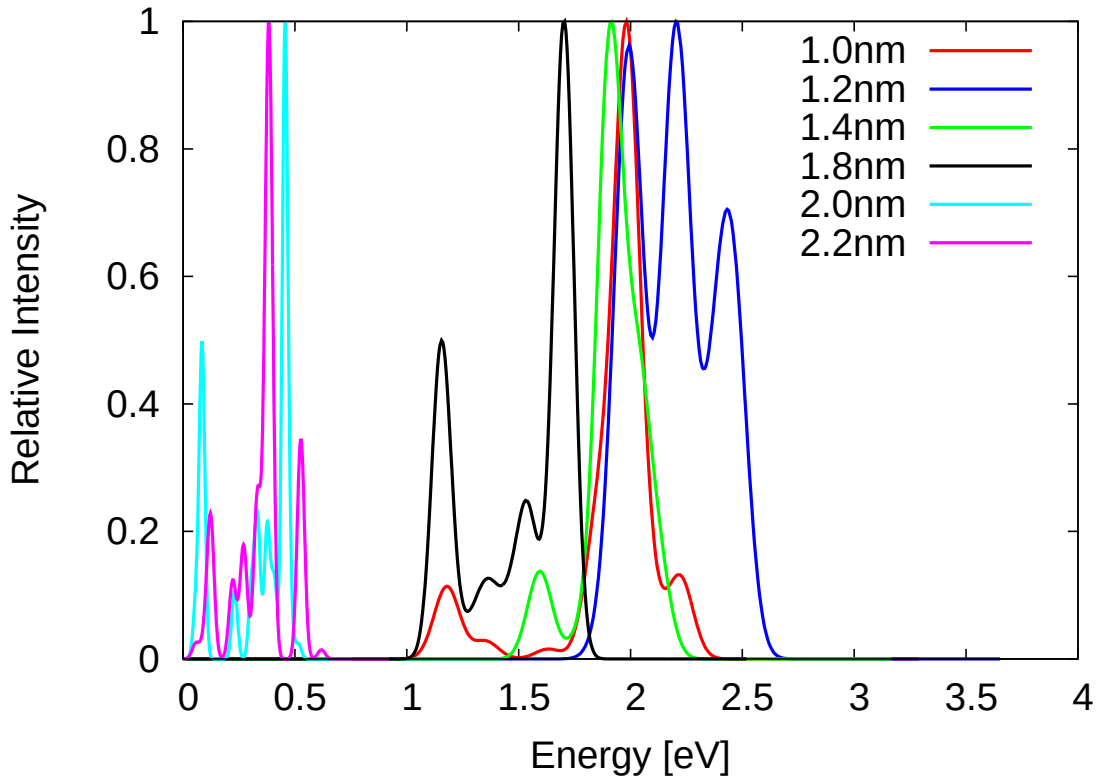

Figure 4.63: Absorption spectra of ZnS quantum dots of different sizes (diameters) obtained from oeINDO.The intensities have been scaled so that the highest intensity is equal to unity.

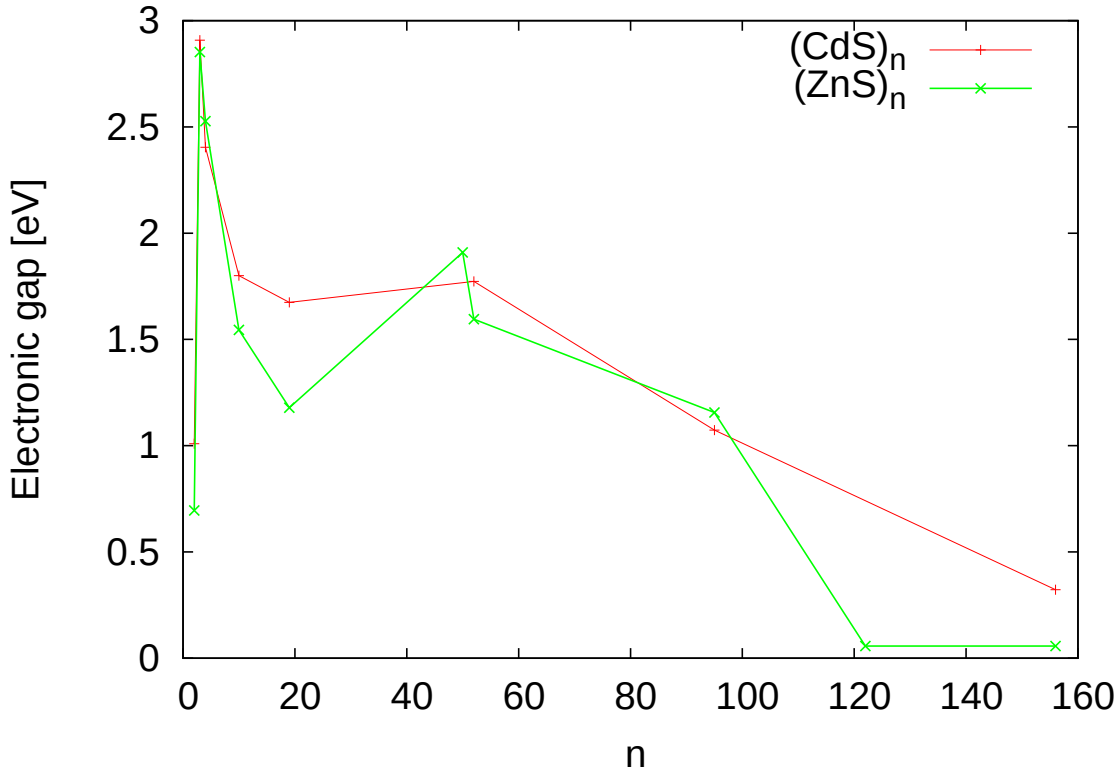

Figure 4.64: Plot of electronic gap for $(CdS)_n$ and $(ZnS)_n$ quantum dots for different number of units, n

Table 4.20: First eight lowest vertical excitation energies (eV) for CdS quantum dots of different sizes

S/N	$(CdS)_{19}$ (1.0nm)	$Cd_{52}S_{52}$ (1.4nm)	$Cd_{95}S_{95}$ (1.8nm)	$Cd_{159}S_{159}$ (2.2nm)
1	1.674	1.773	1.073	0.322
2	1.797	1.829	1.353	0.412
3	1.894	1.980	1.418	0.521
4	1.949	2.006	1.443	0.682
5	1.994	2.044	1.491	0.695
6	2.094	2.051	1.534	0.704
7	2.096	2.090	1.595	0.711
8	2.184	2.132	1.638	0.791

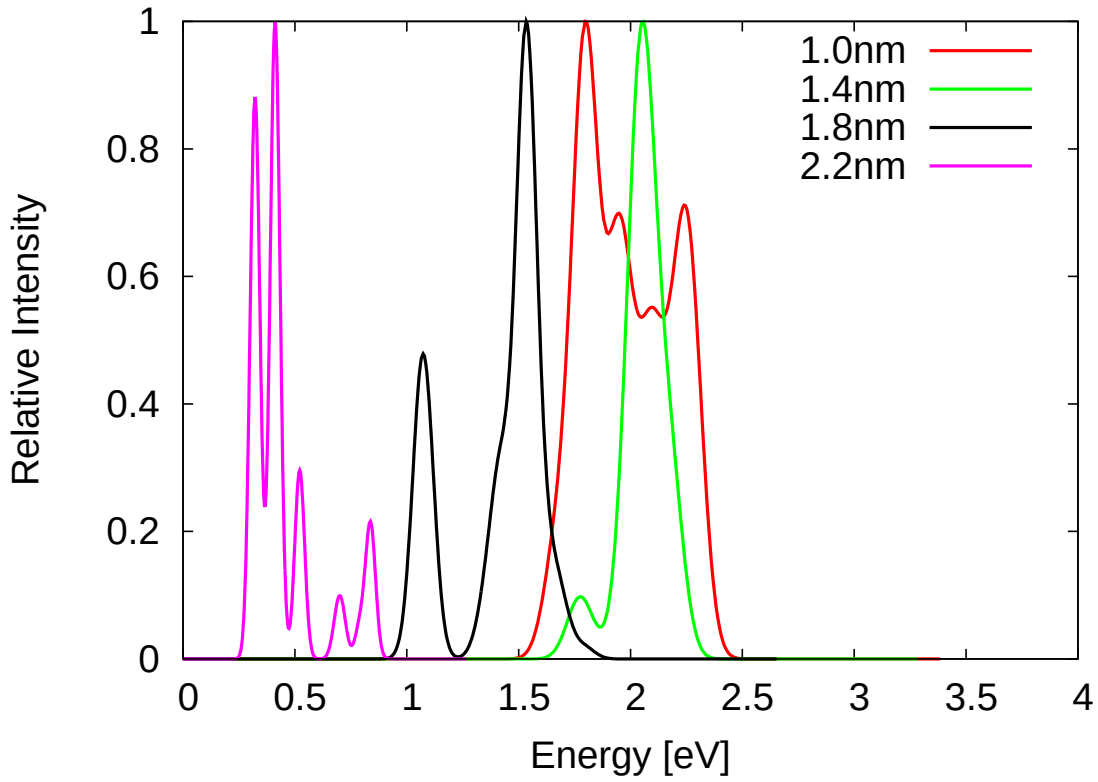

Figure 4.65: Absorption spectra of CdS quantum dots of different sizes (diameters) obtained from oeINDO.The intensities have been scaled so that the highest intensity is equal to unity.

The absorption spectra and the excitation energies obtained from oeINDO for 1.0 - 2.2 nm (corresponding to 59-319 atoms) ZnS quantum dots are presented in Figure 4.63 and Table 4.19, respectively. A confinement effect can be observed and it sets in at the 1.2 nm ZnS quantum dot; a *redshift* is observed in the spectra maxima and first excitation energy with an increase in the size of the dots. The plot of electronic gaps (first excitation energies) against number of atoms (Figure 4.64) shows a decrease in ZnS cluster gap with increase in number of atoms, starting from $(ZnS)_{59}$. This confirm confinement effect in ZnS nano-systems, which set in at $(ZnS)_{59}$. The 1.0-1.8 nm ZnS quantum dots absorb radiation within the visible region of the electromagnetic spectrum with highest peaks at 1.99 eV, 2.21 eV, 1.92 eV and 1.70 eV for 1.0, 1.2, 1.4 and 1.8 nm dot size, respectively. However, the spectra highest peaks for 1.0 nm, 1.4 nm, 1.8 nm ZnS quantum dots, which correspond to the reddish visible region of the electromagnetic spectrum, are already approaching infrared radiation. The 1.2 nm ZnS dot has its absorption band span 1.60 eV to 2.50 eV with two prominent peaks, one at 2.00 eV (orange colour) and the other at 2.21 eV (green colour). The 1.2 nm spherical-like quantum dot (optimised at PM7 level) is theoretically optimal for solar cell application whereas bulk ZnS, which has a wide band gap of about 3.68 eV in the ultraviolet region of the electromagnetic spectrum is not suitable for solar cell application. The optimal band gap for solar cell material is about 1.38 eV for $\approx 33\%$ efficiency (Rühle, 2016).

The eight lowest excitation energies and absorption spectra obtained with the oeINDO model for 1.0 , 1.4, 1.8 and 2.2 nm CdS quantum dots are shown in Table 4.20 and Figure 4.65. Confinement effects set in at the size 1.4 nm CdS dot since from this dot size, a continuous decrease in electronic gap energy (*red-shift*) with increase in the dot size is observed (Figure 4.63). Also, a *red-shift* is observed in the absorption spectra as the dot size increases. The 1.0 and 1.4 nm CdS quantum dots were predicted to absorb light in the visible region of the electromagnetic spectrum, with highest peaks at 1.80 eV (red portion of the visible spectrum) and 2.06 eV (the orange portion of the visible spectrum), respectively. The highest peak of the spectrum for 1.4 nm CdS quantum dot is deeper in the visible region than that from 1.0 nm CdS dot. Thus, the 1.4 nm CdS dot, optimised at the PM7 level is potential for solar cell applications.

Table 4.21: Eight lowest vertical excitation energies (eV) for different CdZnS quantum dots

S/N	$Zn_{95}S_{95}$	$Cd_{38}Zn_{57}S_{95}$	$Cd_{57}Zn_{38}S_{95}$	$Cd_{76}Zn_{19}S_{95}$	$Cd_{95}S_{95}$
1	1.156	1.231	1.149	1.108	1.090
2	1.270	1.323	1.321	1.270	1.229
3	1.311	1.346	1.326	1.318	1.298
4	1.343	1.351	1.349	1.341	1.335
5	1.399	1.448	1.408	1.350	1.470
6	1.475	1.463	1.431	1.423	1.553
7	1.541	1.541	1.525	1.491	1.642
8	1.614	1.666	1.630	1.576	1.655

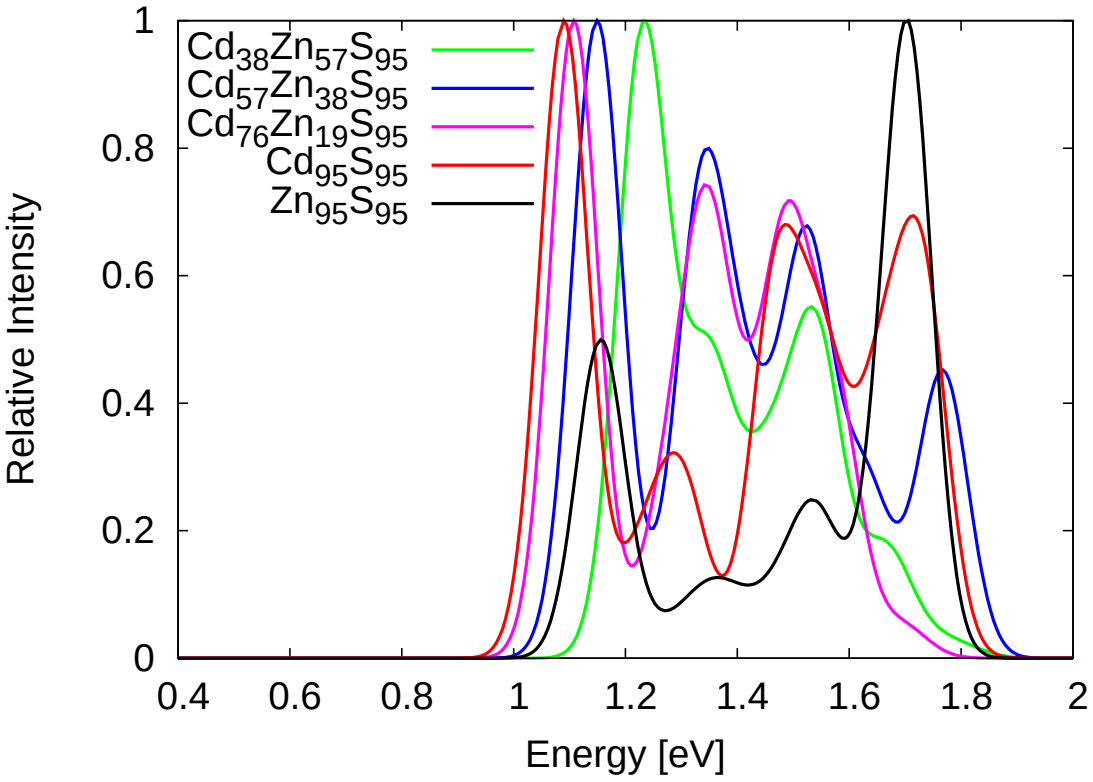

Figure 4.66: Absorption spectra of CdZnS quantum dots obtained from oeINDO.The intensities have been scaled so that the highest intensity is equal to unity.

Table 4.22: Computational time (in minutes) expended in carrying out excitation energies and absorption spectra for some atomic clusters using different methods

Atomic clusters	EOM-CCSD	TDDFT	CIS(D)	oeINDO
Si_3	84.53	12.8	48.27	0.07
Si_4	159.07	15.33	14.67	0.01
Si_5	510.13	20.13	53.87	0.01
Si_{19}	–	1524.48	421.60	0.70
Si_{40}	–	17505	13146.4	0.03
Si_{244}	–	–	–	13.38
Si_{779}	–	–	–	768.73
S_3	194.5	26.0	39.0	0.21
S_5	2102.5	11.6	13.2	0.01
S_39	–	2591.5	4327.5	0.17
S_{190}	–	–	–	13.98
Cd_3	12053.3	37.83	36.33	0.33
Cd_{20}	–	1911.2	7071.7	0.58
Cd_{60}	–	–	–	2.37
Zn_3	554.8	10.17	23.33	0.01
Zn_4	7913.3	68.03	39.33	0.01
$(ZnS)_{10}$	–	1778.67	2684.53	0.15
$(ZnS)_{159}$	–	–	–	76.73
$(CdS)_{19}$	–	23138.93	–	0.91
$(CdS)_{95}$	–	–	–	13.33

The results of the excited state energies and UV-Vis absorption spectra of cadmium-zinc sulphide quantum dots obtained from oeINDO model are presented in Table 4.21 and Figure 4.61 respectively. The effect of cadmium-zinc mixing can clearly be seen in Figure 4.61. Starting from the $Zn_{95}S_{95}$ quantum dot, a *red-shift* (decrease in energy) in spectrum highest peak and the first excitation energy (electronic gap) is observe as cadmium content (replacing the zinc contents) is increased. The trend observed agrees with previous reports (Wageh and Badr, 2008, Gaur and Jeevanandam, 2016, Sethi et al., 2007, Jabeen et al., 2016). The electronic gap decreased from 1.156 eV ($Zn_{95}S_{95}$) to 1.090 eV ($Cd_{95}S_{95}$) and so is with the absorption spectra highest peaks observed at 1.705 eV, 1.231 eV, 1.149 eV, 1.108 eV and 1.090 eV for $Zn_{95}S_{95}$, $Cd_{38}Zn_{57}S_{95}$, $Cd_{57}Zn_{38}S_{95}$, $Cd_{76}Zn_{19}S_{95}$ and $Cd_{95}S_{95}$, respectively.

4.4 Computation Time Expended for Excitation Energies and Absorption Spectra Calculations Using Different Methods

The computation times expended in the calculation of excited state energies and absorption spectra for some atomic clusters using the oeINDO and *ab-initio* methods are presented in Table 4.22. EOM-CCSD was found to be *compute-intensive* and prohibitive for large clusters. It was practically limited to clusters with less than 10 atoms. The B3LYP/TDDFT and CIS(D) methods are less expensive for small-sized clusters but become *compute-intensive* as clusters grew bigger since the needed computational resources/time grew as N^3-N^4, where N is the number of electrons in the system. The oeINDO method, however, is computationally cheap. It uses only a small fraction of the time expended in the computations with EOM-CCSD, TDDFT and CIS(D) (see Table 4.22). For instance, with 1 central processing unit (CPU) of the computer, calculations of excited state energies and absorption spectra for Cd_3 were achieved in over 200 hrs (over 8 days) using EOM-CCSD, 39 minutes with TDDFT, 36 minutes with CIS(D) and 0.33 minutes with oeINDO. The oeINDO computation time is less than a thousandth and hundredth of the computation time of EOM-CCSD and TDDFT/CIS(D), respectively. An important milestone achieved with the oeINDO is the study of bigger systems with reduced computational resources and time. For instance, with 1 CPU, $\approx$ 12 hrs was expended for the computation of excitation energies and absorption spectra of Si_{779}

cluster 4.22 using oeINDO. Even with the available huge computational power, a cluster of this size is prohibitively expensive with EOM-CCSD, TDDFT and CIS(D).

Chapter 5

CONCLUSION AND RECOMMENDATIONS

5.1 Summary and Conclusion

Despite the availability of powerful computing resources, high-level *ab-initio* methods are still computational prohibitive for the calculation of excitation energies and absorption spectra of quantum dots (containing over 1000 electrons). In this work, a new semi-empirical Hamiltonian that is computationally cheap and capable of giving accurate vertical excited state energies and ultra-violet absorption spectra for large atomic clusters and quantum dots was used. The semi-empirical Hamiltonian was parameterised using high-level first principle data from homogeneous dimer geometries. The data were obtained from Equation-Of-Motion Coupled-Cluster with Single and Double (EOM-CCSD) excitations, a method generally regarded as the 'gold standard' in computational chemistry that gives accurate results, which are comparable to experiments. The Zerner Intermediate Neglect of Differential Overlap for spectroscopy(ZINDO/s) or INDO/s Hamiltonian was parameterised using benchmark excitation energies from EOM-CCSD for homogeneous diatomics at different separations.

In this method, benchmark excitation energies for diatomics were calculated using high-level *ab-initio*. The INDO/s Hamiltonian was parameterised to fit the benchmark excitation energies. In addition, the one-center one electron integral parameters, which were not initially directly optimised, were shifted to reproduce first ionization potential energies. The optimised INDO/s parameters were then validated with homogeneous and inhomogeneous atomic clusters not included in the training geometries. Thereafter, the parameters were used to predict excitation energies and absorption spectra for large

atomic clusters and quantum dots.

The parameterisations were performed for silicon, sulphur, cadmium and zinc diatomics and a typical error of 0.23 eV was obtained for the fits. The model obtained from the parameterisations was called optimised for excitations Intermediate Neglect of Differential Overlap (oeINDO).

Without a need for re-parametrization, it was demonstrated that oeINDO is transferable; that is, the optimised parameters obtained give accurate results for complex geometries that are not included in the training geometry sets. Although the Hamiltonian was not directly optimised for the Zn-S and Cd-S heterogeneous diatomics, good results were also obtained for ZnS and CdS clusters The oeINDO excitation energies were found to be accurate with typical error of about 0.30 eV relative to the benchmark (EOM-CCSD) for complex cluster structures. However, the original ZINDO/s has a typical error of about 1.11 eV for the same structures. Even though the absorption spectra were not included in the training data sets, the relative intensities obtained with oeINDO compared well qualitatively with those from accurate *ab-initio* methods (EOM-CCSD, CIS(D) and TDDFT). The oeINDO UV-VIS absorption spectra highest peaks are shifted from those of TDDFT with on MAE of 0.40 eV while the original ZINDO/s spectra highest peaks are shifted with an MAE of 1.49 eV which is 3-4 times larger.

After the validation of oeINDO, it was employed for calculations and predictions of excitation energies and UV-VIS absorption spectra of silicon, sulphur, zinc, cadmium, zinc sulphide and cadmium sulphide quantum dots of different sizes ranging from 1.0 to 3.0 nm (40-779 atom systems). It predicted quantum confinement effects in the quantum dots; a *red-shift* (decrease in energy) in the electronic gap and UV-VIS absorption spectra of the quantum dots as their sizes increase and a *blue-shift* (increase in energy) as the sizes decrease. The oeINDO Hamiltonian also predicted silicon, zinc and cadmium quantum dots as metallic in agreement with earlier literature reports. In addition, the electronic energy gap of 0.24 and 0.401 eV were obtained for Si_{147} and a 1.2 nm Cd cluster, respectively are consistent with reports in literature. The transition of the zinc and cadmium clusters to bulk-like (metallic) behaviour was observed at a cluster size of about $N = 20$ atoms.

The oeINDO was employed in the prediction of optimal size and shape of the quantum dot for solar cell application. It predicted that the 1.2 nm spherical-like ZnS quantum dot, which has its highest absorption peak at 2.21 eV (corresponding to the green portion of the visible region of electromagnetic spectrum), is theoretically optimal for solar cell application. In contrast to bulk ZnS, which has a wide band gap of about 3.68 eV (corresponding to the ultra-violet portion of electromagnetic spectrum), the 1.2 nm spherical-like ZnS quantum dot has its gap to be 1.909 eV (visible region). The 1.4 nm spherical-like CdS quantum dot was predicted theoretically optimal for solar cell application. It has a maximum absorption at 2.06 eV (the orange portion of the visible region) and an electronic gap of 1.773 eV.

Although, both bulk CdS (with band gap 2.42 eV) and quantum dots are suitable for solar cells application, they are not environmentally friendly. The environmentally friendly ZnS quantum dot can serve as a good replacement for CdS for solar cell applications.

A *red-shift* was found in the electronic gap and absorption peak of ZnS quantum dot as cadmium is increasingly substituted for its zinc contents. This agrees with the trend observed in earlier reports.

It is important to mention the computation times for the different methods in order to appreciate the significance of the newly developed approach. The oeINDO achieved accuracy close to EOM-CCSD using less than a hundredth of its computational time and resources. Furthermore, oeINDO obtained results reasonably close to TDDFT and sometimes better, with time and resources less than a hundredth of those of TDDFT.

5.2 Contribution to Knowledge

A new method of obtaining accurate semi-empirical Hamiltonian model parameters from *ab-initio* diatomic data was developed. In particular, the method was employed to obtain a model called optimised for excitation Intermediate Neglect of Differential Overlap (oeINDO), which yielded vertical excitation energies and UV-VIS absorption spectra that are comparable to those from high-level *ab-initio* data at a fraction of the computation cost. The new model, oeINDO, is a significant improvement over the well known

INDO/s (or ZINDO/s) model.

5.3 Recommendations

The oeINDO model, like current semi-empirical models based on the Hartree Fock formalism, neglects the three- and four-center integrals. Future work can be to incorporate the three-center integral implicitly into the oeINDO model in order to improve its accuracy. The four-center effect is less significant and so it can be neglected. In addition, to improve the accuracy of oeINDO model for heterogeneous systems, the combination rule for β may need to be multiplied by 'interaction factors' and further work can determine the values of these factors for heterogeneous diatomics. Also, a new strategy need to be developed for shifting the one center integrals in order to accurately reproduce ionization potentials.

REFERENCES

Abbasi, E., Kafshdooz, T., Bakhtiary, M., Nikzamir, N., Nikzamir, N., Nikzamir, M., Mohammadian, M., and Akbarzadeh, A. (2016). Biomedical and biological applications of quantum dots. *Artificial cells, nanomedicine, and biotechnology*, 44(3):885–891.

Aguado, A., Vega, A., Lebon, A., and von Issendorff, B. (2018). Are zinc clusters really amorphous? A detailed protocol for locating global minimum structures of clusters. *Nanoscale*, 10(40):19162–19181.

Aitken, A. and Learmonth, M. P. (2009). Protein determination by UV absorption. In *The protein protocols handbook*, pages 3–6. Springer.

Allouche, A. (2008). Gabedit is a free graphical user interface for computational chemistry packages. *It is available at http://gabedit. sourceforge. net*.

Allouche, A.-R. (2011). Gabedit A graphical user interface for computational chemistry softwares. *Journal of Computational Chemistry*, 32(1):174–182.

Andersson, K., Malmqvist, P. A., Roos, B. O., Sadlej, A. J., and Wolinski, K. (1990). Second-order perturbation theory with a CASSCF reference function. *Journal of Physical Chemistry*, 94(14):5483–5488.

Andrew, R. L. (2001). *Molecular modelling: principles and applications*. Harlow, England; New York: Prentice Hall.

Anisimov, V. I. (2010). Electronic structure of strongly correlated materials. In *AIP Conference Proceedings*, volume 1297, pages 3–134. AIP.

Atkins, P. W. and Friedman, R. S. (2011). *Molecular quantum mechanics*. United State: Oxford university press.

Bacon, A. D. and Zerner, M. C. (1979). An intermediate neglect of differential overlap theory for transition metal complexes: Fe, Co and Cu chlorides. *Theoretica Chimica Acta*, 53(1):21–54.

Bae, K. H., Chung, H. J., and Park, T. G. (2011). Nanomaterials for cancer therapy and imaging. *Molecules and Cells*, 31(4):295–302.

Barone, V. (2011). *Computational strategies for spectroscopy: from small molecules to nano systems*. New Jersey: John Wiley & Sons.

Bartlett, R. J. (2012). Coupled-cluster theory and its equation-of-motion extensions. *Wiley Interdisciplinary Reviews: Computational Molecular Science*, 2(1):126–138.

Baskoutas, S., Terzis, A., and Voutsinas, E. (2004). Binding energy of donor states in a quantum dot with parabolic confinement. *Journal of Computational and Theoretical Nanoscience*, 1(3):315–319.

Becke, A. D. (1993). Density-functional thermochemistry. III. The role of exact exchange. *Journal Chemical Physics*, 98:5648–5652.

Bene, J. D. and Jaffe, H. H. (1968). Use of the CNDO method in spectroscopy. I. Benzene, pyridine, and the diazines. *The Journal of Chemical Physics*, 48(4):1807–1813.

Bennie, S. J., Curchod, B. F., Manby, F. R., and Glowacki, D. R. (2017). Pushing the limits of EOM-CCSD with projector-based embedding for excitation energies. *The Journal of Physical Chemistry Letters*, 8(22):5559–5565.

Bester, G. (2008). Electronic excitations in nanostructures: an empirical pseudopotential based approach. *Journal of Physics: Condensed Matter*, 21(2):023202.

Blase, X., Duchemin, I., and Jacquemin, D. (2018). The Bethe–Salpeter equation in chemistry: relations with TD-DFT, applications and challenges. *Chemical Society Reviews*, 47(3):1022–1043.

Borah, P., Siboh, D., Kalita, P., Sarma, J., and Nath, N. (2018). Quantum confinement induced shift in energy band edges and band gap of a spherical quantum dot. *Physica B: Condensed Matter*, 530:208–214.

Born, M. and Oppenheimer, J. R. (1927). On the quantum theory of molecules. *Collection of articles for a multimedia electronic educational-methodical complex on the discipline guillemotleft physics of the atom and atomic phenomena guillemotright / ed. ed. Shundalov MB; BSU, Faculty of Physics*.

Børve, K. J., Jensen, V. R., Karlsen, T., Støvneng, J. A., and Swang, O. (1997). Evaluation of PM3 (tm) as a geometry generator in theoretical studies of transition-metal-based catalysts for polymerizing olefins. *Molecular Modeling Annual*, 3(4):193–202.

Bourzac, K. (2013). Quantum dots go on display. *Nature*, 493(7432):283.

Brazis, P. (2017). Quantum dots and their potential impact on lighting and display applications. *Underwriters Laboratories*.

Bredow, T. and Jug, K. (2005). Theory and range of modern semiempirical molecular orbital methods. *Theoretical Chemistry Accounts*, 113(1):1–14.

Brus, L. E. (1984). Electron–electron and electron-hole interactions in small semiconductor crystallites: The size dependence of the lowest excited electronic state. *The Journal of Chemical Physics*, 80(9):4403–4409.

Burke, K. et al. (2007). The abc of dft. *Department of Chemistry, University of California*, page 40.

Caricato, M., Trucks, G. W., Frisch, M. J., and Wiberg, K. B. (2010). Oscillator strength: How does TDDFT compare to EOM-CCSD? *Journal of Chemical Theory and Computation*, 7(2):456–466.

Caricato, M., Trucks, G. W., Frisch, M. J., and Wiberg, K. B. (2011). Oscillator strength: How does TDDFT compare to EOM-CCSD? *Journal of Chemical Theory and Computation*, 7:456 – 466.

Casida, M. E. (1995). Time-dependent density functional response theory for molecules. In *Recent Advances In Density Functional Methods: (Part I)*, pages 155–192. World Scientific.

Casida, M. E. (2009). Time-dependent density-functional theory for molecules and molecular solids. *Journal of Molecular Structure: THEOCHEM*, 914(1-3):3–18.

Chatfield, D. and Christopher, J., C. (2002). Essentials of Computational Chemistry: Theories and Models. *Theoretical Chemistry Accounts: Theory, Computation, and Modeling (Theoretica Chimica Acta)*, 108(6):367–368.

Christensen, A. S., Kubar, T., Cui, Q., and Elstner, M. (2016). Semiempirical quantum mechanical methods for noncovalent interactions for chemical and biochemical applications. *Chemical Reviews*, 116(9):5301–5337.

Christiansen, O., Koch, H., and Jørgensen, P. (1995). The second-order approximate coupled cluster singles and doubles model CC2. *Chemical Physics Letters*, 243(5-6):409–418.

Cohen, M. L. and Bergstresser, T. (1966). Band structures and pseudopotential form factors for fourteen semiconductors of the diamond and zinc-blende structures. *Physical Review*, 141(2):789.

Darghouth, A., Casida, M., Taouali, W., Alimi, K., Ljungberg, M., Koval, P., sanchez Portal, D., and Foerster, D. (2015). Assessment of density-functional tight-binding ionization potentials and electron affinities of molecules of interest for organic solar cells against first-principles GW calculations. *Computation*, 3(4):616–656.

Delerue, C. J. and Lannoo, M. (2013). *Nanostructures: theory and modeling*. New York: Springer Science & Business Media.

Dewar, M. J. and Thiel, W. (1977). Ground states of molecules. 38. The MNDO method. Approximations and parameters. *Journal of the American Chemical Society*, 99(15):4899–4907.

Dewar, M. J., Zoebisch, E. G., Healy, E. F., and Stewart, J. J. (1985). Development and use of quantum mechanical molecular models. 76. AM1: A new general purpose quantum mechanical molecular model. *Journal of the American Chemical Society*, 107(13):3902–3909.

Dhayal, S. S., Ramaniah, L. M., Ruda, H. E., and Nair, S. V. (2014). Electron states in semiconductor quantum dots. *The Journal of Chemical Physics*, 141(20):204702.

Di Bella, S., Fragala, I. L., Ratner, M. A., and Marks, T. J. (1993). Electron donor-acceptor complexes as potential high-efficiency second-order nonlinear optical materials. A computational investigation. *Journal of the American Chemical Society*, 115(2):682–686.

Dral, P. O., Wu, X., Sporkel, L., Koslowski, A., Weber, W., Steiger, R., Scholten, M., and Thiel, W. (2016). Semiempirical quantum-chemical orthogonalization-corrected methods: theory, implementation, and parameters. *Journal of Chemical Theory and Computation*, 12(3):1082–1096.

Dreuw, A. and Head-Gordon, M. (2005). Single-reference ab initio methods for the calculation of excited states of large molecules. *Chemical Reviews*, 105(11):4009–4037.

Dutta, A. K., Vaval, N., and Pal, S. (2018). Lower scaling approximation to eom-ccsd: A critical assessment of the ionization problem. *International Journal of Quantum Chemistry*, 118(14):e25594.

Ekimov, A. and Onushchenko, A. (1982). Quantum size effect in the optical-spectra of semiconductor micro-crystals. *Soviet Physics Semiconductors-USSR*, 16(7):775–778.

Ekimov, A. I., Efros, A. L., and Onushchenko, A. A. (1985). Quantum size effect in semiconductor microcrystals. *Solid State Communications*, 56(11):921–924.

Evarestov, R. A. (2007). *Quantum chemistry of solids: The LCAO first principles treatment of crystals*, volume 153. Berlin Heidelberg: Springer Science & Business Media.

Fanfrlik, J., Bronowska, A. K., Rezac, J., Prenosil, O., Konvalinka, J., and Hobza, P. (2010). A reliable docking/scoring scheme based on the semiempirical quantum mechanical PM6-DH2 method accurately covering dispersion and H-bonding: HIV-1 protease with 22 ligands. *The Journal of Physical Chemistry B*, 114(39):12666–12678.

Fedorov, A., Kuzubov, A., Kholtobina, A., Kovaleva, E., Knaup, J., and Irle, S. (2016). Theoretical investigation of molecular and electronic structures of

buckminsterfullerene-silicon quantum dot systems. *The Journal of Physical Chemistry A*, 120(49):9767–9775.

Feng, J., Li, J., Wang, Z., and Zerner, M. C. (1990). Quantum-chemical investigation of Buckminsterfullerene and related carbon clusters (I): The electronic structure and UV spectra of Buckminsterfullerene, and other C_60 cages. *International Journal of Quantum Chemistry*, 37(4):599–607.

Fu, H., Wang, L.-W., and Zunger, A. (1998). Applicability of the k.p method to the electronic structure of quantum dots. *Physical Review B*, 57(16):9971.

Furmanchuk, A., Leszczynski, J., Tretiak, S., and Kilina, S. V. (2012). Morphology and optical response of carbon nanotubes functionalized by conjugated polymers. *The Journal of Physical Chemistry C*, 116(12):6831–6840.

Gabay, D., Wang, X., Lomakin, V., Boag, A., Jain, M., and Natan, A. (2017). Size dependent electronic properties of silicon quantum dotsAn analysis with hybrid, screened hybrid and local density functional theory. *Computer Physics Communications*, 221:95–101.

Galli, G., Puzder, A., Williamson, A. J., Grossman, J. C., and Pizzagalli, L. (2002). Structural and electronic properties of quantum dot surfaces. In *2002 International Conference on Computational Nanoscience and Nanotechnology: ICCN 2002 San Juan: April 21-25, 2002, San Juan Marriott Resort and Stellaris Casino, San Juan, Puerto Rico, USA*, page 253. Computational Publications.

Gatti, M. (2007). *Correlation effects in valence electron spectroscopy of transition metal oxides: Many-body perturbation theory and alternative approaches*. PhD thesis, PhD thesis, École Polytechnique, Palaiseau.

Gaur, R. and Jeevanandam, P. (2016). Synthesis and Characterization of $Cd_{1-x}Zn_xS$ (x= 0-1) Nanoparticles by Thermal Decomposition of Bis (thiourea) cadmium–zinc acetate Complexes. *ChemistrySelect*, 1(11):2687–2697.

Gieseking, R. L., Ratner, M. A., and Schatz, G. C. (2016). Semiempirical modeling of Ag nanoclusters: New parameters for optical property studies enable determination

of double excitation contributions to plasmonic excitation. *The Journal of Physical Chemistry A*, 120(26):4542–4549.

Govender, K., Gao, J., and Naidoo, K. J. (2014). AM1/d-CB1: A semiempirical model for QM/MM simulations of chemical glycobiology systems. *Journal of Chemical Theory and Computation*, 10(10):4694–4707.

Griffiths, D. (1995). *Introduction to quantum mechanics*. New Jersey: Prentice Hall.

Groom, C. R., Bruno, I. J., Lightfoot, M. P., and Ward, S. C. (2016). The Cambridge structural database. *Acta Crystallographica Section B: Structural Science, Crystal Engineering and Materials*, 72(2):171–179.

Guest*, M. F., Bush, I. J., Van Dam, H. J., Sherwood, P., Thomas, J. M., Van Lenthe, J. H., Havenith, R. W., and Kendrick, J. (2005). The GAMESS-UK electronic structure package: algorithms, developments and applications. *Molecular Physics*, 103(6-8):719–747.

Harrison, P. and Valavanis, A. (2016). *Quantum wells, wires and dots: Theoretical and computational physics of semiconductor nanostructures*. England: John Wiley & Sons.

Harrison, W. A. (1989). Tight-binding theory of molecules and solids. *Pure and Applied Chemistry*, 61(12):2161–2169.

Harrison, W. A. (2012). *Electronic structure and the properties of solids: the physics of the chemical bond*. United State: Courier Corporation.

Harvey, D. (2011). Analytical Chemistry 2.0an open-access digital textbook. *Analytical and Bioanalytical Chemistry*, 399(1):149–152.

Hata, T., Murakami, T., Shibuya, H., and Ono, Y. (2006). Improved CNDO/S calculation of electronic spectra of organic compounds. I. New CNDO/S calculation by using an improved method of one-center electron repulsion integral. *Chemical and Pharmaceutical Bulletin*, 54(5):646–652.

Hoffman, R. (1964). Extended Huckel theory. 4. Carbonium ions. *Journal of ChemicalL Physics*, 40(9):2480.

Hoffmann, R. (1963). An extended Hückel theory. I. hydrocarbons. *The Journal of Chemical Physics*, 39(6):1397–1412.

Hoffmann, R. and Lipscomb, W. N. (1962). Theory of polyhedral molecules. I. Physical factorizations of the secular equation. *The Journal of Chemical Physics*, 36(8):2179–2189.

Hohenberg, P. and Kohn, W. (1964). Inhomogeneous electron gas. *Physical Review*, 136(3B):B864.

Hostavs, J., vezavc, J., and Hobza, P. (2013). On the performance of the semiempirical quantum mechanical PM6 and PM7 methods for noncovalent interactions. *Chemical Physics Letters*, 568:161–166.

Hubbell, J. A. and Chilkoti, A. (2012). Nanomaterials for drug delivery. *Science*, 337(6092):303–305.

Hückel, E. (1931). Quantum-theoretical contributions to the benzene problem. I. The electron configuration of benzene and related compounds. *Z. Physik*, 70(3-4):204–286.

Husch, T., Vaucher, A. C., and Reiher, M. (2018). Semiempirical molecular orbital models based on the neglect of diatomic differential overlap approximation. *International Journal of Quantum Chemistry*, 118(24):e25799.

Hutchison, G. R., Ratner, M. A., and Marks, T. J. (2002). Accurate prediction of band gaps in neutral heterocyclic conjugated polymers. *The Journal of Physical Chemistry A*, 106(44):10596–10605.

Imamoglu, A. (2003). Are quantum dots useful for quantum computation? *Physica E: Low-dimensional Systems and Nanostructures*, 16(1):47–50.

Jabeen, U., Shah, S. M., Hussain, N., Ali, A., Khan, S. U., et al. (2016). Synthesis, characterization, band gap tuning and applications of Cd-doped ZnS nanoparticles in hybrid solar cells. *Journal of Photochemistry and Photobiology A: Chemistry*, 325:29–38.

Jackson, K. and Jellinek, J. (2016). Si clusters are more metallic than bulk Si. *Journal of Chemical Physics*, 145(24):244302.

Jelski, D. A. and George, T. F. (1999). *Computational studies of New Materials*. Singapore: World Scientific.

Jensen, F. (2017). *Introduction to computational chemistry*. Chichester West Sussex, UK; Hoboken, NJ: John wiley & sons.

Jin, Y., Maroulis, G., Kuang, X., Ding, L., Lu, C., Wang, J., Lv, J., Zhang, C., and Ju, M. (2015). Geometries, stabilities and fragmental channels of neutral and charged sulfur clusters: S_n^Q (n= 3–20, Q= 0,$\pm$1). *Physical Chemistry Chemical Physics*, 17(20):13590–13597.

Jin, Y. and Yang, W. (2019). Excitation Energies from the Single-Particle Greens Function with the GW Approximation. *The Journal of Physical Chemistry A*, 123(14):3199–3204.

Jug, K. and Wichmann, D. (2000). MSINDO study of large silsesquioxanes. *Journal of Computational Chemistry*, 21(16):1549–1553.

Jurs, P. C., Lipkowitz, K., and Boyd, D. (1990). Chemometrics and multivariate analysis in analytical chemistry. *Reviews in Computational Chemistry*, 1:169–212.

Kayi, H. (2009). Parameterization of the AM1* semiempirical molecular orbital method for the first-row transition metals and other elements.

Kayi, H. and Clark, T. (2007). Am1* parameters for copper and zinc. *Journal of Molecular Modeling*, 13(9):965–979.

Kilina, S., Ramirez, J., and Tretiak, S. (2012). Brightening of the lowest exciton in carbon nanotubes via chemical functionalization. *Nano Letters*, 12(5):2306–2312.

Koch, W. and Holthausen, M. C. (2015). *A chemist's guide to density functional theory*. VCH Verlag GmbH: John Wiley & Sons.

Kohaut, S. (2017). *Global optimization studies in clusters*. PhD thesis, NT - Naturwissenschaftlich- Technische Fakultt.

Kohaut, S. and Springborg, M. (2016). Growth patterns and structural motifs of cadmium clusters with up to 60 atoms: disordered or not? *Physical Chemistry Chemical Physics*, 18(41):28524–28537.

Kohn, W. and Sham, L. J. (1965). Self-consistent equations including exchange and correlation effects. *Physical review*, 140(4A):A1133.

Koskinen, P. and Mäkinen, V. (2009). Density-functional tight-binding for beginners. *Computational Materials Science*, 47(1):237–253.

Kostko, O., Wrigge, G., Cheshnovsky, O., and Issendorff, B. v. (2005). Transition from a Bloch-Wilson to a free-electron density of states in Zn_n clusters.

Kotzian, M., Rosch, N., and Zerner, M. (1992). Intermediate neglect of differential overlap spectroscopic studies on lanthanide complexes. *Theoretica Chimica Acta*, 81(4-5):201–222.

Kuno, M. (2005). Introduction to nanoscience and nanotechnology: A workbook. *University of Notre Dame, Indiana (US)*, page 370.

Leang, S. S., Zahariev, F., and Gordon, M. S. (2012). Benchmarking the performance of time-dependent density functional methods. *The Journal of Chemical Physics*, 136(10):104101.

Leng, X., Jin, F., Wei, M., and Ma, Y. (2016). GW method and Bethe-Salpeter equation for calculating electronic excitations. *Wiley Interdisciplinary Reviews: Computational Molecular Science*, 6(5):532–550.

Linstrom, P. J. and Mallard, W. G. (2001). The NIST chemistry WebBook: A chemical data resource on the internet. *Journal of Chemical & Engineering Data*, 46(5):1059–1063.

Lopez, X. and York, D. M. (2003). Parameterization of semiempirical methods to treat nucleophilic attacks to biological phosphates: AM1/d parameters for phosphorus. *Theoretical Chemistry Accounts*, 109(3):149–159.

Magnasco, V. (2009). *Methods of molecular quantum mechanics: An introduction to electronic molecular structure*. Chichester, U.K.: John Wiley & Sons.

Magnasco, V. (2013). *Elementary molecular quantum mechanics: mathematical methods and applications*. Netherland: Elsevier.

Maitra, N. T. (2016). Perspective: Fundamental aspects of time-dependent density functional theory. *The Journal of Chemical Physics*, 144(22):220901.

Marques, M. A., Maitra, N. T., Nogueira, F. M., Gross, E. K., and Rubio, A. (2012). *Fundamentals of time-dependent density functional theory*, volume 837. New York: Springer Science & Business Media.

Marques, M. A., Ullrich, C. A., Nogueira, F., Burke, K., Rubio, A., and Gross, E. K. (2006). *Time-dependent density functional theory*, volume 706. New York: Springer Science & Business Media.

Martin, R. M. (2020). *Electronic structure: basic theory and practical methods*. United Kingdom: Cambridge university press.

Marutaphan, A. and Wongchoosuk, C. (2017). SCC-DFTB study on structure, electronic and sensing properties of polypyrrole. In *Journal of Physics: Conference Series*, volume 901, page 012079. IOP Publishing.

Mataga, N. and Nishimoto, K. (1957). Electronic structure and spectra of nitrogen heterocycles. *Zeitschrift fr Physikalische Chemie*, 13:140–157.

Miehlich, B., Savin, A., Stoll, H., and Preuss, H. (1989). Results obtained with the correlation energy density functionals of Becke and Lee, Yang and Parr. *Chemical Physics Letters*, 157(3):200–206.

Moore, C. E. (1949). *Atomic energy levels as derived from analysis of optical spectra: 1H-23V*, volume 1. US Government Printing Office.

Nakanishi, N. (1969). A general survey of the theory of the Bethe-Salpeter equation. *Progress of Theoretical Physics Supplement*, 43:1–81.

Nazir, S., Hussain, T., Ayub, A., Rashid, U., and MacRobert, A. J. (2014). Nanomaterials in combating cancer: therapeutic applications and developments. *Nanomedicine: Nanotechnology, Biology and Medicine*, 10(1):19–34.

Neese, F. (2012). The ORCA program system. *Wiley Interdisciplinary Reviews: Computational Molecular Science*, 2(1):73–78.

Neese, F. (2018). Software update: the ORCA program system, version 4.0. *Wiley Interdisciplinary Reviews: Computational Molecular Science*, 8(1):e1327.

Nelder, J. A. and Mead, R. (1965). A simplex method for function minimization. *The Computer Journal*, 7(4):308–313.

Nilapwar, S. M., Nardelli, M., Westerhoff, H. V., and Verma, M. (2011). Absorption spectroscopy. In *Methods in enzymology*, volume 500, pages 59–75. Elsevier.

Nishimoto, Y. (2015). Time-dependent density-functional tight-binding method with the third-order expansion of electron density. *The Journal of Chemical Physics*, 143(9):094108.

Nozik, A. (2002). Quantum dot solar cells. *Physica E: Low-dimensional systems and nanostructures*, 14(1-2):115–120.

Nozik, A. J. (2008). Multiple exciton generation in semiconductor quantum dots. *Chemical Physics Letters*, 457(1-3):3–11.

NREL, N. (2019). Best research-cell efficiency chart.

Ochsenfeld, C., Kussmann, J., and Lambrecht, D. S. (2007). Linear-scaling methods in quantum chemistry. *Reviews in Computational Chemistry*, 23:1.

Papaconstantopoulos, D. and Mehl, M. (2003). The Slater-Koster tight-binding method: A computationally efficient and accurate approach. *Journal of Physics: Condensed Matter*, 15(10):R413.

Pariser, R. and Parr, R. G. (1953). A semi-empirical theory of the electronic spectra and electronic structure of complex unsaturated molecules. I. *The Journal of Chemical Physics*, 21(3):466–471.

Perdew, J. P., Burke, K., and Ernzerhof, M. (1996). Generalized gradient approximation made simple. *Physical review letters*, 77(18):3865.

Persson, P., Bergstrom, R., and Lunell, S. (2000). Quantum chemical study of photoinjection processes in dye-sensitized TiO_2 nanoparticles. *The Journal of Physical Chemistry B*, 104(44):10348–10351.

Pople, J. (1965). 3289; JA Pople, DP Santry and GA Segal. *J. chem. Phys*, 43:129.

Pople, J., Beveridge, D., and Dobosh, P. (1967). Approximate self-consistent molecular-orbital theory. v. intermediate neglect of differential overlap. *The Journal of Chemical Physics*, 47(6):2026–2033.

Pople, J. A. and Segal, G. A. (1965). Approximate self-consistent molecular orbital theory. II. Calculations with complete neglect of differential overlap. *The Journal of Chemical Physics*, 43(10):S136–S151.

Praveen, P., Babu, R. R., and Ramamurthi, K. (2015). Validation of PM6 & PM7 semiempirical methods on polarizability calculations. In *AIP Conference Proceedings*, volume 1665, page 090011. AIP Publishing.

Predojević, A. (2016). Photon generation efficiency and entanglement in quantum dot systems. *Contemporary Y Materials*, 2(7):162–165.

Press, W. H., Teukolsky, S. A., Vetterling, W. T., and Flannery, B. P. (2007). *Numerical recipes 3rd edition: The art of scientific computing*. Cambridge university press.

Quarti, C., Fazzi, D., and Del Zoppo, M. (2011). A computational investigation on singlet and triplet exciton couplings in acene molecular crystals. *Physical Chemistry Chemical Physics*, 13(41):18615–18625.

Racine, J. (2006). Gnuplot 4.0: A portable interactive plotting utility. *Journal of Applied Econometrics*, 21(1):133–141.

Raghavachari, K. (1986). Theoretical study of small silicon clusters: equilibrium geometries and electronic structures of Si_n (n= 2–7, 10). *Journal Chemical Physics*, 84(10):5672–5686.

Raghavachari, K. and Rohlfing, C. M. (1988). Bonding and stabilities of small silicon clusters: A theoretical study of Si_7–Si_10. *Journal Chemical Physics*, 89(4):2219–2234.

Ramaniah, L. M. and Nair, S. V. (1993). Optical absorption in semiconductor quantum dots: A tight-binding approach. *Physical Review B*, 47(12):7132.

Reimers, J. R. and Hush, N. S. (2001). The need for quantum-mechanical treatment of capacitance and related properties of nanoelectrodes. *The Journal of Physical Chemistry B*, 105(37):8979–8988.

Rezac, J., Fanfrlik, J., Salahub, D., and Hobza, P. (2009). Semiempirical quantum chemical PM6 method augmented by dispersion and H-bonding correction terms reliably describes various types of noncovalent complexes. *Journal of Chemical Theory and Computation*, 5(7):1749–1760.

Rezac, J. and Hobza, P. (2013). Describing noncovalent interactions beyond the common approximations: How accurate is the gold standard, CCSD (T) at the complete basis set limit? *Journal of Chemical Theory and Computation*, 9(5):2151–2155.

Ridley, J. and Zerner, M. (1973). An intermediate neglect of differential overlap technique for spectroscopy: pyrrole and the azines. *Theoretical Chimica Acta*, 32(2):111–134.

Ridley, J. E. and Zerner, M. C. (1976). Triplet states via intermediate neglect of differential overlap: benzene, pyridine and the diazines. *Theoretica Chimica Acta*, 42(3):223–236.

Robles, J., Mayorga, O., Lee, T.-S., and Daz, D. (1999). PM3 semiempirical electronic structure calculation of capped and uncapped CdS nanoparticles. *Nanostructured Materials*, 11(2):283–286.

Rocha, G. B., Freire, R. O., Simas, A. M., and Stewart, J. J. (2006). RM1: A reparameterization of AM1 for H, C , N, O, P, S, F, Cl, Br, and I. *Journal of Computational Chemistry*, 27(10):1101–1111.

Rossetti, R., Nakahara, S., and Brus, L. E. (1983). Quantum size effects in the redox potentials, resonance Raman spectra, and electronic spectra of CdS crystallites in aqueous solution. *The Journal of Chemical Physics*, 79(2):1086–1088.

Rühle, S. (2016). Tabulated values of the Shockley–Queisser limit for single junction solar cells. *Solar Energy*, 130:139–147.

Rühle, S., Shalom, M., and Zaban, A. (2010). Quantum-dot-sensitized solar cells. *ChemPhysChem*, 11(11):2290–2304.

Runge, E. and Gross, E. K. (1984). Density-functional theory for time-dependent systems. *Physical Review Letters*, 52(12):997.

Saadeh, Y., Leung, T., Vyas, A., Chaturvedi, L. S., Perumal, O., and Vyas, D. (2014). Applications of nanomedicine in breast cancer detection, imaging, and therapy. *Journal of nanoscience and nanotechnology*, 14(1):913–923.

Santoprete, R., Koiller, B., Capaz, R., Kratzer, P., Liu, Q., and Scheffler, M. (2003). Tight-binding study of the influence of the strain on the electronic properties of InAs/GaAs quantum dots. *Physical Review B*, 68(23):235311.

Sauri, V., Serrano-Andres, L., Shahi, A. R. M., Gagliardi, L., Vancoillie, S., and Pierloot, K. (2010). Multiconfigurational second-order perturbation theory restricted active space (RASPT2) method for electronic excited states: a benchmark study. *Journal of Chemical Theory and Computation*, 7(1):153–168.

Schautz, F., Buda, F., and Filippi, C. (2004). Excitations in photoactive molecules from quantum Monte Carlo. *The Journal of Chemical Physics*, 121(12):5836–5844.

Schiff, L. (1995). *Quantum mechanics, 2nd edition*. New York: McGraw-Hill.

Schreiber, M., Silva-Junior, M. R., Sauer, S. P., and Thiel, W. (2008). Benchmarks for electronically excited states: CASPT2, CC2, CCSD, and CC3. *The Journal of Chemical Physics*, 128(13):134110.

Schulz, S. (2007). *Electronic and optical properties of quantum dots: a tight-binding approach*. PhD thesis, Universitt Bremen.

Segal, G. (2012). *Semiempirical methods of electronic structure calculation: Part A: Applications*, volume 8. United State: Springer Science & Business Media.

Seifert, G. (2007). Tight-binding density functional theory: an approximate Kohn- Sham DFT scheme. *The Journal of Physical Chemistry A*, 111(26):5609–5613.

Seifert, G. and Joswig, J.-O. (2012). Density-functional tight binding: An approximate density-functional theory method. *Wiley Interdisciplinary Reviews: Computational Molecular Science*, 2(3):456–465.

Service, R. F. (2008). Solar energy. can the upstarts top silicon? *Science (New York, NY)*, 319(5864):718.

Sethi, R., Kumar, L., Sharma, P., Mishra, P., and Pandey, A. (2007). Synthesis and characterization of $Cd_{1-x}Zn_xS$ ternary nanocrystals. In *2007 International Workshop on Physics of Semiconductor Devices*, pages 472–474. IEEE.

Shao, Y., Gan, Z., Epifanovsky, E., Gilbert, A. T., Wormit, M., Kussmann, J., Lange, A. W., Behn, A., Deng, J., Feng, X., et al. (2015). Advances in molecular quantum chemistry contained in the Q-Chem 4 program package. *Molecular Physics*, 113(2):184–215.

Sherrill, C. D. and Schaefer III, H. F. (1999). The configuration interaction method: Advances in highly correlated approaches. In *Advances in quantum chemistry*, volume 34, pages 143–269. Elsevier.

Shi, L. and Papaconstantopoulos, D. A. (2004). Modifications and extensions to Harrisons tight-binding theory. *Physical Review B*, 70(20):205101.

Silva-Junior, M. R., Schreiber, M., Sauer, S. P., and Thiel, W. (2008). Benchmarks for electronically excited states: Time-dependent density functional theory and density functional theory based multireference configuration interaction. *The Journal of Chemical Physics*, 129(10):104103.

Silva-Junior, M. R. and Thiel, W. (2010). Benchmark of electronically excited states for semiempirical methods: MNDO, AM1, PM3, OM1, OM2, OM3, INDO/S, and INDO/S2. *Journal of Chemical Theory and Computation*, 6(5):1546–1564.

Singer, S. and Nelder, J. (2009). Nelder-Mead algorithm. *Scholarpedia*, 4(7):2928.

Slater, J. C. and Koster, G. F. (1954). Simplified LCAO method for the periodic potential problem. *Physical Review*, 94(6):1498.

Soloviev, V., Eichhöfer, A., Fenske, D., and Banin, U. (2001). Size-dependent optical spectroscopy of a homologous series of CdSe cluster molecules. *Journal of the American Chemical Society*, 123(10):2354–2364.

Stanton, J. F. and Bartlett, R. J. (1993). The equation of motion coupled-cluster method. a systematic biorthogonal approach to molecular excitation energies, transition probabilities, and excited state properties. *The Journal of Chemical Physics*, 98(9):7029–7039.

Stewart, J. (1989). The PM3 quantum chemistry program. *Journal Computational Chemistry*, 10:209–215.

Stewart, J. J. (1990). MOPAC: A semiempirical molecular orbital program. *Journal of computer-aided molecular design*, 4(1):1–103.

Stewart, J. J. (2007). Optimization of parameters for semiempirical methods V: modification of NDDO approximations and application to 70 elements. *Journal of Molecular Modeling*, 13(12):1173–1213.

Stewart, J. J. (2013). Optimization of parameters for semiempirical methods VI: more modifications to the NDDO approximations and re-optimization of parameters. *Journal of Molecular Modeling*, 19(1):1–32.

Stradi, D., Jelver, L., Smidstrup, S., and Stokbro, K. (2017). Method for determining optimal supercell representation of interfaces. *Journal of Physics: Condensed Matter*, 29(18):185901.

Struve, W. S. (1989). *Fundamentals of molecular spectroscopy*. New York: Wiley.

Suri, S., Ruan, G., Winter, J., and Schmidt, C. E. (2013). Microparticles and nanoparticles. In *Biomaterials Science*, pages 360–388. Elsevier.

Szabo, A. and Ostlund, N. S. (2012). *Modern quantum chemistry: Introduction to advanced electronic structure theory*. Canada: Courier Corporation.

Szalay, P. G., Muller, T., Gidofalvi, G., Lischka, H., and Shepard, R. (2011). Multiconfiguration self-consistent field and multireference configuration interaction methods and applications. *Chemical Reviews*, 112(1):108–181.

Tam, N. M., Hang, T. D., Pham, H. T., Nguyen, H. T., Pham-Ho, M. P., Denis, P. A., and Nguyen, M. T. (2015). Bonding and singlet–triplet gap of silicon trimer: Effects of protonation and attachment of alkali metal cations. *Journal Computational Chemistry*, 36(11):805–815.

Thiel, W. (2014). Semiempirical quantum chemical methods. *WIREs Computational Molecular Science*, 4(2):145–157.

Thiel, W. et al. (2000). Semiempirical methods. *Modern Methods and Algorithms of Quantum Chemistry*, pages 261–283.

Thiel, W. and Voityuk, A. A. (1996). Extension of MNDO to d orbitals: Parameters and results for the second-row elements and for the zinc Group. *The Journal of Physical Chemistry*, 100(2):616–626.

Tian, W. Q., Feng, J.-K., Wang, Y. A., and Aoki, Y. (2006). Search for suitable approximation methods for fullerene structure and relative stability studies: Case study with C_50. *The Journal of Chemical Physics*, 125(9):094105.

Tran, F. and Blaha, P. (2017). Importance of the kinetic energy density for band gap calculations in solids with density functional theory. *The Journal of Physical Chemistry A*, 121(17):3318–3325.

Valiev, M., Bylaska, E. J., Govind, N., Kowalski, K., Straatsma, T. P., Van Dam, H. J., Wang, D., Nieplocha, J., Apra, E., Windus, T. L., et al. (2010). NWChem: A comprehensive and scalable open-source solution for large scale molecular simulations. *Computer Physics Communications*, 181(9):1477–1489.

Van Catledge, F. A. (1971). Semiempirical investigation of pi.-. sigma. excitations in nonplanar hydrocarbons. *Journal of the American Chemical Society*, 93(18):4365–4374.

van Setten, M. J., Weigend, F., and Evers, F. (2012). The GW-method for quantum chemistry applications: theory and implementation. *Journal of Chemical Theory and Computation*, 9(1):232–246.

Varsano, D. (2006). *First principles description of response functions in low dimensional systems*. PhD thesis, PhD thesis, Thesis, University of the Basque Country.

Vatankhah, C. and Ebadi, A. (2013). Quantum size effects on effective mass and band gap of semiconductor quantum dots. *Research Journal of Recent Sciences*, 2277:2502.

Voityuk, A. A. (2006). Assessment of semiempirical methods for the computation of charge transfer in DNA π-stacks. *Chemical physics letters*, 427(1-3):177–180.

Voityuk, A. A. (2013). Intermediate neglect of differential overlap for spectroscopy. *Wiley Interdisciplinary Reviews: Computational Molecular Science*, 3(5):515–527.

Voityuk, A. A. (2014). Indo/x: A new semiempirical method for excited states of organic and biological molecules. *Journal of Chemical Theory and Computation*, 10(11):4950–4958.

Voityuk, A. A. and Rösch, N. (2000). AM1/d parameters for molybdenum. *The Journal of Physical Chemistry A*, 104(17):4089–4094.

Voityuk, A. A., Zerner, M. C., and Rösch, N. (1999). Extension of the neglect of diatomic differential overlap method to spectroscopy. NDDO-G parametrization and results for organic molecules. *The Journal of Physical Chemistry A*, 103(23):4553–4559.

Wageh, S. and Badr, M. (2008). $Cd_{1-x}Zn_xS$ nanoparticles stabilized by a bifunctional organic molecule. *Physica E*, 40(8):2810–2813.

Wahab, H. S. (2012). Quantum chemical modeling study of adsorption of benzoic acid on anatase TiO_2 nanoparticles. *Journal of Molecular Modeling*, 18(6):2709–2716.

Wang, B.-C., Chou, Y.-M., Deng, J.-P., and Dung, Y.-T. (2008). Structural and optical properties of passivated silicon nanoclusters with different shapes: A theoretical investigation. *The Journal of Physical Chemistry A*, 112(28):6351–6357.

Wang, L. W. and Zunger, A. (1994). Electronic structure pseudopotential calculations of large (. apprx. 1000 atoms) si quantum dots. *The Journal of Physical Chemistry*, 98(8):2158–2165.

Wang, L.-W. and Zunger, A. (1996). Pseudopotential calculations of nanoscale CdSe quantum dots. *Physical Review B*, 53(15):9579.

Wang, L.-W. and Zunger, A. (1997). Pseudopotential theory of nanometer silicon quantum dots. In *Studies in Surface Science and Catalysis*, volume 103, pages 161–207. Elsevier.

Watts, J. D. (2008). An introduction to equation-of-motion and linear-response coupled-cluster methods for electronically excited states of molecules. In *Radiation Induced Molecular Phenomena in Nucleic Acids*, pages 65–92. Springer.

Weigend, F. and Ahlrichs, R. (2005). Balanced basis sets of split valence, triple zeta valence and quadruple zeta valence quality for H to Rn: Design and assessment of accuracy. *Physical Chemistry Chemical Physics*, 7(18):3297–3305.

Wilson, H. F., McKenzie-Sell, L., and Barnard, A. S. (2014). Shape dependence of the band gaps in luminescent silicon quantum dots. *Journal of Materials Chemistry C*, 2(44):9451–9456.

Winget, P. and Clark, T. (2005). Am1* parameters for aluminum, silicon, titanium and zirconium. *Journal of Molecular Modeling*, 11(6):439–456.

Winget, P., Horn, A. H., Selçuki, C., Martin, B., and Clark, T. (2003). AM1* parameters for phosphorus, sulfur and chlorine. *Journal of Molecular Modeling*, 9(6):408–414.

Wolfsberg, M. and Helmholz, L. (1952). The spectra and electronic structure of the tetrahedral ions MnO4-, CrO4–, and ClO4-. *The Journal of Chemical Physics*, 20(5):837–843.

Won, Y.-H., Cho, O., Kim, T., Chung, D.-Y., Kim, T., Chung, H., Jang, H., Lee, J., Kim, D., and Jang, E. (2019). Highly efficient and stable InP/ZnSe/ZnS quantum dot light-emitting diodes. *Nature*, 575(7784):634–638.

Yoffe, A. D. (1993). Low-dimensional systems: quantum size effects and electronic properties of semiconductor microcrystallites (zero-dimensional systems) and some quasi-two-dimensional systems. *Advances in Physics*, 42(2):173–262.

Zerner, M. C. (1991). Semiempirical molecular orbital methods. *Reviews in Computational Chemistry*, pages 313–365.

Zerner, M. C., Loew, G. H., Kirchner, R. F., and Mueller-Westerhoff, U. T. (1980a). An intermediate neglect of differential overlap technique for spectroscopy of transition-metal complexes. Ferrocene. *Journal of the American Chemical Society*, 102(2):589–599.

Zerner, M. C., Lowe, G. H., Kirchner, R. F., and Mueller-Westerhoff, U. T. (1980b). An intermediate neglect of differential dverlap technique for spectroscopy of sransition-metal complexes. Ferrocene. *Journal of the American Chemical Society*, 102:589–599.

Zhou, Y. (2015). *Eco-and renewable energy materials*. Beijing: Springer.

Zonias, N., Lagoudakis, P., and Skylaris, C.-K. (2009). Large-scale first principles and tight-binding density functional theory calculations on hydrogen-passivated silicon nanorods. *Journal of Physics: Condensed Matter*, 22(2):025303.

Appendix A

Materials Used in the Research Work

The materials employd for the research are broadly divided into two, namely hardware and software.

A.1 Hardware

Calculations for the determination of equilibrium structure, ground-state properties, excitation energies, and absorption spectra of large atomic clusters and nano-sized materials were carried out using both high-level and semi-empirical methods. The former calculations are *compute-intensive* and require large computation resources and time. In order to achieve these, High-Performance Computing (HPC) facilities at the Center for High-Performance Computing (CHPC) in South Africa and HPC at the International Centre for Theoretical Physics Trieste, Italy were employed.

A.2 Software algorithms and Packages

The software packages used for this research were ORCA 4.0, Amoeba Optimizer, MOPAC 7, Avogadro, QuantumATK, Gnuplot 4.6 and Gabedit 2.5.0.

A.2.1 ORCA 4.0

ORCA is a self-consistency field molecular orbital package developed by Frank Neese for the execution of first principle and semi-empirical molecular orbital theory approaches (Neese, 2012). In particular, ORCA 4.0 was employed in this research to carry out geometry optimisations and calculate ground state and excitation energies, and UV-VIS absorption spectra both using *ab-initio* and semi-empirical methods. In addition, the calculations with new accurate semi-empirical method developed in this work were carried out using the ORCA 4.0 platform.

A.2.2 Amoeba Optimiser Algorithm

The Amoeba optimiser is a method based on the simplex algorithm used for finding the minimum point of a multidimensional function. It was proposed by Mead and Nelder in 1965 (Nelder and Mead, 1965). The method involves moving and continuous transformation (shrinking, reflecting and stretching) of a simplex (e.g triangle or polygon) around an optimal point until a tolerance error is reached. Each vertex of the simplex corresponds to a set of parameters of the function to be minimized. The detailed algorithm and implementation of this method have been reported in the reference: (Press et al., 2007). Although the simplex method is slow in speed, it is reliable and has been widely employed for optimisation of models parameters (Singer and Nelder, 2009).
In this work, the Amoeba optimizer algorithm was used for the optimisation of semi-empirical Hamiltonian parameters. The required libraries for the code were taken from Numerical Recipes (Press et al., 2007) in the C++ computer language and a C++ code and a bash linux scripts adopted as drivers to drive the libraries.

A.2.3 MOPAC7

MOPAC is an acronym for Molecular Orbital Package. It was developed by James Stewart (Stewart, 1990) to execute semi-empirical methods based on NDDO including the PM3, PM6, and PM7.In this research, the PM7 in the MOPAC7 was employed to perform structure optimisation for large atomic clusters and quantum dots for which *ab-initio* methods are prohibitively expensive. The ZINDO semi-empirical Hamiltonian is

not coded in MOPAC. Thus, we could not use MOPAC for calculations of the absorption spectra and excitation energies which were based on the ZINDO/S Hamiltonian.

A.2.4 QuantumATK

QuantumATK is a powerful tool for modelling different kinds of materials including nanomaterials. It employs a variety of methods like DFT, tight-binding, classical force fields, etc. for its modelling and simulations. It is also composed of a builder used for building varieties of atomic systems like bulk, one-dimensional, two-dimensional and zero-dimensional materials (Stradi et al., 2017). In this work, the Wulff constructor in the quantumATK builder was employed to build large atomic clusters and nano-sized materials (quantum dots).

A.2.5 Gnuplot 4.6

Gnuplot (Racine, 2006) is a command-line visualization tool used to carry out different plots including scatter plots of the excitation energies and plots of the absorption spectra. In particular, version 4.6 was utilized in this research.

A.2.6 Gabedit 2.5.0

Gabedit is a computational package, which interfaces with some molecular orbital packages like MOPAC, Gaussian, ORCA etc. It has different features, which include the display of spectra and geometries from the output files of different packages (Allouche, 2008, 2011). In this work, gabedit 2.5.0 was employed to visualize UV-Vis absorption spectra from ORCA excitation and spectra calculations output files.

Appendix B

Optimized atomic structures

B.1 Zinc clusters

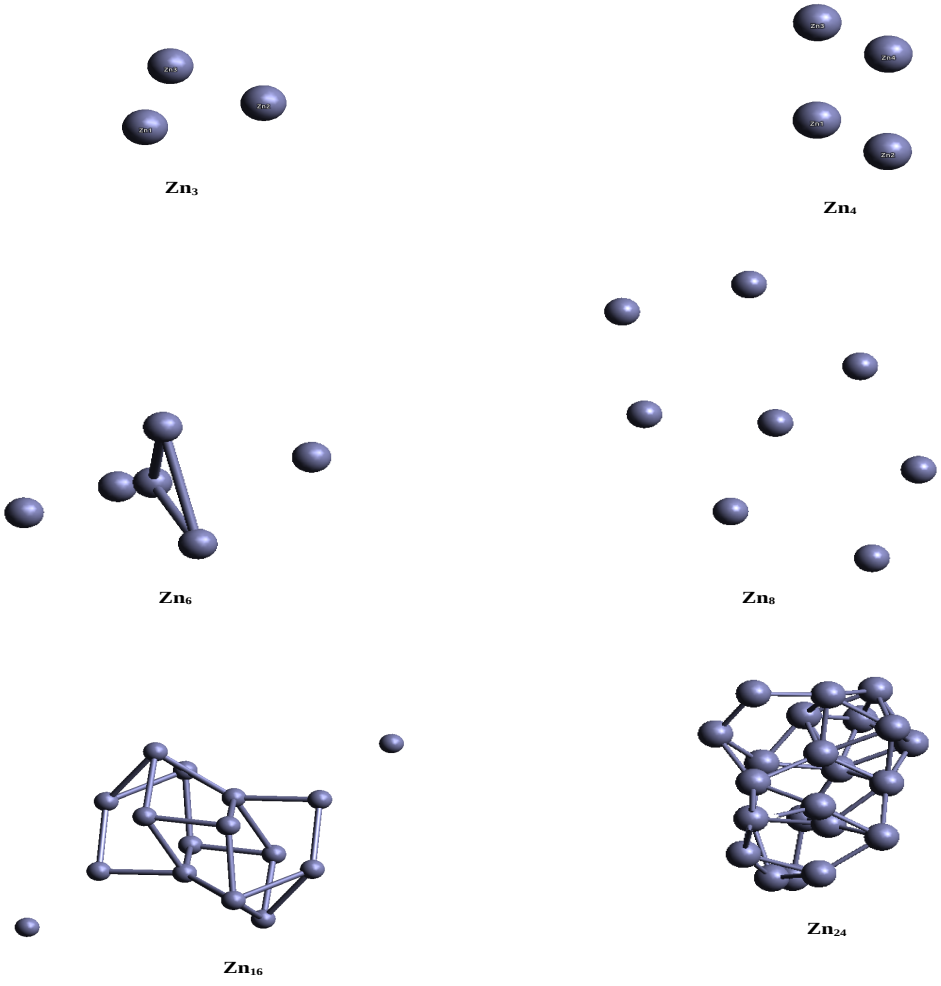

Figure B.1: Equilibrium structures of Zn_n (n= 3, 4, 6, 8, 16, 24). The structures were obtained from geometry optimizations using B3LYP/DEF2-TZVPP for small clusters and B3LYP/DEF2-SVP for moderate-sized clusters.

B.1.1 Cartesian coordinates of equilibrium zinc clusters in Angstrom

Zn_3

	x	y	z
Zn	0.977980	-0.563480	3.710250
Zn	2.665000	-3.488950	3.710250
Zn	4.352020	-0.563480	3.710250

Zn_4

	x	y	z
Zn	1.048700	-0.769410	3.712820
Zn	2.665010	2.399990	3.707680
Zn	2.665010	-3.938440	3.707680
Zn	4.281000	-0.769410	3.712820

Zn_6

	x	y	z
Zn	-1.361706	0.353221	-0.155692
Zn	-0.757604	3.442835	-0.822890
Zn	0.513636	1.602957	1.567345
Zn	1.271224	0.878638	-1.083022
Zn	0.909574	-1.502764	0.994363
Zn	-4.287594	-0.693600	-0.500105

Zn_8

	x	y	z
Zn	-3.892005	1.053449	-0.000563
Zn	-1.320401	2.811341	0.001949
Zn	1.825857	3.181664	-0.001794
Zn	2.834073	-1.463988	0.001509
Zn	0.258744	0.368232	0.002342
Zn	-3.240845	-2.071732	-0.001667
Zn	-0.160721	-2.519134	-0.000238
Zn	4.400197	1.305980	-0.001539

Zn_{16}

	x	y	z
Zn	1.309724	-0.272694	1.697209
Zn	0.592158	1.145879	5.607923
Zn	2.665000	6.283164	3.622037
Zn	2.665000	3.583849	4.892289
Zn	2.665002	-2.572512	2.466663
Zn	2.665002	-1.138558	6.077919
Zn	4.020277	-0.272692	1.697210
Zn	4.737841	1.145881	5.607919
Zn	0.592227	-1.145853	4.286125
Zn	1.309718	0.272708	8.196827
Zn	2.664998	1.138534	3.816186
Zn	2.664998	2.572488	7.427307
Zn	2.664999	-3.583809	5.001698
Zn	2.664994	-6.283241	6.271740
Zn	4.737776	-1.145854	4.286124
Zn	4.020286	0.272711	8.196824

Zn_{24}

	x	y	z
Zn	1.597912	0.940148	2.700771
Zn	0.618412	0.177612	5.203401
Zn	1.436436	0.677550	10.220961
Zn	1.162049	3.565947	3.193973
Zn	1.325607	2.927668	5.846840
Zn	2.425704	3.193143	10.650837
Zn	3.983035	-0.384343	2.923070
Zn	1.444607	-2.129759	6.552442
Zn	1.110823	-3.164985	10.451074
Zn	5.789436	0.143101	4.956837
Zn	5.046609	1.050892	7.567449
Zn	4.885845	2.604712	9.703134
Zn	1.526950	-1.663384	3.292700
Zn	0.402669	0.395812	7.818179
Zn	3.145742	-1.408135	10.976535
Zn	3.251933	0.969379	5.419575
Zn	2.536852	2.181045	8.137949
Zn	3.721663	1.108407	11.748347
Zn	2.586800	-3.833030	4.537654
Zn	-0.512227	-1.989407	8.605535
Zn	4.059498	-2.727034	13.484239
Zn	4.002320	-1.801284	5.797204
Zn	3.074436	-0.670401	8.372065
Zn	5.336890	-0.163653	9.931228

B.2 Cadmium Clusters

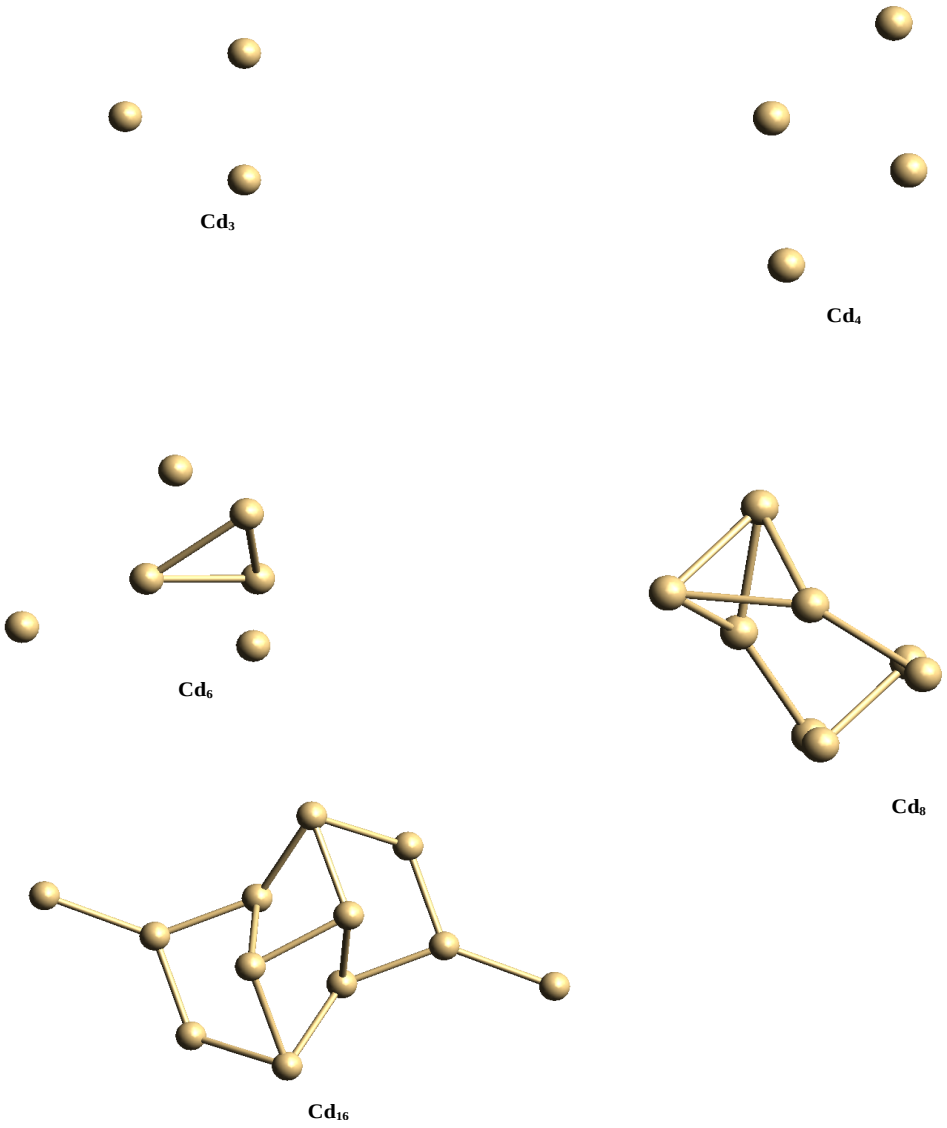

Figure B.2: Equilibrium structures of Cd_n (n= 3, 4, 6, 8, 16). The structures were obtained from geometry optimization using B3LYP/DEF2-TZVPP for small clusters and B3LYP/DEF2-SVP for moderate-sized clusters.

B.2.1 Cartesian coordinates of equilibrium cadmium clusters in Angstrom

Cd_3

	x	y	z
Cd	0.912857	-0.522724	3.710250
Cd	2.665000	-3.570468	3.710250
Cd	4.417143	-0.522724	3.710250

Cd_4

	x	y	z
Cd	0.966913	-0.769323	3.710207
Cd	2.665005	2.468298	3.710293
Cd	2.665005	-4.006928	3.710292
Cd	4.363078	-0.769323	3.710208

Cd_6

	x	y	z
Cd	-1.479310	0.280929	-0.167017
Cd	-0.786582	3.649948	-0.890809
Cd	0.635055	1.744607	1.772220
Cd	1.495986	0.917573	-1.243600
Cd	1.081351	-1.727707	1.095999
Cd	-4.658969	-0.784062	-0.566794

Cd_8

	x	y	z
Cd	0.274865	1.740542	-0.994800
Cd	-2.020659	2.966742	0.912465
Cd	1.180767	3.162451	1.752450
Cd	1.972044	-1.271420	-0.527539
Cd	-0.452511	0.368938	2.084672
Cd	-1.116844	-1.466207	-1.321866
Cd	-0.148486	-2.806631	1.641417
Cd	1.015725	-0.028603	-3.546800

Cd_{16}

	x	y	z
Cd	1.091584	-0.338999	1.224444
Cd	0.252570	1.358260	5.708279
Cd	2.665005	7.055048	3.598561
Cd	2.665003	4.001191	4.802245
Cd	2.665006	-3.002380	2.126086
Cd	2.665002	-1.170568	6.224168
Cd	4.238412	-0.338993	1.224444
Cd	5.077426	1.358264	5.708275
Cd	0.252618	-1.358352	4.185746
Cd	1.091590	0.339060	8.669612
Cd	2.664996	1.170544	3.669924
Cd	2.664995	3.002417	7.767868
Cd	2.664998	-4.001159	5.091708
Cd	2.664996	-7.055049	6.295286
Cd	5.077385	-1.358350	4.185744
Cd	4.238414	0.339065	8.669610

B.3 Zinc Quantum Dots

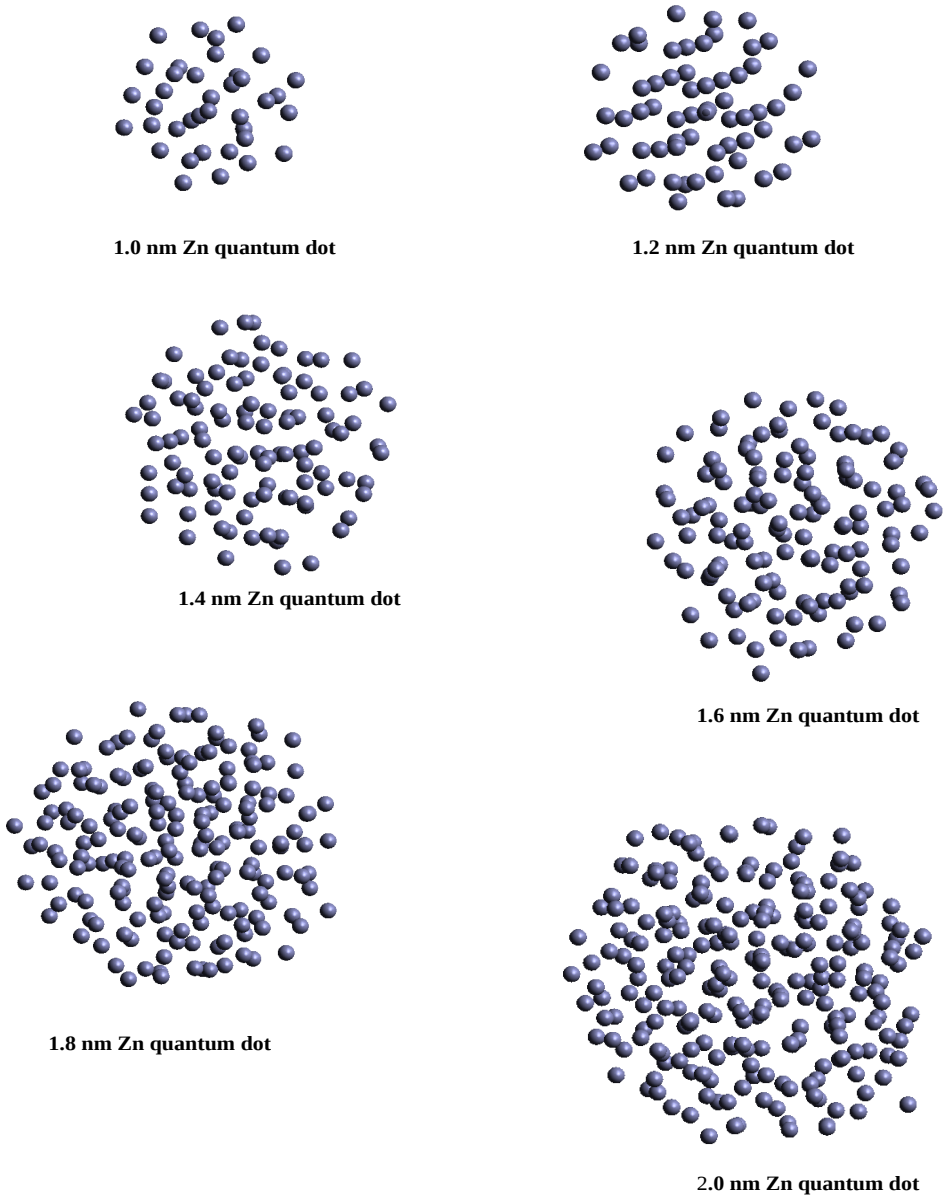

Figure B.3: Equilibrium structures of Zn quantum dots of sizes 1.0, 1.2, 1.4, 1.6, 1.8 and 2.0 nm. The structures were obtained from geometry optimization using PM7 as implemented in MOPAC.

B.3.1 Cartesian coordinates of equilibrium zinc quantum dots in Angstrom

Zn_{62} (1.2nm)

	x	y	z
Zn	2.629584	-0.870628	-9.826427
Zn	-0.041493	-4.843919	-7.080275
Zn	2.953517	-3.549539	-7.676692
Zn	4.077043	-2.401456	-4.702567
Zn	-1.318283	-7.952943	-3.262859
Zn	1.324073	-6.516969	-4.569175
Zn	4.245731	-6.477817	-2.565587
Zn	6.495514	-4.487786	-3.894923
Zn	6.319579	-2.851299	-1.049899
Zn	-2.548582	0.147201	-8.675430
Zn	-4.331853	-2.242587	-7.236227
Zn	-1.886756	-2.858980	-5.169355
Zn	0.229947	-0.999325	-7.413047
Zn	0.687804	2.277681	-7.013707
Zn	3.114602	2.370099	-9.193018
Zn	5.405170	2.618568	-6.765772
Zn	-6.038533	-4.694297	-5.747148
Zn	-3.542814	-5.344626	-3.701779
Zn	0.151477	-4.060252	-2.679671
Zn	2.458891	-0.174461	-1.024263
Zn	1.089103	-0.801923	-4.123150
Zn	2.985121	1.777073	-4.621217
Zn	7.608959	1.994609	-4.167965
Zn	5.196799	3.868441	-2.680507
Zn	-0.763572	-7.931061	2.472881
Zn	-0.822723	-6.281532	-0.386358
Zn	2.364818	-5.675362	0.835820
Zn	2.976062	-3.507547	-1.683677
Zn	4.235945	-1.551206	1.584581
Zn	5.323464	-0.026117	-2.623528
Zn	6.286153	1.038355	0.484140
Zn	8.392288	3.100358	-0.931117
Zn	2.445283	-7.447333	3.587461
Zn	5.445488	-5.995948	4.157065
Zn	5.719707	-5.696375	0.662145
Zn	6.827986	-3.021863	3.060954
Zn	8.581821	-1.257401	0.866518
Zn	-5.525517	-0.041738	-5.113705
Zn	-3.502602	2.311383	-6.369773
Zn	-1.207687	5.116472	-6.920310
Zn	-7.336220	-2.422662	-3.714347
Zn	-5.024147	-3.164109	-1.530306
Zn	-3.172272	-0.764296	-2.822159
Zn	-0.936169	1.963139	-0.479650
Zn	-1.254518	1.572192	-4.098591
Zn	1.174191	5.032685	-4.360632
Zn	4.380797	5.557889	-5.435772
Zn	4.661474	7.520684	-2.522154
Zn	-4.225863	-6.965849	-0.525015
Zn	-2.546457	-3.650948	0.848222
Zn	-0.673964	-0.454392	2.370050
Zn	-0.824723	-1.487355	-0.903927
Zn	1.876834	1.447007	2.059672
Zn	2.067254	3.332314	-1.423756
Zn	4.112118	3.821440	1.173577
Zn	6.622065	5.810179	-0.014783
Zn	-3.954341	-8.635440	2.408646
Zn	-4.399299	-6.002198	4.449300
Zn	-1.407660	-4.887389	3.766720
Zn	1.485561	-1.948906	5.781042
Zn	1.299412	-3.028644	2.608464
Zn	3.750501	0.273109	4.547099
Zn	6.134119	2.520473	3.683212
Zn	7.571209	5.557010	3.142581
Zn	1.065237	-5.663402	5.929042
Zn	4.148344	-4.050339	6.585060
Zn	6.150307	-1.554457	5.867838
Zn	-8.709485	-0.043444	-1.759298
Zn	-6.660627	2.165991	-2.887231
Zn	-6.399591	5.472157	-2.537085
Zn	-4.028738	5.466798	-4.864067

Zn_{104} (1.4nm)

	x	y	z
Zn	2.629584	-0.870628	-9.826427
Zn	-0.041493	-4.843919	-7.080275
Zn	2.953517	-3.549539	-7.676692
Zn	4.077043	-2.401456	-4.702567
Zn	-1.318283	-7.952943	-3.262859
Zn	1.324073	-6.516969	-4.569175
Zn	4.245731	-6.477817	-2.565587
Zn	6.495514	-4.487786	-3.894923
Zn	6.319579	-2.851299	-1.049899
Zn	-2.548582	0.147201	-8.675430
Zn	-4.331853	-2.242587	-7.236227
Zn	-1.886756	-2.858980	-5.169355
Zn	0.229947	-0.999325	-7.413047
Zn	0.687804	2.277681	-7.013707
Zn	3.114602	2.370099	-9.193018
Zn	5.405170	2.618568	-6.765772
Zn	-6.038533	-4.694297	-5.747148
Zn	-3.542814	-5.344626	-3.701779
Zn	0.151477	-4.060252	-2.679671
Zn	2.458891	-0.174461	-1.024263
Zn	1.089103	-0.801923	-4.123150
Zn	2.985121	1.777073	-4.621217
Zn	7.608959	1.994609	-4.167965
Zn	5.196799	3.868441	-2.680507
Zn	-0.763572	-7.931061	2.472881
Zn	-0.822723	-6.281532	-0.386358
Zn	2.364818	-5.675362	0.835820
Zn	2.976062	-3.507547	-1.683677
Zn	4.235945	-1.551206	1.584581
Zn	5.323464	-0.026117	-2.623528
Zn	6.286153	1.038355	0.484140
Zn	8.392288	3.100358	-0.931117
Zn	2.445283	-7.447333	3.587461
Zn	5.445488	-5.995948	4.157065
Zn	5.719707	-5.696375	0.662145
Zn	6.827986	-3.021863	3.060954
Zn	8.581821	-1.257401	0.866518
Zn	-5.525517	-0.041738	-5.113705
Zn	-3.502602	2.311383	-6.369773
Zn	-1.207687	5.116472	-6.920310
Zn	-7.336220	-2.422662	-3.714347
Zn	-5.024147	-3.164109	-1.530306
Zn	-3.172272	-0.764296	-2.822159
Zn	-0.936169	1.963139	-0.479650
Zn	-1.254518	1.572192	-4.098591
Zn	1.174191	5.032685	-4.360632
Zn	4.380797	5.557889	-5.435772
Zn	4.661474	7.520684	-2.522154
Zn	-4.225863	-6.965849	-0.525015
Zn	-2.546457	-3.650948	0.848222
Zn	-0.673964	-0.454392	2.370050
Zn	-0.824723	-1.487355	-0.903927
Zn	1.876834	1.447007	2.059672
Zn	2.067254	3.332314	-1.423756
Zn	4.112118	3.821440	1.173577
Zn	6.622065	5.810179	-0.014783
Zn	-3.954341	-8.635440	2.408646
Zn	-4.399299	-6.002198	4.449300
Zn	-1.407660	-4.887389	3.766720
Zn	1.485561	-1.948906	5.781042
Zn	1.299412	-3.028644	2.608464
Zn	3.750501	0.273109	4.547099
Zn	6.134119	2.520473	3.683212
Zn	7.571209	5.557010	3.142581
Zn	1.065237	-5.663402	5.929042
Zn	4.148344	-4.050339	6.585060
Zn	6.150307	-1.554457	5.867838
Zn	-8.709485	-0.043444	-1.759298
Zn	-6.660627	2.165991	-2.887231
Zn	-6.399591	5.472157	-2.537085
Zn	-4.028738	5.466798	-4.864067
Zn	-2.079011	8.062799	-3.168412
Zn	-8.372367	-2.796864	2.411443
Zn	-6.467873	-0.988077	0.441015
Zn	-4.084526	1.837633	2.919965
Zn	-4.372768	1.598246	-0.627903
Zn	-4.130340	4.943030	-0.254324
Zn	-1.693245	4.623259	-2.600219
Zn	0.256614	6.018195	-0.054248
Zn	1.262738	7.773767	-2.680050
Zn	-5.738232	-4.798030	1.720488
Zn	-6.632513	-1.560456	4.998608
Zn	-4.188169	-1.356042	2.835282
Zn	-1.616453	1.389403	5.244716
Zn	-1.626662	4.012231	1.820710
Zn	0.602239	3.649491	4.265984
Zn	2.276181	6.003239	2.678354
Zn	4.903623	6.867958	4.635921
Zn	-4.699707	-3.515642	6.755307
Zn	-1.776841	-2.085347	8.777748
Zn	-2.001364	-2.146219	5.348214
Zn	0.180751	0.506147	7.772269
Zn	2.635787	2.441744	6.608327
Zn	5.437175	4.181976	6.516112
Zn	1.151041	-3.634840	8.835851
Zn	-7.451233	2.314489	1.186745
Zn	-8.220336	3.323174	4.318625
Zn	-5.588795	5.043727	2.723815
Zn	-2.863179	6.782299	3.407057
Zn	-2.485426	7.853784	0.180747
Zn	-5.849572	1.655543	5.704191
Zn	-3.266672	3.584271	7.024579
Zn	-1.070903	5.824876	5.983720
Zn	-1.687459	2.514850	9.661516

Zn_{128} (1.6 nm)

	x	y	z
Zn	2.856009	-1.992959	-8.349380
Zn	1.905763	1.642131	-8.138038
Zn	0.906421	-5.705138	-6.217056
Zn	3.982520	-4.941109	-7.322336
Zn	4.749978	-3.234884	-4.570032
Zn	4.695799	-0.133343	-6.213961
Zn	7.178954	2.387223	-5.518305
Zn	1.140042	-9.076122	-1.156339
Zn	1.843662	-6.558966	-3.146017
Zn	3.925382	-4.530832	-1.606867
Zn	7.363711	-5.157768	-3.596019
Zn	6.849721	-0.720666	-3.220457
Zn	9.727878	1.028397	-3.716635
Zn	3.722814	-8.523210	1.107989
Zn	5.867125	-7.277791	-1.344224
Zn	7.510774	-5.751012	0.982132
Zn	7.480649	-3.049371	-0.958382
Zn	-2.740857	1.573132	-9.222411
Zn	-0.579352	3.656866	-7.389828
Zn	-3.996499	-1.211777	-7.060843
Zn	-1.893405	-2.569683	-4.583902
Zn	-0.544389	-0.697570	-7.924898
Zn	-2.107406	1.386683	-5.287230
Zn	1.475976	0.767468	-4.758904
Zn	3.842599	3.443554	-5.707785
Zn	-2.635778	-5.600122	-5.839856
Zn	-3.893565	-6.258308	-2.763888
Zn	-0.929524	-4.938827	-2.133474
Zn	1.381109	-2.520428	-1.872164
Zn	1.245921	-2.505587	-5.304194
Zn	3.512561	-0.131811	-2.344006
Zn	4.283223	3.252763	-2.412673
Zn	7.091822	4.845423	-3.098855
Zn	-2.069545	-10.926811	1.458931
Zn	-2.435657	-9.173927	-1.334856
Zn	-1.088007	-6.723136	0.639534
Zn	2.221159	-5.598536	1.061143
Zn	4.687649	-1.802937	0.551865
Zn	6.445528	1.168475	-0.424028
Zn	9.362690	2.604641	2.290501
Zn	9.060542	3.000650	-1.186035
Zn	0.499271	-9.206899	2.480069
Zn	1.239754	-5.998770	4.123335
Zn	4.321627	-7.332144	4.339509
Zn	4.978924	-4.462070	2.674019
Zn	6.799342	-1.449773	3.525252
Zn	8.755600	-0.595108	1.105605
Zn	-6.763967	0.683683	-6.293402
Zn	-4.618559	3.136661	-6.814827
Zn	-2.916430	6.016553	-5.690472
Zn	-0.825949	6.969525	-8.307389
Zn	2.104362	7.590076	-6.690999
Zn	-5.573069	-3.905846	-5.924747
Zn	-4.908972	-2.926207	-2.867809
Zn	-4.927483	0.343914	-3.511158
Zn	-3.324704	1.482354	-0.776600
Zn	-2.275165	3.712596	-3.118035
Zn	0.765273	3.033391	-2.192276
Zn	1.102911	5.006987	-4.903099
Zn	5.120315	6.481582	-5.353943
Zn	-5.602708	-8.499213	-0.199794
Zn	-4.391396	-5.253559	0.524597
Zn	-2.503917	-2.680025	-0.295374
Zn	-0.960492	-0.307795	-2.346768
Zn	-0.842336	0.098450	1.415103
Zn	2.079991	1.351637	0.416495
Zn	3.682288	4.482958	0.653467
Zn	6.130297	6.695719	-0.491023
Zn	-3.693356	-8.219723	2.717618
Zn	-2.983712	-5.821883	4.947953
Zn	-1.312330	-4.098966	2.815491
Zn	2.639202	-2.953450	4.589780
Zn	1.335754	-2.426059	1.407370
Zn	3.608460	0.002442	3.447064
Zn	5.534660	2.606642	2.414694
Zn	7.552107	1.502671	5.065466
Zn	-0.886769	-8.348052	5.558859
Zn	0.178761	-6.814079	8.266627
Zn	3.129524	-5.622397	7.250743
Zn	3.771113	-2.129554	7.637401
Zn	4.562555	0.881604	6.439536
Zn	-7.510505	0.543946	-1.466135
Zn	-8.649579	2.347396	-4.061932
Zn	-5.660630	3.815446	-3.587779
Zn	-4.946971	7.080665	-3.000491
Zn	-0.907334	7.345173	-3.156927
Zn	1.659116	9.229497	-3.906969
Zn	-7.229055	-3.368239	1.121646
Zn	-8.074964	-2.655814	-1.954516
Zn	-5.057797	-0.781934	0.648404
Zn	-5.826050	3.690440	-0.379346
Zn	-3.051171	5.580586	-0.475828
Zn	0.584189	5.786365	-0.520439
Zn	3.195031	8.610148	0.434668
Zn	3.229591	6.675396	-2.596051
Zn	-6.867232	-6.637330	2.826341
Zn	-5.470433	-3.676283	4.200714
Zn	-3.175927	-1.275110	3.500281
Zn	-2.513736	2.207595	4.962003
Zn	-2.276095	3.395612	1.992625
Zn	0.962337	3.837002	2.785885
Zn	4.207705	6.811772	3.108403
Zn	7.338813	5.499475	2.644241
Zn	-5.140389	-3.274990	7.516734
Zn	-0.410493	-2.002943	5.682021
Zn	0.487468	0.917139	4.301535
Zn	1.450611	2.272907	7.141629
Zn	3.729553	4.017592	4.954840
Zn	6.898050	4.652024	5.851612
Zn	-1.892978	-4.290696	7.647503
Zn	0.840372	-0.903239	8.454877
Zn	-8.476037	1.888361	1.499074
Zn	-7.248503	6.735894	-0.400550
Zn	-4.809335	7.857683	1.494984
Zn	-2.628759	9.168092	-0.868023
Zn	-9.263691	-1.214082	2.654865
Zn	-5.682657	1.427253	3.095780
Zn	-8.574545	5.168038	2.310168
Zn	-5.398420	4.809350	2.996504
Zn	-2.029927	6.646207	3.261709
Zn	-0.196127	8.536436	1.290890
Zn	-7.093057	-0.793349	5.102899
Zn	-6.082275	1.258110	7.644107
Zn	-4.975635	4.022282	6.253155
Zn	-2.568762	4.949021	8.297970
Zn	-0.452454	4.787846	5.769586
Zn	-3.382117	-0.470051	7.006210
Zn	-1.571354	1.769817	8.789662

Zn_{190} (1.8 nm)

	x	y	z
Zn	4.450044	-5.057248	-9.209072
Zn	2.864786	-7.929026	-8.896859
Zn	5.361033	-8.845652	-7.025274
Zn	-1.079610	-5.308266	-7.524607
Zn	-0.810370	-2.321019	-9.591908
Zn	1.654838	0.063464	-10.060566
Zn	2.284018	2.448649	-12.261581
Zn	5.016076	3.240839	-10.679064
Zn	-1.325635	-9.923702	-6.597350
Zn	1.002284	-7.661194	-6.150716
Zn	2.460978	-4.803094	-5.004898
Zn	2.063283	-3.294843	-7.841893
Zn	5.380471	-2.212699	-6.233826
Zn	7.355282	-0.151963	-7.904553
Zn	8.350857	0.979528	-4.817667
Zn	-1.238976	-10.220410	-3.185370
Zn	1.760508	-9.645098	-1.492276
Zn	3.338928	-9.361877	-4.453671
Zn	4.779514	-6.940011	-2.899440
Zn	5.627591	-5.650107	-6.084335
Zn	8.195711	-5.500010	-3.716619
Zn	7.674563	-2.175302	-3.960205
Zn	10.779027	0.294239	-2.503225
Zn	2.243863	-9.713462	2.230611
Zn	4.709236	-8.557258	0.219988
Zn	7.758556	-8.381775	-1.715645
Zn	8.775429	-6.305825	0.732260
Zn	10.771597	-5.113271	-1.654778
Zn	9.338714	-2.228310	-0.912634
Zn	-5.426676	-1.476261	-9.621989
Zn	-2.863851	0.542508	-9.461031
Zn	-0.160581	2.267636	-8.402387
Zn	0.493951	4.717113	-10.452040
Zn	3.516254	5.878810	-9.502212
Zn	-6.317887	-5.824949	-7.041661
Zn	-4.021014	-3.506124	-7.575792
Zn	-1.704016	-0.968346	-6.446578
Zn	1.545751	-0.361260	-6.372276
Zn	1.739801	2.316556	-4.257350
Zn	4.224741	1.220662	-8.125879
Zn	5.337489	4.363663	-5.324241
Zn	5.088044	7.347315	-6.753077
Zn	-4.490194	-9.373229	-3.654624
Zn	-3.416012	-7.333155	-5.971999
Zn	-0.954001	-6.959686	-3.515270
Zn	-0.885411	-3.733176	-4.656402
Zn	0.690267	-2.990107	-1.538127
Zn	2.842485	-1.838691	-3.785506
Zn	5.260985	-1.550453	-1.678470
Zn	4.957952	1.066423	-4.708087
Zn	5.106135	2.082264	-1.578683
Zn	7.761076	3.792869	-2.974032
Zn	-2.360779	-9.626533	-0.087948
Zn	-3.586328	-10.427171	2.920574
Zn	-0.087155	-7.535068	0.978058
Zn	1.324043	-5.236735	3.163414
Zn	1.620025	-6.081950	-1.772289
Zn	3.586111	-5.315712	0.779513
Zn	6.492450	-4.463554	-0.834217
Zn	7.379464	0.025925	0.532531
Zn	9.348628	2.417353	-0.409776
Zn	10.585884	3.157351	2.645091
Zn	-1.021614	-8.699994	3.992876
Zn	1.191608	-9.576041	6.262756
Zn	3.317263	-7.565430	4.609075
Zn	5.873762	-3.797724	5.488831
Zn	6.037166	-6.457828	2.940483
Zn	6.286563	-2.882449	2.163915
Zn	9.454774	-3.367571	2.388231
Zn	9.089386	-0.010345	3.422931
Zn	4.580075	-6.233755	7.355495
Zn	8.896541	-2.438177	5.897602
Zn	-6.958414	4.770494	-8.039016
Zn	-8.859511	-0.571491	-4.334994
Zn	-6.792056	0.122504	-7.110698
Zn	-4.819627	1.960859	-4.178173
Zn	-4.499392	2.652093	-7.482034
Zn	-1.848382	4.261966	-6.213351
Zn	-0.792507	6.748901	-8.158198
Zn	1.746367	7.071082	-6.139404
Zn	-9.273110	-5.529918	-2.369146
Zn	-7.398412	-3.878958	-4.476671
Zn	-6.513602	-1.482931	-1.871654
Zn	-4.694252	-1.271169	-4.754081
Zn	-2.126552	-1.130908	-2.287531
Zn	-1.463628	1.617103	-4.238048
Zn	0.110566	5.611943	-3.618422
Zn	2.543611	3.796997	-6.995229
Zn	3.571284	4.794098	-2.627378
Zn	5.816925	8.554957	-3.679310
Zn	-6.973385	-7.074396	-0.478136
Zn	-3.878667	-6.969218	-1.453601
Zn	-3.980089	-4.538882	-3.950216
Zn	-4.065198	-3.236666	-0.651136
Zn	-0.895857	0.277793	0.502965
Zn	1.975568	0.720428	-1.295551
Zn	1.399689	3.826880	-0.166226
Zn	3.613020	4.735789	2.074189
Zn	6.367537	6.361022	-1.190687
Zn	8.222838	8.112481	0.892039
Zn	-5.532172	-7.838072	2.601909
Zn	-2.923357	-5.791671	1.688084
Zn	-1.449080	-5.501806	5.105808
Zn	-0.753446	-3.231414	1.478089
Zn	-0.230835	-1.039358	3.987479
Zn	3.172855	-1.913273	0.807426
Zn	4.258736	0.993896	1.884128
Zn	6.505220	3.901114	1.023538
Zn	6.363870	3.103895	4.599035
Zn	8.431919	5.694273	3.070691
Zn	0.234960	-6.675898	7.664889
Zn	2.156428	-3.953643	7.525331
Zn	2.716487	-2.555679	4.352046
Zn	3.154715	0.128636	6.552882
Zn	5.767471	-0.208781	4.420050
Zn	7.352494	0.108137	7.528336
Zn	9.238606	2.379023	5.851645
Zn	4.980054	-2.126014	8.268121
Zn	-9.108759	2.526696	-7.135584
Zn	-6.809979	5.879823	-4.912633
Zn	-10.541954	-0.144764	-1.354873
Zn	-7.917083	1.722178	-0.763729
Zn	-8.057609	2.738362	-3.925526
Zn	-5.673286	4.499917	-0.561554
Zn	-3.966206	5.139063	-3.560925
Zn	-1.924441	8.134883	-3.641160
Zn	0.555264	10.056500	-5.096507
Zn	-0.045509	10.067929	-1.440676
Zn	-9.258022	-2.953853	-0.296107
Zn	-10.984246	-2.938881	2.528757
Zn	-6.978710	-0.928733	1.697959
Zn	-7.411557	2.246765	2.793276
Zn	-4.360626	1.200829	-1.086430
Zn	-1.792670	3.401391	-1.556463
Zn	-2.689696	5.850891	0.912398
Zn	0.296122	6.756735	-0.224049
Zn	2.725249	8.245365	-2.792678
Zn	3.609480	7.628059	0.396067
Zn	-8.616283	-4.616380	4.079636
Zn	-6.678780	-4.397538	1.452267
Zn	-7.257902	-1.793742	5.072854
Zn	-3.822424	-1.092417	1.893876
Zn	-3.132477	0.770523	4.919202
Zn	-4.181296	2.503035	2.119131
Zn	-0.743744	3.213980	2.260630
Zn	0.784348	6.343001	3.423380
Zn	5.307843	6.369320	4.605867
Zn	5.598770	9.199051	2.565925
Zn	-5.930726	-6.182034	5.375930
Zn	-4.349143	-3.707978	3.980693
Zn	-4.038832	-1.757279	6.722550
Zn	-0.988756	-2.657711	6.868008
Zn	-0.198904	1.212928	6.957787
Zn	1.688724	1.776205	3.885054
Zn	2.405494	4.394213	5.671904
Zn	5.404882	6.160143	7.890483
Zn	-1.710834	-4.634859	9.542286
Zn	1.147215	-3.352905	10.548429
Zn	2.780945	-0.234966	10.178417
Zn	3.242251	3.070337	10.345670
Zn	4.909255	2.822938	7.516917
Zn	-11.784289	1.454074	1.354398
Zn	-9.811695	4.085397	0.708522
Zn	-8.476921	5.837612	-1.934739
Zn	-7.492227	8.345176	-0.049601
Zn	-4.350647	7.939103	-1.182530
Zn	-2.911961	10.499533	0.125112
Zn	-9.977004	0.020663	3.690169
Zn	-9.587019	1.692456	6.584481
Zn	-9.000477	4.648792	4.883135
Zn	-6.098536	4.646855	6.600620
Zn	-7.135500	5.803332	2.111829
Zn	-4.333392	5.353830	3.937319
Zn	-1.551434	8.749749	2.488471
Zn	1.509076	10.042549	1.614121
Zn	-8.574700	-1.206972	8.051097
Zn	-5.762211	0.402014	8.883009
Zn	-6.407040	1.431918	5.728273
Zn	-3.494820	2.972666	8.085935
Zn	-1.621674	4.060110	5.359470
Zn	-0.915448	7.210820	6.382361
Zn	2.691403	8.650052	4.658746
Zn	-3.616755	-1.938830	10.283134
Zn	-0.672389	-0.458308	9.761820
Zn	-1.558612	2.550654	10.839504
Zn	0.595110	4.040158	8.708765
Zn	2.211296	7.184498	7.731935
Zn	-5.138395	7.507194	7.949527
Zn	-3.692202	8.320953	5.049552
Zn	-2.369317	6.042631	9.057175

Zn_{244} (2.0 nm)

	x	y	z
Zn	5.566306	-3.542519	-9.025397
Zn	7.383936	-1.138372	-10.859204
Zn	8.705073	-2.849639	-7.724835
Zn	4.589129	-8.965170	-6.966378
Zn	6.077246	-5.998624	-6.575043
Zn	6.590977	-2.718355	-5.038963
Zn	9.404719	-5.721512	-5.882812
Zn	10.954600	-2.668223	-5.010716
Zn	5.816188	-9.786851	-3.882707
Zn	7.844630	-8.511791	-1.336700
Zn	8.054742	-5.371984	-2.862106
Zn	10.548933	-3.537924	-1.764388
Zn	-4.131432	-6.948366	-8.672612
Zn	-1.330592	-5.109942	-9.816634
Zn	0.385215	-2.799536	-7.929180
Zn	0.708812	-0.188671	-10.116402
Zn	4.106079	-0.239807	-10.367635
Zn	5.751481	2.626701	-9.745874
Zn	7.393521	5.246287	-8.472904
Zn	-2.273756	-9.170774	-6.767360
Zn	0.177414	-7.248047	-7.685188
Zn	-1.324712	-4.909841	-5.783857
Zn	2.807892	-4.925079	-7.198110
Zn	3.363567	-3.600770	-4.150775
Zn	4.752187	-0.747226	-7.061797
Zn	7.778416	0.534684	-7.930094
Zn	9.983141	2.945309	-8.549333
Zn	9.532563	4.081875	-5.436884
Zn	-0.949878	-10.895117	-4.133076
Zn	2.509101	-10.737422	-3.429818
Zn	2.185596	-7.806803	-4.989381
Zn	4.945210	-6.524618	-3.538327
Zn	5.829339	-2.941511	-1.471553
Zn	8.532877	-0.979565	-0.931823
Zn	8.826016	-0.283329	-4.160843
Zn	11.143086	1.997447	-3.466804
Zn	1.752104	-9.656265	-0.392651
Zn	5.196901	-10.941310	-0.550763
Zn	4.508442	-7.478562	-0.214351
Zn	7.198214	-7.105671	3.536519
Zn	7.148489	-5.431445	0.602443
Zn	10.175271	-4.618659	1.387867
Zn	5.201255	-11.054178	2.847423
Zn	7.351848	-9.881871	5.209003
Zn	10.761717	-9.359945	4.960005
Zn	10.099922	-5.944604	4.465823
Zn	-4.535063	-3.552035	-9.745499
Zn	-2.801501	-0.673989	-10.079527
Zn	-2.322646	2.636727	-9.408932
Zn	0.365520	2.948750	-11.302170
Zn	1.433407	4.626073	-8.346542
Zn	3.543062	4.610268	-11.159737
Zn	5.323834	7.234454	-10.092734
Zn	-5.908694	-6.257032	-5.849315
Zn	-4.208689	-3.332220	-6.473143
Zn	-1.061622	-1.929068	-3.889098
Zn	-2.222921	-0.833935	-6.889591
Zn	0.145413	1.501095	-7.280479
Zn	3.826025	2.576735	-7.081854
Zn	2.467941	2.248243	-4.163468
Zn	5.296855	5.353393	-5.919828
Zn	6.941633	8.548083	-6.712210
Zn	-7.069371	-8.221378	-3.206423
Zn	-3.155160	-7.188737	-4.315172
Zn	-4.939696	-6.131848	-1.649633
Zn	0.693442	-5.181518	-3.218510
Zn	2.021367	-1.282667	-1.850144
Zn	1.745288	-0.925897	-5.568698
Zn	4.851977	0.079754	-3.312099
Zn	6.842388	2.280792	-5.050684
Zn	7.000517	3.885569	-1.991744
Zn	7.815929	6.527319	-3.944812
Zn	-4.195230	-10.152540	-2.967328
Zn	-3.058223	-8.729456	-0.130042
Zn	-0.588011	-8.116704	-2.255249
Zn	-8.257800	5.364507	-5.397174
Zn	-6.018621	3.212541	-3.795351
Zn	-0.035161	-6.445917	0.800906
Zn	2.815486	-4.831522	-0.389281
Zn	3.744727	-1.433227	0.818962
Zn	5.935867	1.092607	-0.329718
Zn	7.574962	2.672217	2.393935
Zn	9.673688	2.264352	-0.515338
Zn	11.776387	3.115489	1.889368
Zn	-1.139254	-10.979064	1.357709
Zn	0.861390	-9.036734	3.196617
Zn	4.036204	-7.878479	2.940209
Zn	2.923553	-4.815532	2.974653
Zn	5.910961	-3.483742	3.123163
Zn	8.393375	-3.267531	5.635764
Zn	8.965228	-1.750998	2.337067
Zn	10.061239	1.048872	3.928188
Zn	2.625989	-11.222695	4.941098
Zn	4.324697	-8.736255	6.344848
Zn	6.225520	-5.903987	6.435441
Zn	9.056131	-7.365257	7.483484
Zn	9.345862	-4.259586	8.689614
Zn	-8.179865	2.872018	-8.170269
Zn	-4.992008	4.101376	-10.660372
Zn	-3.468395	7.087465	-10.322091
Zn	-10.254531	-1.443397	-4.625843
Zn	-7.400661	-1.982980	-9.026555
Zn	-6.691931	-1.080398	-5.852294
Zn	-5.873121	0.891396	-9.568369
Zn	-4.346256	1.726661	-6.564540
Zn	-1.799109	5.429108	-7.845492
Zn	1.058468	5.350763	-4.918023
Zn	3.272306	7.359541	-7.559086
Zn	3.110492	9.773452	-5.155254
Zn	-10.636540	-4.327611	-2.588485
Zn	-7.376791	-3.793950	-3.866919
Zn	-4.157674	-3.128873	-3.097400
Zn	-5.485427	0.163375	-2.837792
Zn	-2.201130	0.797770	-2.575877
Zn	-1.773569	3.285652	-5.172482
Zn	0.132453	4.940694	-1.806198
Zn	3.636116	6.984692	-3.421319
Zn	6.013091	8.483285	-1.634664
Zn	6.216255	10.592790	-4.172506
Zn	-9.288211	-7.181047	-0.964557
Zn	-7.594903	-4.401720	-0.237542
Zn	-5.020689	-2.224413	-0.027200
Zn	-0.504515	-3.110922	-0.547851
Zn	-2.412554	-0.458649	0.571289
Zn	2.945840	2.141373	1.037376
Zn	0.679157	1.656605	-1.385487
Zn	3.758572	4.258609	-1.658246
Zn	3.808488	6.450478	0.773105
Zn	7.337089	5.972315	0.560990
Zn	-5.470732	-9.556499	3.711872
Zn	-6.444649	-8.456036	0.749079
Zn	-3.242182	-4.779645	0.918924
Zn	-0.347254	-5.254063	3.977980
Zn	0.668285	-2.578719	6.070842
Zn	0.806382	-2.056678	2.377775
Zn	5.886596	-0.115787	3.359694
Zn	4.627137	4.159981	3.046714
Zn	6.939527	3.393142	5.918798
Zn	9.618167	5.363642	3.177008
Zn	-2.910426	-11.707367	4.081667
Zn	-1.620251	-9.179377	5.964354
Zn	-2.814734	-7.557636	3.299581
Zn	1.015578	-7.186755	6.315926
Zn	3.204918	-4.567354	6.191977
Zn	5.043666	-1.869947	7.286563
Zn	7.714097	0.004355	6.124000
Zn	9.513968	1.540513	8.639037
Zn	10.240869	3.590190	6.044082
Zn	2.628177	-8.193456	9.266896
Zn	2.682762	-4.867835	9.460301
Zn	6.035466	-4.288074	9.357493
Zn	-11.896391	3.052100	-4.941315
Zn	-8.373477	-1.079769	-1.726080
Zn	-7.774725	0.020560	1.249417
Zn	-3.069369	3.847464	-1.564785
Zn	-1.433847	2.699655	1.272929
Zn	-3.249429	6.104672	0.945931
Zn	-0.386473	7.881714	1.572220
Zn	1.548312	8.021435	-1.160367
Zn	3.577374	10.508495	0.021971
Zn	-8.748103	-5.282290	4.513425
Zn	-6.166171	-5.564732	2.420985
Zn	-5.891704	-2.178504	3.288212
Zn	-5.192169	1.767510	0.270876
Zn	-4.484252	0.850128	3.637771
Zn	0.613868	1.091628	3.309078
Zn	0.730567	4.308999	4.758785
Zn	0.923045	4.868193	1.513012
Zn	3.387495	6.475208	5.561882
Zn	6.128878	8.874720	2.248454
Zn	-6.658863	-7.478000	6.106069
Zn	-4.129226	-5.292676	5.328204
Zn	-2.591310	-2.721260	3.450154
Zn	-3.050145	-2.421946	7.365188
Zn	-1.535407	0.017558	5.377353
Zn	0.726415	1.287670	7.683714
Zn	3.089922	-0.194285	5.080387
Zn	3.618886	2.792480	6.300018
Zn	6.759606	6.556599	4.669800
Zn	-3.360060	-7.116051	8.035380
Zn	-2.376450	-5.865545	11.148272
Zn	-0.591174	-4.933825	8.256529
Zn	-0.719242	-2.465399	10.711649
Zn	2.009560	-1.558260	8.983293
Zn	4.686615	1.002915	9.113191
Zn	6.820356	3.528169	9.128686
Zn	-10.305255	5.276144	-2.808968
Zn	-8.841608	8.400654	-1.787205
Zn	-6.553965	8.041800	-4.548842
Zn	-4.015116	10.089564	-3.808173
Zn	-10.957246	1.182301	1.314325
Zn	-7.212096	4.184222	-0.897704
Zn	-5.664383	7.193720	-1.090080
Zn	-6.919280	7.412199	2.029604
Zn	-5.037613	10.472740	-0.570745
Zn	-1.491384	10.665554	-0.492095
Zn	-10.668353	-0.647077	4.241039
Zn	-7.911059	0.997344	4.633400
Zn	-5.784320	4.298314	2.620164
Zn	-2.596729	3.936713	4.052475
Zn	-3.801830	9.293678	2.359585
Zn	-3.434516	7.070764	4.973519
Zn	-1.555978	10.766087	4.406560
Zn	0.716797	11.366556	2.003604
Zn	-10.056956	-2.930692	6.739230
Zn	-9.527404	-4.555311	9.649238
Zn	-6.619865	-3.206803	6.347631
Zn	-5.619166	-0.033241	7.200115
Zn	-3.414432	2.464388	6.989081
Zn	-0.736195	4.401519	7.927245
Zn	-0.345278	7.747999	4.970681
Zn	1.099382	7.210404	8.071281
Zn	2.751087	8.693404	3.192245
Zn	-6.403897	-5.360756	8.926846
Zn	-4.282760	-3.214443	10.395341
Zn	-5.073918	0.138039	10.418075
Zn	-1.956990	0.348558	9.386696
Zn	-1.541518	3.206571	10.923237
Zn	1.976074	2.628147	10.450266
Zn	3.664915	5.025137	8.932857
Zn	-9.574735	6.126512	0.708221
Zn	-8.344119	8.363395	4.927373
Zn	-0.054215	8.449281	-4.524554
Zn	1.173810	11.253279	-2.572616
Zn	-11.404678	-1.830078	-0.347971
Zn	-9.399640	-2.838018	2.174491
Zn	-2.171013	7.769406	-2.148680
Zn	-3.933584	5.874510	-4.422221
Zn	-7.982960	10.392817	0.939372
Zn	-6.250260	10.873059	3.985297
Zn	-9.079892	3.562278	2.870977
Zn	-9.336006	5.185495	5.704662
Zn	-5.967654	4.768011	5.999626
Zn	-6.550118	7.831632	7.669745
Zn	-4.278848	10.025068	6.518665
Zn	-7.660728	2.605446	7.940334
Zn	-4.838274	3.543770	9.909053
Zn	-3.513464	6.314705	8.378378
Zn	-2.665097	8.431438	-6.451054
Zn	-12.347793	0.327098	-2.878251
Zn	-9.753331	2.007863	-1.721796
Zn	-8.802387	1.659909	-5.178969
Zn	-5.436870	4.844871	-7.424525
Zn	-5.624627	8.083974	-7.887501

B.4 Sulphur Quantum Dots

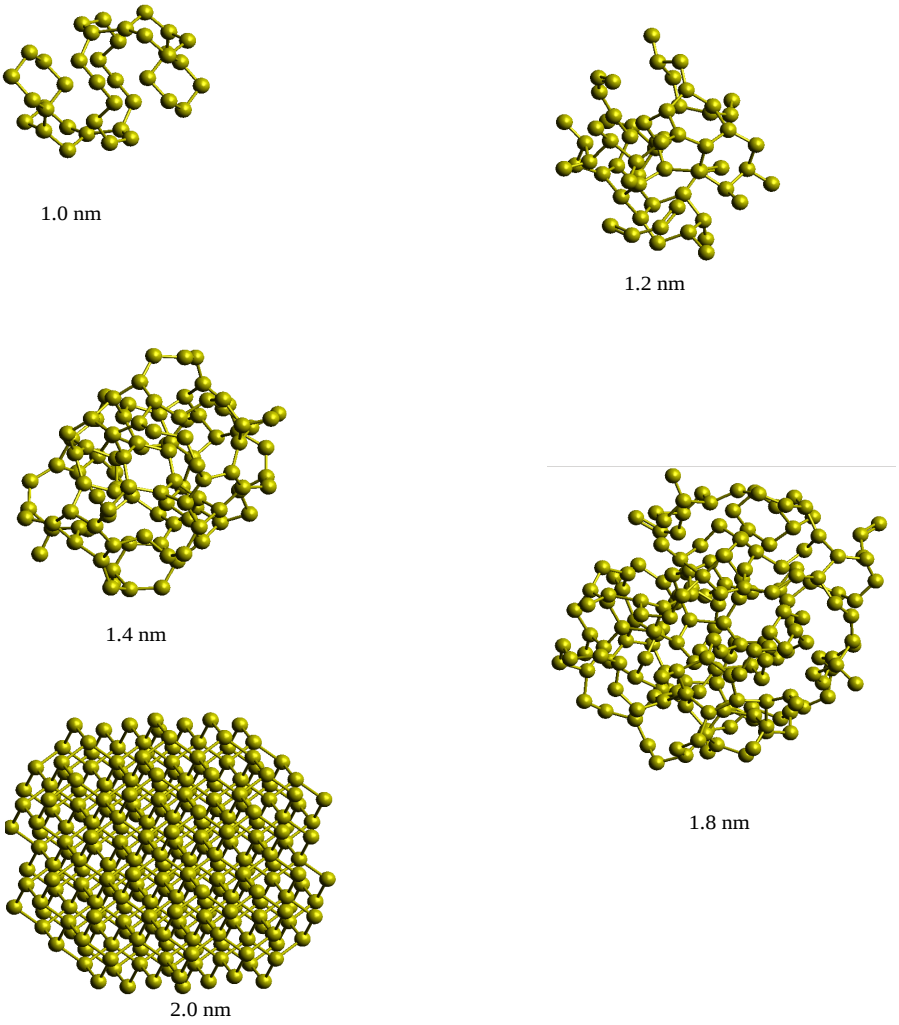

Figure B.4: Equilibrium structures of S quantum dots of sizes 1.0, 1.2, 1.4, 1.8 and 2.0 nm. The structures were obtained from geometry optimization using PM7 as implemented in MOPAC.

B.4.1 Cartesian coordinates (Angstroms) of equilibrium sulphur quantum dots

S_{38} (1.0 nm)

	x	y	z
S	-2.350686	-2.999812	-5.180103
S	0.556609	0.054883	-3.791009
S	-2.347042	-4.509889	-2.224432
S	-1.174186	-3.450986	-3.556104
S	0.887437	-3.179158	-2.581361
S	1.643917	-1.348418	-3.050974
S	4.504577	1.254414	-1.790281
S	0.199805	-4.037109	0.705408
S	1.471867	-3.744204	-0.738990
S	4.678764	-1.865693	-0.727515
S	5.772360	-0.286169	-1.401329
S	-4.941267	-2.662744	-3.170141
S	-3.760358	-1.697809	-4.489916
S	-3.806411	1.290394	-1.052466
S	-0.484792	1.408525	-2.837875
S	0.728337	2.621046	-1.681816
S	-3.792671	-3.229489	-1.533757
S	-3.663602	-1.830050	0.012065
S	-2.507146	-0.208431	-0.633530
S	2.510792	0.212778	0.625913
S	3.671445	1.838621	-0.002899
S	3.799969	3.230331	1.548606
S	-0.728923	-2.641470	1.695159
S	0.481649	-1.415925	2.839899
S	3.803782	-1.295133	1.029271
S	3.748398	1.687301	4.498089
S	4.937622	2.658205	3.190248
S	-5.757991	0.311221	1.404400
S	-4.670367	1.882492	0.702351
S	-1.470969	3.745401	0.742042
S	-0.193445	4.027017	-0.701719
S	-4.491130	-1.229350	1.796824
S	-1.647607	1.343729	3.052595
S	-0.890087	3.174857	2.583246
S	1.167163	3.442003	3.552131
S	2.346593	4.506776	2.230198
S	-0.560001	-0.060610	3.789121
S	2.332398	2.985666	5.182259

S_{62} (1.2 nm)

	x	y	z
S	3.765302	-0.912514	-4.070353
S	2.828926	-5.654661	-3.279289
S	6.867076	-1.977083	-0.606269
S	-1.451330	-2.021947	-4.027713
S	-1.353278	-1.408001	-5.941783
S	-0.275617	0.387704	-5.847209
S	0.250995	1.015921	-7.537903
S	-1.187215	-4.247688	-1.037559
S	-0.467140	-3.361492	-2.806640
S	1.437757	-2.659107	-2.293107
S	2.465528	-1.110707	-2.767915
S	4.328385	2.608974	-2.906254
S	4.426430	3.551296	-4.478993
S	-0.142590	-5.897386	-0.525902
S	1.757359	-5.179369	-0.014303
S	2.676479	-4.399251	-1.910480
S	4.056771	-2.309525	1.198888
S	5.368810	-0.995713	-0.022039
S	5.922009	0.606427	1.224614
S	2.858461	-6.531450	0.682814
S	4.924805	-3.193274	2.607609
S	-3.238777	2.187093	-5.908706
S	-3.542657	-1.311740	-0.984763
S	1.168975	3.181617	-2.011677
S	0.809982	5.063906	-2.364662
S	-2.383960	-2.827842	-0.067730
S	-1.313240	-1.991554	1.448130
S	0.296407	-0.979985	0.805549
S	-0.179098	0.792456	-0.053683
S	3.109678	2.728657	-1.405280
S	3.257914	3.189062	0.640345
S	-3.047230	-4.751884	3.009713
S	-1.725869	-5.377130	4.144640
S	0.034851	-4.861194	4.436751
S	2.399616	-1.141383	1.595960
S	2.816509	0.531255	2.778939
S	4.210303	1.599889	1.595148
S	1.066793	-3.518437	3.663770
S	-2.844584	2.530557	-1.857881
S	-0.493611	7.863802	-1.332503
S	-5.186367	-0.725652	-0.023395
S	-4.600513	0.734672	1.370060
S	-3.723104	4.120271	-1.274342
S	-3.776776	5.070297	0.318275
S	-0.121571	6.109836	-0.739507
S	1.250609	6.128275	0.857653
S	-5.904495	-0.962715	4.106119
S	-4.354826	-0.509524	3.159590
S	-3.050443	0.886572	4.284560
S	-0.987779	2.083744	1.246292
S	0.439397	2.872239	2.482828
S	1.626692	4.245511	1.402809
S	-1.890191	-1.800789	6.095939
S	-1.453677	-0.528371	4.759026
S	0.072225	0.790256	5.355531
S	1.110495	1.284315	3.730804
S	-5.875069	2.125572	1.566294
S	-2.906228	4.801515	1.925157
S	-3.944626	1.712969	5.707427
S	-2.648986	-0.775051	-2.813242
S	-1.836633	1.169835	-2.916052
S	-1.682423	1.849773	-4.921243

S_{104} (1.4 nm)

	x	y	z
S	0.334411	-2.653798	-7.017321
S	0.478079	-4.641201	-3.928979
S	1.284745	-3.298521	-5.413022
S	2.643878	-2.208994	-4.332576
S	0.559920	-7.485439	-2.068174
S	1.497897	-5.729500	-2.353385
S	3.001321	-4.446909	-1.759176
S	4.124973	-3.191408	-3.086919
S	5.908703	-2.629627	-2.339395
S	-2.311400	0.101822	-7.735747
S	-3.969460	-3.640652	-6.912633
S	-2.718004	-2.707880	-5.842320
S	-1.283395	-1.454433	-6.892218
S	0.873408	1.932069	-5.586746
S	2.032878	3.560631	-5.512628
S	2.793224	3.850286	-3.674648
S	-2.455219	-7.255387	-5.196917
S	-2.461208	-6.360699	-3.571726
S	-1.463540	-4.589152	-3.391191
S	0.839344	-1.918380	-1.550772
S	1.810936	-0.854965	-3.000139
S	1.631303	3.740346	3.808016
S	3.343243	4.858357	3.814680
S	4.295343	4.899752	5.586917
S	-3.524010	-3.437233	3.356005
S	-2.711726	-2.347070	4.838737
S	-1.475547	-0.860485	4.328654
S	1.976777	2.396078	7.601963
S	5.462236	3.201861	6.055001
S	7.221328	3.630980	6.530643
S	0.077827	4.755057	4.663812
S	0.040983	2.798296	7.726672
S	-0.830908	3.349205	5.994291
S	2.441734	1.065556	-1.918870
S	3.886525	2.412120	-2.542744
S	5.239573	2.776724	-0.962503
S	-2.564271	-7.492614	-0.342172
S	-1.414972	-7.595157	-1.983717
S	0.927981	-5.401420	2.042440
S	2.241809	-2.988870	-0.472832
S	2.770397	-1.600705	1.136547
S	5.297514	-1.086225	-1.075794
S	6.931902	-0.195209	-0.175117
S	6.919340	1.722601	-0.805809
S	1.906176	-5.269809	3.777076
S	2.841520	-3.489962	3.930250
S	4.064453	-2.368804	2.574939
S	5.487533	-0.886915	2.957952
S	7.057400	-0.835719	1.724741
S	-4.581294	0.107851	-5.031103
S	-3.369736	1.166893	-6.397930
S	-2.469585	2.540720	-5.097025
S	-6.904676	-5.279385	-3.760192
S	-6.150388	-3.608216	-3.410888
S	-3.404695	-1.472747	-4.382068
S	-2.222607	1.017224	-1.393366
S	-0.699186	1.755287	-4.432080
S	0.389076	3.953154	-1.453495
S	1.957783	5.080282	-2.167656
S	3.067806	5.925983	-0.627051
S	-4.760609	-4.492207	-0.413469
S	-4.488355	-3.542049	-2.199151
S	-2.322128	-1.160911	0.924491
S	-2.202252	-0.963918	-1.068605
S	0.961365	1.499959	1.292337
S	1.130707	2.084086	-0.739589
S	4.304198	4.311089	2.011183
S	4.604425	4.560392	-0.035973
S	-3.139372	-5.685728	0.266291
S	-2.422485	-4.695642	1.980857
S	-0.503136	-4.123520	1.606881
S	0.489860	-1.234330	3.804560
S	1.328482	-0.463649	2.012815
S	5.273299	2.054905	4.225905
S	5.998464	3.060553	2.568169
S	7.659711	3.956486	2.734166
S	2.000220	-1.902805	5.032432
S	3.100979	-0.353147	5.888922
S	4.827131	0.088411	4.762438
S	-7.489899	-0.479841	-3.047399
S	-5.864611	0.562794	-3.397500
S	-4.953833	2.318267	-2.671762
S	-3.476198	3.605712	-3.513745
S	-2.858690	5.110225	-2.328710
S	-7.781056	-2.918571	-0.408069
S	-7.585829	-2.314732	-2.305164
S	-4.747590	1.345481	1.135682
S	-4.096266	1.762373	-0.853017
S	-1.781663	3.772348	0.991541
S	-1.505728	4.570432	-0.953984
S	1.957055	7.672820	2.090006
S	2.624091	7.672105	0.229456
S	-6.118038	-3.258575	0.689796
S	-5.030314	-2.493911	2.233260
S	-4.228118	-0.638625	1.598054
S	-1.789582	1.102426	3.650694
S	-0.959615	2.019796	1.900162
S	2.697044	0.561307	7.612416
S	-5.219310	2.670023	2.576982
S	-3.752832	3.630305	3.541188
S	-2.430047	4.995420	2.534726
S	-0.792972	6.057257	3.231034
S	0.054771	7.772942	2.610622
S	-2.436956	2.617675	4.911359

S_{190} (1.8 nm)

	x	y	z
S	2.165664	-6.428788	-9.326861
S	5.329255	-5.610920	-6.003172
S	6.905619	-4.896406	-5.103533
S	-3.258890	-4.481287	-7.891604
S	-2.232438	-3.874895	-9.398107
S	-0.193887	-3.969377	-9.560437
S	0.615902	-2.132474	-9.563089
S	1.023472	-1.186185	-7.873642
S	-0.809979	-7.206100	-4.123211
S	0.652265	-6.992707	-5.463881
S	2.037012	-5.634901	-5.206220
S	0.583916	-5.635563	-8.712712
S	3.630209	-2.256609	-5.825721
S	2.914502	-1.159230	-7.299967
S	7.563010	2.194020	-3.016438
S	-0.777108	-8.695835	-2.793154
S	-0.199303	-8.195379	-0.905432
S	3.885055	-6.417142	-4.709366
S	4.495334	-5.961911	-2.803989
S	7.151063	-2.977038	-4.708930
S	6.374892	-2.217769	-3.051616
S	8.647512	1.717987	-1.379730
S	9.966347	3.070999	-0.822402
S	1.694554	-8.908073	-0.508937
S	2.963933	-7.304272	-0.195328
S	4.514323	-7.379055	-1.477254
S	6.592034	-3.948789	-0.159783
S	7.216502	-2.242887	-1.259938
S	8.540978	-1.343538	0.003989
S	-4.314990	-1.301831	-6.796151
S	-3.684539	-0.193133	-8.306324
S	-2.810244	1.571105	-8.081074
S	-0.951354	2.040359	-8.686782
S	0.330513	2.840203	-7.346323
S	-3.728761	-4.394104	-4.523898
S	-3.470117	-3.209698	-6.295832
S	-1.245493	-1.763940	-4.185265
S	-0.312491	-0.157437	-4.733564
S	-0.101275	1.452472	-3.641279
S	2.012958	2.292283	-6.353597
S	3.803540	2.445869	-5.895655
S	4.890847	3.908053	-6.086201
S	-4.600162	-8.257701	-0.415908
S	-2.176881	-5.515598	-3.848382
S	-1.353981	-4.556504	-2.155827
S	-0.257517	-2.991904	-2.840514
S	1.975706	-2.752881	-2.961759
S	3.151139	-1.502157	-4.014395
S	4.317587	1.692058	-2.186895
S	5.813892	2.987697	-2.461537
S	8.999391	6.253901	-1.141287
S	10.179552	7.012060	-2.337271
S	-4.029849	-9.444068	1.021331
S	-2.191239	-8.934887	1.774948
S	-0.918124	-7.451687	1.076910
S	0.230099	-5.832034	1.419604
S	2.681936	-3.649521	-1.303779
S	2.910542	-2.387888	0.212485
S	4.658009	0.198618	-0.944314
S	5.276508	0.531098	0.897957
S	9.179010	4.733845	0.114522
S	9.366152	4.575653	2.133574
S	-2.725939	-8.495266	3.776136
S	-1.371152	-7.906335	5.018195
S	2.197113	-6.185986	1.485562
S	2.985913	-6.922739	3.289770
S	2.137167	-8.463860	3.987652
S	8.678949	-4.009766	3.517239
S	-5.208662	4.173459	-6.484085
S	-7.054107	-2.451839	-4.346661
S	-5.995737	-1.029455	-5.534875
S	-5.406821	0.348798	-4.093553
S	-3.598933	2.981822	-6.596642
S	-2.120932	3.630191	-5.216742
S	-0.596718	4.385618	-6.303191
S	1.794401	6.594322	-4.286870
S	-7.300675	-5.888439	-0.507484
S	-5.394182	-3.554082	-3.552450
S	-4.744212	-2.259564	-2.083262
S	-4.017461	-0.599770	-2.951055
S	-2.578117	2.047377	-1.535103
S	-1.799777	2.586882	-3.379113
S	1.434629	3.209912	-1.357521
S	3.166612	5.582461	-3.208151
S	4.689660	6.729094	-2.403229
S	5.952514	7.471720	-3.589349
S	-5.406996	-6.449517	-0.176122
S	-4.149872	-4.890974	0.511919
S	-2.712068	-4.613245	-0.737398
S	-2.745998	-1.174026	0.568888
S	-1.928632	0.386744	-0.499384
S	0.250216	0.173607	-0.230419
S	1.237028	1.912717	0.178890
S	3.950565	4.021605	1.160699
S	5.405269	5.183934	0.538492
S	6.319296	6.162130	2.109876
S	-5.289184	-5.794274	3.553695
S	-3.611418	-5.233916	2.500126
S	-2.184083	-4.677710	4.120419
S	-1.623976	-2.537282	1.551036
S	0.043461	-1.778472	2.462414
S	1.299694	-1.330346	0.754007
S	3.192393	-0.486558	3.449301
S	4.080695	0.950263	2.411576
S	6.280874	3.285269	4.011592
S	7.553979	4.769144	3.027531
S	-0.714205	-5.981206	4.775826
S	1.105481	-5.138316	5.490051
S	2.984746	-5.216884	4.547691
S	4.523556	-4.859934	5.703100
S	4.290768	-1.743426	4.494223
S	5.523529	-1.148588	5.914769
S	7.362802	1.533473	4.213165
S	4.863052	-5.376627	7.462691
S	-6.749667	3.341144	-5.481851
S	-5.345978	7.433916	-4.103214
S	-8.601417	-1.931542	-3.176133
S	-8.292400	-0.631420	-1.660500
S	-6.223732	2.497056	-3.758945
S	-5.891151	3.565669	-2.109323
S	-3.792339	6.485865	-3.942621
S	-2.671338	6.382200	-2.445535
S	0.854866	7.915258	-3.063654
S	2.261244	9.201476	-2.365876
S	-8.664430	-5.210254	0.624919
S	-8.472462	-3.096327	0.849112
S	-7.412912	-1.500808	0.105295
S	-6.235694	-0.138312	1.062193
S	-3.027349	3.498037	-0.180447
S	-1.927461	3.751670	1.436260
S	0.336613	4.832557	-0.915504
S	1.351991	5.993675	0.419123
S	3.608217	8.197324	-1.171582
S	4.766102	8.845492	0.302287
S	-7.615446	-2.097635	5.640232
S	-4.208809	-0.383999	1.763290
S	-3.604739	1.249577	3.045546
S	-1.861455	2.146233	2.666905
S	1.612203	3.844288	3.308278
S	2.319564	5.073922	1.928637
S	4.214683	8.286252	3.650172
S	5.457360	8.147359	2.019429
S	-3.716746	-3.539801	6.903638
S	-2.739608	-3.128642	5.357608
S	-0.824466	-2.228774	5.783178
S	-0.396455	-0.996412	4.252445
S	0.028038	2.214456	5.856320
S	1.544337	2.591602	4.763616
S	3.343580	2.283043	5.715964
S	4.902633	3.422716	5.468364
S	0.712485	-3.440026	6.622928
S	1.254915	-3.354966	8.556326
S	2.192070	-1.709652	9.129821
S	4.171953	-1.596282	9.020655
S	4.825447	-0.366168	7.591784
S	-9.275479	1.055778	-1.043523
S	-8.266320	2.425513	0.023189
S	-7.502831	3.985708	-1.017659
S	-4.074395	7.760966	0.277720
S	-2.357273	7.729302	-0.948093
S	-1.113754	9.090188	-0.086569
S	-10.231320	-2.552910	1.804120
S	-10.017090	-1.385927	3.382060
S	-7.197618	1.658568	1.680461
S	-7.105315	2.100706	3.659907
S	-3.572943	7.221259	2.118951
S	-2.321241	8.598139	3.101518
S	-0.621473	8.454466	1.790111
S	1.154314	9.293199	2.415128
S	-9.567837	-2.277444	5.119469
S	-5.021276	0.746414	6.247556
S	-5.057167	1.700025	4.410173
S	-2.524225	4.560111	5.849099
S	-1.242080	5.510682	4.560039
S	-0.032602	6.875843	5.424368
S	2.483051	9.071250	3.640643
S	-3.193793	0.578701	6.947478
S	-2.410640	2.047632	8.021959
S	-1.093819	3.402316	7.237569
S	0.237353	4.818707	7.901807
S	1.313913	5.918031	6.587746
S	-8.448454	1.423729	4.799135
S	-2.990840	10.315416	3.402735
S	-3.727301	5.574831	6.852180
S	8.488091	-1.067858	1.951554
S	8.405742	0.666294	2.938643
S	7.441838	-2.720433	2.959398
S	5.982561	-3.336943	1.615993
S	-6.659046	-4.387678	3.330597
S	-6.433945	-2.582520	4.120997

S_{244} (2.0 nm)

	x	y	z
S	2.165664	-6.428788	-9.326861
S	5.329255	-5.610920	-6.003172
S	6.905619	-4.896406	-5.103533
S	-3.258890	-4.481287	-7.891604
S	-2.232438	-3.874895	-9.398107
S	-0.193887	-3.969377	-9.560437
S	0.615902	-2.132474	-9.563089
S	1.023472	-1.186185	-7.873642
S	-0.809979	-7.206100	-4.123211
S	0.652265	-6.992707	-5.463881
S	2.037012	-5.634901	-5.206220
S	0.583916	-5.635563	-8.712712
S	3.630209	-2.256609	-5.825721
S	2.914502	-1.159230	-7.299967
S	7.563010	2.194020	-3.016438
S	-0.777108	-8.695835	-2.793154
S	-0.199303	-8.195379	-0.905432
S	3.885055	-6.417142	-4.709366
S	4.495334	-5.961911	-2.803989
S	7.151063	-2.977038	-4.708930
S	6.374892	-2.217769	-3.051616
S	8.647512	1.717987	-1.379730
S	9.966347	3.070999	-0.822402
S	1.694554	-8.908073	-0.508937
S	2.963933	-7.304272	-0.195328
S	4.514323	-7.379055	-1.477254
S	6.592034	-3.948789	-0.159783
S	7.216502	-2.242887	-1.259938
S	8.540978	-1.343538	0.003989
S	-4.314990	-1.301831	-6.796151
S	-3.684539	-0.193133	-8.306324
S	-2.810244	1.571105	-8.081074
S	-0.951354	2.040359	-8.686782
S	0.330513	2.840203	-7.346323
S	-3.728761	-4.394104	-4.523898
S	-3.470117	-3.209698	-6.295832
S	-1.245493	-1.763940	-4.185265
S	-0.312491	-0.157437	-4.733564
S	-0.101275	1.452472	-3.641279
S	2.012958	2.292283	-6.353597
S	3.803540	2.445869	-5.895655
S	4.890847	3.908053	-6.086201
S	-4.600162	-8.257701	-0.415908
S	-2.176881	-5.515598	-3.848382
S	-1.353981	-4.556504	-2.155827
S	-0.257517	-2.991904	-2.840514
S	1.975706	-2.752881	-2.961759
S	3.151139	-1.502157	-4.014395
S	4.317587	1.692058	-2.186895
S	5.813892	2.987697	-2.461537
S	8.999391	6.253901	-1.141287
S	10.179552	7.012060	-2.337271
S	-4.029849	-9.444068	1.021331
S	-2.191239	-8.934887	1.774948
S	-0.918124	-7.451687	1.076910
S	0.230099	-5.832034	1.419604
S	2.681936	-3.649521	-1.303779
S	2.910542	-2.387888	0.212485
S	4.658009	0.198618	-0.944314
S	5.276508	0.531098	0.897957
S	9.179010	4.733845	0.114522
S	9.366152	4.575653	2.133574
S	-2.725939	-8.495266	3.776136
S	-1.371152	-7.906335	5.018195
S	2.197113	-6.185986	1.485562
S	2.985913	-6.922739	3.289770
S	2.137167	-8.463860	3.987652
S	8.678949	-4.009766	3.517239
S	-5.208662	4.173459	-6.484085
S	-7.054107	-2.451839	-4.346661
S	-5.995737	-1.029455	-5.534875
S	-5.406821	0.348798	-4.093553
S	-3.598933	2.981822	-6.596642
S	-2.120932	3.630191	-5.216742
S	-0.596718	4.385618	-6.303191
S	1.794401	6.594322	-4.286870
S	-7.300675	-5.888439	-0.507484
S	-5.394182	-3.554082	-3.552450
S	-4.744212	-2.259564	-2.083262
S	-4.017461	-0.599770	-2.951055
S	-2.578117	2.047377	-1.535103
S	-1.799777	2.586882	-3.379113
S	1.434629	3.209912	-1.357521
S	3.166612	5.582461	-3.208151
S	4.689660	6.729094	-2.403229
S	5.952514	7.471720	-3.589349
S	-5.406996	-6.449517	-0.176122
S	-4.149872	-4.890974	0.511919
S	-2.712068	-4.613245	-0.737398
S	-2.745998	-1.174026	0.568888
S	-1.928632	0.386744	-0.499384
S	0.250216	0.173607	-0.230419
S	1.237028	1.912717	0.178890
S	3.950565	4.021605	1.160699
S	5.405269	5.183934	0.538492
S	6.319296	6.162130	2.109876
S	-5.289184	-5.794274	3.553695
S	-3.611418	-5.233916	2.500126
S	-2.184083	-4.677710	4.120419
S	-1.623976	-2.537282	1.551036
S	0.043461	-1.778472	2.462414
S	1.299694	-1.330346	0.754007
S	3.192393	-0.486558	3.449301
S	4.080695	0.950263	2.411576
S	6.280874	3.285269	4.011592
S	7.553979	4.769144	3.027531
S	-0.714205	-5.981206	4.775826
S	1.105481	-5.138316	5.490051
S	2.984746	-5.216884	4.547691
S	4.523556	-4.859934	5.703100
S	4.290768	-1.743426	4.494223
S	5.523529	-1.148588	5.914769
S	7.362802	1.533473	4.213165
S	4.863052	-5.376627	7.462691
S	-6.749667	3.341144	-5.481851
S	-5.345978	7.433916	-4.103214
S	-8.601417	-1.931542	-3.176133
S	-8.292400	-0.631420	-1.660500
S	-6.223732	2.497056	-3.758945
S	-5.891151	3.565669	-2.109323
S	-3.792339	6.485865	-3.942621
S	-2.671338	6.382200	-2.445535
S	0.854866	7.915258	-3.063654
S	2.261244	9.201476	-2.365876
S	-8.664430	-5.210254	0.624919
S	-8.472462	-3.096327	0.849112
S	-7.412912	-1.500808	0.105295
S	-6.235694	-0.138312	1.062193
S	-3.027349	3.498037	-0.180447
S	-1.927461	3.751670	1.436260
S	0.336613	4.832557	-0.915504
S	1.351991	5.993675	0.419123
S	4.214683	8.286252	3.650172
S	5.457360	8.147359	2.019429
S	-3.716746	-3.539801	6.903638
S	-2.739608	-3.128642	5.357608
S	-0.824466	-2.228774	5.783178
S	-0.396455	-0.996412	4.252445
S	0.028038	2.214456	5.856320
S	1.544337	2.591602	4.763616
S	3.343580	2.283043	5.715964
S	4.902633	3.422716	5.468364
S	0.712485	-3.440026	6.622928
S	1.254915	-3.354966	8.556326
S	2.192070	-1.709652	9.129821
S	4.171953	-1.596282	9.020655
S	4.825447	-0.366168	7.591784
S	-9.275479	1.055778	-1.043523
S	-8.266320	2.425513	0.023189
S	-7.502831	3.985708	-1.017659
S	-4.074395	7.760966	0.277720
S	-2.357273	7.729302	-0.948093
S	-1.113754	9.090188	-0.086569
S	-10.231320	-2.552910	1.804120
S	-10.017090	-1.385927	3.382060
S	-7.197618	1.658568	1.680461
S	-7.105315	2.100706	3.659907
S	-3.572943	7.221259	2.118951
S	-2.321241	8.598139	3.101518
S	-0.621473	8.454466	1.790111
S	1.154314	9.293199	2.415128
S	-9.567837	-2.277444	5.119469
S	-5.021276	0.746414	6.247556
S	-5.057167	1.700025	4.410173
S	-2.524225	4.560111	5.849099
S	-1.242080	5.510682	4.560039
S	-0.032602	6.875843	5.424368
S	2.483051	9.071250	3.640643
S	-3.193793	0.578701	6.947478
S	-2.410640	2.047632	8.021959
S	-1.093819	3.402316	7.237569
S	0.237353	4.818707	7.901807
S	1.313913	5.918031	6.587746
S	-8.448454	1.423729	4.799135
S	-2.990840	10.315416	3.402735
S	-3.727301	5.574831	6.852180
S	-4.208809	-0.383999	1.763290
S	-3.604739	1.249577	3.045546
S	-1.861455	2.146233	2.666905
S	1.612203	3.844288	3.308278
S	2.319564	5.073922	1.928637
S	3.608217	8.197324	-1.171582
S	4.766102	8.845492	0.302287
S	-6.659046	-4.387678	3.330597
S	-6.433945	-2.582520	4.120997
S	-7.615446	-2.097635	5.640232
S	8.488091	-1.067858	1.951554
S	8.405742	0.666294	2.938643
S	5.982561	-3.336943	1.615993
S	7.441838	-2.720433	2.959398

B.5.1 Cartesian coordinates (Angstroms) of equilibrium silicon quantum dots

Si_{128} (1.6 nm)

	x	y	z
Si	0.678825	-2.036475	-7.467075
Si	3.425001	0.685102	-7.583179
Si	0.962133	-4.494602	-5.034891
Si	1.965147	-3.197148	-6.401497
Si	3.477724	-2.064418	-5.222039
Si	4.559163	-0.508377	-6.404960
Si	5.922193	0.536831	-5.068959
Si	0.664426	-6.989434	-2.652309
Si	1.969399	-5.894418	-3.771945
Si	3.478855	-4.746077	-2.597622
Si	4.598667	-3.225088	-3.727596
Si	6.153479	-2.059330	-2.540138
Si	6.996188	-0.800648	-3.998943
Si	3.455211	-7.173590	0.086589
Si	4.572698	-5.961975	-1.078727
Si	5.938426	-4.642943	-0.002842
Si	6.999584	-3.548282	-1.322289
Si	-2.045384	0.642410	-7.531821
Si	0.657505	3.303983	-7.450149
Si	-3.037010	-3.866291	-5.864395
Si	-1.965384	-2.070317	-5.175612
Si	-0.721336	-0.712759	-6.573019
Si	0.671186	0.592051	-5.157687
Si	2.043716	1.943365	-6.567716
Si	3.154812	3.113728	-4.954613
Si	-2.967110	-5.247227	-4.408967
Si	-1.950894	-4.730834	-2.582815
Si	-0.550631	-3.321289	-3.815147
Si	0.728696	-2.031459	-2.489100
Si	2.033070	-0.711961	-3.834373
Si	3.360021	0.583480	-2.498758
Si	4.737998	2.002847	-3.881678
Si	5.899169	3.092819	-2.322940
Si	-2.020044	-7.138335	0.071086
Si	-0.689693	-6.140617	-1.256235
Si	0.687494	-4.752947	0.072419
Si	2.040724	-3.395775	-1.203743
Si	3.366278	-2.087925	0.118183
Si	4.698798	-0.755003	-1.196061
Si	6.106845	0.532337	0.116510
Si	7.074637	1.937436	-1.164363
Si	0.708332	-7.094840	2.732410
Si	2.081836	-6.194308	1.380109
Si	3.185054	-4.599866	2.581666
Si	4.763156	-3.501551	1.502089
Si	5.918587	-1.962697	2.630703
Si	7.089005	-0.773652	1.488983
Si	-4.453757	0.844296	-4.981269
Si	-3.145857	1.843131	-6.341699
Si	-2.044587	3.358687	-5.171791
Si	-0.523874	4.546089	-6.351599
Si	0.531007	5.840222	-4.969303
Si	-6.122316	-3.046443	-3.722945
Si	-4.587401	-2.055325	-2.518089
Si	-3.283886	-0.757262	-3.855713
Si	-1.957427	0.583409	-2.488644
Si	-0.619024	1.921798	-3.793290
Si	0.697870	3.228884	-2.472263
Si	2.060923	4.664532	-3.851077
Si	3.217395	5.769165	-2.322262
Si	-4.466071	-4.597355	0.293085
Si	-3.294876	-3.428344	-1.260659
Si	-1.961450	-2.097291	0.116038
Si	-0.630398	-0.750266	-1.177074
Si	0.708103	0.552353	0.148339
Si	2.037440	1.892228	-1.143907
Si	3.366315	3.234065	0.223774
Si	4.521079	4.416282	-1.338300
Si	-3.136161	-5.964217	1.282355
Si	-2.007572	-4.838292	2.824763
Si	-0.619717	-3.427165	1.422129
Si	0.705574	-2.115704	2.754102
Si	2.041474	-0.771219	1.460111
Si	4.679719	1.856551	1.484282
Si	6.174708	2.966903	2.647921
Si	-0.504348	-6.030084	3.972243
Si	0.536086	-4.672052	5.306239
Si	2.059532	-3.533527	4.148767
Si	3.216791	-2.038610	5.306455
Si	4.538908	-1.012206	3.971434
Si	-7.005999	0.587481	-2.518572
Si	-5.844081	1.770575	-3.655782
Si	-4.677832	3.308045	-2.546331
Si	-3.156209	4.443784	-3.640638
Si	-1.981797	5.974190	-2.455364
Si	-0.707860	6.969905	-3.824891
Si	-7.010102	-2.119776	0.129457
Si	-6.038010	-0.714751	-1.137045
Si	-4.620634	0.562391	0.172082
Si	-3.285914	1.898854	-1.136869
Si	-1.963511	3.208809	0.172574
Si	-0.592760	4.550092	-1.105565
Si	0.777289	5.947553	0.228674
Si	2.140772	6.940120	-1.056487
Si	-5.834239	-3.290770	1.292878
Si	-4.694993	-2.194075	2.861360
Si	-3.281469	-0.783919	1.471319
Si	-1.953402	0.511232	2.804394
Si	-0.649430	1.831746	1.465000
Si	0.628028	3.129134	2.783623
Si	2.027167	4.528950	1.562300
Si	3.073579	5.076465	3.369434
Si	-3.116279	-3.290187	3.916369
Si	-1.937238	-2.151627	5.541681
Si	-0.585623	-0.796471	4.125309
Si	0.798885	0.516159	5.535786
Si	2.044328	1.878384	4.139984
Si	3.107722	3.684763	4.821853
Si	-0.671297	-3.565171	6.501508
Si	2.155088	-0.798864	6.503362
Si	-6.934684	3.358119	0.276096
Si	-5.858206	4.469463	-1.031697
Si	-4.495283	5.772132	0.061094
Si	-3.337132	6.936265	-1.124295
Si	-6.904581	0.638891	2.983311
Si	-6.075712	1.879151	1.507096
Si	-4.519332	3.028686	2.706938
Si	-3.401467	4.543106	1.578410
Si	-1.887026	5.703458	2.734327
Si	-0.641531	6.799552	1.558286
Si	-5.851768	-0.710301	4.042364
Si	-4.469948	0.313165	5.385024
Si	-3.391214	1.866121	4.197574
Si	-1.881553	3.015032	5.372508
Si	-0.880805	4.309127	4.004521
Si	-3.320976	-0.878731	6.541677
Si	-0.584256	1.855372	6.432346
Si	3.370890	0.573388	2.825023

Si_{172} (1.8 nm)

	x	y	z
Si	-2.036475	-4.751775	-7.467075
Si	-0.670591	-3.641489	-8.484146
Si	0.495405	-2.132321	-7.664170
Si	1.308303	-0.320471	-8.644490
Si	2.963017	0.347037	-7.494293
Si	-2.066255	-7.407551	-4.811975
Si	-1.029138	-6.065548	-6.112257
Si	0.516641	-4.886483	-4.983504
Si	1.651448	-3.384715	-6.157868
Si	3.149054	-2.277703	-5.017074
Si	4.281353	-0.739227	-6.196005
Si	5.631570	0.266206	-4.870118
Si	-0.823807	-8.484034	-3.609976
Si	0.578294	-7.608369	-2.267160
Si	1.669562	-5.992005	-3.469198
Si	3.208424	-4.873880	-2.352218
Si	4.323915	-3.408935	-3.544198
Si	5.884371	-2.314206	-2.432140
Si	6.995853	-0.795324	-3.604772
Si	5.692257	-4.721886	0.194231
Si	7.006451	-3.433705	-0.884533
Si	8.032578	-2.404375	0.525679
Si	-4.643119	-2.031799	-7.495482
Si	-3.494925	-0.845064	-8.670204
Si	-2.125334	0.430471	-7.665666
Si	-0.278763	1.261097	-8.585672
Si	0.399583	2.942331	-7.480195
Si	-4.678967	-4.676908	-4.766973
Si	-3.547954	-3.593166	-6.321062
Si	-2.147044	-2.217768	-4.886193
Si	-0.833467	-0.887847	-6.153112
Si	0.526256	0.466701	-4.858869
Si	1.965623	1.905909	-6.258389
Si	3.090312	2.989387	-4.736332
Si	-4.673920	-7.382995	-2.104046
Si	-3.568602	-6.233169	-3.664588
Si	-2.139114	-4.848481	-2.265687
Si	-0.820405	-3.530352	-3.579657
Si	0.517324	-2.199444	-2.274287
Si	1.845186	-0.873351	-3.588779
Si	3.186777	0.444441	-2.277432
Si	4.565261	1.798820	-3.640811
Si	5.714991	2.962356	-2.168162
Si	-3.560000	-8.580289	-0.924777
Si	-2.189842	-7.596342	0.371039
Si	-0.809533	-6.182885	-0.950421
Si	0.517755	-4.836176	0.371844
Si	1.842103	-3.515827	-0.956964
Si	3.179647	-2.166927	0.322517
Si	4.532522	-0.880294	-0.985434
Si	5.885968	0.454418	0.323796
Si	7.304670	1.762466	-1.024822
Si	8.173191	3.194958	0.244150
Si	-0.775969	-8.472032	1.711307
Si	0.425283	-7.374538	2.943444
Si	1.953584	-6.212923	1.766862
Si	3.100550	-4.706803	2.861985
Si	4.582316	-3.573651	1.747037
Si	5.744700	-2.072617	2.835437
Si	7.305067	-0.840675	1.691479
Si	8.297309	0.463800	3.042976
Si	-7.334940	-2.032761	-4.799481
Si	-5.998670	-1.043480	-6.138146
Si	-4.805196	0.500843	-4.966902
Si	-3.244633	1.609917	-6.116585
Si	-2.155173	3.133180	-4.979351
Si	-0.638940	4.249624	-6.168157
Si	0.370490	5.600753	-4.841873
Si	-7.339477	-4.702854	-2.139090
Si	-6.191448	-3.539184	-3.634383
Si	-4.769780	-2.175020	-2.253780
Si	-3.446740	-0.868412	-3.578875
Si	-2.114743	0.456399	-2.258056
Si	-0.783861	1.781470	-3.561381
Si	0.547849	3.122872	-2.259197
Si	1.925727	4.499554	-3.627445
Si	3.098365	5.619327	-2.140341
Si	-6.020648	-6.019859	-1.115213
Si	-4.840322	-4.849068	0.436124
Si	-3.441205	-3.504740	-0.941857
Si	-2.105389	-2.177816	0.367420
Si	-0.784433	-0.862595	-0.950097
Si	0.553177	0.462818	0.362781
Si	1.880160	1.784746	-0.953636
Si	3.207186	3.091522	0.376730
Si	4.600440	4.467445	-1.034478
Si	5.763116	5.622363	0.511637
Si	-3.286340	-5.970398	1.533327
Si	-2.167727	-4.862344	3.068420
Si	-0.777619	-3.495933	1.677301
Si	0.560083	-2.177752	2.990561
Si	1.889953	-0.858413	1.671770
Si	3.237367	0.464493	2.979819
Si	4.561646	1.784421	1.661950
Si	3.042823	-7.379527	0.224846
Si	4.366631	-6.017963	-0.795045
Si	5.969428	3.195997	3.070029
Si	7.104168	4.329326	1.543217
Si	-0.626325	-6.001355	4.204424
Si	0.406331	-4.689879	5.526918
Si	1.949470	-3.554651	4.336823
Si	3.108616	-2.033228	5.438925
Si	4.637284	-0.899536	4.326235
Si	5.795715	0.649525	5.519580
Si	7.133923	1.665632	4.187630
Si	-8.465848	-0.759354	-3.683834
Si	-7.487546	0.515517	-2.294610
Si	-5.928287	1.644460	-3.463700
Si	-4.801502	3.145939	-2.326471
Si	-3.268006	4.265037	-3.454565
Si	-2.196106	5.836639	-2.360569
Si	-0.661944	6.943690	-3.525999
Si	0.553369	8.138344	-2.421191
Si	-8.504605	-3.603161	-0.886664
Si	-7.516158	-2.218903	0.381959
Si	-6.105816	-0.857967	-0.927960
Si	-4.744697	0.474533	0.390583
Si	-3.421874	1.783106	-0.937401
Si	-2.074382	3.103863	0.371717
Si	-0.769197	4.441487	-0.946193
Si	0.572158	5.787702	0.362715
Si	1.858838	7.184105	-1.039051
Si	3.342873	8.002863	0.185436
Si	-5.944199	-3.334153	1.588793
Si	-4.769805	-2.197277	3.067146
Si	-3.398526	-0.841429	1.692842
Si	-2.057666	0.469217	3.003107
Si	-0.746968	1.795719	1.688362
Si	0.592761	3.120008	2.997755
Si	1.909677	4.446492	1.677352
Si	3.333303	5.841680	3.074859
Si	4.459508	6.965096	1.529822
Si	-3.259762	-3.333078	4.213969
Si	-2.120924	-2.220044	5.750816
Si	-0.741742	-0.851094	4.323709
Si	0.598277	0.465222	5.662789
Si	1.912423	1.780282	4.307099
Si	3.287594	3.144181	5.719809
Si	4.423169	4.282819	4.196894
Si	-0.579713	-3.355139	6.879925
Si	0.673594	-2.267442	8.051584
Si	1.951996	-0.877612	7.075529
Si	3.351461	0.395216	8.048951
Si	4.437122	1.626706	6.874732
Si	-8.444189	1.886953	-0.973681
Si	-7.281090	3.007770	0.258410
Si	-5.941597	4.321878	-0.777189
Si	-4.600940	5.635880	0.221462
Si	-3.305179	6.982180	-0.826179
Si	-2.174770	8.019347	0.492940
Si	-8.313251	-0.947021	1.842511
Si	-7.262404	0.367482	2.957642
Si	-6.137119	1.887460	1.808572
Si	-4.558940	2.994877	2.865662
Si	-3.418951	4.493603	1.734082
Si	-1.917116	5.644291	2.866352
Si	-0.708761	7.207407	1.747207
Si	0.612718	8.180142	3.100813
Si	-5.897406	-0.675381	4.239998
Si	-4.574539	0.310794	5.569667
Si	-3.450278	1.890651	4.417019
Si	-1.864420	2.989060	5.466079
Si	-0.758331	4.522771	4.361287
Si	0.810475	5.662929	5.546021
Si	1.827596	7.005796	4.217122
Si	-3.238184	-0.682430	6.883945
Si	-2.130339	0.561592	8.057658
Si	-0.716156	1.817538	7.094815
Si	0.569167	3.203697	8.066685
Si	1.790440	4.295695	6.888682
Si	8.078192	0.552396	-2.555247
Si	1.940991	-8.577776	-0.956471

B.5 Silicon Quantum Dots

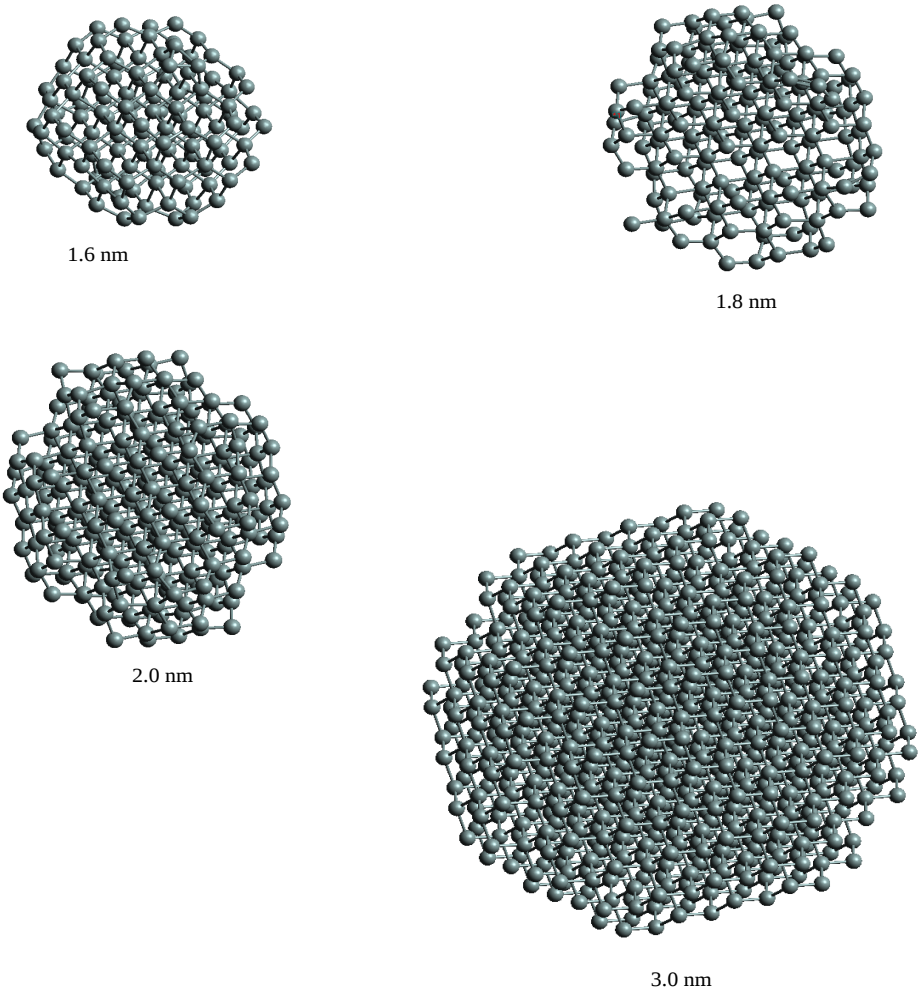

Figure B.5: Equilibrium structures of Si quantum dots of sizes 1.6, 1.8, 2.0 and 3.0 nm. The structures were obtained from geometry optimization using PM7 as implemented in MOPAC.

Si_{244} (2.0 nm)

	x	y	z
Si	3.394125	-4.751775	-7.467075
Si	4.610993	-3.588989	-8.526417
Si	5.767047	-2.239570	-7.250359
Si	3.522360	-7.156096	-4.419005
Si	4.442187	-5.876150	-5.925856
Si	6.039052	-4.689372	-4.771920
Si	7.193282	-3.151004	-5.905940
Si	8.342157	-1.946984	-4.755317
Si	4.684050	-8.480267	-3.444580
Si	5.767706	-7.151374	-2.283137
Si	7.215084	-5.789450	-3.208873
Si	8.333513	-4.709608	-1.944991
Si	-1.868748	-4.529765	-7.169138
Si	-0.574322	-3.392716	-8.222697
Si	0.713867	-1.963196	-7.356315
Si	2.001678	-0.645219	-8.385180
Si	3.312677	0.656301	-7.366461
Si	4.711505	1.889466	-8.399837
Si	5.831468	3.120456	-7.266537
Si	-1.872494	-7.189245	-4.522494
Si	-0.842309	-5.838163	-5.829392
Si	0.701509	-4.673218	-4.674128
Si	1.989806	-3.416122	-6.057828
Si	3.294897	-2.034529	-4.683499
Si	4.637862	-0.686733	-6.024963
Si	5.959761	0.632443	-4.679144
Si	7.182765	2.208537	-5.814142
Si	8.470619	3.418924	-4.714983
Si	-0.595464	-8.258030	-3.351213
Si	0.692928	-7.337127	-1.960780
Si	1.985088	-5.963534	-3.311756
Si	3.302556	-4.609659	-1.975374
Si	4.617778	-3.319047	-3.345404
Si	5.950710	-2.003134	-2.019860
Si	7.332269	-0.722489	-3.354154
Si	8.368759	0.621106	-2.049507
Si	2.004022	-8.381786	-0.683314
Si	3.311943	-7.364398	0.623781
Si	4.664899	-5.982299	-0.661008
Si	5.946299	-4.642594	0.657789
Si	7.328624	-3.326833	-0.661381
Si	8.345176	-1.987538	0.631633
Si	4.688962	-8.287551	1.938599
Si	5.860282	-7.225098	3.186502
Si	7.122737	-5.606520	2.348022
Si	8.609342	-4.690535	3.391334
Si	-4.473383	-1.818158	-7.184581
Si	-3.364298	-0.638473	-8.331130
Si	-1.958201	0.680011	-7.328716
Si	-0.714294	2.035763	-8.347812
Si	0.647190	3.313825	-7.344501
Si	1.883429	4.716753	-8.383155
Si	3.130183	5.819384	-7.258527
Si	-4.490444	-4.457379	-4.466490
Si	-3.374456	-3.368630	-6.014334
Si	-1.957836	-1.970743	-4.621281
Si	-0.642193	-0.661310	-5.950336
Si	0.665382	0.662752	-4.643737
Si	1.984272	1.983697	-5.980932
Si	3.296979	3.281405	-4.658039
Si	4.677144	4.662782	-6.139660
Si	5.794732	5.777364	-4.535482
Si	-4.490147	-7.172338	-1.834015
Si	-3.375693	-6.015082	-3.380759
Si	-1.960630	-4.611245	-1.987722
Si	-0.634106	-3.309288	-3.322593
Si	0.671178	-1.985442	-1.991832
Si	1.987616	-0.684327	-3.370974
Si	3.297842	0.635586	-2.014220
Si	4.604526	1.951744	-3.332202
Si	5.954614	3.295193	-1.999190
Si	7.135521	4.419594	-3.535750
Si	-3.337213	-8.337787	-0.634911
Si	-1.986418	-7.323505	0.668382
Si	-0.657915	-5.941053	-0.671968
Si	0.667305	-4.629956	0.654182
Si	1.976886	-3.305283	-0.673197
Si	3.283410	-1.975522	0.631247
Si	4.623759	-0.676520	-0.693576
Si	5.944189	0.649356	0.621989
Si	7.348217	1.941405	-0.732390
Si	8.249766	3.323422	0.586644
Si	-0.684299	-8.347707	1.977050
Si	0.616169	-7.344787	3.300573
Si	1.976192	-5.978607	1.960004
Si	3.263315	-4.669203	3.278768
Si	4.546036	-3.314570	1.937345
Si	5.914535	-2.002948	3.251478
Si	7.320553	-0.684905	1.959150
Si	8.320177	0.601135	3.338399
Si	1.886598	-8.386959	4.668803
Si	3.094618	-7.268402	5.835498
Si	4.663124	-6.149503	4.727234
Si	5.758581	-4.525033	5.777220
Si	7.084638	-3.667988	4.240153
Si	-4.545824	3.433484	-7.183497
Si	-3.327790	4.724179	-8.263550
Si	-2.058491	5.914674	-7.220337
Si	-7.168219	-1.820380	-4.481311
Si	-5.812700	-0.841173	-5.799000
Si	-4.647278	0.707480	-4.632040
Si	-3.319116	1.973412	-5.939917
Si	-1.968782	3.341970	-4.623011
Si	-0.617511	4.678653	-5.953129
Si	0.680184	5.983298	-4.635233
Si	2.266926	7.175719	-5.778278
Si	3.436713	8.489707	-4.703224
Si	-7.167161	-4.488424	-1.838190
Si	-6.005106	-3.331566	-3.345478
Si	-4.592771	-1.961256	-1.981127
Si	-3.279571	-0.640530	-3.311725
Si	-1.979920	0.676614	-1.997381
Si	-0.651120	1.995201	-3.323916
Si	0.644035	3.304184	-1.994891
Si	1.968104	4.591540	-3.313743
Si	3.300488	5.932897	-1.990466
Si	4.403509	7.116189	-3.555836
Si	-5.819495	-5.821614	-0.822639
Si	-4.622726	-4.650488	0.709935
Si	-3.285998	-3.297332	-0.648403
Si	-1.983468	-1.972046	0.661183
Si	-0.656241	-0.660956	-0.681285
Si	0.661430	0.661431	0.641841
Si	1.974978	1.972922	-0.691020
Si	3.296479	3.290467	0.628481
Si	4.648945	4.640252	-0.721122
Si	5.811624	5.810418	0.807380
Si	-4.382611	-7.094197	3.550180
Si	-3.293828	-5.938713	1.988128
Si	-1.971979	-4.571947	3.315790
Si	-0.654006	-3.296782	1.970526
Si	0.655969	-1.981275	3.294470
Si	1.970957	-0.660573	1.963490
Si	3.295729	0.657366	3.279432
Si	4.618082	1.972025	1.941410
Si	6.005346	3.349194	3.368845
Si	7.166411	4.504063	1.852664
Si	-3.445583	-8.481153	4.722625
Si	-2.273968	-7.149856	5.764124
Si	-0.676786	-5.963697	4.636851
Si	0.638563	-4.656416	5.960366
Si	1.957197	-3.325613	4.581980
Si	3.314346	-1.996511	5.925338
Si	4.634703	-0.710311	4.610806
Si	4.464505	-3.511740	7.087568
Si	-7.134309	3.569380	-4.412760
Si	-5.811985	4.504052	-5.835625
Si	-4.677361	6.092973	-4.759054
Si	-3.113254	7.252395	-5.861543
Si	-1.929043	8.398345	-4.718557
Si	-8.335013	-0.583790	-3.362819
Si	-7.322088	0.675473	-1.975685
Si	-5.935214	2.005070	-3.293810
Si	-4.580607	3.330904	-1.971499
Si	-3.287051	4.673343	-3.309656
Si	-1.975051	5.982080	-1.986858
Si	-0.655766	7.358499	-3.330882
Si	0.697590	8.287066	-1.980832
Si	-8.331609	-3.375242	-0.613584
Si	-7.316024	-2.010427	0.655636
Si	-5.932993	-0.665496	-0.655490
Si	-4.628992	0.671129	0.662808
Si	-3.298357	1.988889	-0.662029
Si	-1.986002	3.316030	0.649617
Si	-0.667996	4.636525	-0.669477
Si	0.655442	5.939478	0.663168
Si	1.997010	7.298049	-0.646903
Si	3.393501	8.398835	0.579354
Si	-7.146994	-4.520434	3.478189
Si	-5.949600	-3.324111	1.993242
Si	-4.622867	-1.953890	3.330182
Si	-3.311761	-0.656286	1.986227
Si	-1.995417	0.657041	3.281028
Si	-0.670088	1.984128	1.965888
Si	0.639366	3.308964	3.288073
Si	1.983392	4.603540	1.971653
Si	3.393507	5.994654	3.366575
Si	4.522203	7.119394	1.819005
Si	-5.833612	-5.793223	4.497060
Si	-4.724583	-4.689469	6.114904
Si	-3.320046	-3.281916	4.661773
Si	-1.992492	-1.964636	5.983158
Si	-0.666676	-0.653774	4.604345
Si	0.655545	0.647916	5.917851
Si	1.965813	1.986463	4.599089
Si	3.387613	3.367131	5.991481
Si	4.524703	4.474255	4.504279
Si	-3.145981	-5.794114	7.241917
Si	-1.921614	-4.659978	8.369386
Si	-0.650210	-3.295742	7.334412
Si	0.674639	-1.985275	8.338295
Si	1.992226	-0.699644	7.298502
Si	3.340629	0.637653	8.310382
Si	4.484457	1.832426	7.150307
Si	-8.491055	4.747565	-3.385142
Si	-7.145434	5.756245	-2.240590
Si	-5.841196	7.225610	-3.231945
Si	-4.684355	8.287418	-1.949831
Si	-8.337475	1.995676	-0.661839
Si	-7.363708	3.347284	0.638925
Si	-5.959902	4.655119	-0.667281
Si	-4.649116	5.982518	0.640366
Si	-3.293346	7.360114	-0.632673
Si	-1.979893	8.395898	0.660600
Si	-8.362831	-0.705914	1.962866
Si	-7.363752	0.617602	3.286567
Si	-5.980524	1.981901	1.980540
Si	-4.664044	3.305139	3.281848
Si	-3.320595	4.613802	1.959168
Si	-1.996004	5.951904	3.314624
Si	-0.702738	7.328850	1.963947
Si	0.591590	8.232809	3.377969
Si	-8.331039	-3.376714	4.724159
Si	-7.200648	-2.113921	5.890465
Si	-5.977096	-0.638144	4.670723
Si	-4.636923	0.677900	5.957987
Si	-3.288321	-0.601236	7.322160
Si	-1.975280	0.669835	8.374955
Si	-0.695230	1.957042	7.304770
Si	0.665284	3.291195	8.246139
Si	1.858072	4.530280	7.154902
Si	-8.416619	4.654522	1.912477
Si	-7.265484	5.821627	3.106970
Si	-5.822951	7.192099	2.200576
Si	-4.716979	8.465882	3.416373
Si	-8.235224	1.840538	4.747394
Si	-7.234390	3.177517	5.861969
Si	-6.149280	4.727806	4.673057
Si	-4.525343	5.798090	5.785363
Si	-3.530021	7.125718	4.446094
Si	-5.685411	2.292738	7.164281
Si	-4.697301	3.398298	8.504768
Si	-3.601948	4.344680	7.113516
Si	-0.714732	4.648812	4.647637
Si	0.817289	5.804533	5.794627
Si	1.882893	7.153816	4.519632
Si	-5.875337	-3.154359	7.283070
Si	-4.697139	-1.859942	8.280191
Si	5.801444	0.835121	5.799047
Si	7.166720	1.823694	4.477711
Si	2.161455	-5.818405	7.173969
Si	3.433661	-4.703127	8.419013
Si	-3.319017	1.976220	4.569812
Si	-1.994135	3.300270	5.936949

B.6.1 Cartesian coordinates (Angstroms) of equilibrium ZnS quantum dots

$Zn_{19}S_{19}$ (1.0 nm)

	x	y	z
S	-2.680919	-2.264999	-4.161032
S	0.296397	0.611870	-4.710072
S	-1.825081	-4.958336	-1.837858
Zn	-0.840470	-3.402812	-3.064184
S	0.825196	-2.174364	-2.100975
Zn	1.681124	-0.373144	-3.324087
S	3.290616	0.818163	-2.123186
S	0.874690	-4.891125	0.883489
Zn	1.873136	-3.412069	-0.379669
S	3.580818	-2.152532	0.723541
Zn	2.841431	-0.257686	-0.220887
S	-4.215999	-2.320498	-2.653386
Zn	-3.035081	-0.382111	-2.813235
S	-1.767756	1.025221	-1.759025
Zn	-0.279760	2.115636	-3.199673
S	0.772309	3.866289	-2.285845
Zn	-3.061812	-3.445993	-0.812979
S	-2.105024	-2.168263	0.812944
Zn	-0.596237	-0.826748	-0.621040
S	0.773591	0.438073	0.758106
Zn	2.597876	2.875080	-1.335987
S	3.734420	3.453768	0.630578
Zn	-0.386334	-3.406082	1.872594
S	0.705018	-2.136512	3.574583
Zn	2.754470	-1.682324	2.762575
S	3.606220	0.457194	3.611954
Zn	4.101579	1.746739	1.872696
S	-4.706121	0.632904	0.242192
Zn	-3.195905	2.167318	-0.279301
S	-2.286145	3.905556	0.780644
Zn	-0.290485	4.208603	-0.295503
Zn	-3.326241	-0.359140	1.634717
S	-2.137139	0.825190	3.255365
Zn	-1.335393	2.890554	2.595942
S	0.624972	3.445324	3.752186
Zn	1.632129	4.145541	1.645517
Zn	-0.225546	-0.242207	2.808408
Zn	1.863374	1.736024	4.119810

$Zn_{31}S_{31}$ (1.2 nm)

	x	y	z
S	3.605832	-1.933996	-2.793934
S	3.632944	-3.776379	-1.853517
S	-1.872624	-2.550859	-4.042484
S	0.830832	0.422135	-4.431769
S	-2.190777	-5.197045	-1.029794
Zn	-1.066877	-3.697899	-2.316337
S	0.529881	-2.196832	-1.328496
Zn	1.318609	-1.332826	-3.229933
S	4.138465	1.795449	-2.428993
Zn	2.654400	1.753574	-4.162679
S	0.691800	-4.984885	1.232690
Zn	1.845235	-3.879001	-0.398510
S	3.979893	-0.366072	0.836690
Zn	3.892742	-0.120557	-1.354902
Zn	3.933378	-3.026497	1.809829
S	-1.597418	3.837438	-2.690294
S	-4.941116	-2.148988	-1.497662
Zn	-3.232152	-1.347750	-2.742631
S	-2.046184	0.529328	-1.963869
Zn	-0.630551	1.766621	-3.309693
S	1.893434	5.082888	-2.126957
Zn	1.340151	4.117598	-4.175458
Zn	-4.106892	-4.139050	-1.149268
S	-1.910547	-1.807252	1.027333
Zn	-0.739587	-0.437388	-0.299120
S	0.553310	1.071400	0.953437
Zn	3.198644	3.478427	-1.194365
S	3.576479	3.701666	1.003959
S	-3.079024	-4.303706	2.826396
Zn	-1.567582	-4.368927	1.102402
S	0.882515	-1.652500	3.647517
Zn	1.913315	-0.453843	1.939796
S	4.646442	1.283756	3.966238
Zn	4.404783	1.736869	1.759671
Zn	1.435044	-3.667058	2.852219
S	-3.530538	3.711704	-2.007436
S	-4.861152	0.751731	0.819644
Zn	-3.634534	1.737664	-0.773531
S	-0.375404	5.051858	1.000493
Zn	-0.081799	4.724113	-1.158579
S	-4.799915	-3.341266	2.152137
Zn	-4.335171	-1.508804	0.798890
S	-2.121410	0.552467	4.031256
Zn	-0.421232	1.775330	3.127173
S	1.004398	3.315691	4.018756
Zn	1.527764	4.152244	1.873554
Zn	-1.373790	-1.400797	3.152220
Zn	2.739060	2.108316	4.424067
Zn	-2.174772	3.614902	1.437616
Zn	-3.566695	1.474566	2.500282

$Zn_{52}S_{52}$ (1.4 nm)

	x	y	z
S	-0.335373	-2.712679	-7.485542
S	0.390677	-4.693930	-4.862874
Zn	1.444209	-2.999087	-6.019525
S	3.203983	-2.081183	-5.063055
S	-0.513078	-7.440280	-2.851307
Zn	1.245100	-6.003153	-3.177693
S	3.044415	-5.155663	-2.213966
Zn	4.082489	-3.522746	-3.484606
S	5.825307	-2.696223	-2.462210
S	-2.013888	1.060956	-7.449845
Zn	-1.746163	-3.839205	-5.998591
S	-1.839498	-1.787934	-4.539996
Zn	-0.995464	-0.654318	-6.549379
S	0.766670	0.567639	-4.864878
Zn	2.217766	2.062771	-5.320006
S	3.598642	3.558784	-4.613709
Zn	-2.116249	-6.063070	-3.731234
S	-1.821557	-4.492536	-1.735783
Zn	-0.537355	-3.075358	-3.061545
S	0.973928	-1.862768	-1.831004
Zn	2.240996	-0.719115	-3.454065
S	3.540938	0.666296	-1.968422
Zn	4.710039	2.356543	-2.915387
S	6.007386	3.673541	-1.593701
S	-2.177783	-7.498932	0.918369
Zn	-1.017715	-6.549290	-0.679384
S	0.756229	-4.991860	0.585271
Zn	2.188523	-3.586317	-0.746523
S	3.504555	-2.116286	0.649797
Zn	5.073840	-1.152408	-1.083473
S	6.868555	-0.117152	-0.142835
Zn	6.615728	2.149952	-0.068052
Zn	2.222029	-5.377412	2.089116
S	3.607283	-4.669465	3.580927
Zn	4.726019	-2.998472	2.332526
S	6.056198	-1.680479	3.617342
Zn	6.643905	-0.116427	2.124034
S	-4.805374	0.865738	-4.513385
Zn	-3.124126	1.792802	-5.722850
S	-1.786042	3.538061	-4.616594
Zn	-4.106901	-4.210234	-4.294908
S	-4.834349	-2.674673	-2.714800
Zn	-3.651792	-0.819028	-3.452976
S	-1.996966	0.569422	-2.047157
Zn	-0.644470	1.795592	-3.500248
S	0.746921	3.153665	-2.016054
Zn	2.196579	4.575116	-3.076298
S	3.083397	6.230938	-1.819169
S	-4.859296	-4.463807	0.830419
Zn	-3.671810	-3.425245	-0.846480
S	-1.968708	-2.066133	0.611023
Zn	-0.671991	-0.692600	-0.677757
S	0.681553	0.661145	0.693322
Zn	2.184357	1.911765	-0.563790
S	3.079404	3.516343	0.937294
Zn	4.308950	4.747266	-0.518810
Zn	-3.214394	-5.754422	1.722347
S	-1.845877	-4.746674	3.486337
Zn	-0.663647	-3.600467	1.790486
S	0.698385	-2.156794	3.207753
Zn	2.105122	-0.755768	1.872654
S	3.029507	0.719845	3.427114
Zn	4.509247	2.533946	2.648784
S	6.664271	2.231902	2.268822
Zn	2.225630	-3.127503	4.613212
S	3.134989	-1.843360	6.240927
Zn	4.359009	-0.608666	4.693192
S	-7.803104	1.251464	-1.726815
Zn	-5.983719	1.752016	-2.812097
S	-4.753033	3.560812	-1.686529
Zn	-3.321948	4.012602	-3.210991
S	-0.975372	6.493216	-0.799868
S	-7.770094	-1.588957	1.374281
Zn	-7.342384	-0.351430	-0.353078
S	-4.766682	0.293620	0.332385
Zn	-3.417042	1.821421	-0.734938
S	-2.046598	3.158827	0.668997
Zn	-0.812319	4.291431	-0.868174
S	1.219719	7.158760	1.721442
Zn	1.394496	6.826689	-0.523396
Zn	-5.987159	-2.773561	1.789423
S	-4.705551	-1.713387	3.612190
Zn	-3.376832	-0.757638	1.858597
S	-2.016345	0.639728	3.214709
Zn	-0.535276	2.041471	2.068987
S	0.508607	3.529016	3.468861
Zn	2.040564	5.191596	2.466654
S	3.538078	5.615298	4.136938
Zn	-3.304950	-3.278399	4.003501
S	-0.845523	-0.697925	6.539136
Zn	-0.786247	-0.910622	4.338128
S	1.383742	1.856691	7.005704
Zn	2.094486	2.478583	4.972683
S	4.072716	3.704964	4.717958
Zn	1.526067	-0.421804	6.773233
Zn	-5.779978	1.610554	1.723672
S	-5.100814	3.100152	3.163829
Zn	-3.513921	4.308704	1.993332
S	-2.464141	5.971708	3.133006
Zn	-1.000236	6.673496	1.606358
Zn	-3.465280	1.989886	4.360060
S	-2.389983	3.187428	5.967200
Zn	-1.260940	4.530600	4.469691
Zn	-0.867348	1.701890	6.626861

B.6 ZnS Quantum Dots

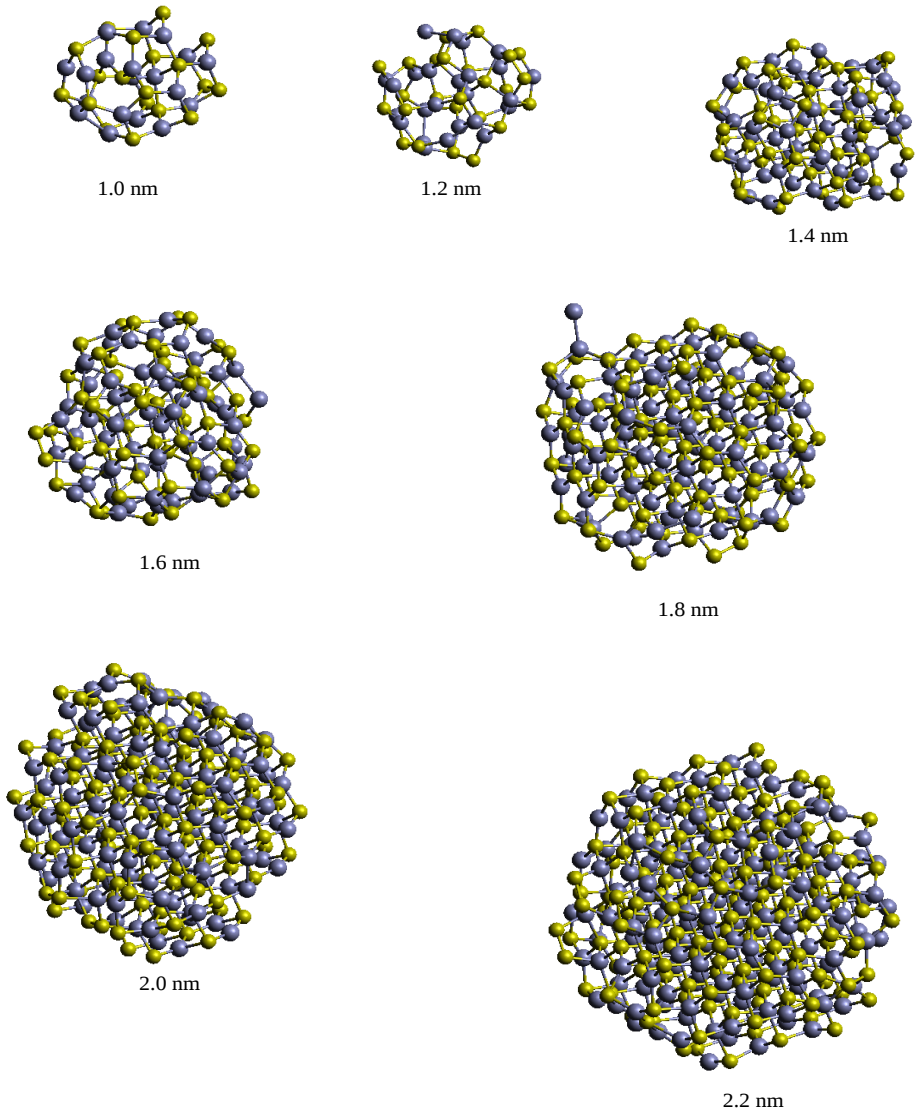

Figure B.6: Equilibrium structures of ZnS quantum dots of sizes 1.0, 1.2, 1.4, 1.6, 1.8, 2.0 and 2.2 nm. The structures were obtained from geometry optimization using PM7 as implemented in MOPAC.

$Zn_{95}S_{95}$ (1.8 nm)

	x	y	z
S	3.745444	-5.487903	-5.841981
S	1.770894	-8.141490	-3.343905
S	5.502625	-4.669484	-5.093786
S	-2.172881	-4.741965	-7.555176
Zn	-0.702933	-3.230349	-8.108517
S	1.543856	-3.140020	-8.384123
Zn	1.582866	-0.904997	-8.231444
S	2.954428	0.673766	-7.705829
S	-2.023790	-7.554238	-4.717571
Zn	-1.124610	-5.846855	-5.886502
S	0.521612	-4.674353	-4.829457
Zn	2.248312	-3.658505	-6.274263
S	3.110902	-1.986775	-4.866326
Zn	4.157459	-0.360838	-6.049033
S	5.889033	0.663131	-5.176675
Zn	-0.476699	-8.046498	-3.249554
S	-0.845518	-8.127015	-0.879270
Zn	2.358040	-5.993943	-3.965965
S	3.283514	-4.666673	-2.218032
Zn	4.722846	-3.203604	-3.466990
S	6.134372	-1.961740	-2.195874
Zn	7.008647	-0.344963	-3.480328
S	8.691878	1.054612	-2.862237
Zn	2.262428	-7.880605	-1.228324
S	3.578041	-7.360232	0.371182
Zn	4.659324	-5.540691	-0.580995
S	6.311235	-4.517006	0.482796
Zn	7.265451	-2.561791	-0.196026
S	8.972524	-1.552390	0.812176
S	-4.847395	-1.961516	-7.488962
Zn	-3.370968	-0.432918	-8.009983
S	-0.998348	-0.806443	-8.130513
Zn	-1.279174	2.230251	-7.921345
S	0.325129	3.553299	-7.432711
S	-4.831961	-4.780912	-4.730380
Zn	-3.628632	-3.510689	-6.176864
S	-2.166124	-2.045541	-4.726781
Zn	-0.832887	-0.609704	-5.839397
S	0.512434	0.751369	-4.763001
Zn	1.831116	2.183029	-6.242243
S	3.245269	3.404533	-4.987744
Zn	7.849006	4.593021	-5.893718
S	-4.765243	-7.554106	-2.006854
Zn	-3.546400	-6.209929	-3.516493
S	-2.074189	-4.726060	-2.091156
Zn	-0.728634	-3.355713	-3.428727
S	0.561132	-2.000832	-2.079458
Zn	1.879319	-0.634305	-3.438251
S	3.248323	0.698937	-2.205723
Zn	4.524042	2.079168	-3.657870
S	6.051394	3.249689	-2.341483
Zn	7.904927	2.911865	-3.877346
Zn	-3.236172	-8.092680	-0.546046
S	-3.144365	-8.272866	1.714762
Zn	-0.633084	-5.839126	-0.759575
S	0.729468	-4.726935	0.546999
Zn	2.026478	-3.314668	-0.804534
S	3.366880	-2.050813	0.531692
Zn	4.593506	-0.641182	-0.875460
S	5.917099	0.601799	0.487220
Zn	7.293015	1.852351	-0.906497
S	8.800175	2.779307	0.690126
Zn	-0.914246	-8.131923	1.760217
S	0.720251	-7.602323	3.051864
Zn	2.206466	-6.156676	1.883849
S	8.958777	0.334880	3.844293
Zn	9.622369	-3.950789	4.322517
Zn	8.270984	-1.958672	3.116305
S	-3.423926	1.816298	-8.093079
S	-7.603567	-2.048299	-4.594108
Zn	-5.937738	-1.032418	-5.750276
S	-4.836210	0.598175	-4.600007
Zn	-3.930892	2.423436	-5.922216
S	-2.176414	3.334510	-4.616811
Zn	-0.548230	4.652526	-5.580434
S	0.580992	6.266615	-4.602963
S	-7.551831	-4.718080	-1.893441
Zn	-6.194829	-3.535606	-3.424508
S	-4.710852	-2.092145	-2.001156
Zn	-3.400885	-0.653289	-3.315040
S	-2.000658	0.619127	-1.990576
Zn	-0.705895	2.111202	-3.277854
S	0.682162	3.458336	-2.071263
Zn	2.156276	4.855591	-3.522369
S	3.864114	6.030843	-2.541169
Zn	3.022118	7.847786	-1.639687
Zn	-5.821824	-5.859421	-0.969973
S	-4.652795	-4.740027	0.637709
Zn	-3.302170	-3.383713	-0.631527
S	-1.923759	-2.013237	0.626493
Zn	-0.556587	-0.586732	-0.616800
S	0.780733	0.725623	0.678714
Zn	2.054779	2.115903	-0.819653
S	3.424616	3.369084	0.536374
Zn	4.854801	4.707132	-0.962081
S	6.274387	5.774135	0.612429
S	-5.458451	-5.666169	3.876816
Zn	-3.634220	-6.143595	2.378243
S	-1.912370	-4.772138	3.212384
Zn	-0.538768	-3.368705	1.969652
S	0.785729	-2.070100	3.308117
Zn	2.132936	-0.778086	1.953857
S	3.402200	0.593421	3.375650
Zn	4.634569	1.858984	1.833306
S	6.058545	3.128739	3.458482
Zn	7.193775	4.030353	1.643042
Zn	-0.257035	-5.943312	4.298210
S	0.770440	-4.967866	5.987126
Zn	2.148570	-3.577329	4.681690
S	3.346233	-2.287791	6.190511
Zn	4.691383	-1.071229	4.797072
S	5.904045	0.440479	6.251519
Zn	7.056107	1.265747	4.410788
Zn	2.113112	-0.742599	7.097787
S	-5.797520	3.834440	-5.413836
S	-5.027841	5.587109	-4.608161
Zn	-8.083929	-0.558430	-3.093903
S	-8.353282	1.665898	-3.004438
Zn	-6.244100	2.355922	-3.593245
S	-4.806410	3.188487	-1.936679
Zn	-3.388466	4.823749	-3.154299
S	-2.119910	6.170202	-1.874535
Zn	-0.207683	7.249535	-2.719323
S	0.899444	8.784153	-1.590524
Zn	-8.018044	-3.281106	-0.336315
S	-8.061471	-0.772296	-0.521003
Zn	-5.752574	-0.742216	-0.567435
S	-4.652338	0.631293	0.771994
Zn	-3.324019	1.977527	-0.654533
S	-2.024881	3.307234	0.681308
S	-8.146016	-3.275495	1.907366
Zn	-5.980503	-3.818789	2.460696
S	-4.582472	-2.082168	3.291396
Zn	-3.186480	-0.693638	2.060805
S	-1.926873	0.697313	3.409491
Zn	-0.648817	2.027565	1.990591
S	0.656165	3.412401	3.357678
Zn	2.010411	4.673583	1.804491
S	3.451547	6.048590	3.318670
Zn	4.547124	6.941548	1.475289
S	-4.626023	-4.875370	5.610204
Zn	-3.123076	-3.339448	4.756801
S	-1.814257	-2.011781	6.065585
Zn	-0.495813	-0.734060	4.649686
S	0.770396	0.734548	6.014936
Zn	1.863709	1.849767	4.414142
S	3.835410	3.945470	6.561523
Zn	4.405146	4.357613	4.376974
Zn	-0.553769	-3.641496	7.154720
S	-0.891924	-3.527857	9.357890
Zn	0.451874	-1.926141	9.677727
S	1.997364	-0.385499	9.425018
Zn	4.350702	1.848059	6.667109
Zn	-8.153888	1.740693	-0.778484
S	-7.593548	3.178457	0.746544
Zn	-5.894767	4.338038	-0.332466
S	-4.899200	5.956993	0.751152
Zn	-3.237508	7.264732	-0.228686
S	-2.919119	9.061079	0.999238
Zn	-7.963997	-1.066642	2.098956
S	-7.381683	0.454851	3.534347
Zn	-6.184954	1.908749	2.132923
S	-4.813670	3.221286	3.352851
Zn	-3.371898	4.681554	1.979497
S	-2.121948	6.219977	3.335425
Zn	-1.465088	8.260732	2.432571
S	0.633468	8.883056	3.030809
Zn	-5.573263	-0.527919	4.603268
S	-4.525911	0.607662	6.205961
Zn	-3.346180	2.056858	4.773101
S	-2.413873	3.793400	5.958725
Zn	-0.811851	4.846444	4.652875
S	0.688062	6.118384	5.900537
Zn	1.592187	7.182191	4.101707
Zn	-2.691699	-0.286169	7.256026
S	-1.787124	0.956396	8.883414
Zn	0.572024	1.322914	9.257056
S	0.561063	3.546603	8.735395
Zn	1.644753	4.377958	6.961387
Zn	-5.638128	4.951611	4.618427
Zn	-3.920167	6.898955	4.530668
Zn	-1.502987	2.972347	7.744146
S	6.012679	-2.160943	3.400600
Zn	8.966665	0.693717	1.568154
Zn	1.282823	8.386096	0.816248
S	3.649441	8.662035	0.476395
S	3.404555	-4.807497	3.218543
Zn	4.794132	-3.450689	2.008180
Zn	-0.654462	4.739645	-0.632704
S	0.561398	6.007461	0.784089

$Zn_{122}S_{122}$ (2.0 nm)

	x	y	z
S	3.051308	-4.965739	-7.646906
Zn	4.370638	-3.250897	-8.251833
S	6.089714	-2.153526	-7.475535
S	3.043604	-7.603172	-4.895791
Zn	4.210019	-5.851535	-5.962359
S	5.927346	-4.961443	-4.836691
Zn	7.210555	-3.197135	-5.733710
S	8.728119	-2.055895	-4.756176
Zn	4.613497	-7.989994	-3.468365
S	6.011075	-7.568798	-1.954706
Zn	7.238821	-5.707637	-3.040882
S	8.725652	-5.030053	-1.657685
S	-2.287796	-5.104257	-7.831066
Zn	-0.914842	-3.514425	-8.283333
S	0.572424	-2.062019	-7.840390
Zn	2.669092	-0.917013	-8.049290
S	2.871812	1.308647	-8.168162
Zn	4.627902	2.282356	-7.276759
S	6.341706	3.537149	-7.062990
S	-2.310197	-7.813601	-5.047529
Zn	-1.232521	-6.086510	-6.088376
S	0.389545	-4.962178	-4.928434
Zn	1.781479	-3.466088	-6.211919
S	3.165832	-2.198297	-4.791546
Zn	4.910077	-0.873294	-5.886327
S	5.994961	0.581646	-4.634382
Zn	7.461611	2.245892	-5.427218
S	8.943748	3.193750	-4.163864
Zn	-0.983298	-8.238258	-3.431477
S	0.608565	-7.767470	-2.091994
Zn	1.801738	-6.132923	-3.477029
S	3.159335	-4.885465	-2.113812
Zn	4.623944	-3.415282	-3.394167
S	5.888482	-2.167702	-2.066326
Zn	7.617463	-0.787426	-3.290854
S	8.754054	0.022750	-1.457270
Zn	1.602151	-8.395073	-0.109461
S	3.527735	-7.465351	0.757055
Zn	4.899582	-5.914681	-0.720641
S	5.984258	-4.617219	0.741392
Zn	7.665465	-3.319699	-0.681865
S	8.781474	-1.453295	0.041378
Zn	4.991151	-7.386272	2.393208
S	6.574734	-6.989342	3.743645
Zn	7.562987	-5.281786	2.395766
S	8.967458	-3.948874	3.353851
S	-5.037265	-2.311288	-7.848312
Zn	-3.421547	-0.967995	-8.284029
S	-1.977098	0.522032	-7.852207
Zn	-1.142422	2.650638	-8.566930
S	0.662752	3.761595	-7.518767
Zn	2.451632	4.987601	-7.416732
S	3.823477	6.531044	-6.947044
S	-5.091665	-5.108937	-5.158304
Zn	-3.760235	-3.804920	-6.439831
S	-2.275668	-2.305116	-5.126429
Zn	-0.732208	-0.817556	-6.297171
S	0.470114	0.483565	-4.912083
Zn	1.576688	2.033816	-6.162412
S	3.101523	3.110623	-4.794481
Zn	5.568561	5.377721	-5.867617
S	6.478431	6.260419	-4.034513
S	-5.007599	-7.743608	-2.262493
Zn	-3.781217	-6.344677	-3.828974
S	-2.284141	-4.975727	-2.373064
Zn	-0.919696	-3.488391	-3.644341
S	0.390686	-2.170296	-2.322682
Zn	1.911833	-0.740470	-3.502322
S	3.179161	0.478627	-2.105501
Zn	4.574635	1.931649	-3.363734
S	5.863612	3.113872	-1.966244
Zn	-5.837096	4.207665	-5.937897
S	-4.976548	5.914115	-4.773747
Zn	-3.227532	7.245187	-5.664680
S	-2.181817	8.770745	-4.580892
Zn	-8.200224	-0.958746	-3.509971
S	-7.718475	0.581032	-2.120884
Zn	-6.067790	1.786595	-3.501145
S	-4.857684	3.161249	-2.112490
Zn	-3.371105	4.609741	-3.429709
S	-2.145294	5.854325	-2.039523
Zn	-0.799293	7.578448	-3.301907
S	0.075650	8.676549	-1.400939
Zn	-8.161926	-3.351538	-0.985894
S	-7.630318	-1.958011	0.547945
Zn	-6.007822	-0.774960	-0.934010
S	-4.650892	0.441300	0.376941
Zn	-3.235742	1.897361	-0.934404
S	-2.107033	3.136750	0.584239
Zn	-0.740157	4.574133	-0.762294
S	0.603040	5.728496	0.639509
Zn	1.825889	7.291223	-0.724489
S	2.720461	8.607594	1.244013
S	-7.590673	-4.845616	2.883801
Zn	-6.061381	-3.341456	1.763485
S	-4.896542	-2.048601	3.229069
Zn	-3.361987	-0.813446	1.947753
S	-2.107217	0.505674	3.240776
Zn	-0.671265	1.875416	2.006210
S	0.589406	3.196934	3.353657
Zn	1.956742	4.431317	1.981970
S	3.384210	5.831178	3.400156
Zn	4.311456	7.011770	1.693626
Zn	-5.871489	-5.901018	4.032012
S	-4.912765	-4.901561	5.784041
Zn	-3.381585	-3.385752	4.613318
S	-2.146746	-2.112249	5.932034
Zn	-0.718226	-0.713260	4.814923
S	0.560916	0.624743	6.054518
Zn	1.936707	1.900695	4.822921
S	3.289382	3.392118	6.178197
Zn	4.478541	4.208602	4.517736
Zn	-3.208714	-5.670479	7.245863
S	-2.068808	-4.814520	8.839106
Zn	-0.809195	-3.314198	7.756075
S	-0.024590	-1.443589	8.848312
Zn	1.921673	-0.614382	7.721624
S	3.365998	0.561922	8.918267
Zn	4.350708	1.646125	7.331853
Zn	-7.975889	4.573118	-3.428312
S	-7.570222	5.981825	-1.916929
Zn	-5.732693	7.232179	-3.007996
S	-5.040051	8.703848	-1.602074
Zn	-8.415290	1.685108	-0.215296
S	-7.465990	3.557817	0.772461
Zn	-5.887352	4.871728	-0.707349
S	-4.582877	5.973454	0.759952
Zn	-3.318231	7.600913	-0.712879
S	-1.408993	8.691259	0.092828
Zn	-8.008261	-0.067199	1.903146
S	-7.859302	0.582003	3.964082
Zn	-5.621499	2.154809	1.465112
S	-4.753541	3.059786	3.278538
Zn	-3.205408	4.636770	2.032587
S	-1.840131	5.924193	3.258510
Zn	-0.692043	7.344536	1.855407
S	1.245933	8.612842	2.741184
Zn	-8.025658	-3.494986	4.529183
S	-7.588248	-2.229058	6.152188
Zn	-6.118940	-0.726047	5.053034
S	-4.700151	0.603555	6.180387
Zn	-3.270786	1.797412	4.811925
S	0.458467	-4.617727	0.363363
Zn	1.940171	-3.209010	-0.946261
S	3.178741	-2.075900	0.550811
Zn	4.741021	-0.703981	-0.711218
S	5.975422	0.591097	0.613650
Zn	7.619428	1.930963	-0.604032
S	8.717942	3.629642	0.316833
Zn	-0.129259	-7.900581	2.019356
S	0.613972	-7.811471	4.050092
Zn	2.177141	-5.577113	1.463836
S	3.032972	-4.727694	3.298157
Zn	4.704884	-3.174422	1.987361
S	5.894402	-1.829066	3.247879
Zn	7.670898	-0.587932	1.967211
S	8.843086	0.534639	3.471650
Zn	2.590828	-6.745019	4.540045
S	3.803604	-6.927816	6.337570
Zn	5.697150	-5.802202	5.603041
S	6.474549	-3.907034	6.440047
Zn	7.413362	-2.952928	4.603000
S	-4.952498	3.057364	-7.609973
Zn	-3.268118	4.443489	-8.283227
S	-2.265111	6.206733	-7.431964
S	-7.755688	-2.297253	-5.105163
Zn	-6.004874	-1.227600	-6.115621
S	-4.880516	0.402348	-4.961611
Zn	-3.384591	1.806676	-6.263388
S	-2.142701	3.212471	-4.858135
Zn	-0.742284	5.037967	-6.026157
S	0.634109	6.137558	-4.586273
Zn	2.431691	7.516244	-5.270332
S	3.416860	8.858123	-3.857309
S	-7.741649	-4.981241	-2.296003
Zn	-6.312872	-3.771319	-3.847614
S	-4.958449	-2.277520	-2.386415
Zn	-3.441219	-0.931355	-3.655960
S	-2.162776	0.395612	-2.312740
Zn	-0.776245	1.923667	-3.499327
S	0.536480	3.149068	-2.130794
Zn	1.944918	4.611129	-3.367447
S	3.167735	5.862051	-1.890694
Zn	4.698559	7.213506	-3.067924
Zn	-5.988837	-5.973665	-1.237297
S	-4.833535	-4.813410	0.366658
Zn	-3.448174	-3.456046	-1.015341
S	-2.207222	-2.205572	0.426996
Zn	-0.734171	-0.751320	-0.781206
S	0.535855	0.529239	0.547751
Zn	1.958998	1.895621	-0.713194
S	3.289989	3.174241	0.618640
Zn	4.705966	4.587268	-0.684606
S	5.943518	6.171355	0.548972
S	-4.780294	-7.590582	2.886598
Zn	-3.320257	-6.016156	1.749140
S	-2.039860	-4.854503	3.229246
Zn	-0.770662	-3.338211	1.953955
S	0.527882	-2.049402	3.236225
Zn	1.971167	-0.649050	2.002627
S	3.246746	0.678426	3.307453
Zn	4.754760	1.893294	1.974045
S	6.123649	3.378660	3.319217
Zn	7.156501	4.458745	1.562421
Zn	-3.389316	-7.984116	4.508655
S	-2.214871	-7.547055	6.199924
Zn	-0.655503	-6.095395	5.183561
S	0.617869	-4.598516	6.239660
Zn	1.834300	-3.204319	4.822807
S	3.165052	-1.862315	5.988266
Zn	4.681214	-0.595765	4.784675
S	6.005204	0.762590	6.085206
Zn	7.243280	1.636707	4.417229
Zn	-5.704169	-3.187100	7.228764
S	-4.885626	-2.004422	8.812536
Zn	-3.362440	-0.775040	7.727683
S	-1.505862	0.047669	8.823735
Zn	-0.629427	1.965699	7.720203
S	0.288832	3.677984	8.797572
Zn	1.566310	4.474101	7.243630
Zn	-7.374282	5.024117	2.397393
S	-6.950115	6.621051	3.728589
Zn	-5.237782	7.583330	2.384273
S	-3.813326	8.925670	3.336248
Zn	-6.820404	2.546839	4.505522
S	-7.030360	3.772190	6.290254
Zn	-5.888579	5.651068	5.626177
S	-4.005898	6.439271	6.501722
Zn	-3.046939	7.334494	4.693014
Zn	-5.482767	2.397651	7.535123
S	-4.238285	3.390342	9.004219
Zn	-3.117142	4.545585	7.478058
Zn	7.442411	4.415725	-3.072003
Zn	-3.370253	-8.152068	-0.951132
S	-1.943674	-7.610485	0.546640
Zn	-0.761883	-6.006860	-0.913208
S	-1.984609	3.189187	5.971611
Zn	-0.664979	4.615573	4.798675
S	0.579845	6.202527	6.006635
Zn	1.710560	7.025855	4.349024
Zn	2.465816	-5.370747	7.563344
S	3.442271	-4.065717	8.989206
Zn	4.610779	-3.009725	7.414571
S	-7.592261	3.021983	-4.872238

B.7.1 Cartesian coordinates (Angstroms) of equilibrium CdS quantum dots

$Cd_{19}S_{19}$ (1.0 nm)

	x	y	z
S	-1.604550	-1.666159	-4.289204
S	-0.168635	-0.214354	-4.794729
S	-2.086553	-5.311817	-1.900860
Cd	-0.642976	-3.590751	-2.601041
S	1.172676	-2.192317	-1.620241
Cd	1.904421	-0.726212	-3.479746
S	3.694502	0.721596	-2.497154
S	0.857558	-5.414099	0.466009
Cd	2.625541	-3.993630	0.045212
S	4.213420	-2.290817	0.951199
Cd	4.464051	-0.828486	-0.856089
S	-5.262795	-2.079342	-1.841908
Cd	-3.531337	-0.705727	-2.667858
S	-2.191946	1.145593	-1.658527
Cd	-0.740683	1.884862	-3.537850
S	0.681088	3.693139	-2.639218
Cd	-4.031256	-4.054216	-1.428652
S	-2.203529	-2.188273	0.328419
Cd	-0.414058	-0.435941	-0.304533
S	0.995857	1.032970	0.967955
Cd	2.338475	2.337019	-0.934352
S	3.569428	4.116780	0.275553
Cd	-0.685966	-3.848106	1.424515
S	0.632084	-2.524353	3.326712
Cd	2.469494	-0.940151	2.403131
S	3.638739	0.444650	4.089169
Cd	5.194244	2.106381	2.026783
S	-5.443098	0.950421	0.530916
Cd	-3.979483	2.623370	-0.100051
S	-2.276286	4.235622	0.830002
Cd	-0.806460	4.479642	-0.979017
Cd	-3.877782	-0.667120	1.331984
S	-2.510662	0.754094	3.285958
Cd	-0.971915	2.458622	2.279829
S	0.673123	3.849606	3.744387
Cd	2.153823	4.634883	1.957695
Cd	-0.991600	-0.938608	3.827096
Cd	2.097583	2.018900	4.552455

$Cd_{52}S_{52}$ (1.4 nm)

	x	y	z
S	0.206556	-2.352673	-7.685863
S	0.529716	-5.466660	-4.782727
Cd	1.513758	-3.440846	-5.863167
S	3.666211	-2.200406	-5.409181
S	1.120152	-7.761005	-0.947457
Cd	1.925948	-6.264762	-2.918110
S	3.839296	-4.961533	-1.977464
Cd	4.900566	-3.551700	-3.709792
S	6.808356	-2.226775	-2.693733
S	-2.363704	0.177254	-7.707812
Cd	-2.261386	-2.266150	-6.835073
S	-2.104239	-2.102745	-4.446755
Cd	0.113659	0.124410	-7.375085
S	1.336898	1.318269	-5.489170
Cd	2.890219	2.985199	-5.936159
S	4.444467	4.366212	-4.818240
Cd	-5.263964	-7.225573	-0.215033
S	-2.825997	-5.576027	-2.073013
Cd	-1.388625	-4.331676	-3.568269
S	0.979572	-1.885874	-2.763199
Cd	2.657924	-0.424853	-3.931593
S	4.029666	0.993356	-2.201312
Cd	5.400877	2.705344	-3.155950
S	7.296211	4.048021	-1.968943
S	-3.131259	-8.036187	0.790571
Cd	-1.300903	-7.018362	-0.794979
S	0.526275	-4.569184	0.111224
Cd	2.251521	-3.077388	-1.034962
S	3.987728	-1.804302	0.577676
Cd	5.669746	-0.882619	-1.267184
S	6.943506	0.722044	0.700413
Cd	4.939482	-3.740955	1.639431
S	6.671662	-2.620211	3.512688
Cd	7.623555	-1.012075	2.239343
S	-5.502969	0.513072	-4.779918
Cd	-3.504875	1.489002	-5.904680
S	-2.230749	3.609747	-5.453381
Cd	-7.248113	-5.204222	-0.147375
S	-5.590923	-2.808591	-2.061334
Cd	-4.343511	-1.390170	-3.575010
S	-1.921756	0.934946	-2.757094
Cd	-0.482413	2.571510	-3.985279
S	1.068865	4.004468	-2.369679
Cd	2.857774	5.514563	-3.051829
S	4.273215	7.156999	-1.926053
S	-4.711548	-4.702937	1.582520
Cd	-3.705607	-3.679040	-0.495195
S	-1.969584	-2.004454	0.430474
Cd	-0.714827	-0.719679	-1.364124
S	0.787242	0.792779	0.560727
Cd	2.122986	2.266284	-0.855250
S	3.944554	3.672546	0.507073
Cd	5.798143	5.571423	-0.439094
Cd	-3.022474	-6.368148	2.589835
S	-1.599236	-4.898434	3.908546
Cd	-0.644378	-3.490480	1.986719
S	0.928017	-2.140486	3.679045
Cd	2.100771	-0.701628	2.105735
S	3.882085	0.750523	3.647247
Cd	4.958100	1.957602	1.854240
S	5.948634	6.586483	1.748331
Cd	2.363635	-4.053745	4.208540
S	3.487688	-2.626393	6.209651
Cd	4.909955	-1.286722	4.822801
S	-7.715325	1.156610	-0.882981
Cd	-6.262369	1.930849	-2.895113
S	-4.959929	3.826378	-1.980931
Cd	-3.556673	4.878263	-3.730003
S	-2.213729	6.762207	-2.786034
S	-8.001638	-3.058055	0.864726
Cd	-7.005911	-1.257214	-0.764704
S	-4.519442	0.500908	0.179897
Cd	-3.072793	2.250925	-1.015989
S	-1.783728	3.976948	0.491965
Cd	-0.798622	5.655021	-1.384955
S	0.897405	6.661361	0.508301
Cd	2.935659	7.990373	-0.081802
Cd	-6.281885	-2.927511	2.614882
S	-4.756981	-1.582295	3.945668
Cd	-3.317528	-0.598299	2.038888
S	-1.984464	1.021543	3.668929
Cd	-0.597375	2.290545	2.071905
S	0.955675	3.914513	3.633567
Cd	2.554353	5.066538	2.151665
S	4.004001	7.211185	2.178812
Cd	-3.264609	-3.327783	4.961358
S	-3.629661	-3.724368	7.465832
Cd	-2.162287	-2.230546	8.208803
S	-0.932632	-0.975044	6.513468
Cd	2.270189	2.268671	5.003223
S	1.574264	1.461235	7.065814
Cd	1.540907	-1.152229	6.637842
Cd	-6.284720	2.067349	0.970851
S	-5.438601	3.710424	2.792432
Cd	-3.613886	4.981644	1.715746
S	-2.348463	6.613459	3.506041
Cd	-0.637803	7.381876	2.126867
Cd	-3.930681	2.393304	4.253420
S	-2.482058	3.471663	6.282775
Cd	-1.130637	4.907497	4.910269
Cd	-1.079868	1.494734	6.694264
Cd	8.064045	2.458519	-0.508862
Cd	2.056681	-6.379680	0.904999
S	3.694106	-5.553495	2.735874

$Cd_{95}S_{95}$ (1.8 nm)

	x	y	z
S	2.200766	-3.550781	-9.081055
S	4.529615	-7.023918	-5.256327
S	5.257857	-5.168093	-5.862422
S	-2.036820	-5.473624	-7.936869
Cd	-0.281395	-3.945424	-8.519666
S	-0.622564	-1.449701	-8.869649
Cd	2.170149	-1.045021	-8.892531
S	3.598679	0.711300	-8.264511
S	-2.354523	-8.440919	-4.942595
Cd	-0.932471	-6.764885	-6.077180
S	0.778815	-5.072351	-5.352995
Cd	3.339691	-4.145851	-7.052185
S	3.713498	-2.106699	-5.277974
Cd	5.055705	-0.388919	-6.491806
Cd	-3.269846	7.763512	5.284107
Cd	-4.007347	5.870547	7.130077
Cd	1.943727	7.922865	4.656430
Cd	-3.536965	-0.433582	7.818824
S	-1.706934	0.107322	9.400250
Cd	-0.732142	2.404325	8.168396
S	0.527410	3.951277	9.457341
S	6.725341	0.975311	-5.389468
Cd	-1.074761	-9.314834	-3.159485
S	1.128224	-7.977848	-2.580052
Cd	2.479023	-6.436705	-4.056678
S	3.830673	-5.022488	-2.147166
Cd	5.198788	-3.546048	-3.716821
S	6.729424	-2.103669	-2.310863
Cd	7.828618	-0.321755	-3.665958
S	9.579019	1.176468	-2.503367
Cd	2.562790	-8.694584	-0.878887
S	3.977350	-7.959965	0.825061
Cd	5.268412	-6.068507	-0.410150
S	6.896814	-4.912039	0.954617
Cd	8.019900	-3.070674	-0.309034
S	9.577288	-1.497539	0.686169
S	-4.996103	-2.384641	-8.286291
Cd	-3.208167	-1.140097	-9.190626
S	-2.534820	1.072585	-8.080872
Cd	-0.796593	2.474831	-8.862670
S	0.788486	3.974711	-8.154592
S	-5.298730	-5.329812	-5.234657
Cd	-3.693345	-4.000190	-6.598816
S	-2.297559	-2.235046	-5.162985
Cd	-0.841221	-0.630478	-6.431120
S	0.744552	0.800332	-5.244447
Cd	2.295625	2.387976	-6.707716
S	3.820241	3.796363	-5.368398
Cd	6.147441	3.649554	-7.413666
S	-5.425533	-8.082710	-2.000206
Cd	-3.971921	-6.718190	-3.673231
S	-2.247630	-5.208530	-2.297227
Cd	-0.700348	-3.690133	-3.768026
S	0.729496	-2.245072	-2.257496
Cd	2.144200	-0.766612	-3.779244
S	3.605798	0.693682	-2.316607
Cd	4.955920	2.316464	-3.815077
S	6.485460	3.137014	-1.854840
Cd	8.520828	3.313947	-2.959848
Cd	-3.809422	-8.809871	-0.381822
S	-1.323939	-8.996648	-0.660159
Cd	-0.648754	-6.472766	-0.871316
S	0.778190	-5.218305	0.700523
Cd	2.225045	-3.634959	-0.752281
S	3.709308	-2.246539	0.782738
Cd	5.040201	-0.653262	-0.799814
S	6.489145	0.303994	1.012723
Cd	8.669273	0.967640	-0.143202
S	9.517156	2.615054	1.779704
Cd	-1.172796	-8.686059	2.440354
S	0.659330	-8.025823	3.782095
Cd	2.253604	-6.649386	2.300596
S	3.579348	-5.046621	3.716118
Cd	5.229101	-3.543660	2.396166
S	6.712741	-2.216795	4.020336
Cd	8.527756	-1.041773	2.850650
S	9.491182	1.364730	3.492187
Cd	4.664587	-6.060949	5.729596
Cd	7.414439	-3.493306	6.083982
S	-5.333087	4.455013	-7.075541
S	-8.004567	-2.080006	-5.310824
Cd	-6.154381	-0.941346	-6.615882
S	-5.288535	0.817660	-5.084624
Cd	-3.982671	2.482815	-6.599326
S	-2.147420	3.760713	-5.129208
Cd	-0.467126	5.252004	-6.240238
S	0.900083	6.877473	-5.175185
S	-8.287149	-4.962396	-2.214097
Cd	-6.639500	-3.729552	-3.857380
S	-5.090273	-2.277675	-2.249370
Cd	-3.668137	-0.655877	-3.681891
S	-2.194776	0.771297	-2.229243
Cd	-0.697760	2.277096	-3.675106
S	0.818660	3.761029	-2.336779
Cd	2.438553	5.328260	-3.794650
S	4.014078	6.686868	-2.378391
Cd	5.942975	7.922085	-4.133042
Cd	-6.647293	-6.243125	-0.853144
S	-5.308163	-5.041104	0.873500
Cd	-3.628914	-3.730364	-0.746984
S	-2.211942	-2.222504	0.688112
Cd	-0.725908	-0.728601	-0.799581
S	0.745776	0.731004	0.648154
Cd	2.185377	2.265798	-0.854750
S	3.767603	3.623637	0.611312
S	-2.313402	3.891840	6.573708
Cd	-0.767231	5.132878	4.911146
Cd	5.277252	5.184341	-0.975387
S	6.952025	6.445818	0.683627
S	-3.569477	-8.924405	2.165275
Cd	-4.302004	-6.608879	2.698255
S	-2.132283	-5.177791	3.626763
Cd	-0.768246	-3.717999	2.128880
S	0.663866	-2.186225	3.606110
Cd	2.181506	-0.738299	2.138505
S	3.591556	0.693211	3.723646
Cd	5.028953	2.040259	2.086485
S	6.419503	3.623764	3.716989
Cd	7.905608	4.581610	1.874950
Cd	-0.479143	-6.152608	5.180855
S	0.775755	-4.988693	6.901127
Cd	2.129611	-3.372101	5.248263
S	3.600160	-2.190665	6.848737
Cd	4.983028	-0.681524	5.312518
S	6.652088	0.646009	6.795459
Cd	7.679859	2.006053	5.130291
Cd	5.196888	-4.090927	7.593042
S	-9.071610	2.060155	-3.498033
S	-5.915283	5.053836	-5.165781
Cd	-8.668978	-0.403348	-3.753724
S	-8.705992	-0.656397	-1.086821
Cd	-6.853465	2.977766	-4.159812
S	-5.217412	3.638213	-2.115307
Cd	-3.687806	5.180883	-3.638808
S	-2.296781	6.670584	-2.248456
Cd	-0.334536	8.061840	-3.315486
S	0.661537	9.474194	-1.719237
Cd	-9.075634	-3.255410	-0.749193
S	-9.333596	-3.067758	1.721485
Cd	-6.278512	-0.708727	-0.740194
S	-5.173997	0.807981	0.802581
Cd	-3.641443	2.245542	-0.722605
S	-2.237192	3.735789	0.731887
Cd	-0.742733	5.136425	-0.806561
S	0.911384	6.506218	0.489682
Cd	2.571779	8.210671	-0.992194
S	3.494420	9.284109	1.353911
S	-7.205940	-5.325164	4.524945
Cd	-7.044335	-3.927178	2.540732
S	-5.325327	-2.107631	3.574681
Cd	-3.671699	-0.757701	2.164073
S	-2.278041	0.792347	3.591257
Cd	-0.746331	2.206871	2.084580
S	0.753440	3.616568	3.582575
Cd	2.174832	5.023126	1.989785
S	3.740484	6.393531	3.656071
Cd	5.196292	7.592346	1.981376
S	-5.241176	-5.854324	4.962238
Cd	-3.875349	-3.674166	5.017769
S	-2.407305	-2.230479	6.408396
Cd	-0.796659	-0.649753	4.994441
S	0.573895	0.744943	6.580028
Cd	2.071638	2.153063	5.176813
S	3.515640	3.665654	6.797021
Cd	4.809222	4.844473	5.187862
Cd	-0.682911	-3.304248	7.909250
S	-0.240587	-1.425966	9.483469
Cd	2.028412	-0.481611	8.384450
S	3.638290	0.644660	9.708779
Cd	4.873377	1.882195	8.133671
Cd	-8.882754	2.286570	-1.058443
S	-8.234297	3.747940	0.652739
Cd	-6.323854	5.144202	-0.499392
S	-5.297313	6.789978	0.870784
Cd	-3.505646	8.050734	-0.433996
S	-2.333251	9.653367	0.857210
Cd	-9.027839	-0.758045	2.227639
S	-8.219499	0.846045	3.745140
Cd	-6.786158	2.379473	2.233366
S	-5.213612	3.737219	3.619857
Cd	-3.672045	5.313847	2.241335
S	-1.996860	6.805362	3.389675
Cd	-0.372913	8.510070	1.465216
S	1.859268	9.466292	2.696991
Cd	-6.358537	-0.374083	5.021248
Cd	1.629213	5.268449	7.841182
Cd	-6.119737	5.104402	5.557577
S	-5.212988	0.939547	6.732018
Cd	-3.596863	2.347514	5.140150
S	0.554422	6.947347	6.344526

B.7 CdS Quantum Dots

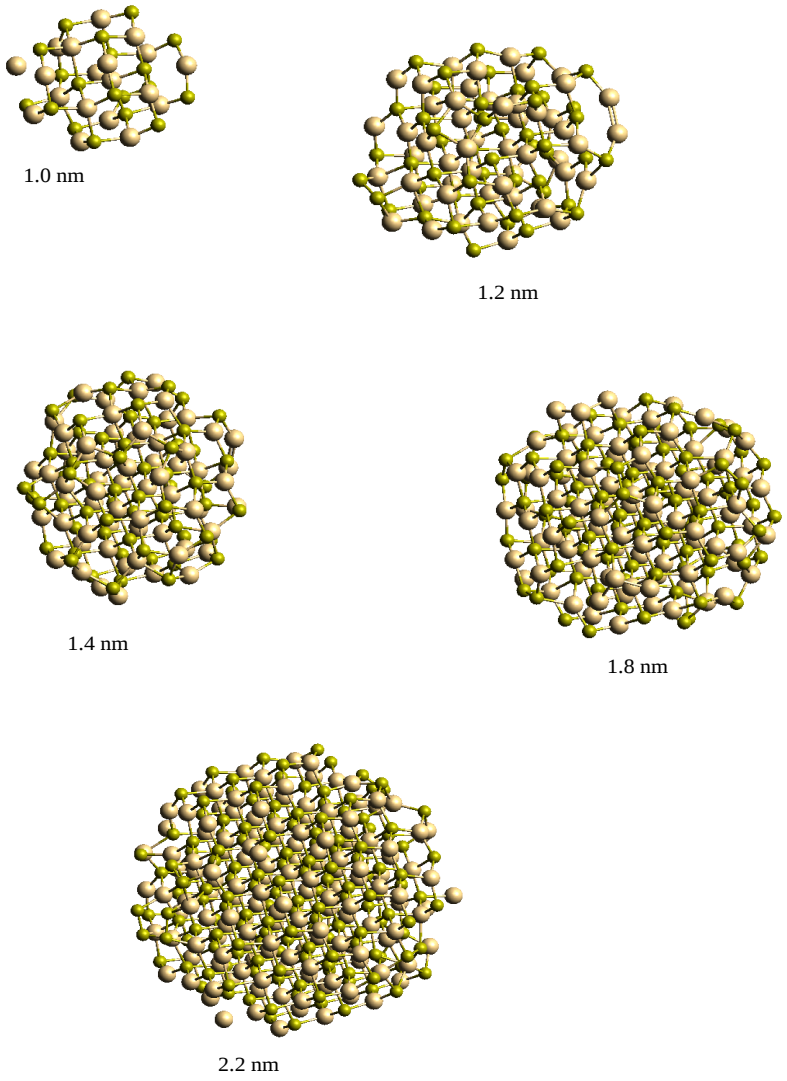

Figure B.7: Equilibrium structures of CdS quantum dots of sizes 1.0, 1.2, 1.4, 1.8 and 2.2 nm. The structures were obtained from geometry optimization using PM7 as implemented in MOPAC.

$Cd_{159}S_{159}$

	x	y	z
S	0.208606	-5.475552	-10.867429
S	3.148362	-2.453242	-11.028980
S	0.392281	-8.441842	-7.936217
Cd	1.620091	-6.763361	-9.052108
S	3.477956	-5.345169	-8.065812
Cd	4.581213	-3.478526	-9.405316
S	6.465089	-2.202910	-8.335574
S	0.807713	-11.175075	-4.599894
Cd	1.685099	-9.715717	-6.158200
S	3.632399	-8.231537	-5.062921
Cd	4.778526	-6.616091	-6.382066
S	6.554207	-5.225156	-5.225420
Cd	7.625992	-3.471377	-6.681654
S	9.435900	-2.150578	-5.421916
S	3.992839	-11.183456	-1.985467
Cd	4.986202	-9.594906	-3.321286
S	6.781686	-8.214515	-2.058454
Cd	7.760072	-6.636066	-3.458194
S	9.596769	-5.275524	-2.248712
Cd	10.206905	-3.775669	-3.912784
S	-0.663822	-0.834395	-11.253320
S	0.820823	0.657171	-11.410895
S	3.723545	3.635304	-10.876182
Cd	-1.906920	-5.727811	-9.733594
S	-1.722171	-4.885677	-7.598764
Cd	0.669802	-3.093383	-10.220281
S	1.141660	-1.950539	-7.993842
Cd	2.804335	-0.163883	-10.086201
S	3.926602	0.960177	-8.161553
Cd	5.377768	2.767804	-9.366026
S	7.005541	4.042202	-8.035548
Cd	-4.057321	-9.896332	-6.552707
S	-2.396005	-8.364011	-4.782814
Cd	-0.999606	-7.004027	-6.222290
S	0.688039	-5.285411	-5.015816
Cd	1.936141	-3.760377	-6.493794
S	3.682087	-2.218559	-5.197619
Cd	5.065852	-0.714975	-6.718023
S	6.645279	0.788721	-5.228599
Cd	7.974496	2.574107	-6.408355
S	9.740721	3.881385	-5.071388
S	-1.346166	-11.105097	-0.985196
Cd	-0.791049	-9.832734	-3.353186
S	0.750064	-8.104364	-2.023702
Cd	2.125328	-6.709716	-3.485220
S	3.736335	-5.164120	-2.147213
Cd	5.009176	-3.679639	-3.670776
S	6.591215	-2.196349	-2.252500
Cd	7.995883	-0.716718	-3.737439
S	9.578282	0.633189	-2.068061
Cd	10.397254	2.251402	-3.541979
S	0.364257	-11.219467	0.257537
Cd	2.271862	-9.922740	-0.851037
S	3.682593	-8.141158	0.691776
Cd	5.179099	-6.734842	-0.667986
S	6.686756	-5.167050	0.774971
Cd	8.014942	-3.725463	-0.816831
S	9.600333	-2.196161	0.569087
Cd	11.510048	0.138386	0.286778
S	3.498930	-11.006566	3.521633
Cd	4.980568	-9.469569	2.388556
S	6.766764	-8.267282	3.767548
Cd	7.885017	-6.646275	2.450495
S	9.706518	-5.321292	3.744579
Cd	10.352579	-3.777327	2.128081
S	-5.182979	0.135302	-11.165709
S	-2.229468	3.025239	-11.164455
Cd	-5.600329	-2.002103	-10.130670
S	-4.712279	-2.118247	-7.998377
Cd	-2.785580	0.447767	-10.342520
S	-1.758647	1.039570	-8.086735
Cd	0.044669	2.702472	-10.144826
S	1.066473	3.891368	-8.207812
Cd	2.887849	5.360753	-9.479719
S	4.046574	7.014252	-8.083303
Cd	-7.417002	-4.775792	-7.534859
S	-5.425697	-5.334820	-5.228959
Cd	-3.761464	-4.023395	-6.381511
S	3.602515	3.616455	0.715407
Cd	5.013371	4.993994	-0.907258
S	6.306207	6.422555	0.581219
S	-2.199291	-2.274633	-5.138716
Cd	-0.885541	-1.007174	-6.895480
S	0.720469	0.681802	-5.279413
Cd	2.164986	2.118717	-6.705726
S	3.753617	3.740803	-5.265274
Cd	5.391531	5.397473	-6.499800
S	6.841414	6.915844	-5.080633
Cd	-5.973057	-9.887425	-1.819136
S	-5.042750	-7.760756	-1.618342
Cd	-3.925377	-6.781392	-3.640292
S	-2.307674	-5.200951	-2.174891
Cd	-0.805992	-3.785858	-3.588527
S	0.749487	-2.209867	-2.202989
Cd	2.126805	-0.769752	-3.772230
S	3.652289	0.739425	-2.267833
Cd	5.081025	2.205642	-3.745968
S	6.685573	3.660526	-2.284002
Cd	8.129617	5.395507	-3.612698
S	9.631189	6.908871	-1.977659
S	-5.667780	-10.949627	0.320792
Cd	-3.206369	-10.306190	0.582753
S	-2.013955	-7.989838	1.164896
Cd	-0.913605	-6.781441	-0.700619
S	0.741166	-5.169451	0.724503
Cd	2.176145	-3.715218	-0.727728
S	3.710299	-2.218673	0.772256
Cd	5.045809	-0.768627	-0.790901
S	6.523871	0.742533	0.745796
Cd	7.964757	2.110062	-0.727681
S	9.603607	3.647902	0.984068
Cd	10.395174	5.293769	-0.484672
S	-2.343215	-11.071509	3.001988
Cd	-0.081597	-9.991280	2.416713
S	1.023601	-8.189778	3.763018
Cd	2.229781	-6.646335	2.112159
S	3.806978	-5.241136	3.729030
Cd	5.153519	-3.722403	2.247330
S	6.699631	-2.247803	3.751010
Cd	7.970683	-0.841979	2.063591
S	9.731394	0.629063	3.293895
Cd	11.012687	3.090962	3.060838
Cd	2.760878	-9.600784	5.242912
S	3.990222	-8.230040	6.903612
Cd	5.372438	-6.727239	5.278036
S	6.857827	-5.272175	6.792118
Cd	8.144461	-3.867721	5.249938
S	9.798568	-2.246431	6.693201
Cd	10.458702	-0.723708	5.006990
S	-8.140352	0.294306	-8.349555
Cd	-6.441149	1.590647	-9.470992
S	-5.195846	3.411270	-8.282703
Cd	-3.280975	4.494202	-9.646193
S	-2.166598	6.410214	-8.451274
Cd	-10.050157	-1.982381	-5.817030
S	-7.955989	-1.819165	-4.821236
Cd	-6.452170	-0.974779	-6.608305
S	-5.065271	0.683323	-5.189601
Cd	-3.532648	1.944593	-6.675534
S	-2.152556	3.666513	-5.259262
Cd	-0.649841	5.019488	-6.829238
S	0.734084	6.616903	-5.275577
Cd	2.476143	7.908338	-6.535343
S	3.736004	9.763866	-5.214133
Cd	-10.022836	-6.399033	-4.027086
S	-8.407050	-4.837155	-2.259500
Cd	-6.668964	-3.794833	-3.694948
S	-5.193485	-2.178664	-2.212341
Cd	-3.630962	-0.852385	-3.649568
S	-2.172038	0.742054	-2.211656
Cd	-0.718464	2.088370	-3.792153
S	0.733481	3.647278	-2.277864
Cd	2.192144	5.040922	-3.802787
S	3.620620	6.665837	-2.334373
Cd	5.245193	8.166537	-3.719127
S	6.710569	9.836259	-2.152155
S	-8.536683	-7.980882	0.565763
Cd	-7.080616	-6.345289	-0.877949
S	-5.320795	-5.056776	0.726211
Cd	-3.767795	-3.698389	-0.773323
S	-2.215073	-2.227204	0.754284
Cd	-0.766319	-0.800510	-0.737969
Cd	7.833357	8.053492	-0.601450
Cd	-6.807478	-9.126954	1.751914
S	-5.329297	-8.138596	3.554740
Cd	-3.796550	-6.541168	1.988246
S	-2.204573	-5.192880	3.678060
Cd	-0.743684	-3.757788	2.162845
S	0.782798	-2.254985	3.684161
Cd	2.208132	-0.763510	2.210492
S	3.700698	0.737654	3.729870
Cd	5.110899	2.244723	2.249374
S	6.538107	3.753482	3.765427
Cd	7.920059	5.317366	2.358202
S	8.762359	7.521640	3.065565
Cd	-3.343108	-9.540614	4.483987
S	-2.099632	-8.418184	6.376909
Cd	-0.653793	-6.803496	4.918607
S	0.832711	-5.276199	6.513265
Cd	2.320898	-3.734814	5.062217
S	3.783385	-2.238618	6.657720
Cd	5.185973	-0.754216	5.128978
S	6.808318	0.775985	6.592330
Cd	8.198060	2.359205	5.165987
S	10.338061	3.562225	5.202533
Cd	2.503092	-6.617979	7.810855
S	3.833021	-5.307312	9.641926
Cd	5.312974	-3.851075	8.036932
S	6.821985	-2.228044	9.686819
Cd	8.070846	-0.999281	7.908387
S	-11.105092	0.179049	-5.531211
Cd	-9.333221	1.588366	-6.643828
S	-8.241614	3.414300	-5.313599
Cd	-6.543007	4.598303	-6.598273
S	-5.314612	6.369549	-5.338288
Cd	-3.533409	7.454049	-6.823950
S	-2.376001	9.323079	-5.493276
S	-11.195046	-1.014343	-1.197461
Cd	-10.396944	0.475430	-3.053004
S	-8.053689	1.104171	-1.945800
Cd	-6.603540	1.938699	-3.679425
S	-5.181829	3.632477	-2.224282
Cd	-3.695292	4.897529	-3.750030
S	-2.276641	6.517390	-2.305458
Cd	-0.858147	7.935763	-3.846399
S	0.499014	9.528981	-2.223340
Cd	2.073717	10.387192	-3.743836
S	-11.165433	-4.531365	1.031408
Cd	-9.841131	-3.424777	-0.668310
S	-8.117414	-2.046103	0.831338
Cd	-6.793830	-0.742814	-0.816433
S	-5.153873	0.722833	0.746416
Cd	-3.718709	2.116619	-0.745067
S	-2.233956	3.665372	0.769766
Cd	-0.824883	4.982284	-0.833169
S	0.656017	6.545111	0.684741
Cd	1.984277	7.885092	-0.927136
S	3.546221	9.518674	0.721865
Cd	5.130412	10.608895	-0.754485
Cd	-9.749878	-6.189353	1.836969
S	-8.203164	-5.086881	3.733286
Cd	-6.701675	-3.539539	2.183428
S	-5.146959	-2.162588	3.757886
Cd	-3.710215	-0.770013	2.174770
S	-2.223569	0.759504	3.703260
Cd	-0.739130	2.190578	2.231431
S	0.748565	3.730833	3.717603
Cd	2.212838	5.124061	2.167363
S	3.624365	6.732424	3.585524
Cd	5.291111	8.147243	2.410935
S	7.598068	8.978710	2.105303
Cd	-6.578914	-6.452319	4.843934
S	-5.168893	-5.274208	6.590054
Cd	-3.664529	-3.708553	5.028781
S	-2.198046	-2.267179	6.616104
Cd	-0.788861	-0.827976	5.040843
S	0.711689	0.676984	6.540454
Cd	2.217636	2.218171	5.168352
S	3.641360	3.704785	6.664708
Cd	5.008729	5.208978	5.128859
S	4.997120	7.010464	7.234800
Cd	-3.395511	-6.814867	7.537161
S	-2.078081	-5.561967	9.375095
S	3.568643	0.714703	9.446451
Cd	5.344778	2.342934	7.923191
S	5.965711	3.656039	9.941393
Cd	2.224395	-3.795165	10.323444
Cd	5.220445	-0.701422	10.346440
S	-11.135814	2.937331	-2.245681
Cd	-9.632873	4.390473	-3.269291
S	-8.426205	6.296389	-2.146087
Cd	-6.833771	7.356273	-3.513471
S	-5.542156	9.240594	-2.310943
Cd	-4.074828	9.918363	-3.994992
S	-11.257777	0.254822	0.496873
Cd	-9.999181	2.377183	0.035632
S	-8.170720	3.755499	1.052237
Cd	-6.802507	4.857392	-0.658697
S	-5.242313	6.483070	0.748450
Cd	-3.864103	7.830630	-0.851798
S	-2.277077	9.459922	0.539722
Cd	-0.916967	11.718153	-0.817007
S	-11.121092	-1.925061	4.180901
Cd	-9.924405	-0.902018	2.362636
S	-8.083600	0.664599	3.712036
Cd	-6.611467	2.098299	2.256744
S	-5.206975	3.722831	3.813578
Cd	-3.728488	5.023972	2.297577
S	-2.239162	6.640697	3.782641
Cd	-0.963543	7.858337	2.036730
S	0.639602	9.484604	3.666994
Cd	2.065799	10.569174	2.162596
Cd	-9.539973	-3.352148	5.077353
S	-8.130441	-2.068547	6.853958
Cd	-6.672338	-0.693969	5.230017
S	-5.106935	0.767344	6.740821
Cd	-3.672750	2.225711	5.177450
S	-2.215528	3.732382	6.720792
Cd	-0.686371	5.121710	5.253931
S	0.750307	6.629569	6.852065
Cd	2.226105	8.034179	5.400537
S	4.180222	8.821372	6.615448
Cd	-6.561313	-3.499577	7.798761
S	-5.160686	-2.325629	9.646750
Cd	-3.669723	-0.845907	8.107748
S	-2.165463	0.656059	9.667699
Cd	-0.795682	1.994700	8.017204
S	0.894032	3.719627	9.153205
Cd	3.315649	5.733133	8.478714
S	4.204655	4.565654	10.610981
Cd	-3.672323	-4.048253	10.168621
Cd	-0.148507	-0.355429	11.634533
Cd	2.582816	2.676550	10.634181
S	-10.994854	3.438764	3.417913
Cd	-9.670824	5.243014	2.779335
S	-8.245886	6.908053	3.924497
Cd	-6.666340	7.737287	2.362527
S	-5.382334	9.635905	3.672426
Cd	-3.877645	10.279773	2.052023
Cd	-9.447086	2.348162	4.949539
S	-8.260056	3.768481	6.720049
Cd	-6.742168	5.271174	5.312294
S	-5.293875	6.831392	6.772755
Cd	-3.938988	8.050345	5.168846
S	-2.402344	9.843507	6.698034
Cd	-0.960406	10.556118	5.113646
Cd	-6.620854	2.459495	7.838455
S	-5.316886	3.834080	9.636498
Cd	-3.848713	5.298194	8.034371
S	-2.231206	6.815929	9.646307
Cd	-1.028486	8.041278	7.834567
Cd	-3.769284	2.256875	10.322308
Cd	-0.586489	5.220781	10.132783
S	0.617823	-2.278152	9.524318
Cd	2.130673	2.116652	-0.765491
S	0.719192	0.716748	0.776664
Cd	-0.711847	-3.882886	7.881208

Appendix C

Vertical excitation energies from different methods for various atomic clusters

C.1 Excited State Energies (eV) for Si_3

Table C.1: First Eight Lowest Excited State Energies (eV) for Si_3

EOM-CCSD	oeINDO	INDO/s	TDDFT	CIS(D)
1.406	1.310	−0.047	1.267	1.447
1.478	1.342	2.258	1.343	1.653
1.981	1.497	2.797	1.896	2.118
2.197	2.316	3.292	2.142	2.307
2.583	2.458	3.630	2.475	2.787
2.998	2.538	3.875	3.026	3.230
3.494	3.211	4.274	3.364	3.965
3.619	3.342	4.341	3.535	3.995

C.2 Excited State Energies (eV) for Zn_4

Table C.2: First Eight Lowest Excited State Energies (eV) for Zn_4

EOM-CCSD	oeINDO	INDO/s	TDDFT	CIS(D)
3.696	3.180	1.963	3.475	3.699
3.714	3.341	2.705	3.645	3.745
3.880	3.415	2.760	3.772	3.871
4.143	3.419	2.921	3.793	4.188
4.231	3.865	3.084	3.829	4.267
4.234	3.970	3.342	3.849	4.297
4.314	4.268	4.568	4.387	4.344
4.684	4.432	4.713	4.389	4.610

C.3 Excited State Energies (eV) for Zn_6

Table C.3: First Eight Lowest Excited State Energies (eV) for Zn_6

oeINDO	INDO/s	TDDFT	CIS(D)
2.143	1.261	3.217	3.106
2.433	1.613	3.292	3.155
2.527	1.755	3.411	3.179
2.694	1.758	3.469	3.349
2.833	1.912	3.478	3.397
2.951	2.045	3.592	3.407
2.968	2.141	3.638	3.428
3.084	2.171	3.676	3.546

C.4 Excited State Energies (eV) for Zn_8

Table C.4: First Eight Lowest Excited State Energies (eV) for Zn_8

oeINDO	INDO/s	TDDFT	CIS(D)
2.060	0.985	2.569	2.207
2.131	1.493	2.613	2.341
2.480	2.758	2.678	2.342
2.506	2.772	2.853	2.714
2.571	3.008	2.962	2.769
2.576	3.376	3.015	2.825
2.721	3.396	3.026	2.842
2.816	3.691	3.123	2.852

C.5 Excited State Energies (eV) for Zn_{16}

Table C.5: First Eight Lowest Excited State Energies (eV) for Zn_{16}

oeINDO	INDO/s	TDDFT	CIS(D)
1.116	0.388	1.599	1.355
1.124	0.524	1.672	1.510
1.153	1.490	1.800	1.613
1.211	1.655	1.818	1.770
1.448	1.687	1.965	1.781
1.508	1.913	1.991	1.897
1.821	1.972	2.046	1.905
1.892	1.977	2.069	1.919

C.6 Excited State Energies (eV) for Zn_{24}

Table C.6: First Eight Lowest Excited State Energies (eV) for Zn_{24}

oeINDO	INDO/s	TDDFT	CIS(D)
0.844	0.421	1.420	1.420
1.083	0.765	1.440	1.440
1.224	0.916	1.583	1.583
1.311	1.092	1.608	1.608
1.486	1.244	1.624	1.624
1.489	1.256	1.660	1.660
1.527	1.515	1.691	1.691
1.593	1.592	1.710	1.710

C.7 Excited State Energies (eV) for Cd_4

Table C.7: First Eight Lowest Excited State Energies (eV) for Cd_4

oeINDO	INDO/s	TDDFT	CIS(D)
3.042	5.586	3.251	3.840
3.251	5.639	3.519	4.004
3.372	5.652	3.534	4.021
3.655	5.670	3.572	4.255
3.732	5.816	3.697	4.445
3.854	5.830	3.743	4.447
4.207	5.835	4.226	4.550
4.513	5.835	4.243	4.828

C.8 Excited State Energies (eV) for Cd_6

Table C.8: First Eight Lowest Excited State Energies (eV) for Cd_6

oeINDO	INDO/s	TDDFT	CIS(D)
2.849	5.290	3.000	3.600
3.091	5.393	3.162	3.620
3.157	5.497	3.201	3.679
3.218	5.517	3.225	3.706
3.225	5.558	3.275	3.869
3.444	5.580	3.318	3.900
3.555	5.613	3.384	3.904
3.746	5.706	3.407	3.961

C.9 Excited State Energies (eV) for Cd_8

Table C.9: First Eight Lowest Excited State Energies (eV) for Cd_8

oeINDO	INDO/s	TDDFT	CIS(D)
2.724	5.220	2.679	3.100
2.776	5.295	2.813	3.181
2.809	5.394	2.867	3.246
2.932	5.401	2.937	3.327
3.109	5.407	2.939	3.356
3.156	5.436	2.992	3.387
3.252	5.448	3.038	3.395
3.311	5.479	3.058	3.450

C.10 Excited State Energies (eV) for Cd_{16}

Table C.10: First Eight Lowest Excited State Energies (eV) for Cd_{16}

oeINDO	INDO/s	TDDFT	CIS(D)
1.390	5.064	1.767	1.919
1.495	5.087	1.866	2.011
1.585	5.208	1.880	2.040
1.799	5.217	1.939	2.074
1.805	5.232	1.991	2.115
1.888	5.261	2.013	2.238
1.948	5.273	2.122	2.277
1.992	5.280	2.193	2.285

C.11 Excited State Energies (eV) for S_3

Table C.11: First Eight Lowest Excited State Energies (eV) for S_3

EOM-CCSD	oeINDO	INDO/s	TDDFT	CIS(D)
1.779	0.672	0.424	1.620	10.066
1.786	1.106	0.588	1.662	10.311
3.372	2.752	2.637	3.621	10.319
5.198	4.370	4.293	4.941	10.354
5.352	4.658	4.310	5.225	10.747
5.449	4.894	4.909	5.345	11.232
5.540	5.114	5.304	5.371	1.801
5.747	5.403	5.810	6.125	1.865

C.12 Excited State Energies (eV) for S_5

Table C.12: First Eight Lowest Excited State Energies (eV) for S_5

EOM-CCSD	oeINDO	INDO/s	TDDFT	CIS(D)
2.827	3.178	4.561	2.621	2.842
3.499	3.624	5.395	3.180	3.539
3.713	4.366	5.471	3.345	3.810
4.018	4.384	5.714	3.560	4.080
4.040	4.561	5.938	3.692	4.084
4.192	4.744	6.050	3.891	4.243
4.432	4.833	6.272	4.086	4.332
4.515	5.182	6.374	4.102	4.341

C.13 Excited State Energies (eV) for S_5

Table C.13: First Eight Lowest Excited State Energies (eV) for S_5

EOM-CCSD	oeINDO	INDO/s	TDDFT	CIS(D)
2.827	3.178	4.561	2.621	2.842
3.499	3.624	5.395	3.180	3.539
3.713	4.366	5.471	3.345	3.810
4.018	4.384	5.714	3.560	4.080
4.040	4.561	5.938	3.692	4.084
4.192	4.744	6.050	3.891	4.243
4.432	4.833	6.272	4.086	4.332
4.515	5.182	6.374	4.102	4.341

C.14 Excited State Energies (eV) for S_6

Table C.14: First Eight Lowest Excited State Energies (eV) for S_6

oeINDO	INDO/s	TDDFT	CIS(D)
4.039	5.406	3.405	3.952
4.039	5.436	3.406	3.952
4.113	5.436	3.781	4.440
4.113	5.631	3.901	4.484
4.244	5.631	3.901	4.508
4.513	5.913	4.044	4.508
4.582	6.299	4.099	4.544
4.584	6.502	4.110	4.600

C.15 Excited State Energies (eV) for S_{10}

Table C.15: First Eight Lowest Excited State Energies(eV) for S_{10}

oeINDO	INDO/s	TDDFT	CIS(D)
3.346	5.004	3.242	3.943
3.399	5.072	3.434	4.014
3.552	5.078	3.558	4.171
3.798	5.255	3.670	4.198
3.976	5.266	3.775	4.357
4.011	5.398	3.885	4.551
4.131	5.609	3.905	4.618
4.322	5.616	3.969	4.675

C.16 Excited State Energies (eV) for S_{20}

Table C.16: First Eight Lowest Excited State Energies (eV) for S_{20}

oeINDO	INDO/s	TDDFT
3.431	5.065	3.490
3.442	5.096	3.519
3.512	5.131	3.623
3.573	5.145	3.648
3.610	5.172	3.691
3.660	5.189	3.727
3.712	5.221	3.761
3.781	5.268	3.777

C.17 Excited State Energies (eV) for $(ZnS)_2$

Table C.17: First Eight Lowest Excited State Energies (eV) for $(ZnS)_2$ cluster

oeINDO	INDO/s	TDDFT	CIS(D)
0.695	−1.116	1.147	1.645
2.222	−0.575	1.752	2.005
2.851	1.935	2.209	2.933
3.040	2.462	2.884	3.497
3.127	3.161	3.516	3.635
3.492	3.302	3.518	3.912
3.586	3.390	3.925	4.147
3.748	3.916	3.969	4.521

C.18 Excited State Energies (eV) for $(ZnS)_3$

Table C.18: First Eight Lowest Excited State Energies (eV) for $(ZnS)_3$ cluster

oeINDO	INDO/s	TDDFT	CIS(D)
2.852	4.295	3.372	4.042
2.853	4.296	3.372	4.043
4.268	5.144	4.107	4.814
4.393	5.876	4.444	4.894
4.395	5.878	4.447	4.895
4.590	6.079	4.483	5.012
4.604	6.079	4.484	5.021
4.754	6.462	4.592	5.187

C.19 Excited State Energies (eV) for $(ZnS)_4$

Table C.19: First Eight Lowest Excited State Energies (eV) for $(ZnS)_4$ cluster

oeINDO	INDO/s	TDDFT	CIS(D)
2.527	3.795	3.612	4.016
3.377	4.229	3.777	4.510
3.377	4.229	4.076	4.546
4.123	4.784	4.076	4.546
4.338	5.860	4.246	4.945
4.354	5.860	4.246	4.945
4.399	5.914	4.554	5.129
4.676	6.615	4.691	5.131

C.20 Excited State Energies (eV) for $(ZnS)_{10}$

Table C.20: First Eight Lowest Excited State Energies (eV) for $(ZnS)_{10}$ cluster

oeINDO	INDO/s	TDDFT	CIS(D)
1.545	3.408	1.635	1.935
1.746	3.477	1.870	2.143
1.778	3.657	1.887	2.279
2.121	3.760	2.265	2.618
2.137	3.837	2.268	2.677
2.280	4.091	2.432	2.934
2.398	4.698	2.520	3.012
2.432	4.731	2.621	3.035

C.21 Excited State Energies (eV) for $(ZnS)_{19}$

Table C.21: First Eight Lowest Excited State Energies (eV) for $(ZnS)_{19}$ cluster

oeINDO	INDO/s	TDDFT
2.685	4.492	2.421
2.729	4.982	2.734
2.944	5.494	2.885
3.005	5.750	2.916
3.046	5.765	3.019
3.099	5.913	3.090
3.179	5.984	3.107
3.244	6.010	3.227

C.22 Excited State Energies (eV) for $(CdS)_2$

Table C.22: First Eight Lowest Excited State Energies(eV) for $(CdS)_2$ cluster

oeINDO	INDO/s	TDDFT
1.009	−2.484	0.940
2.618	−2.036	1.854
3.220	0.776	2.486
3.328	1.166	2.542
3.614	1.446	3.367
3.916	1.539	3.542
4.059	1.841	3.759
4.226	1.871	4.011

C.23 Excited State Energies (eV) for $(CdS)_3$

Table C.23: First Eight Lowest Excited State Energies (eV) for $(CdS)_3$ cluster

oeINDO	INDO/s	TDDFT
2.908	3.178	3.412
2.909	3.435	3.412
4.083	3.436	4.311
4.086	3.958	4.314
4.539	3.959	4.430
4.665	4.102	4.773
4.666	4.318	4.841
4.868	4.493	4.841

C.24 Excited State Energies (eV) for $(CdS)_{10}$

Table C.24: First Eight Lowest Excited State Energies (eV) for $(CdS)_{10}$ cluster

oeINDO	INDO/s	TDDFT
1.800	2.570	1.573
2.180	2.749	1.857
2.244	2.879	1.890
2.451	3.127	2.134
2.466	3.171	2.303
2.697	3.208	2.338
2.716	3.289	2.357
2.854	3.383	2.448

C.25 Excited State Energies (eV) for $(CdS)_{19}$

Table C.25: First Eight Lowest Excited State Energies (eV) for $(CdS)_{19}$ cluster

oeINDO	INDO/s	TDDFT
2.570	1.039	3.605
2.837	1.258	3.845
2.912	1.669	3.904
3.002	1.920	4.208
3.097	2.015	4.274
3.201	2.094	4.555
3.247	2.267	4.876
3.297	2.366	4.983

Appendix D

Published Paper from the Thesis

Chemical Physics Letters 721 (2019) 12–17

Contents lists available at ScienceDirect

Chemical Physics Letters

journal homepage: www.elsevier.com/locate/cplett

Research paper

Efficient determination of excitation energies and absorption spectra for quantum dots and large systems from *ab initio* data

Ezekiel Oyeniyi[a,*], Omololu Akin-Ojo[b,a]

[a] Department of Physics, University of Ibadan, Nigeria
[b] ICTP East Africa Institute for Fundamental Research, University of Rwanda, Rwanda

HIGHLIGHTS

- Computing excited states of big systems is costly; a new method is proposed for this.
- This method parameterizes a Hamiltonian using ab inito excitation energies of ***diatomics***.
- The new method is applied to Si_2 with EOM-CCSD energies and the INDO Hamiltonian.
- The parameterized Hamiltonian is transferable with mean error of 0.3 eV.
- Excitation energies and UV–VIS spectra are predicted for large clusters up to Si_{779}.

ARTICLE INFO

Keywords:
Excitation energy
Absorption spectra
ZINDO/S
EOM-CCSD
TDDFT
CIS(D)

ABSTRACT

A semi-empirical Hamiltonian with the INDO approximation and CIS was parameterized to reproduce EOM-CCSD excitation energies for diatomic silicon Si_2 with different inter-atomic separations. The model Hamiltonian is transferable, producing excitation energies for clusters, Si_n (n = 3, 4, 5) with mean absolute errors (MAEs) of 0.26, 0.18, and 0.09 eV, respectively, from the EOM-CCSD energies. The absorption spectra are also in qualitative agreement with the EOM-CCSD spectra. For clusters Si_{10} and Si_{40}, comparison with TDDFT gave MAEs of 0.32 and 0.12 eV, respectively. Predictions of excitation energies and absorption spectra are also given for Si_n (n = 124, 147, 172, 779) using the model Hamiltonian.

1. Introduction

Nanoscience and nanotechnology have opened up a large vista of possibilities in the development of novel materials and new products. Certain nanomaterials, called quantum dots, are being used in photovoltaic cells, light-emitting diodes, sensors, detectors, and for biomedical imaging. These nanosized materials have characteristics which are typically different from those of the corresponding bulk compounds and have the advantage that their properties can be tuned by changing their sizes and/or shapes. The electronic and optical behavior of quantum dots depend on their electronic excitation energies and ultraviolet–visible (UV–VIS) absorption spectra. Both experimental and theoretical approaches are employed in the study of the excitation energies and absorption spectra of materials. However, the experimental approach is sometimes limited by high infrastructure costs and the sophistication involved in the experiments. Hence, simple, reliable, and accurate theoretical methods are sought for in order to augment experiments and make predictions useful for experimentalists [1]. Theoretical methods can give insight and provide deep understanding of processes in these nanomaterials and, thus, complement experimental work.

Theoretical methods that can be used in the calculation of excitation energies and absorption spectra include the GW [2] method, solutions of the Bethe-Salpeter equation (BSE) [3–5], Quantum Monte Carlo (QMC), the equation-of-motion coupled-cluster with single and double excitations (EOM-CCSD) method [6], the complete active-space second-order perturbation theory (CASPT2) [7], the configuration interaction with singles (CIS) and doubles [CIS(D)] excitations methods [8], time-dependent density functional theory (TDDFT) [9,10] and others. Although these methods can give excitation energies and absorption spectra which are accurate to different degrees, their use is limited in practice by the size of the system [11,12]. They become very computationally expensive and sometimes prohibitive as the system size increases.

* Corresponding author.
E-mail addresses: ezekiellere@gmail.com, eo.oyeniyi@mail1.ui.edu.ng (E. Oyeniyi).

https://doi.org/10.1016/j.cplett.2019.02.014
Received 21 November 2018; Received in revised form 11 February 2019; Accepted 12 February 2019
Available online 19 February 2019
0009-2614/

The *ab initio* EOM-CCSD method has been found to give accurate excitation energies [13] and, in fact, in a previous study, [14] the method produced the most accurate excitation energies in comparison to experimental results. However, EOM-CCSD calculations are compute-intensive and can only be used in practice for the accurate determination of the excited state properties of systems with only a few ($\lesssim 50$) electrons. A pragmatic alternative to EOM-CCSD for obtaining excitation energies is the TDDFT method. TDDFT is being used extensively for calculations of excitation energies and absorption spectra and can routinely handle moderately large systems with up to approximately 100 atoms ($\sim$ 200–500 electrons). It serves as a useful compromise between accuracy and computational expense and is typically accurate within a mean absolute error of 0.3–0.5 eV [12]. In this work, our goal is to describe a procedure that can give excitation energies with near-EOM-CCSD accuracy and which can be used in practice for systems with well over 1000 electrons.

This work is divided as follows. In the next section, we describe our approach. This is followed by Section 3 where we apply the method and present our results. We end by making theoretical predictions for large clusters and giving our conclusion and suggestions for further work.

2. Theory

Our new method consists in determining the parameters of a semi-empirical Hamiltonian in order to reproduce the *ab initio* EOM-CCSD excitation energies for diatomics at different atom–atom separations. This model Hamiltonian can then be used for systems that are more complex than diatomics, for example, quantum dots. Our approach is different from other methods which parameterize the energies of structures that are more complex than diatomics. Later on, it is seen that our parameterization of diatomics does indeed give models which are 'transferable', i.e., the same model/parameters obtained for diatomics give good results for more complex structures.

The semi-empirical Hamiltonian that we have chosen to parameterize is Zeiner's Intermediate Neglect of Differential Overlap (ZINDO) [15] model Hamiltonian. The ZINDO Hamiltonian systematically omits certain integrals from the Hartree-Fock (HF) method while some other integrals are parameterized. In addition, only valence electrons are considered. Although these approximations drastically reduce the number of integrals and, thus, allow semi-empirical methods to handle large systems, the same approximations generally make these methods less accurate [16]. On the other hand, although based on HF, some electron correlation effects are incorporated into these Hamiltonians through model parameters. A variation of ZINDO, which we denote as ZINDO/S is the INDO approach which was parameterized to give good excitation energies when the HF-INDO process is followed by CIS calculations. The theory behind ZINDO and ZINDO/S, like other semi-empirical methods can be found, for example, in Refs. [17–19] and will not be discussed in details here. However, for completeness, and to establish some notation, we give highlights.

In the ZINDO approach, as in the HF formalism, we seek to solve the following secular equation:

$$FC = ESC \tag{1}$$

where F is the Fock matrix, C the basis vector and E is the orbital energy. In the INDO approximation, of which ZINDO is a variant, the overlap matrix S in the equation above is taken to be a unit matrix following from the neglect of differential overlap (NDO). Thus, in ZINDO, we solve:

$$FC = EC \tag{2}$$

Within INDO, the Fock matrix elements can be divided into three categories. For the unrestricted Fock matrix, we have:

1. The diagonal Fock matrix elements (atoms $A = B$ and indices $\mu = \nu$):

$$F^u_{\mu\mu} = H^{core}_{\mu\mu} + \sum_{\lambda on A} \sum_{\sigma on A} [P_{\lambda\sigma}\langle\mu\mu|\lambda\sigma\rangle - P^u_{\lambda\sigma}\langle\mu\lambda|\mu\sigma\rangle] \tag{3}$$

where

$$H^{core}_{\mu\mu} = U_{\mu\mu} + \sum_{A\neq B} [P_{BB} - Z_B]\gamma_{AB} \tag{4}$$

$$P_{DD} = \sum_{k on D} P_{kk} \tag{5}$$

$$P_{mn} = \sum_{i=1} C_{mi}C_{ni} \tag{6}$$

$$U_{\mu\mu} = \langle\mu| -\frac{1}{2}\nabla^2 - \frac{Z}{|r_i - R_A|}|\mu\rangle \tag{7}$$

2. The off-diagonal one center matrix elements (atoms $A = B$ and indices $\mu \neq \nu$):

$$F^u_{\mu\nu} = H^{core}_{\mu\nu} + \sum_{\lambda on A} \sum_{\sigma on A} [P_{\lambda\sigma}\langle\mu\nu|\lambda\sigma\rangle - P^u_{\lambda\sigma}\langle\mu\lambda|\nu\sigma\rangle] \tag{8}$$

$$H^{core}_{\mu\nu} = 0 \tag{9}$$

3. The off-diagonal two center matrix elements (atoms $A \neq B$ and indices $\mu \neq \nu$)

$$F^u_{\mu\nu} = H^{core}_{\mu\nu} - P^u_{\mu\nu}\gamma_{AB} \tag{10}$$

$$H^{core}_{\mu\nu} = \frac{1}{2}(\beta_\mu + \beta_\nu)S_{\mu\nu} \tag{11}$$

In all the equations above, the superscript u represents the spin component: $u = \alpha$ ('spin up') or β ('spin down'). For the restricted Hartree Fock case, $P^u_{\mu\nu} = \frac{1}{2}P_{\mu\nu}$ for both values of u. The important terms and parameters are: the one-electron one center integral $U_{\mu\mu}$, the two-center electron-nuclear attraction V_{AB}, and the two-center two-electron repulsion integral $\langle\mu\nu|\lambda\sigma\rangle$. Details on previous determination of these parameters and terms can be found in Refs. [18,20], for example.

Finally, after solving Eq. (2), the CIS approach is used as a post-Hartree-Fock-like method in order to calculate excitation energies; UV–VIS absorption spectra can also be computed. In CIS, the wave-function is expanded as a linear combination of the ground state and singly excited Slater determinants. Details of the CIS method can be found in Ref. [21], for example.

In principle, another semi-empirical Hamiltonian which can be used is the popular tight-binding method or its density functional theory (DFT)-based method, the tight-binding DFT (DFTB) approach [22]. Unfortunately, however, it is not straightforward to obtain the absorption spectra from DFTB.

3. Computational details

We tested our method with silicon. First, accurate *ab initio* excitation energies for Si_2 were obtained at each of eight different Si–Si separations from 1.6 to 3.0 Å in steps of 0.2 Å. These energies were obtained using the EOM-CCSD method with the triple-zeta valence basis functions having two sets of polarization functions (the "def2-tzvpp" basis functions of Ref. [23]). At each geometry, the eight lowest vertical excitation energies from the ground state were calculated, yielding a

total of 64 excitation energies for all eight geometries. For inter-atomic separations between 1.6 and 3.0 Å, the ground state of Si_2 is the triplet state. This was confirmed by carrying out CCSD/def2-tzvpp calculations for both the singlet and triplet states. All energy calculations were performed with the ORCA 4.0 program [24] unless otherwise stated.

Having obtained these 'benchmark' or 'training' energies, we proceeded to parameterize the ZINDO/S Hamiltonian so as to reproduce the EOM-CCSD energies. For this purpose, we minimized the following quantity with respect to the parameters of the model Hamiltonian:

$$\chi^2 = \frac{1}{N_{\text{data}}} \sum_{i=1}^{N_{\text{data}}} \|E_i^{\text{fit}} - E_i^{\text{ai}}| - \epsilon| \tag{12}$$

where $N_{\text{data}} = 64$ is the number of excitation energies that were fitted, E_i^{ai} is the ith *ab initio* excitation energy in the training data set and E_i^{fit} the ith excitation energy from the ZINDO/CIS result. The constant $\epsilon = 0.1$ eV is a practical difference in energy that we expected for each excitation energy in the parameterization although a value of 0 eV will be ideal.

The simplex method was used for the optimization with the ZINDO/S parameters as the initial guess. Eight parameters were optimized, namely, U_{pp}, ζ_s, ζ_p, β_s, β_p, γ_{ss}, F^2_{pp} and G_{sp}. The parameters γ_{sp}, and γ_{pp} were not directly optimized but were set equal to γ_{ss} while U_{ss} was initially fixed at zero. At the end of the parameterization, the mean absolute error (MAE) calculated as

$$\text{MAE} = \frac{1}{N_{\text{data}}} \sum_{i=1}^{N_{\text{data}}} |E_i^{\text{fit}} - E_i^{\text{ai}}| \tag{13}$$

was determined. A value of 0.21 eV was obtained for the training dataset and, in Fig. 1, we show a scatter plot which compares the excitation energies resulting from our optimized parameters in INDO/CIS with those of EOM-CCSD. All the points in the plot would lie on the diagonal line if the MAE were zero. We also compare the original ZINDO/S with EOM-CCSD. Our new parameters perform better than the original ZINDO/S parameters which gave an MAE of 0.67 eV.

After the optimization of excitation energies, the best values of U_{ss} and U_{pp} which reproduce the *ab initio* first ionization potential (IP_{ai}) of the silicon atom were determined. IP_{ai} was calculated using the "delta-SCF" approach, namely: $IP_{ai} = E(N-1) - E(N)$ where, $E(X)$ is the *ab initio* (CCSD) energy of the X-electron system. For the silicon atom, we obtained $IP_{ai} = 8.069$ eV at the CCSD/def2-tzvpp level which is in agreement with the experimental value [25] of 8.1517 eV. By varying U_{pp} and keeping $(U_{pp} - U_{ss})$ fixed at the value obtained in the previous

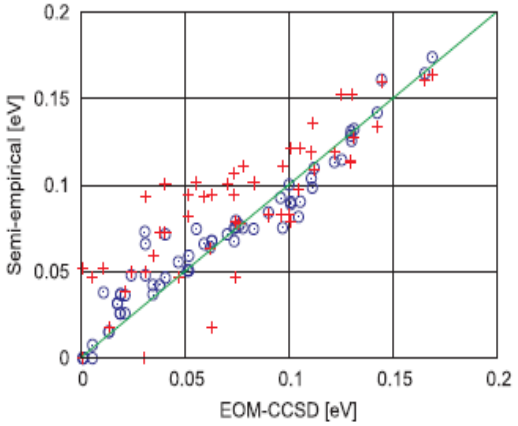

Fig. 1. Scatter plot of oeINDO (blue circles) and original ZINDO/S (red pluses) excitation energies against EOM-CCSD energies for diatomics. All the points would lie on the diagonal green line if the MAE were zero. (For interpretation of the references to color in this figure legend, the reader is referred to the web version of this article.)

Table 1
Our parameters (oeINDO), optimized for diatomics and the original ZINDO/S parameters.

Parameters	oeINDO	ZINDO/S
U_{ss}	− 25.4244 eV	− 36.235929 eV
U_{pp}	− 13.6400 eV	− 28.594917 eV
ζ_s	1.430753 bohrs	1.52 bohrs
ζ_p	1.411963 bohrs	1.52 bohrs
β_s	29.06189 eV	13.0 eV
β_p	9.062134 eV	13.0 eV
γ_{ss}	2.311795 eV	7.57 eV
γ_{sp}	2.311795 eV	7.57 eV
γ_{pp}	2.311795 eV	7.57 eV
F^2_{pp}	1.750264 eV	2.2627 eV
G_{sp}	3.132682 eV	4.8122 eV

fit to excitation energies, we found the values of U_{pp} and U_{ss} which best reproduced the CCSD IP_{ai} without changing the energies obtained in the previous optimization of the excitation energies. Our INDO parameters, optimized for excitation (oe) energies are listed in Table 1 as "oeINDO" along with the original ZINDO/S parameters.

4. Results and discussions

The key question for our approach is whether the parameters we obtained are 'transferable' or not, i.e., whether the same model parameters which we obtained for diatomics will lead to accurate excitation energies for structures more complex than diatomics which were not included in the training set. We verified the transferability of our model by computing the excitation energies for different Si_n complexes with $n = 3, 4, 5, 19, 40$. The equilibrium geometries of Si_n ($n = 3, 4, 5, 19, 40$) have been reported in literature [26–28] and we used these as well as perturbations around the $n = 3, 4, 5$ structures. For Si_3, Si_4 and Si_5, the equilibrium structures are isosceles triangle, planar rhombus and squashed trigonal bi-pyramid, respectively, and all have singlet ground state configurations [27,28]. For the larger clusters (Si_{19} and Si_{40}) for which EOM-CCSD calculations were prohibitive, we have used the TDDFT approach with the 'B3LYP' exchange correlation functional [29] as well as the CIS and CIS(D) approaches but only after estimating their accuracies for smaller silicon clusters.

4.1. Excitation of the equilibrium Si_3 structure

We have determined the excitation energies for the eight lowest lying states of the equilibrium Si_3 structure which has sides 2.292, 2.292, 2.960 Å. The first excitation energy from oeINDO is 1.3 eV while EOM-CCSD/def2-tzvpp gives 1.4 eV. The absorption spectra for this structure is shown in Fig. 2 in which the relative intensity, scaled such that the largest intensity has a value of unity, is plotted. There is reasonable agreement in the results although the highest peak of oeINDO is red-shifted from that of EOM-CCSD by about 0.5 eV. The MAE for the eight excitations is 0.22 eV from the EOM-CCSD results. In comparison, TDDFT/B3LYP and CIS(D) give MAEs of 0.17 and 0.39 eV from the EOM-CCSD energies for this cluster.

4.2. Excitation of the equilibrium Si_4 structure

For the Si_4 equilibrium structure, there is good agreement between the oeINDO absorption spectra and the EOM-CCSD ones: the MAE of oeINDO energies relative to EOM-CCSD is only 0.18 eV and the absorption spectra, shown in Fig. 3, has the highest peak of oeINDO blue-shifted from the EOM-CCSD one by only about 0.10 eV.

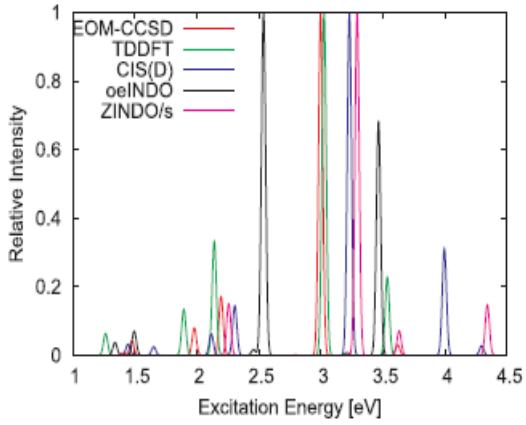

Fig. 2. Computed UV–VIS absorption spectra of the Si_3 equilibrium structure.

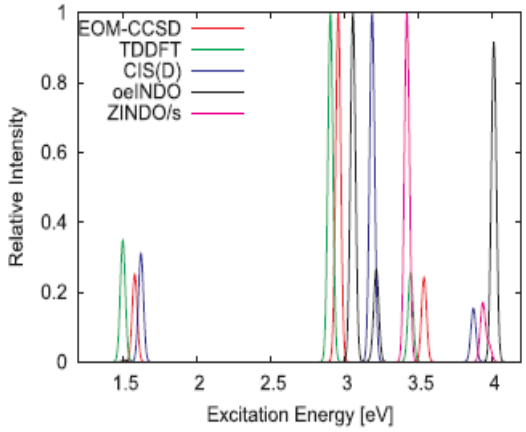

Fig. 3. Computed UV–VIS absorption spectra of the Si_4 equilibrium structure.

4.3. Excitation of the equilibrium Si_5 structure

The excitation energies and the UV–VIS spectra of the equilibrium Si_5 cluster are also well predicted by oeINDO. The spectra is shown in Fig. 4 together with the EOM-CCSD, TDDFT, and CIS(D) spectra. The position of the highest peak of oeINDO deviates by only 0.09 eV from that of the EOM-CCSD. In addition, the MAEs of oeINDO excitation energies from the EOM-CCSD, TDDFT, and CISD energies are 0.09, 0.04, and 0.16 eV, respectively.

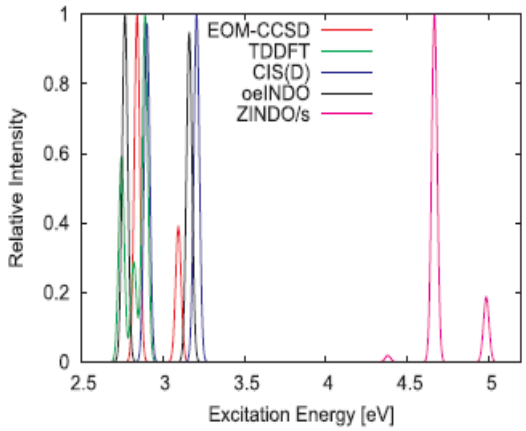

Fig. 4. Computed UV–VIS absorption spectra of the Si_5 equilibrium structure.

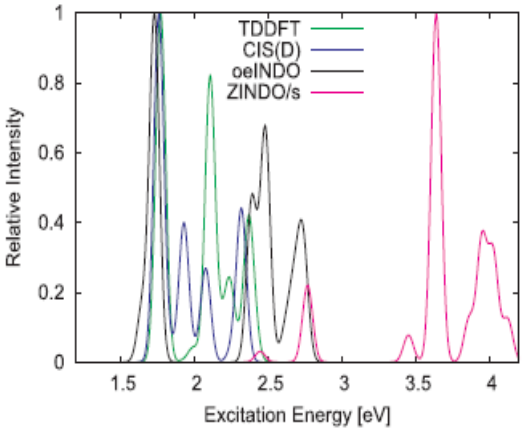

Fig. 5. Computed UV–VIS absorption spectra of the Si_{19} equilibrium structure.

4.4. Excitations of the equilibrium Si_{19} and Si_{40} structures

For the Si_n ($n = 19, 40$) equilibrium structures, we did not have enough computational resources to carry out EOM-CCSD calculations, thus, we compared with TDDFT/B3LYP and CIS(D) excitation energies. The MAE for the oeINDO excitation energies for Si_{19} compared to the TDDFT/B3LYP and CIS(D) energies are 0.32 eV and 0.36 eV respectively. For Si_{40}, the corresponding MAEs are 0.12 eV and 0.03 eV when oeINDO is benchmarked against TDDFT/B3LYP and CIS(D), respectively. For all ($n = 3, 4, 5, 19, 40$) equilibrium structures, the MAE of our oeINDO with respect to the TDDFT/B3LYP energies is 0.15 eV and 0.25 eV with respect to the CIS(D) excitation energies. The corresponding results for ZINDO/S are 1.23 and 1.13 eV, respectively. We present the UV–VIS absorption spectra for Si_{19} and Si_{40}, in Figs. 5 and 6, respectively. The oeINDO results compare favorably well with the TDDFT and CIS(D) spectra. The highest peak of the oeINDO spectra for Si_{19} matches well with that of TDDFT and CIS(D) while the Si_{40} spectra reproduces the CIS(D) pattern in the same energy range.

We have summarized the results of the eight lowest lying excitation energies for each of the Si_3, Si_4, Si_5, Si_{19}, and Si_{40} equilibrium structures in Table 2. For a total of 24 excitation energies, eight for each of these (Si_3, Si_4, and Si_5) equilibrium structures, the MAE of our oeINDO energies with respect to the EOM-CCSD energies is 0.16 eV. This compares favorably with the TDDFT/B3LYP and CIS(D) energies which have MAEs of 0.09 eV and 0.11 eV, respectively, with respect to EOM-CCSD

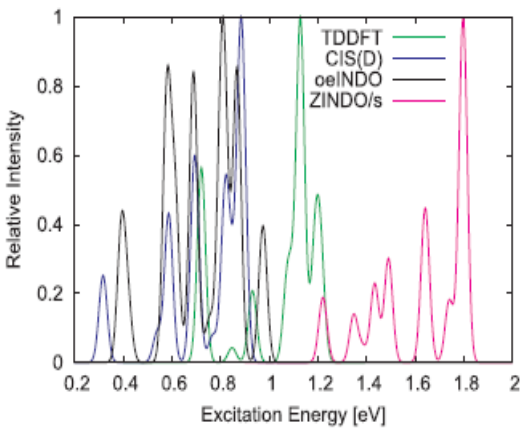

Fig. 6. Computed UV–VIS absorption spectra of Si_{40} equilibrium structure.

Table 2
MAE in eV of oeINDO and ZINDO/S from the EOM-CCSD, TDDFT, and CIS(D) *ab initio* excitation energies of Si_n equilibrium geometries (n = 3, 4, 5, 19, 40). The EOM-CCSD calculations for Si_{19} and Si_{40} were beyond our computational capacity.

Methods	EOM-CCSD	TDDFT	CIS(D)
	Si_3		
oeINDO	0.22	0.17	0.39
ZINDO/S	0.91	0.98	0.74
	Si_4		
oeINDO	0.18	0.24	0.31
ZINDO/S	1.38	1.71	1.25
	Si_5		
oeINDO	0.09	0.04	0.16
ZINDO/S	1.47	1.52	1.39
	Si_{19}		
oeINDO	–	0.32	0.36
ZINDO/S	–	1.42	1.46
	Si_{40}		
oeINDO	–	0.12	0.03
ZINDO/S	–	0.68	0.80

excitation energies. The original ZINDO/S energies have an MAE of 1.28 eV from EOM-CCSD results.

4.5. Excitations of equilibrium and non-equilibrium Si_n structures

We have also included structures that are perturbed from the equilibrium Si_n (n = 3, 4, 5) geometries in our evaluation of the accuracy and transferability of our oeINDO model. The ones we examined were such that the equilibrium inter-atomic distances were scaled by the factors 0.9, 1.1 and 1.2, respectively. This procedure led to 12 structures in all, including the equilibrium geometries. The MAEs of the excitation energies of these structures from the EOM-CCSD energies are presented in Table 3. A scatter plot which compares the oeINDO energies with the EOM-CCSD ones for these small clusters is also shown in Fig. 7. The TDDFT/B3LYP and CIS(D) energies are also compared with the EOM-CCSD energies. Clearly, from the table and figure, the oeINDO model parameters are transferable with an accuracy between 0.01 and 0.5 eV. This accuracy is similar to the TDDFT/B3LYP one which typically range from 0.01 to 0.3 eV.

4.6. Excitations of large silicon clusters

Lastly, we carried out calculations and predicted the spectra for large Si_n (n = 124, 147, 172, 779) clusters using the oeINDO model. Fig. 8 shows the results for the absorption spectra of these clusters. The largest (smallest) one has a diameter of 3.0 (1.6) nm. The absorption edges and excitation energies results agree with the report by Jackson et al. which predict that large Si clusters are more metallic than bulk silicon [30]. In addition, the absorption edge and the first excitation energy of about 0.3 eV for the Si_{147} equilibrium cluster determined by oeINDO agrees with the electronic gap predicted in the same report [30].

Table 3
MAEs of oeINDO, ZINDO/S and TDDFT/B3LYP excitation energies (eV) with respect to EOM-CCSD energies for different (equilibrium and non-equilibrium) Si_n (n = 3, 4, 5) clusters. The data used consisted of 32 excitation energies for each cluster size.

Methods	Si_3	Si_4	Si_5
oeINDO	0.25	0.27	0.11
ZINDO/S	0.87	1.32	1.31
TDDFT/B3LYP	0.06	0.11	0.08
CIS(D)	0.13	0.15	0.06

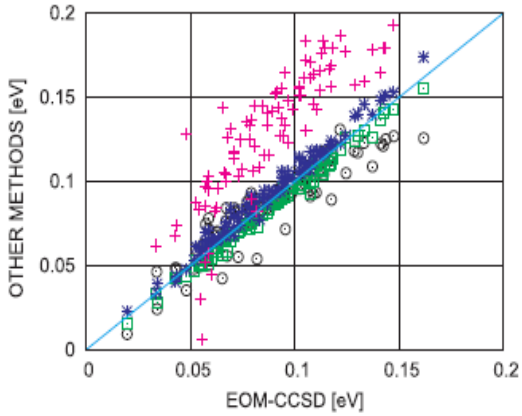

Fig. 7. Scatter plot of oeINDO (black circles), original ZINDO/S (pink pluses), CIS(D) (blue asterisks) and TDDFT (green square) excitation energies against EOM-CCSD energies for equilibrium and non-equilibrium Si_n (n = 3, 4, 5) clusters. The data used consisted of 32 excitation energies for each cluster size. All the points would lie on the diagonal line if the MAE were zero. (For interpretation of the references to color in this figure legend, the reader is referred to the web version of this article.)

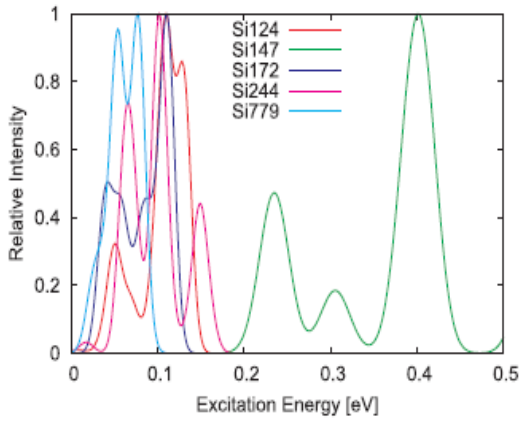

Fig. 8. Computed UV–VIS absorption spectra of Si_n (n = 124, 147, 172, 779) geometries.

5. Conclusion

We have presented a method that can give excitation energies of clusters which are accurate to better than 0.5 eV. This method consists in parameterizing a semi-empirical Hamiltonian using high-level *ab initio* data of diatomics. In this case, the reference *ab initio* data was at the EOM-CCSD level although, in principle, *ab initio* data from other methods such as GW or multireference EOM-CCSD can also be used. We parameterized the ZINDO/S Hamiltonian and demonstrated that the parameters obtained for diatomics are transferable to more complex systems. In particular, we obtained excitation energies with accuracies of 0.5 eV and less as well as UV–VIS spectra in qualitative agreement with the EOM-CCSD ones. However, unlike EOM-CCSD which is computationally prohibitive, oeINDO is not compute intensive and we were able to carry out calculations for quantum dots silicon clusters with 779 atoms (more than 10,000 electrons). Our results for large clusters show that these clusters become more metallic when compared to bulk silicon which has a band gap of approximately 1.2 eV.

It is worth mentioning the calculation times in order to give a good idea of the usefulness of this method. We achieved an accuracy close to EOM-CCSD accuracy using less than a hundredth of the time and resources. The oeINDO results are also reasonably close to TDDFT results and sometimes better but with calculations that take not more than a tenth of the TDDFT calculation time, depending on the size of the system.

We note here that we have experimented with other semi-empirical methods, namely PM3 [31] and AM1 [32]. These model Hamiltonians gave small MAEs for small ($n = 3, 4, 5$) clusters but large MAEs for the larger ($n = 19, 40$) clusters. The reason for this poor performance for large clusters is possibly due to the form of the two-electron two-center integrals in these models. We plan to investigate this further in future work.

The oeINDO model, like the ZINDO/S and other INDO semi-empirical models neglect three- and four-center terms. Future work can investigate improvement of the accuracy of oeINDO through the inclusion of explicit three-center terms into the model Hamiltonian; we expect the four-center terms to be much less important.

Declaration of interests

The authors declare that they have no known competing financial interests or personal relationships that could have appeared to influence the work reported in this paper.

Acknowledgement

Computing resources from the Center for High Performance Computing (CHPC) South Africa and from the International Center for Theoretical Physics (ICTP), Italy are acknowledged.

References

[1] M. Gatti, Correlation Effects in Valence Electron Spectroscopy of Transition Metal Oxides: Many-body Perturbation Theory and Alternative Approaches (Ph.D. thesis), École Polytechnique, Palaiseau, 2007.
[2] M.J. van Setten, F. Weigend, F. Evers, The gw-method for quantum chemistry applications: theory and implementation, J. Chem. Theory Comput. 9 (1) (2012) 232–246.
[3] N. Nakanishi, A general survey of the theory of the Bethe-Salpeter equation, Prog. Theoret. Phys. Suppl. 43 (1969) 1–81.
[4] X. Leng, F. Jin, M. Wei, Y. Ma, Gw method and Bethe-Salpeter equation for calculating electronic excitations, Wiley Interdiscip. Rev.: Comput. Mol. Sci. 6 (5) (2016) 532–550.
[5] X. Blase, I. Duchemin, D. Jacquemin, The Bethe–Salpeter equation in chemistry: relations with td-dft, applications and challenges, Chem. Soc. Rev. 47 (3) (2018) 1022–1043.
[6] O. Christiansen, H. Koch, P. Jørgensen, The second-order approximate coupled cluster singles and doubles model cc2, Chem. Phys. Lett. 243 (5–6) (1995) 409–418.
[7] K. Andersson, P.A. Malmqvist, B.O. Roos, A.J. Sadlej, K. Wolinski, Second-order perturbation theory with a Casscf reference function, J. Phys. Chem. 94 (14) (1990) 5483–5488.
[8] R. Krishnan, H. Schlegel, J. Pople, Derivative studies in configuration-interaction theory, J. Chem. Phys. 72 (8) (1980) 4654–4655.
[9] M.A. Marques, N.T. Maitra, F.M. Nogueira, E.K. Gross, A. Rubio, Fundamentals of Time-dependent Density Functional Theory vol. 837, Springer Science & Business Media, 2012.
[10] M.E. Casida, Time-dependent density-functional theory for molecules and molecular solids, J. Mol. Struct.: THEOCHEM 914 (1–3) (2009) 3–18.
[11] A.A. Voityuk, Indo/xc a new semiempirical method for excited states of organic and biological molecules, J. Chem. Theory Comput. 10 (11) (2014) 4950–4958.
[12] M.R. Silva-Junior, W. Thiel, Benchmark of electronically excited states for semiempirical methods: Mndo, am1, pm3, om1, om2, om3, indo/s, and indo/s2, J. Chem. Theory Comput. 6 (5) (2010) 1546–1564.
[13] M. Caricato, G.W. Trucks, M.J. Frisch, K.B. Wiberg, Oscillator strength: How does tddft compare to eom-ccsd? J. Chem. Theory Comput. 7 (2011) 456–466.
[14] D. Jacquemin, V. Wathelet, E.A. Perpete, C. Adamo, J. Chem. Theory Comput. 5 (2009) 2420–2435.
[15] M.C. Zerner, G.H. Lowe, R.F. Kirchner, U.T. Mueller-Westerhoff, An intermediate neglect of differential overlap technique for spectroscopy of transition-metal complexes. Ferrocene, J. Am. Chem. Soc. 102 (1980) 589–599.
[16] W. Thiel, Semiempirical quantum–chemical methods, WIREs Comput. Mol. Sci. 4 (2) (2014) 145–157.
[17] A.R. Leach, Molecular Modelling: Principles and Applications, Prentice Hall, 2001.
[18] J. Ridley, M. Zerner, An intermediate neglect of differential overlap technique for spectroscopy: pyrrole and the azines, Theor. Chim. Act. 32 (2) (1973) 111–134.
[19] G. Segal, Semiempirical Methods of Electronic Structure Calculation: Part B: Applications vol. 8, Springer Science and Business Media, 2012.
[20] A.A. Voityuk, Intermediate neglect of differential overlap for spectroscopy, Wiley Interdiscip. Rev.: Comput. Mol. Sci. 3 (5) (2013) 515–527.
[21] A. Szabo, N.S. Ostlund, Modern Quantum Chemistry: Introduction to Advanced Electronic Structure Theory, Courier Corporation, 2012.
[22] M. Elstner, D. Porezag, G. Jungnickel, J. Elsner, M. Haugk, T. Frauen-heim, S. Suhai, G. Seifert, Self-consistent-charge density-functional tight-binding method for simulations of complex materials properties, Phys. Rev. B 58 (11) (1998) 7260.
[23] F. Weigend, R. Ahlrichs, Balanced basis sets of split valence, triple zeta valence and quadruple zeta valence quality for h to rn: design and assessment of accuracy, PCCP 7 (18) (2005) 3297–3305.
[24] F. Neese, The orca program system, Wiley Interdiscip. Rev.: Comput. Mol. Sci. 2 (1) (2012) 73–78.
[25] W.C. Martin, R. Zalubas, Energy levels of silicon, si i through si xiv, J. Phys. Chem. Ref. Data 12 (1983) 323–380.
[26] N.M. Tam, T.D. Hang, H.T. Pham, H.T. Nguyen, M.P. Pham-Ho, P.A. Denis, M.T. Nguyen, Bonding and singlet–triplet gap of silicon trimer: effects of protonation and attachment of alkali metal cations, J. Comp. Chem. 36 (11) (2015) 805–815.
[27] K. Raghavachari, Theoretical study of small silicon clusters: equilibrium geometries and electronic structures of si n (n= 2–7, 10), J. Chem. Phys. 84 (10) (1986) 5672–5686.
[28] K. Raghavachari, C.M. Rohlfing, Bonding and stabilities of small silicon clusters: a theoretical study of si7–si10, J. Chem. Phys. 89 (4) (1988) 2219–2234.
[29] A.D. Becke, Density-functional thermochemistry. iii. The role of exact exchange, J. Chem. Phys. 98 (1993) 5648–5652.
[30] K. Jackson, J. Jellinek, Si clusters are more metallic than bulk Si, J. Chem. Phys. 145 (24) (2016) 244302.
[31] J.J.P. Stewart, Optimization of parameters for semiempirical methods. i. Method, J. Comp. Chem. 10 (1989) 209–220.
[32] M.J.S. Dewar, E.G. Zoebisch, E.F. Healy, Am1: a new general purpose quantum mechanical molecular model, J. Am. Chem. Soc. 107 (1985) 3902–3909.